The Enskog-2σ model, a new viscosity model for simple fluids and alkanes

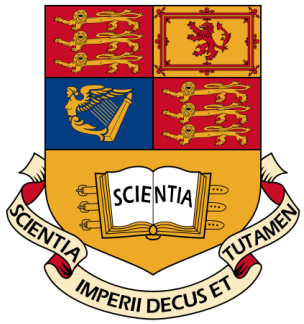

Rudolf Umla

Department of Earth Science and Engineering

Qatar Carbonates and Carbon Storage Research Centre

Imperial College London

A thesis submitted for the degree of

Doctor of Philosophy

February 24, 2013

Abstract

This thesis describes the development of a new model for viscosity, the Enskog-2σ model. The model is based on Enskog theory in which the viscosity of a hard sphere fluid is computed from the hard sphere interactions on the molecular level. The idea of the Enskog-2σ model is to introduce two effective weakly temperature dependent diameters in Enskog's approach. One of the diameters is linked to the collision rate between the fluid molecules, the other diameter to the molecule size.

The optimisation of the two effective temperature dependent diameters allows the Enskog-2σ model to reproduce the viscosity data of simple fluids, i.e. fluids with non-polar, fairly spherical molecules, very well over a wide range of pressures and temperatures. For argon, for example, the model covers a pressure range from 0 to 400 MPa and temperatures from $0.6T_c$ to $4.6T_c$ (T_c = critical temperature of argon) and correlates the experimental reference correlation within $\pm 10\%$. Making use of the universal behavior of the diameters for various simple fluids, the number of free parameters can be reduced to one or two constant scaling parameters that can be predicted well from viscosity data along one isotherm.

The Enskog-2σ approach has been extended to model n-alkanes from ethane to octane. The molecules of n-alkanes are described as chains of equally sized hard spheres and a collision between two chains is modelled as collision between two spherical segments of the colliding chains. The Enskog-2σ model for n-alkanes contains two effective weakly temperature dependent chain lengths. The number of free parameters can be reduced by relating the chain lengths to the carbon number or to the chain lengths of a reference n-alkane. The remaining free parameters can usually be determined satisfactorily from viscosity data along one isotherm.

Acknowledgements

I would like to thank my academic supervisors Prof. Dr. Velisa Vesovic and Dr. Nicolas Riesco for their excellent support throughout my PhD. Also, I would like to thank my parents Helmut Umla and Silvia Umla as well as my grandmother Johanna Aubertin for encouraging my research kindly. I am grateful as well to my co-workers in the Qatar Carbonates and Carbon Research Center for inspiring discussions and presentations. Finally, I gratefully acknowledge funding from the Qatar Carbonates and Carbon Storage Research Centre (QCCSRC), provided jointly by Qatar Petroleum, Shell, and Qatar Science & Technology Park

All material in this thesis is based on my own work unless referenced otherwise.

Contents

List of Figures

List of Tables

1

Introduction

The main aim of this work is to develop a new model for viscosity that provides us with a realistic and fairly accurate viscosity model for dense fluids. In more detail, the new viscosity model has been derived from Enskog's theory for hard sphere fluids and validated for simple fluids with fairly spherical, non-polar molecules as well as n-alkanes over a wide range of pressures and temperatures in the supercritical as well as liquid phase.

1.1 Petroleum Engineering

Petroleum engineering is a field of engineering related to the production of hydrocarbons. Hydrocarbons have played a vital role in satisfying the global energy demands in the 20th century and will continue to do so for the coming decades. Thus, the efficient production of hydrocarbons from reservoirs is an important task in petroleum engineering and leads increasingly to the application of enhanced oil recovery methods. Important enhanced oil recovery methods are chemical flooding, hydrocarbon as well as gas injection and thermal recovery methods (Lyons & Plisga, 2004). To select an appropriate recovery method for a given reservoir and adjust the process parameters like the injection and production rates optimally, the properties of the reservoir rocks, the reservoir fluids and the injected fluids have to be determined fairly accurately. A crucial fluid parameter is the viscosity of the fluids involved, i.e., the viscosity of the reservoir fluids, that usually consist mainly of n-alkanes, and the viscosity of the injected fluids such as nitrogen, oxygen, carbon dioxide, water and polymers. The viscosity of these

fluids is also of great interest for other petroleum engineering applications like flow through pipelines and carbon capture storage.

1.2 Viscosity

Viscosity or more precisely shear viscosity measures the resistance of fluids to deformation by shear stress. Deformation by shear stress is found relevant in many kinds of fluid flow, e.g., flow through a pipe, flow within a porous medium or flow around an obstacle. Thus, viscosity determines often crucially how a fluid flows and appears as one of the key parameters in fluid dynamics. Moreover, models to describe fluid flows are ubiquitous in science as well as industry and are often sensitive to the viscosity values. Especially, as outlined above, in the petroleum industry an accurate knowledge of viscosity can be of enormous value. For the fluids considered in this work, i.e., pure Newtonian fluids such as nitrogen, oxygen, carbon dioxide and n-alkanes up to octane, viscosity can be described fully as function of temperature and fluid density. We do not deal with fluid mixtures, in which viscosity depends also on the concentration of the mixture components, or non-Newtonian fluids like certain polymers, for which viscosity changes with the shear rate. For the fluids under investigation, viscosity is independent of the shear rate such that the velocity gradient in the fluid changes linearly with the applied shear stress, i.e.,

$$\tau = \eta \frac{\partial u}{\partial y}, \tag{1.1}$$

where τ is the shear stress, η the shear viscosity and $\frac{\partial u}{\partial y}$ the local shear velocity. In addition to shear viscosity, there is bulk viscosity, also called volume viscosity or second viscosity. The bulk viscosity describes the internal friction encountered when a fluid is compressed or expanded. The bulk viscosity becomes important only when the compression or expansion is fast, such as in sound and shock waves. In this work, we will deal only with shear viscosity.

1.3 Measuring viscosity

Experimental measurements are hitherto the most accurate way to determine viscosity of dense fluids. Traditional measurement instruments for viscosity include capillary

viscometers, falling-body viscometers, rolling ball viscometers, oscillating-body viscometers and vibrating wire viscometers (Wakeham *et al.*, 1991; Ciotta, 2010). Under favourable conditions, these viscometers allow to measure the viscosity with a relative accuracy of a few percent. For example, in (Vogel *et al.*, 2000), the viscosity of methane has been determined with a vibrating wire viscometer over a temperature range from 260K to 360K and a pressure range from 0.3 MPa to 29 Mpa with an estimated accuracy of ±0.3%. Another recent example are the viscosity measurements for argon with a oscillating-body viscometer by (Evers *et al.*, 2002). There, the viscosity has been measured from 233K to 523K and from 0.1 MPa to 28 MPa with an estimated accuracy of better than ±1%. (Wakeham *et al.*, 1991) and (Ciotta, 2010) give a detailed review of experimental viscosity measurements.

1.4 Experimental reference correlations for viscosity

Based on the most accurate experimental measurements available, experimental reference correlations for viscosity have been developed for a number of fluids. These correlations reproduce viscosity with estimated uncertainties of a few percent over a wide range of pressures and temperatures. Some examples are the correlation by (Lemmon & Jacobson, 2004) for argon, oxygen, nitrogen and air, the correlation by (Vogel *et al.*, 2000) for methane and the correlation by (Huber *et al.*, 2004) for n-octane, n-nonane and n-decane. The drawback of these correlations is that they are merely empirical and do not possess a theoretical background. Viscosity models with a theoretical background, however, are desirable as they are often superior in extrapolating viscosity data and because they can serve as basis for viscosity models of fluid mixtures.

1.5 Viscosity models with theoretical background

Theoretically based viscosity models assume a certain intermolecular potential and strive to compute the viscosity from this potential. Traditionally, viscosity models distinguish between three different contributions to viscosity η,

$$\eta = \eta^0 + \Delta\eta_c + \Delta\eta, \tag{1.2}$$

the viscosity η^0 in the dilute gas limit, the critical enhancement $\Delta\eta_c$ of viscosity close to the critical point and the excess viscosity $\Delta\eta$. The critical enhancement $\Delta\eta_c$ contributes significantly to viscosity only in a small temperature and density region close to the critical point and can be neglected outside this region (Millat *et al.*, 1996). The critical enhancement has been measured experimentally and predicted for many fluids fairly well by theoretical models (Sengers, 1985; Millat *et al.*, 1996).

In recent years, great advances have been made in the ability to calculate the viscosity η^0 in the dilute gas limit from an intermolecular potential by means of classical trajectory calculations (Bock *et al.*, 2002; Hellmann *et al.*, 2008, 2009, 2011). The starting point for classical trajectory calculations is Boltzmann's equation which has first been derived in 1872 by Boltzmann (Ferziger & Kaper, 1972). Boltzmann's equation describes the statistics of gas particles in terms of a particle distribution function and, in principle, allows to derive the viscosity of a fluid for a given intermolecular potential. In (Bock *et al.*, 2002; Hellmann *et al.*, 2008, 2009, 2011), classical trajectory computations have been carried out for carbon dioxide, methane, water and hydrogen sulfide and the calculations predict the bulk of the dilute gas viscosity data over wide range of temperatures very well within ±1%. These calculations, however, are restricted to the dilute gas limit and cannot be used to compute the excess viscosity $\Delta\eta$ for dense fluids.

Boltzmann's equation in combination with kinetic theory offers a possible formal way of linking the viscosity of dense fluids to the intermolecular potential (McCourt *et al.*, 1991; Chapman & Cowling, 1970) and thus utilizing the molecular approach that has been so successful for dilute gases (Bock *et al.*, 2002; Hellmann *et al.*, 2008, 2009, 2011; McCourt *et al.*, 1991; Chapman & Cowling, 1970). However, a general solution to Boltzmann's equation is still lacking and hence no rigorous kinetic theory is available (Chapman & Cowling, 1970). One has therefore to rely on approximate solutions. One of the historically earliest attempts was that by Enskog (Chapman & Cowling, 1970; Enskog, 1922), who solved Boltzmann's equation by assuming that molecules in a fluid can be replaced by hard spheres and by making further assumptions about their interaction. In Enskog's approach, fluid molecules interact only via the infinitely steep, repulsive hard sphere potential. A slightly more realistic potential that also considers attractive forces between fluid molecules is the square well potential which is characterised by three potential parameters. In (Davis *et al.*, 1961), an equation

for viscosity of square well fluids has been derived from Boltzmann's equation. Based on this equation, a large body of work has been devoted to approximate the viscosity of real fluids with the one of a square well fluid (Monnery *et al.*, 1996, 1997, 1998). Another popular and fairly realistic intermolecular potential for simple molecules is the Lennard-Jones potential which contains both attraction and repulsion as a continuous function of distance between the molecules. A viscosity expression for Lennard-Jones fluids has been derived from Boltzmann's integro-differential equation only after further simplifications have been introduced (Karkheck *et al.*, 1988). Alternatively, the viscosity of a Lennard-Jones fluid has been calculated within ±5% by molecular dynamics (MD) simulations (Meier *et al.*, 2004; Galliéro *et al.*, 2005, 2006) and approximated by a number of analytical approaches that are not based on kinetic theory. The best-known of these approaches are the stochastic theory by (Polewczak & Stell, 2002), the renormalized Kirkwood theory (Kirkwood *et al.*, 1949) and the mode-coupling theory by (Egorov, 2008). All approaches introduce a series of further simplifications before an expression for viscosity is derived and the resulting viscosity expression often involves integrals that have to be solved by numerical integration. The intermolecular potentials used for the classical trajectory calculations in (Bock *et al.*, 2002; Hellmann *et al.*, 2008, 2009, 2011) constitute a very good approximation for the intermolecular potential of the respective real fluid under investigation. These potentials however are more complicated than the Lennard-Jones potential and it is to be expected that one has to make strong simplifications in order to derive transport properties for dense fluids from these potentials. Thus, although the chosen intermolecular potential might be quite realistic, the accuracy of the approach as a whole is expected to reduce greatly due to the simplifications necessary to derive an expression for viscosity. Also, MD simulations for more complicated fluid potentials are still in their infancy, for some examples see (Bordat & Müller-Plathe, 2002; Hess, 2002; Galliéro & Boned, 2009).

1.6 Enskog theory

Enskog theory has become a cornerstone for developing molecular-based viscosity models (Dymond, 1985; Millat *et al.*, 1996). The wide-spread use of Enskog theory (Barker & Henderson, 1967; Weeks *et al.*, 1971; Andersen *et al.*, 1971; Hanley *et al.*, 1972; Andrews, 1976; Lado, 1984; Speedy *et al.*, 1989; Silva & Liu, 2008; Vesovic & Wakeham,

1989b,a) follows from the fact that the hard sphere potential captures the major effects in a dense gas (Silva & Liu, 2008) and that Enskog theory leads to easy to use, explicit expressions for viscosity, thermal conductivity and mass diffusion. One of the underlying drawbacks of the model is that it cannot be used to directly predict the viscosity of real fluids, as the assumptions made are sufficiently drastic to preclude this possibility. In particular, the attractive potential part of a real fluid is neglected and the repulsive potential part is modelled as infinitely steep which are rather crude approximations. However, if the size of the hard sphere is used as an effective parameter, the Enskog model can be shown to describe the viscosity of real fluids reasonably well (Millat *et al.*, 1996; Silva & Liu, 2008). Hence, most models based on the original Enskog model make use of a single effective diameter, usually weakly temperature and possibly density dependent, to ensure good agreement between experiments and prediction (Barker & Henderson, 1967; Weeks *et al.*, 1971; Andersen *et al.*, 1971; Hanley *et al.*, 1972; Andrews, 1976; Lado, 1984; Speedy *et al.*, 1989). In essence, the deficiencies of the Enskog hard sphere model are absorbed by the use of an effective sphere diameter for the real fluid molecules.

1.7 The Enskog-2σ model

In this work, we argue that the predictions of the Enskog model can be greatly improved if we make a more physically based choice of the effective parameters. Enskog's assumptions broadly address the simplification of collisional dynamics and the estimation of the excluded volume of a molecule. Although the excluded volume of a molecule contributes to the increased probability of collision, there is no reason to believe that the effective sizes of a molecule contributing to the dynamics and the geometry of molecular interactions in a dense fluid are the same. Hence, we propose the Enskog-2σ model, where we base our choice of the effective parameters on the physical effects corrected in Enskogs treatment; namely, the excluded volume of a molecule and the increased probability of collision in comparison to the dilute gas. We further show that the Enskog-2σ describes the viscosity of real fluids more accurately than the standard Enskog model and illustrate that the Enskog-2σ model can be generalized to predict the viscosity of one fluid from the knowledge of another. The developed Enskog-2σ

model provides us with a realistic and fairly accurate viscosity model for dense fluids.

1.8 Structure of this work

The present work is structured as follows:

- In **chapter 2**, the theoretical foundations are established upon which the Enskog-2σ model will be based.
- In **chapter 3**, the Enskog-2σ model is derived for simple fluids with fairly spherical, non-polar molecules.
- In **chapter 4**, the Enskog-2σ model is modified to deal with n-alkanes.
- In **chapter 5**, the results of the Enskog-2σ model for simple fluids are discussed.
- In **chapter 6**, the results of the Enskog-2σ model for n-alkanes are presented.
- In **chapter 7**, the results of this work are summarised.

2

Theoretical foundations

In the present chapter, the theory is established upon which we will develop the Enskog-2σ model. First, Boltzmann's kinetic theory is introduced leading to viscosity results applicable to dilute gases. Next, we discuss Enskog's theory which is an extension of Boltzmann's approach to moderately dense gases and which will serve as basis for the Enskog-2σ model. To extend the Enskog-2σ model to high densities, Enskog's theory is corrected by molecular dynamics simulations which are discussed next. Enskog's theory describes a hard sphere fluid and hence it is a suitable approximation for fluids with fairly spherical molecules. For fluids with chain like molecules like n-alkanes, a modification of Enskog's viscosity expression has been proposed in (de Wijn *et al.*, 2008). This modification is the theoretical foundation of the Enskog-2σ model for n-alkanes and hence is also described in this chapter. Finally, we review the VW method (Vesovic & Wakeham, 1989b,a). The VW method allows to predict the viscosity of fluid mixtures from the viscosities of the pure mixture components and is closely related to the Enskog-2σ model. The description of Boltzmann's approach and Enskog theory, given in the first two sections, follows (Ferziger & Kaper, 1972; Maitland *et al.*, 1981).

2.1 Boltzmann's Kinetic Theory of Gases

Kinetic theory aims at modelling transport properties of gases (e.g. viscosity, thermal conductivity and self diffusion) starting from a description on the molecular scale. On the molecular scale, a gas is represented by a large number of particles (atoms or molecules). How these particles behave statistically determines the properties of a gas

on the macroscopic scale.
In Boltzmann's approach, the statistics of the gas particles are described by the particle distribution function $f(\mathbf{r}, \mathbf{v}, t)$. The particle distribution function is defined by setting

$$f(\mathbf{r}, \mathbf{v}, t) d\mathbf{r} d\mathbf{v} \tag{2.1}$$

equal to the number of particles which, at time t, are located in the volume element $d^3\mathbf{r}$ about $\mathbf{r}$ and have a velocity in $d^3\mathbf{v}$ about $\mathbf{v}$. To derive an equation which allows to compute how f changes in time from a given initial state, Boltzmann introduced the following assumptions:

(i) only binary collisions are taken into account,

(ii) external forces have negligible influence on the outcome of a collision,

(iii) the expected number of collisions in a given volume element between particles that belong to different velocity ranges can be calculated statistically. This assumption is called the molecular chaos assumption or Stosszahlansatz which means collision number assumption in German.

Making use of these assumptions, Boltzmann derived the Boltzmann equation that can be written as (Ferziger & Kaper, 1972)

$$\left(\frac{\partial}{\partial t} + \mathbf{v} \cdot \nabla_{\mathbf{r}} + \mathbf{F}(\mathbf{r}, t) \cdot \nabla_{\mathbf{v}} \right) f(\mathbf{r}, \mathbf{v}, t) = \left(\frac{\partial f}{\partial t} \right)_{\text{coll}} . \tag{2.2}$$

The quantity $\mathbf{F}(\mathbf{r}, t)$ is the external force per unit mass on a particle at position $\mathbf{r}$ at time t. The term on the right hand side denotes the rate at which the particle distribution function f changes by particle collisions. The collisions are assumed to be elastic in Boltzmann's approach. The collision rate can be expressed in terms of f by

$$J(ff) = \int \int \left(f(\mathbf{r}, \mathbf{v}', t) f(\mathbf{r}, \mathbf{v}_1', t) - f(\mathbf{r}, \mathbf{v}, t) f(\mathbf{r}, \mathbf{v}_1, t) \right) g d\tilde{\Omega} d^3\mathbf{v}_1 \tag{2.3}$$

with the velocities $\mathbf{v}, \mathbf{v}_1$ and $\mathbf{v}', \mathbf{v}_1'$ before and after the collision of the two particles and the absolute value g of the relative velocities before and after collision,

$$g = |\mathbf{v} - \mathbf{v}_1| = \left| \mathbf{v}' - \mathbf{v}_1' \right| . \tag{2.4}$$

The latter equality holds true as the collisions are assumed to be elastic. The term $d\tilde{\Omega}$ indicates the integration over all possible relative orientations of the colliding particles,

which can be specified by two scattering angles. The velocities $\mathbf{v}', \mathbf{v}_1'$ after collision can be expressed in terms of the scattering angles as well as the velocities $\mathbf{v}, \mathbf{v}_1$ before collision via the conversation equations for momentum and kinetic energy. To obtain macroscopic transport equations from the Boltzmann equation, the distribution function is related to the macroscopic fluxes through appropriate averages, e.g., to the momentum flux through a velocity average. The most popular approach in which this link is worked out in detail is the Chapman–Enskog theory. Starting point is a gas in the absence of an external force, i.e., $\mathbf{F} = \mathbf{0}$, that is described by the macroscopic observables number density $n(\mathbf{r}, t)$, hydrodynamic velocity $\mathbf{u}(\mathbf{r}, t)$ and temperature $T(\mathbf{r}, t)$. The macroscopic quantities are assumed to change on a much longer time scale than the time between collisions of the gas particles which is a reasonable assumption for most real gas systems. As $f(\mathbf{r}, \mathbf{v}, t)$ changes with every particle collision, the particle distribution function will adjust itself rapidly to the macroscopic observables $n(\mathbf{r}, t)$, $\mathbf{u}(\mathbf{r}, t)$ and $T(\mathbf{r}, t)$. Consequently, on the macroscopic time scale, the time dependence of f can be fully described through the time dependence of the macroscopic observables n, $\mathbf{u}$ and T such that one can write (Maitland *et al.*, 1981)

$$\frac{\partial f(\mathbf{r}, \mathbf{v}, t)}{\partial t} = \frac{\partial f}{\partial n} \cdot \frac{\partial n}{\partial t} + \frac{\partial f}{\partial \mathbf{u}} \cdot \frac{\partial \mathbf{u}}{\partial t} + \frac{\partial f}{\partial T} \cdot \frac{\partial T}{\partial t}. \tag{2.5}$$

Next, the particle distribution function is decomposed in terms of successive approximations which describe increasingly large departures from thermal equilibrium,

$$f = f_0 + \zeta f_1 + \zeta^2 f_2 + ..., \tag{2.6}$$

where $1/\zeta$ measures the collision frequency in the gas. Due to the introduction of the varying collision frequency ζ, the Boltzmann equation, Eq. (2.2), is modified to

$$\frac{\partial f}{\partial t} + \mathbf{v} \cdot \frac{\partial f}{\partial \mathbf{r}} = \frac{1}{\zeta} J(ff). \tag{2.7}$$

After substitution of the expansion (2.6) for f into Eq. (2.7), the right hand side of Eq. (2.7) can be written as

$$\frac{1}{\zeta} J(f_0 f_0) + \{J(f_1 f_0) + J(f_0 f_1)\} + ... \tag{2.8}$$

To find a similar expansion for the left hand side of Eq. (2.7), the derivatives $\partial n/\partial t$, $\partial \mathbf{u}/\partial t$ and $\partial T/\partial t$ are expressed more explicitly through the conversation equations of

molecular number, momentum and energy in the gas. These conversation equations can be obtained by multiplying both sides of Eq. (2.7) by 1, $m\mathbf{v}$, and $mv^2/2$ respectively and integrating with respect to $\mathbf{v}$. Taking additionally into account that the collision term on the right hand side of Eq. (2.7) conserves the number of particles, their momentum and energy, the conversation equations can be written in the form (Maitland *et al.*, 1981):

$$\frac{\partial n}{\partial t} = -\sum_{j=1}^{3} u_j \frac{\partial n}{\partial x_j} - n \sum_{j=1}^{3} \frac{\partial u_j}{\partial x_j}, \tag{2.9}$$

$$nm\frac{\partial u_i}{\partial t} = -nm \sum_{j=1}^{3} u_j \frac{\partial u_i}{\partial x_j} - \sum_{j=1}^{3} \frac{\partial p_{ij}}{\partial x_j}, \qquad i = 1,\ 2,\ 3, \tag{2.10}$$

$$3/2nk_B\frac{\partial T}{\partial t} = -\frac{3}{2}nk_B \sum_{j=1}^{3} u_j \frac{\partial T}{\partial x_j} - \sum_{i=1}^{3} \frac{\partial q_i}{\partial x_i} - \sum_{i=1}^{3}\sum_{j=1}^{3} p_{ij}\frac{\partial u_i}{\partial x_j} \tag{2.11}$$

with the stress tensor

$$p_{ij} = \int f(m(V_i V_j))d^3\mathbf{v} \qquad i,j = 1,\ 2,\ 3, \tag{2.12}$$

and the heat vector

$$q_i = \int f(\frac{1}{2}mV^2)V_i d^3\mathbf{v} \qquad i = 1,\ 2,\ 3. \tag{2.13}$$

The quantity k_B is the Boltzmann constant, m the particle mass, $\mathbf{V}$ the peculiar velocity $\mathbf{v} - \mathbf{u}$ and the x_i's are the Cartesian coordinates. Using the expansion for f, Eq. (2.6), the conversation equations (2.9) to (2.11) can also be expanded in terms of the reciprocal collision frequency ζ (Maitland *et al.*, 1981):

$$\frac{\partial n}{\partial t} = \left(\frac{\partial n}{\partial t}\right)^{(0)}, \tag{2.14}$$

$$\frac{\partial u_i}{\partial t} = \left(\frac{\partial u_i}{\partial t}\right)^{(0)} + \zeta\left(\frac{\partial u_i}{\partial t}\right)^{(1)} + \zeta^2\left(\frac{\partial u_i}{\partial t}\right)^{(2)} + ..., \tag{2.15}$$

$$\frac{\partial T}{\partial t} = \left(\frac{\partial T}{\partial t}\right)^{(0)} + \zeta\left(\frac{\partial T}{\partial t}\right)^{(1)} + \zeta^2\left(\frac{\partial T}{\partial t}\right)^{(2)} + ..., \tag{2.16}$$

where

$$\left(\frac{\partial n}{\partial t}\right)^{(0)} = -\sum_{j=1}^{3} u_j \frac{\partial n}{\partial x_j} - n\sum_{j=1}^{3} \frac{\partial u_j}{\partial x_j}, \tag{2.17}$$

$$\left(\frac{\partial u_i}{\partial t}\right)^{(0)} = -\sum_{j=1}^{3} u_j \frac{\partial u_i}{\partial x_j} - \frac{1}{nm}\sum_{j=1}^{3} \frac{\partial p^0_{ij}}{\partial x_j}, \qquad i = 1,\ 2,\ 3, \tag{2.18}$$

$$\left(\frac{\partial u_i}{\partial t}\right)^{(1)} = -\frac{1}{nm}\sum_{j=1}^{3} \frac{\partial p^1_{ij}}{\partial x_j}, \qquad i = 1,\ 2,\ 3, \tag{2.19}$$

$$\left(\frac{\partial T}{\partial t}\right)^{(0)} = -\sum_{i=1}^{3} u_j \frac{\partial T}{\partial x_j} - \frac{2}{3nk_B}\left\{\sum_{i=1}^{3} \frac{\partial q_i^{(0)}}{\partial x_i} + \sum_{i=1}^{3}\sum_{j=1}^{3} p_{ij}^{(0)} \frac{\partial u_i}{\partial x_j}\right\}, \tag{2.20}$$

$$\left(\frac{\partial T}{\partial t}\right)^{(1)} = -\frac{2}{3nk_B}\left\{\sum_{i=1}^{3} \frac{\partial q_i^{(1)}}{\partial x_i} + \sum_{i=1}^{3}\sum_{j=1}^{3} p_{ij}^{(1)} \frac{\partial u_i}{\partial x_j}\right\}. \tag{2.21}$$

Substituting Eqs. (2.14) to (2.16) for $\partial f/\partial t$ in Eq. (2.7) and ordering the terms in ζ yields the following equation for the zeroth-order approximation f_0,

$$J(f_0 f_0) = 0, \tag{2.22}$$

and for the first order approximation f_1,

$$\left(\frac{\partial f_0}{\partial n}\right)\left(\frac{\partial n}{\partial t}\right)^{(0)} + \left(\frac{\partial f_0}{\partial \mathbf{u}}\right)\left(\frac{\partial \mathbf{u}}{\partial t}\right)^{(0)} + \left(\frac{\partial f_0}{\partial T}\right)\left(\frac{\partial T}{\partial t}\right)^{(0)} + \mathbf{v}\cdot\frac{\partial f_0}{\partial \mathbf{r}} = J(f_0 f_1) + J(f_1 f_0). \tag{2.23}$$

The solution of Eq. (2.22) is the Maxwell-Boltzmann distribution (Maitland *et al.*, 1981)

$$f_0 = n\left(\frac{m}{2\pi k_B T}\right)^{3/2} e^{-V^2}. \tag{2.24}$$

When the Maxwell-Boltzmann distribution, Eq. (2.24), is used in Eq. (2.15) and only the zeroth-order term in ζ is considered, we obtain the Euler equations of hydrodynamics with an equation of state which is the ideal gas law. Since the gas is modelled as inviscid at this level, the zero-order approximation is not sufficient for our means. To derive the first-order approximation, f_0 is substituted in Eq. (2.23) and the equation is solved which gives an expression for f_1. Then, if f_1 is used in Eq. (2.15) and only the terms up to first order in ζ are considered, we obtain the Navier–Stokes equations which are on the relevant level of approximation for this work. The next higher approximation yields the Burnett equations. The Burnett equations have the potential to

be more accurate than the Navier–Stokes equations in special situations only such as hypersonic flows or the description of boundary layers. The viscosity at the first order level of approximation is related to the stress tensor by

$$p_{12}^{(1)} = -\eta \left(\frac{\partial u_1}{\partial x_2} + \frac{\partial u_2}{\partial x_1} \right) \tag{2.25}$$

where the components of $\mathbf{u}$ are considered up to first order in ζ. By means of variational calculus, the viscosity can be expressed as (Maitland *et al.*, 1981)

$$\eta = \frac{5}{16} \frac{\sqrt{\pi m k_B T}}{\bar{\Omega}^{(2,2)}(T)} \tag{2.26}$$

with the collision integral $\bar{\Omega}^{(2,2)}$ which depends on the intermolecular forces between the particles. Higher order corrections to the viscosity expression above are usually negligible, as can be seen for example in (Bock *et al.*, 2002) or (Hellmann *et al.*, 2008). An important example for which the collision integral $\bar{\Omega}^{(2,2)}$ can be calculated analytically is the case in which the intermolecular potential ϕ is given by the hard sphere potential, i.e., by

$$\phi(r) = \begin{cases} \infty, & \text{for } r \leq \sigma, \\ 0, & \text{for } r > \sigma. \end{cases} \tag{2.27}$$

For the hard sphere potential, the result for viscosity reads (Ferziger & Kaper, 1972)

$$\eta = \frac{5}{16} \frac{\sqrt{m k_B T \pi}}{\pi \sigma^2}. \tag{2.28}$$

Next, to understand the range of applicability of the Boltzmann equation, we discuss the main assumptions inherent in Boltzmann's approach. An important assumption is that only binary collisions of molecules are considered while collision events are neglected in which more than two particles are involved. In addition, the molecular chaos assumption is applied. This assumption states that the positions or velocities of the particles are not correlated prior to a collision. The previous two assumptions are reasonable as long as the mean free path (i.e. the average distance covered by a particle between two successive collisions) is large in comparison to the diameter of the particles. Such a situation prevails in gases at low densities. At higher densities, multiple collisions and correlations between particles become important and Boltzmann's equation will result in poor predictions.

2.2 Enskog Theory

In order to obtain a theory for dense gases, Enskog modified Boltzmann's approach. His modifications resulted in the Enskog theory. In Enskog theory, gas particles are represented by hard spheres which interact via the hard sphere potential as written in Eq. (2.27). To account for the fact that a sphere occupies a volume which is excluded for any other sphere, Enskog included a factor χ in the collision integral of Boltzmann's equation (2.2) which considers an increase in the probability of a collision. In addition, he reformulated the equation in order to consider that spheres are at different positions in the event of a collision. For comparison, the Boltzmann equation (2.2) is formulated in a way which implies that the particles are at the same position in a collision event (this follows from the assumption in Boltzmann's approach that spatial correlations are completely neglected prior to a collision). As a result of the modifications outlined above, Enskog arrived at a new equation for the particle distribution function, Enskog's equation. Enskog's equation has the same form as the Boltzmann equation (2.2) but it possesses a modified collision term which reads (Enskog, 1922; Ferziger & Kaper, 1972)

$$J(ff) = \int\int (\chi(\mathbf{r}+\frac{1}{2}\sigma\mathbf{k})f(\mathbf{r},\mathbf{v}',t)f(\mathbf{r}+\sigma\mathbf{k},\mathbf{v}_1',t) - \chi(\mathbf{r}-\frac{1}{2}\sigma\mathbf{k})f(\mathbf{r},\mathbf{v},t)f(\mathbf{r}-\sigma\mathbf{k},\mathbf{v}_1,t))gd\tilde{\Omega}d^3c_1 \quad (2.29)$$

where $\mathbf{k}$ is the unit vector along the line through the centres of the two colliding spheres.

2.2.1 Enskog theory for viscosity

To obtain a viscosity expression from Enskog's equation (2.29), the terms $\chi(\mathbf{r}+\frac{1}{2}\sigma\mathbf{k})$, $f(\mathbf{r}+\sigma\mathbf{k},\mathbf{v}_1',t)$ and $f(\mathbf{r}-\sigma\mathbf{k},\mathbf{v}_1,t)$ are expanded in a Taylor series near $\mathbf{r}$ and terms higher than third order are neglected. From the resulting equation, macroscopic transport equations can be deduced in a similar fashion as done for the Boltzmann equation in section 2.1. On the first-order approximation level, the Navier–Stokes equations are obtained with the following expression for viscosity (Ferziger & Kaper, 1972):

$$\eta = \eta_0\left(\frac{1}{\chi}+\alpha\rho+\frac{1}{\beta}\chi\alpha^2\rho^2\right) \quad (2.30)$$

with the molar density ρ and $\beta = (1/4+3/\pi)^{-1} = 0.8299$. The quantity α is proportional to the excluded volume $V_{\text{excl}} = 4/3\pi\sigma^3$ of a sphere and is given by

$$\alpha = \frac{8N_A}{15}\pi\sigma^3 = \frac{2N_A}{5}V_{\text{excl}}. \quad (2.31)$$

N_A is Avogadro's constant, σ the hard sphere diameter and η_0 the dilute gas viscosity viscosity of a hard sphere fluid, Eq. (2.28). χ is the factor which Enskog included in Boltzmann's equation in order to consider the increased collision probability. Enskog approximated χ by the equilibrium radial distribution function g at contact, i.e., g evaluated at a distance of σ. χ converges in the thermodynamic limit to the radial distribution function at contact which can be shown by making use of the Clausius virial expression for pressure, see (Chapman & Cowling, 1970). The radial distribution function at contact is linked to the compressibility factor Z via

$$\chi = \frac{Z-1}{4y}, \tag{2.32}$$

see for example (Hansen & McDonald, 2006). The compressibility factor Z can be computed from the equation of state (EOS) of a hard sphere fluid via its definition

$$Z = \frac{PV_m}{RT} \tag{2.33}$$

with the universal gas constant R and the molar volume V_m. A number of EOS have been suggested for the hard sphere fluid (Thiele, 1963; Wertheim, 1963; Reiss *et al.*, 1959; Wertheim, 1964; Ree & Hoover, 1964; Guggenheim, 1965; Yelash *et al.*, 1999) and an overview about various hard sphere EOS can be found in (Miandehy & Modarress, 2003). In this work, we make use of Carnahan and Starling's EOS (Carnahan & Starling, 1969), that describes the compressibility factor and hence χ very well up to high densities, as can be shown by the aid of computer simulations (Miandehy & Modarress, 2003). The radial distribution function in Carnahan and Starling's approach is given by

$$\chi = \frac{(1-0.5y)}{(1-y)^3} \tag{2.34}$$

in terms of the packing fraction y (Carnahan & Starling, 1969). The packing fraction y is defined as ratio between the volume V_{spheres} occupied by the spheres and the total volume V_{tot} available to the fluid, i.e.,

$$y = \frac{V_{\text{spheres}}}{V_{\text{tot}}} = \frac{N_A \frac{4}{3}\pi \left(\frac{\sigma}{2}\right)^3}{1/\rho} = \frac{\pi N_A}{6}\rho\sigma^3. \tag{2.35}$$

Altogether, knowing only the hard sphere diameter, it is possible to calculate the viscosity of a hard sphere fluid at any temperature and density by means of Eqs. (2.30), (2.31), (2.34) and (2.35). In this work, we refer to the traditional Enskog model also as Enskog-1σ model since it requires knowledge of a single hard-sphere diameter.

2.2.2 Shortcomings of Enskog theory

The main assumptions inherent in Enskog's approach are as follows:

(i) as in Boltzmann's approach, only binary collisions are considered.

(ii) while spatial correlations are treated at least approximately by including the radial distribution function, velocity correlations are still neglected.

(iii) the intermolecular potential is described by the hard sphere potential.

The first two assumptions cause Enskog theory to deviate with increasing density from the true behaviour of a hard sphere system. The effect of these deviations on the viscosity are quantified in section 2.3 where we compare Eq. (2.30) with molecular dynamics simulation (MD) results for hard sphere fluids. Apart from MD simulations, there have been several analytical approaches that aim at abandoning assumptions (i) and (ii) for the sake of obtaining a theory which is valid for high densities. Interesting analytical approaches in this direction are, for instance, the solution of a generalized Boltzmann equation (Ferziger & Kaper, 1972) and mode coupling theories (Leutheuser, 1982; Egorov, 2008). The analytical approaches contain a series of approximations and, compared to MD simulations, describe the viscosity of a hard sphere fluid less accurately. Thus, we focus on the correction of Enskog theory with MD simulation results. Assumption (iii) is a simplification for real gases. First, particles in real gases do not interact only by repulsive forces but also by an attractive potential part. Secondly, the repulsive potential part in real gases is not infinitely steep. To correct Enskog theory for the simplifications inherent in assumption (iii) when a real fluid is modelled, the hard sphere diameter is treated as an effective parameter; this will be discussed in more detail in section 2.2.3.

2.2.3 Estimation of the hard sphere diameter

To compute the viscosity of a real fluid from the Enskog's viscosity expression, the hard sphere diameter σ needs to be estimated. To improve the ability of the Enskog model to reproduce the viscosity of real fluids, the hard sphere diameter is assumed to be an effective parameter that depends weakly on temperature and possibly weakly on density, see (Silva & Liu, 2008). First, we discuss approaches in which σ depends on

temperature only. In (Hanley *et al.*, 1972), the hard sphere diameter σ is obtained from the modified Enskog theory (MET). The basic idea of MET is to account for attractive forces by replacing the pressure P in the equation of state of a hard sphere fluid by the thermal pressure $P_t = T(\partial P/\partial T)_V$ of the real gas (Chapman & Cowling, 1970). After this substitution, a virial expansion is carried out which allows to relate the hard sphere diameter σ to the second order virial coefficient of the real gas. As a result, one obtains a weakly temperature dependent *sigma* with which the viscosity equation (2.30) can be evaluated. Hanley and co-workers (Hanley *et al.*, 1972) have shown that the modified Enskog theory can reproduce experimental viscosity data of simple fluids like argon and oxygen with deviations less than 15% up to the critical density.

In (Kirkwood & Boggs, 1942), it has been noted that that the form of the radial distribution function for dense fluids is primarily determined by repulsive forces, while attractive interactions play a secondary role. This observation has lead to the development of several perturbation approaches, which usually combine the Enskog model as an appealing and tractable first approximation for the major excluded volume effects with an effective diameter, to account for the softness of the repulsive potential. One such approach is the Boltzmann criterion (Andrews, 1976; Speedy *et al.*, 1989). The Boltzmann criterion approximates σ by the distance of closest approach of a colliding pair of molecules with average kinetic energy, $E_{\text{kin}} = 3/2k_BT$, subjected to a soft repulsive interaction potential. Another perturbation approach is the one by Barker and Henderson published first in (Barker & Henderson, 1967). Here, the LJ-potential,

$$\phi_{\text{LJ}}(r) = 4\epsilon\left[\left(\frac{\sigma_{\text{LJ}}}{r}\right)^{12} - \left(\frac{\sigma_{\text{LJ}}}{r}\right)^{6}\right], \tag{2.36}$$

is assumed to be the perturbation potential to the unperturbed hard sphere potential. The Lennard–Jones potential is shown in figure 2.1. As can be seen, σ_{LJ} corresponds to the distance r between the particles at which the potential vanishes and ϵ to the depth of the potential well. The effective σ in Barker and Henderson's approach is obtained from integration over the repulsive potential part as

$$\sigma = \int_0^{\sigma_{\text{LJ}}} \left[1 - \exp(-\phi_{\text{LJ}}(r)/k_BT)\right] dr. \tag{2.37}$$

A popular approach that yields a weakly temperature and density dependent effective diameter is the Weeks, Chandler and Andersen (WCA) theory, see (Weeks *et al.*, 1971; Andersen *et al.*, 1971). In WCA theory, the LJ potential is splitt up into a reference

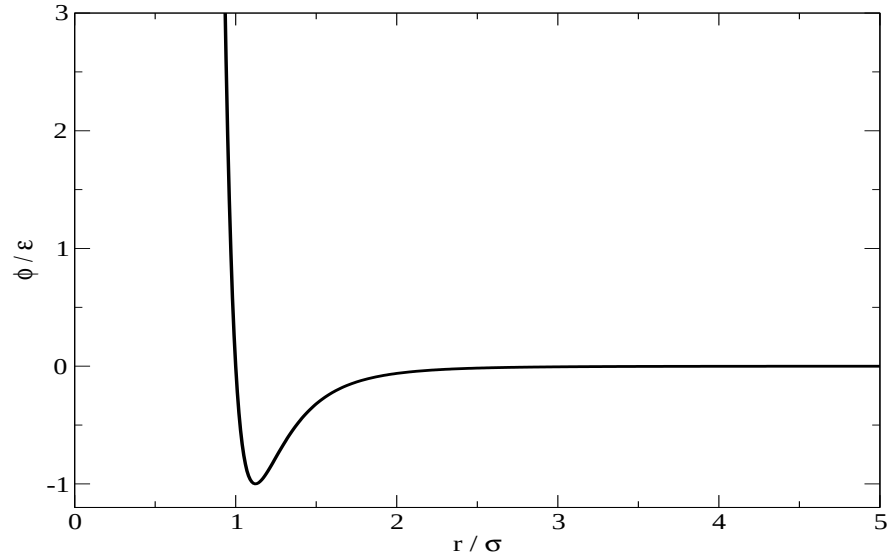

Figure 2.1: Plot of the Lennard–Jones potential.

part containing all repulsive forces, and a perturbing part containing all forces of attraction. In (Lado, 1984), Lado has proposed a modification of the WCA approach which is known as LWCA theory. LWCA theory corrects the WCA for thermodynamic inconsistencies and leads as well to a weakly temperature and density dependent effective diameter. (Silva & Liu, 2008) is recommended as overview about effective hard sphere expressions in Enskog theory.

2.3 Molecular dynamics corrections of Enskog theory

The predictions based on Enskog theory deviate from the true behaviour of a hard sphere system as the density increases since only binary collisions are considered and velocity correlations are neglected. The importance of velocity correlations at high densities can be illustrated by the following generic example which describes the back scattering effect, see also (Dymond & Alder, 1966). In a dense fluid, a sphere is surrounded closely by a shell of other spheres. The back scattering effect refers to the fact that the velocity of a sphere in the shell is likely to be reversed in a collision. This first back scattering collision is dominant since the correlation between the velocity of the sphere and its velocity before the first collision decreases fast in subsequent collision

events. As a result, one might expect that momentum in a hard sphere fluid is transported more slowly than stated by Enskog theory or, in other words, that the viscosity is larger (this is indeed true as we will see below).

To extend Enskog theory to high densities, molecular dynamics (MD) simulations can be used. In MD simulations, the time evolution of an ensemble of particles is simulated from a given initial state based on the equations of motion. After computing the positions and velocities of the particles as a function of time t, the viscosity can be determined by the generalized Einstein relation:

$$\eta = \frac{k_B T m^2}{V} \lim_{t\to\infty} \frac{1}{2t} \left\langle \left(\sum_{i=1}^{N} [v_{ix}(t) r_{iy}(t) - v_{ix}(0) r_{iy}(0)] \right)^2 \right\rangle, \tag{2.38}$$

where the limit is taken at a sufficiently large time in practice. N is the particle number, V the volume of the simulation box, v_{ix} the x-component of the velocity of particle i, r_{iy} the y-component of the position of particle i and the remaining quantities are defined as before. The brackets $\langle\cdot\rangle$ denote the canonical ensemble average, which is defined by

$$\langle F \rangle = \frac{\int F(\mathbf{r},\mathbf{v}) e^{-E(\mathbf{r},\mathbf{v})/k_B T} d\mathbf{r}^{3N} d\mathbf{v}^{3N}}{\int e^{-E(\mathbf{r},\mathbf{v})/k_B T} d\mathbf{r}^{3N} d\mathbf{v}^{3N}}, \tag{2.39}$$

where $E(\mathbf{r},\mathbf{v})$ is the total energy of the system with particle positions $\mathbf{r}_1, ..., \mathbf{r}_N$ and velocities $\mathbf{v}_1, ..., \mathbf{v}_N$. The generalized Einstein relation has been used to obtain the results which are presented in the following. Alternative formulae to the generalized Einstein relation and more details about MD simulations can be found in (Millat *et al.*, 1996), (Rapaport, 2004) and (Smith *et al.*, 1997).

The MD corrections of Enskog's result for viscosity are often expressed in form of a correction factor f,

$$\eta_{\mathrm{MD}}(\rho, T) = \eta(\rho, T) f(V_0/V), \tag{2.40}$$

with the close-packing volume V_0 of spheres, $V_0/V = \left[N_A/\sqrt{2}\right] \rho\sigma^3 = \left[6/(\pi\sqrt{2})\right] y$ and with η referring to the viscosity in Enskog theory, Eq. (2.30), as well as η_{MD} to the MD corrected viscosity. The correction factor stated in (van der Gulik & Trappeniers, 1986) based on the calculations (Dymond, 1974) and (Michels & Trappeniers, 1980)

reads

$$f(V_0/V) = \begin{cases} 1.02 & \text{if } V_0/V < 0.42, \\ 1.02 + 15(V_0/V - 0.35)^3 & \text{if } 0.42 \leq V_0/V \leq 0.575, \\ 1.02 + 15(V_0/V - 0.35)^3 + 350(V_0/V - 0.575)^3 & \text{if } 0.575 < V_0/V. \end{cases} \tag{2.41}$$

In (Michels & Trappeniers, 1980), the accuracy of the calculations leading to this factor is estimated to be between 5% and 7% from the zero density limit up to the packing fraction $y_s \approx 0.494$ at which the hard sphere system still represents a stable fluid, see, for example, (Sigurgeirsson & Heyes, 2003). If the packing fraction increases beyond this value, fluid states become metastable and for high enough packing fractions a transition to the solid state occurs.

The factor in Eq. (2.41) has been obtained from simulations with 108 spheres. The more recent computations by (Sigurgeirsson & Heyes, 2003) with systems consisting of 4000 spheres lead to the factor

$$f(V_0/V) = \begin{cases} 1.02 & \text{if } V_0/V < 0.42, \\ 1.02 + 18(V_0/V - 0.35)^3 & \text{if } 0.42 \leq V_0/V \leq 0.575, \\ 1.02 + 18(V_0/V - 0.35)^3 + 575(V_0/V - 0.575)^3 & \text{if } 0.575 < V_0/V. \end{cases} \tag{2.42}$$

In figure 2.2, both factors are plotted against the packing fraction. The deviations of the molecular dynamics simulations from Enskog theory remain within 5% up to $V_0/V \approx 0.468$ ($y \approx 0.345$). With increasing packing fractions, the deviations become larger until the correction factor of (Sigurgeirsson & Heyes, 2003) reaches a value close to 2 at $y = y_s$. Enskog theory underestimates the viscosity of a true hard sphere system which might be partially explained by the back scattering effect discussed above. The two correction factors depart from each other with increasing packing fraction. At $y = y_s$, both factors deviate about 14%. These deviation are not discussed in the original work by (Sigurgeirsson & Heyes, 2003) but might be caused mainly by finite-size effects in a system consisting only of 108 spheres. Both correction factors are defined such that a discontinuity occurs at $V_0/V = 0.42$, $y \approx 0.311$, see also Fig. 2.2. However, this discontinuity is smaller than 0.0062 and plays a negligible role for the results in this work.

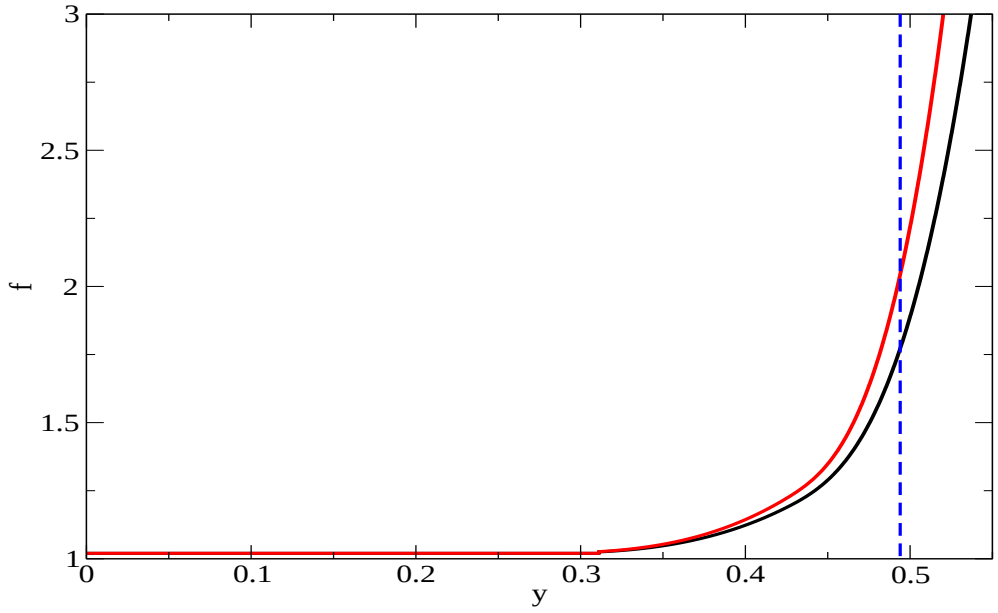

Figure 2.2: MD correction factors are shown against the packing fraction y. The black line depicts the factor by (van der Gulik & Trappeniers, 1986), the red one the factor by (Sigurgeirsson & Heyes, 2003). The blue line indicates the highest packing fraction y_s up to which a hard sphere fluid is in a stable fluid state.

2.4 Modification of Enskog theory for chain fluids

In (de Wijn *et al.*, 2008), Enskog theory has been extended to model fluid molecules as chains formed from equally sized hard spheres. Within this approach, the viscosity of a fluid consisting of N chains, each made up of m segments, is approximated by that of a fluid consisting of Nm hard spheres. In (de Wijn *et al.*, 2012), this fluid is also referred to as a segment fluid. In the segment fluid, the collision dynamics is governed principally by collisions between the spherical segments and one can make use of Enskog theory for hard spheres. In doing so, Enskog's viscosity expression is modified for the presence of the other segments in the chain and reads

$$\eta = \tilde{\eta}_0 \left(\frac{1}{\tilde{\chi}} + \tilde{\alpha}\tilde{\rho} + \frac{1}{\beta}\tilde{\chi}\tilde{\alpha}^2\tilde{\rho}^2 \right). \tag{2.43}$$

The quantities with tilde refer to the segments instead of free hard spheres as in Enskog's original viscosity expression, Eq. (2.30). $\tilde{\rho}$ denotes the molar segment density and, as

in Eq. (2.30), $\beta = (1/4 + 3/\pi)^{-1} = 0.8299$. The quantity $\tilde{\alpha}$ is proportional to the excluded volume $\tilde{V}_{\text{excl}}$ of a segment and has been derived in (de Wijn *et al.*, 2008) from geometric considerations as

$$\tilde{\alpha} = \frac{2N_A}{5}\tilde{V}_{\text{excl}} = \frac{2N_A}{5}V_{\text{excl}}\left[1 + \frac{11}{8}(m-1) + \frac{3}{40\pi}\left(11\pi - 18\arctan\sqrt{2} - 2\sqrt{2}\right)(m-1)^2\right] \tag{2.44}$$

with the excluded volume $V_{\text{excl}} = 4/3\pi\sigma^3$ of a free spherical segment with diameter σ. In the thermodynamic limit, $\tilde{\chi}$ converges to the radial distribution function of the segments at contact and can be approximated according to (de Wijn *et al.*, 2008) by

$$\tilde{\chi} = \chi - \chi_{\text{corr}} = \frac{(1-0.5y)}{(1-y)^3} - \frac{m-1}{m}\frac{\frac{5}{8} - \frac{1}{4}y}{(1-\frac{1}{2}y)(1-y)} \tag{2.45}$$

in terms of the packing fraction y, Eq. (2.35). In this expression, the radial distribution at contact χ of free spherical segments is corrected by the term χ_{corr} for the change in collision rate due to the presence of neighbouring segments in the chain. The zero-density viscosity $\tilde{\eta}_0$ of the segments is related to the zero-density viscosity η_0 of the fluid via

$$\tilde{\eta}_0 = \eta_0\tilde{\chi}(y=0) = \eta_0\left(1 - \frac{5}{8}\left(\frac{m-1}{m}\right)\right). \tag{2.46}$$

Eqs. (2.43) to (2.46) define the viscosity of the segment fluid within the Enskog framework. The approach describes a real chain fluid best at moderate densities. At low densities, after a collision, a chain segment will transfer momentum through the entire chain before any of its segments collide again. Thus, the segments are strongly correlated at low densities and the segment fluid approach, in which those correlations are not considered, does not describe a chain fluid well. At large enough densities, on the contrary, the collision rate is sufficiently high for the segments in the chain to collide before they transfer momentum to their neighbours in the chain and a chain fluid can be approximated well by the segment fluid approach. In the regime of very high densities, the neglect of binary collisions and velocity correlations between the segments, which are inherent in Enskog's approach, see section 2.2.2, become important and lead to larger deviations from the true behaviour of a chain fluid.

2.5 The VW method

The VW method is a predictive scheme for the viscosity of fluid mixtures. As input, the viscosity of the pure mixture components are used without the use of any adjustable

parameter. As we will see in section 3.4, the VW approach is closely related to the Enskog-2σ model and hence is introduced here. Following (Royal *et al.*, 2005), we summarise the mixing rules of the latest version of the VW method based on Enskog's hard sphere theory. We demonstrate next how these mixing rules are used to compute the viscosity of the fluid mixture. The VW method has been validated for a wide range of fluid mixtures, see (Vesovic & Wakeham, 1989b,a; Vesovic *et al.*, 1998; Assael *et al.*, 2001; Royal *et al.*, 2003, 2005; de Wijn *et al.*, 2012). A brief overview about these results is given in the last section.

2.5.1 The VW mixing rules

The latest version of the VW method based on Enskog's hard sphere theory is described in (Royal *et al.*, 2005). The approach expresses the viscosity η of an N-component mixture in the form

$$\eta = -\begin{vmatrix} H_{11} & \cdots & H_{1N} & Y_1 \\ \vdots & & \vdots & \vdots \\ H_{N1} & \cdots & H_{NN} & Y_N \\ Y_1 & \cdots & Y_N & 0 \end{vmatrix} \Bigg/ \begin{vmatrix} H_{11} & \cdots & H_{1N} \\ \vdots & & \vdots \\ H_{N1} & \cdots & H_{NN} \end{vmatrix} + k_{\text{mix}}, \tag{2.47}$$

$$Y_i = x_i \left[1 + \sum_{j=1}^{N} \frac{M_j}{M_i + M_j} x_j \bar{\alpha}_{ij} \bar{\chi}_{ij} \rho \right], \tag{2.48}$$

$$H_{ii} = \frac{x_i^2 \bar{\chi}_{ii}}{\eta_i^0} + \sum_{j \neq i} \frac{x_i x_j \bar{\chi_{ij}}}{2 A_{ij}^* \eta_{ij}^{(0)}} \frac{M_i M_j}{(M_i + M_j)^2} \left[\frac{20}{3} + \frac{4 M_j}{M_i} A_{ij}^* \right], \tag{2.49}$$

$$H_{ij} = -\frac{x_i x_j \bar{\chi_{ij}}}{2 A_{ij}^* \eta_{ij}^{(0)}} \frac{M_i M_j}{(M_i + M_j)^2} \left[\frac{20}{3} - 4 A_{ij}^* \right], \tag{2.50}$$

$$k_{\text{mix}} = \frac{3}{\pi} \rho^2 \sum_{i=1}^{N} \sum_{j=1}^{N} x_i x_j \bar{\chi_{ij}} \bar{\alpha}_{ij}^2 \eta_{ij}^{(0)}. \tag{2.51}$$

Table 2.1 summarises the definition of all quantities appearing in the mixing rules above. The interaction functions, $\bar{\chi}_{ij}$ and $\bar{\alpha}_{ij}$, are computed from the following mixing rules:

$$\bar{\chi}_{ij} = \frac{1}{1 - \sum_{k=1}^{N} x_k w_k} + \frac{3 w_i^{1/3} w_j^{1/3} \sum_{k=1}^{N} x_k w_k^{2/3}}{(w_i^{1/3} + w_j^{1/3}) \left(1 - \sum_{k=1}^{N} x_k w_k\right)^2}, \tag{2.52}$$

$$w_i = \left[\sum_{l=1}^{N} x_l \frac{(f_i^{1/3} + f_l^{1/3})}{2}\right]^3, \qquad f_i = \frac{4\bar{\chi}_i + 1 - (24\bar{\chi}_i + 1)^{1/2}}{4\bar{\chi}_i} \tag{2.53}$$

and

$$\bar{\alpha}_{ij}^{1/3} = \frac{1}{2}(\bar{\alpha}_{ii}^{1/3} + \bar{\alpha}_{jj}^{1/3}) \quad \text{with} \quad \bar{\alpha}_{ii}^{1/3} = \sum_{l=1}^{N} x_l \left(\frac{\bar{\alpha}_i^{1/3} + \bar{\alpha}_j^{1/3}}{2}\right). \tag{2.54}$$

The mixing rules for $\bar{\chi}_{ij}$ and $\bar{\alpha}_{ij}$ are based on the Lebowitz's solution of the Percus-Yevick integral equation for the radial distribution function of a multicomponent mixture (Reed & Gubbins, 1973) and on the assumption (Royal *et al.*, 2003) that the presence of molecules of type j in a mixture influences the interaction between like species i. The reasoning for preferring this set of mixing rules is explained in detail in (Royal *et al.*, 2003), where the set is named RVW/LPY scheme. The zero-density binary interaction parameters η_{ij}^0 and A_{ij}^* are available for only a few mixtures, primarily, due to lack of experimental data. As standard, see (Vesovic & Wakeham, 1989b,a; Vesovic *et al.*, 1998; Assael *et al.*, 2001; Royal *et al.*, 2003, 2005), the two interaction parameters are calculated from empirical mixing rules which have been obtained by analysing the transport property data of several gases (Maitland *et al.*, 1981).

Table 2.1: Definition of the quantities appearing in the mixing rules of the VW method, Eqs. (2.47) to (2.51). In order to distinguish between the molecular interactions in the pure fluid and in the mixture, a single subscript i is used to indicate an i-i pair interaction in the pure fluid and a double subscript ii to indicate an i-i pair interaction in the presence of all other species in the mixture. The bar above a symbol indicates that it represents a pseudo or effective quantity.

Quantity	Definition
ρ	Molar density of the mixture
x_i	Molar fraction of species i
M_i	Molar weight of species i
η_i^0	Viscosity of species i in the zero density limit
$\bar{\chi}_i$	Pseudo-radial distribution function of species i
η_{ij}^0	Interaction viscosity of i-j pair in the zero density limit
A_{ij}^*	Weakly temperature-dependent for an i-j pair interaction
$\bar{\alpha}_{ij}$	Temperature dependent function taking into account the mean free path shortening for an i-j collision in the dense fluid
$\bar{\chi}_{ij}$	Pseudo-radial distribution function at contact for the species i and j

2.5.2 Evaluation of the VW mixing rules

To evaluate the VW mixing rules in section 2.5.1, the pure species parameters $\bar{\chi}_i$, $\bar{\alpha}_i$ are computed from the viscosity η_i of species i. According to (Chapman & Cowling, 1970; Vesovic & Wakeham, 1989b), the pseudo-radial distribution for species i is related to η_i via

$$\bar{\chi}_i(T,\rho) = \frac{\beta}{2}\frac{(\eta_i - \rho\bar{\alpha}_i\eta_i^{(0)})}{\rho^2\bar{\alpha}_i^2\eta_i^{(0)}} \pm \beta\left[\left(\frac{(\eta_i - \rho\bar{\alpha}_i\eta_i^{(0)})}{2\rho^2\bar{\alpha}_i^2\eta_i^{(0)}}\right)^2 - \frac{1}{\beta\rho^2\bar{\alpha}_i^2}\right]^{1/2} \tag{2.55}$$

with $\beta = (1/4 + 3/\pi)^{-1} = 0.8299$. The pure species viscosity η_i on the right hand side of Eq. (2.55) is evaluated at the same temperature T and density ρ as $\bar{\chi}_i$ and the temperature-dependent quantities $\bar{\alpha}_i$, $\eta_i^{(0)}$ at the same temperature. Eq. (2.55) yields two solutions which we denote by $\bar{\chi}_i^+$, $\bar{\chi}_i^-$ corresponding to the positive and negative sign before the bracketed term. As the collision frequency of the fluid molecules is

expected to increase monotonically with increasing density, one has to insure that $\bar{\chi}_i$ grows monotonically with ρ. This is achieved by switching from the solution $\bar{\chi}_i^-$ to $\bar{\chi}_i^+$ at the density ρ_i^* at which both solutions are equal (Sandler & Fiszdon, 1979; Vesovic & Wakeham, 1989b). The density ρ_i^* is called switch-over density, depends only on the temperature T and is obtained, as shown in (Vesovic & Wakeham, 1989b), at each T from the equation

$$\left(\frac{\partial \eta_i}{\partial \rho}\right) = \frac{\eta_i}{\rho}. \tag{2.56}$$

If ρ_i^* is computed from Eq. (2.56), the quantity $\bar{\alpha}_i$ at temperature T follows from

$$\bar{\alpha}_i(T) = \frac{1}{1+\frac{2}{\beta}} \frac{\eta_i(T,\rho_i^*)}{\eta_i^0(T)\rho_i^*}. \tag{2.57}$$

Substituting $\bar{\alpha}_i$ into Eq. (2.55) allows to calculate the pseudo-radial distribution function $\bar{\chi}_i$ for species i and hence to evaluate the VW mixing rules in section 2.5.1.
It should be noted that, if T is smaller than the critical temperature of species i , it is possible that the switch-over density ρ_i^* lies in the two-phase region of species i. In this case, the viscosity $\eta_i^*(T,\rho_i^*)$ is not uniquely defined. This problem is usually solved by obtaining $\eta_i^*(T,\rho_i^*)$ as an appropriately interpolated value of the viscosities at the saturated vapour and saturated liquid density at temperature T.

2.5.3 Application of the VW method

The VW method has been applied to a wide range of fluid mixtures. Mixtures investigated include gas mixtures (Vesovic & Wakeham, 1989b,a; Vesovic *et al.*, 1998), hydrocarbon mixtures (Assael *et al.*, 2001; Royal *et al.*, 2003) and mixtures of refrigerants (Assael *et al.*, 2001; Royal *et al.*, 2005). The accuracy of the VW method is found to be satisfactory to very good in general. The accuracy decreases when accurate pure species viscosity data is lacking which is needed as input. The VW approach works best for mixtures consisting of pure species with similar features. For asymmetric mixtures consisting of components with largely different molecular masses, the accuracy of the VW method is found to diminish (Assael *et al.*, 2001). In (de Wijn *et al.*, 2012), the VW method has recently been extended to mixtures of chain like fluids based on the theory outlined in section 2.4. The approach shows good predictive power for the viscosity of n-alkane mixtures and even predicts the viscosity of a highly asymmetric mixture, consisting of methane and n-decane, well within 14%.

3

Theory of the Enskog-2σ model for simple fluids

This chapter introduces the theory of the Enskog-2σ model for simple fluids. First, we explain the idea behind the Enskog-2σ model. Then, the methodology of the approach up to moderate densities is outlined and the model equations are summarised. The extension of the Enskog-2σ model to high densities is discussed next. The next section compares the Enskog-2σ model with the VW method, introduced in section 2.5. Finally, we summarise the experimental reference correlations with which we will validate the Enskog-2σ model for simple fluids.

3.1 Model idea

As discussed in section 2.2.1, Enskog modified Boltzmann's approach by assuming that (a) the spheres possess an excluded volume and hence are at a different position at collision and (b) that the probability of a collision is increased in comparison to the dilute gas. Assumption (a) and (b) appear via the terms α and χ in Enskog's viscosity expression, Eq. (2.30). If a hard sphere is modelled, it is sensible to assume that α and χ are computed using the hard sphere diameter σ. For a real fluid, on the contrary, there is no reason to believe that a single diameter can correctly account for both the geometry of the molecules and the dynamics of the molecular interactions. Thus, we modify the Enskog's approach by rewriting Eqs. (2.31) and (2.35) in terms of two

effective diameters,

$$\alpha = \frac{8\pi N_A}{15}\sigma_\alpha^3, \tag{3.1}$$

$$y = \frac{\pi N_A}{6}\rho\sigma_\chi^3, \tag{3.2}$$

such that the effective diameter σ_α is used to calculate the parameter α, while the effective diameter σ_χ is used to calculate the packing fraction y, and consequently the radial distribution function at contact, χ. In principle there are a number of ways one can introduce the two effective diameters. For instance, one can use one effective diameter to account for the low-density behaviour, described by the first two terms of Enskog's viscosity expression, Eq. (2.30), and another effective diameter to account for the high-density behaviour, described by the last term of Eq. (2.30). In this work, we ascribe the different effective parameters to two different physical effects corrected in Enskogs treatment; namely, the excluded volume of a molecule and the increased probability of collision in comparison to the dilute gas. Thus, with this choice we have separated the geometric effects from the collisional ones.

3.2 Methodology up to moderate densities

In section 2.3, we have illustrated that the Enskog model needs to be corrected to reproduce the behaviour of viscosity at high packing fractions. Hence, in order to avoid these high packing fractions, we limit our investigation first to supercritical temperatures and moderate densities. To obtain the effective σ for the Enskog-1σ model and the effective σ_α and σ_χ for the Enskog-2σ model, we minimise the maximum deviation between model and the experimental viscosity reference correlations. The fitting is limited to densities up to

$$\rho_{\mathrm{MD}} = \frac{0.31}{\frac{\pi}{6}N_A\sigma_\alpha^3} \tag{3.3}$$

or the maximum pressure at which a given correlation is valid, whichever range is smaller. The factor 0.31 in Eq. (3.3) refers to the packing fraction y up to which Enskog's theory describes a hard sphere fluid without MD corrections, see section 2.3. The maximum pressures are stated in Table 3.1 and the corresponding densities are estimated using the NIST webbook (McLinden *et al.*, 2010). The non-linear optimisation problem associated with obtaining the optimal effective σ's is solved using the

LMDIF routine in the MINPACK library (Moré *et al.*, 1984). As we are interested in the viscosity behaviour as a function of density, we use the zero-density viscosity values obtained directly from correlations, rather than making use of the zero-density viscosity of a hard sphere fluid, Eq. (2.28). The expression for the maximum density, Eq. (3.3), and the following equations define the Enskog-2σ model proposed at supercritical conditions up to moderate densities:

$$\eta = \eta_0 \left(\frac{1}{\chi} + \alpha\rho + \frac{1}{\beta}\chi\alpha^2\rho^2 \right), \tag{3.4}$$

$$\alpha = \frac{8\pi N_A}{15}\sigma_\alpha^3, \tag{3.5}$$

$$\chi = \frac{(1-0.5y)}{(1-y)^3}, \tag{3.6}$$

$$y = \frac{\pi N_A}{6}\rho\sigma_\chi^3. \tag{3.7}$$

3.3 Extension to high densities

In order to extend the Enskog-2σ model to high densities, we correct Enskog theory for its deficiencies at high packing fractions. As explained in section 2.3, this correction is achieved by multiplying Enskog's viscosity expression, Eq. (2.30), by the molecular-dynamics factor f_{MD} by (Sigurgeirsson & Heyes, 2003), see Eq. (2.42). The correction factor is a function of the packing fraction only and thus depends on the effective diameter σ chosen through y. We denote the corresponding σ as σ_{MD}. The diameter σ_{MD} corresponds to the diameter of the spheres when the correction factor is used in the Enskog-1σ model. In the Enskog-2σ model, there is no such clear correspondence between σ_{MD} and the effective diameters σ_α and σ_χ. The diameter σ_{MD} is neither directly related to the excluded volume nor to the collision rate. In fact, the relations chosen between σ_{MD} and the effective diameters σ_α and σ_χ is arbitrary and purely empirical. In this work, we propose and analyse the following generic choices for σ_{MD}:

- $\sigma_{\mathrm{MD}} = \sigma_\alpha$,
- $\sigma_{\mathrm{MD}} = \sigma_\chi$,
- $\sigma_{\mathrm{MD}} = (\sigma_\alpha + \sigma_\chi)/2$,

- $\sigma_{\mathrm{MD}} = \sqrt{\sigma_\alpha \sigma_\chi}$.

For a given choice of σ_{MD}, the maximum density $\rho_{\max}$ is consistently defined by

$$\rho_{\max} = \min\left(\rho_{y_s}, \rho_{\exp}\right) \quad \text{where} \quad \rho_{y_s} = \frac{0.494}{N_A \pi / 6 \sigma_{\mathrm{MD}}^3}. \tag{3.8}$$

The factor 0.494 in Eq. (3.8) is equal to the packing fraction y_s up to which a hard sphere system still represents a stable fluid (see section 2.3) and hence represents the packing fraction up to which the MD correction factor has a physical foundation. At supercritical conditions, the effective temperature-dependent diameters σ_α and σ_χ are computed by minimising the maximum deviation between the model with MD corrections and experimental reference correlation from the dilute gas limit to $\rho_{\max}$ at each given temperature. The same is done in the liquid phase but the optimisation is carried out from the saturated liquid density to $\rho_{\max}$. Altogether, the Enskog-2σ model proposed for high densities in the supercritical and liquid phase is defined by the expression for the maximum density, Eq. (3.8), the choice of σ_{MD}, Eqs. (3.5) to (3.7) and Enskog's viscosity expression corrected by the MD correction factor f_{MD},

$$\eta = \eta_0 \left(\frac{1}{\chi} + \alpha\rho + \frac{1}{\beta} \chi \alpha^2 \rho^2 \right) f_{\mathrm{MD}}(\rho \sigma_{\mathrm{MD}}^3), \tag{3.9}$$

$$f_{MD}(V_0/V) = \begin{cases} 1.0 & \text{if } V_0/V < 0.42, \\ 1.0 + \frac{18}{1.02}(V_0/V - 0.35)^3 & \text{if } 0.42 \leq V_0/V \leq 0.575, \\ 1.0 + \frac{18}{1.02}(V_0/V - 0.35)^3 + \frac{575}{1.02}(V_0/V - 0.575)^3 & \text{if } 0.575 < V_0/V, \end{cases} \tag{3.10}$$

$$V_0/V = \left[N_A/\sqrt{2} \right] \rho \sigma_{\mathrm{MD}}^3 = \left[6/(\pi\sqrt{2}) \right] y_{\mathrm{MD}}. \tag{3.11}$$

Note that the MD correction factor, Eq. (2.42), has been divided by 1.02 to model the zero-density viscosity η_0 correctly. Furthermore, it is interesting to notice that including the MD correction factor in the optimisation of σ_α and σ_χ weakens the link of the diameters to the excluded volume and the collision rate. Therefore, we will also look at alternatives that do not include the MD correction factor in the optimisation of σ_α and σ_χ and thus keep a full link between the effective diameters and the excluded volume as well as the collision rate. This is done by optimising the effective diameters σ_α and σ_χ up to

$$\rho^* = \frac{0.31}{N_A \pi / 6 \sigma_{\mathrm{mean}}^3} \quad \text{with} \quad \sigma_{\mathrm{mean}} = \frac{\sigma_\alpha + \sigma_\chi}{2} \tag{3.12}$$

to minimise the maximum deviation between model and the experimental reference correlations at each temperature. The factor 0.31 corresponds to the packing fraction up to which Enskog's theory is a correct description of a hard sphere fluid (see section 2.3). Here, up to ρ^*, no MD correction factor is used such that the link between the effective diameters and the excluded volume as well as the collision rate is kept fully. In section 5.2.5, we will investigate two alternatives for the calculation of σ_{MD}:

(i) σ_{MD} is obtained from

$$\sigma_{\mathrm{MD}} = \sigma_{\mathrm{mean}} =: \sigma_{\mathrm{MD,mean}}, \tag{3.13}$$

(ii) σ_{MD} is optimised at each temperature by minimising the maximum deviation between model and experimental reference correlation

$$\sigma_{\mathrm{MD}} =: \sigma_{\mathrm{MD,opti}}. \tag{3.14}$$

In both cases, we define the maximum density by

$$\rho_{\mathrm{max}} = \min\left(\rho_{y_{s,\mathrm{mean}}}, \rho_{\mathrm{exp}}\right) \quad \text{where} \quad \rho_{y_{s,\mathrm{mean}}} = \frac{0.494}{N_A \pi / 6 \sigma_{\mathrm{mean}}^3}. \tag{3.15}$$

3.4 Comparison with the VW method

It is interesting to compare the Enskog-2σ methodology to how a pure fluid is treated within the VW method. As outlined in section 2.5.2, the pure species parameters $\bar{\chi}$, $\bar{\alpha}$ in the VW approach are computed from the viscosity η of the pure component. Using Eq. (2.34) for $\bar{\chi}$ and Eq. (2.31) for $\bar{\alpha}$, the parameters $\bar{\chi}$, $\bar{\alpha}$ can be related to effective diameters $\bar{\sigma}_\chi$, $\bar{\sigma}_\alpha$. Just as σ_α in the Enskog-2σ model, the effective diameter $\bar{\sigma}_\alpha$ depends on the temperature only whereas $\bar{\sigma}_\chi$ depends in general on the temperature and weakly on density. The density dependence in $\bar{\sigma}_\chi$ guarantees that the experimental reference correlation of the pure species is reproduced exactly. This is done however at the expense that a density and temperature depending diameter appears in Carnahan and Starling's expression, Eq. (2.34), which weakens the link to Enskog's original theory. In the Enskog-2σ model, σ_χ depends on the temperature only such that the density dependence in χ is fully captured by Carnahan and Starling's expression and the link to Enskog theory is not impaired.

3.5 Reference correlations for simple fluids

In order to evaluate the Enskog-2σ model, we investigate the viscosity of seven simple fluids. As both Enskog theory and Carnahan-Starling expression are strictly valid for hard spheres, we have, in the first instance, limited our investigation to fluids made of relatively spherical molecules. The choice of fluids was also guided by the existence of accurate viscosity correlations that span a large temperature and pressure range. Table 3.1 lists the fluids together with the respective temperature and pressure ranges. It can be inferred from table 3.1 that the viscosity correlation for sulphur hexafluoride (SF_6) covers a much smaller range in the reduced temperature and pressure than for the other six fluids. Nevertheless, the SF_6 molecule is by far the largest of the seven considered and it will thus provide a test on the applicability of the proposed model as the molecular size increases. Over the pressure and temperature ranges depicted in table 3.1, the estimated uncertainties of the reference correlation is ±2% for sulphur hexafluoride, ±3% for ethane and ±5% for argon, methane, nitrogen, carbon dioxide and oxygen. In the critical region, the estimated uncertainties of the reference correlation for argon, nitrogen and oxygen are larger. As the uncertainties inherent in the reference correlations are only estimated, we will validate the accuracy of the Enskog-2σ model also directly against primary experimental viscosity measurements.

Table 3.1: Summary of experimental reference correlations used for simple fluids.

Fluid	P-range (MPa)	T-range (K)	Viscosity correlation
Ar	0-400	90-700	(Lemmon & Jacobson, 2004)
CH_4	0-100	115-600	(Vogel *et al.*, 2000)
C_2H_6	0-60	250-500	(Hendl *et al.*, 1994)
N_2	0-100	85-600	(Lemmon & Jacobson, 2004)
CO_2	0-300	270-700	(Vesovic *et al.*, 1990; Fenghour *et al.*, 1998)
O_2	0-80	85-700	(Lemmon & Jacobson, 2004)
SF_6	0-50	325-500	(Quiñones-Cisneros *et al.*, 2012)

4

Theory of the Enskog-2σ model for alkanes

The theory of the Enskog-2σ model for alkanes is introduced in this chapter. First, the methodology up to moderate densities at supercritical conditions is described and the corresponding model equations are formulated. Then, we discuss extensions of the model to high densities and to the liquid phase. Finally, we summarise the experimental reference correlations with which we will validate the Enskog-2σ model for alkanes.

4.1 Methodology up to moderate densities

The theoretical foundation of the Enskog-2σ model for alkanes is the modification of Enskog theory for chain fluids described in section 2.4. The chain fluid is modelled as a segment fluid with an Enskog-like expression for viscosity, Eq. (2.43). Analogously to section 3.1, we introduce two effective temperature-dependent diameters σ_α and σ_χ. The diameter σ_α is related to the geometry of the segments and is used to calculate $\tilde{\alpha}$ via Eq. (2.44), while the diameter σ_χ is related to the collision dynamics between the segments and is used to compute $\tilde{\chi}$ via Eq. (2.45). In the chain fluid approach, the fluid molecules are characterised as well by the chain length m. Consistently to using two effective diameters, we introduce two effective temperature-dependent chain lengths, m_α and m_χ. The chain length m_α is related to the geometry of the molecules and is used to calculate $\tilde{\alpha}$ via Eq. (2.44) as well as the segment density $\tilde{\rho} = m_\alpha \rho$ where ρ is the molar density of the chain fluid. The chain length m_χ is related to the collision

dynamics between the segments and is used to calculate $\tilde{\chi}$ via Eq. (2.45).
Altogether, the Enskog-2σ model for alkanes contains four effective parameters, σ_α, σ_χ, m_α, m_χ. To reduce the number of free parameters, we make use the following chain length constraint

$$\sigma_\alpha(m_\alpha - 1) = \sigma_\chi(m_\chi - 1). \tag{4.1}$$

This constraint has been introduced in (de Wijn *et al.*, 2012) and ensures that the distance between the end segments using σ_α as well as m_α, and σ_χ as well as m_χ are equal. In order to reduce the number of free parameters further on, we assume that the diameter of a chain segment is approximately equal to the diameter of a methane molecule at the same temperature. Thus, we set σ_α equal to the σ_α of methane at the same temperature where σ_α is obtained from the methodology outlined in section 3.2 and will be calculated in section 5.1.
There are no molecular dynamics simulations available that indicate in which packing fraction range the viscosity expression of the segment fluid, Eq. (2.43), is a good approximation for the viscosity of a chain fluid. From the theoretical considerations in section 2.4, we know that the segment fluid approach describes a chain fluid best at moderate densities. The issue that the segment fluid is a rather crude approximation for a chain fluid at low densities can be circumvented when we are modelling the viscosity of alkanes. This is done by using the experimental dilute gas viscosity of the respective alkane in Eq. (2.46). By doing so, the Enskog-2σ model reproduces the viscosity of the alkane accurately in the zero-density limit and presents a promising model approach for the viscosity of alkanes from the dilute gas limit up to moderate densities. To avoid further complications, we restrict the Enskog-2σ model to moderate densities by choosing the following maximum density

$$\rho_{\max} = \min(\rho_{\exp}, \rho^*) \tag{4.2}$$

where $\rho_{\exp}$ is the maximum density of the experimental reference correlation and ρ^* is given by

$$\rho^* = \rho_{\max,C_1} \frac{\rho_{c,C_n}}{\rho_{c,C_1}} \tag{4.3}$$

where the maximum density of methane, $\rho_{\max,C_1}$, is evaluated at the same reduced temperature T/T_c as $\rho_{\max}$. The densities ρ_{c,C_1} and ρ_{c,C_n} are the critical densities of methane and the respective alkane. The maximum density of methane, $\rho_{\max,C_1}$, is

computed from the methodology in section 3.2 and is depicted in Fig. 6.1 in section 6.1.1.

Altogether, the Enskog-2σ model for alkanes up to moderate densities is represented by the chain length constraint, Eq. (4.1), the expression for the maximum density, Eq. (4.2), and the equations

$$\eta = \tilde{\eta}_0 \left(\frac{1}{\tilde{\chi}} + \tilde{\alpha}\tilde{\rho} + \frac{1}{\beta}\tilde{\chi}\tilde{\alpha}^2\tilde{\rho}^2 \right), \tag{4.4}$$

$$\tilde{\alpha} = \frac{2N_A}{5}\tilde{V}_{\text{excl}} = \frac{2N_A}{5}V_{\text{excl}} \left[1 + \frac{11}{8}(m_\alpha - 1) + \frac{3}{40\pi}\left(11\pi - 18\arctan\sqrt{2} - 2\sqrt{2} \right)(m_\alpha - 1)^2 \right], \tag{4.5}$$

$$V_{\text{excl}} = 4/3\pi\sigma_\alpha^3, \qquad \tilde{\rho} = m_\alpha \rho, \tag{4.6}$$

$$\tilde{\chi} = \chi - \chi_{\text{corr}} = \frac{(1 - 0.5y)}{(1-y)^3} - \frac{m_\chi - 1}{m_\chi} \frac{\frac{5}{8} - \frac{1}{4}y}{(1 - \frac{1}{2}y)(1-y)}, \tag{4.7}$$

$$\tilde{\eta}_0 = \eta_0 \tilde{\chi}(y = 0) = \eta_0 \left(1 - \frac{5}{8} \left(\frac{m_\chi - 1}{m_\chi} \right) \right), \tag{4.8}$$

$$y = \frac{\pi N_A}{6}\rho\sigma_\chi^3, \tag{4.9}$$

with the molar density of the alkane, ρ, the experimental dilute gas viscosity of the alkane, η_0, and the effective diameter σ_α from methane as described above. Using these model equations, we compute at each temperature optimised effective chain lengths m_α, m_χ, by minimising the maximum deviation between model and experimental reference correlation for the respective alkane from the dilute gas limit up to ρ_{max}. The non-linear optimisation problem associated with obtaining the optimal m's is solved using the LMDIF routine in the MINPACK library (Moré *et al.*, 1984).

4.2 Extension to high densities

As discussed in section 2.4, the segment viscosity expression, Eq. (2.43), is expected to deviate with increasing density from the viscosity of a chain fluid owing to the neglect of binary collisions and velocity correlations between the segments. For simple fluids, we corrected Enskog's viscosity expression for hard spheres by an MD correction factor to improve the description at high densities, see section 3.3. For the segment fluid, there is no such correction factor available. As first approximation, however, we can correct the segment fluid by the hard sphere MD correction factor, Eq. (2.42), with an

appropriate definition of the packing fraction in the MD correction factor, y_{MD}. The packing fraction y_{MD} is given as

$$y_{\mathrm{MD}} = \frac{\pi N_A}{6}\tilde{\rho}_{\mathrm{MD}}\sigma_{\mathrm{MD}}^3 = \frac{\pi N_A}{6}\rho m_{\mathrm{MD}}\sigma_{\mathrm{MD}}^3 \tag{4.10}$$

with an effective chain length m_{MD} and an effective diameter σ_{MD}. Analogously to the approach for simple fluids in section 3.3, we relate both effective parameters m_{MD} and σ_{MD} to the model parameters σ_α, σ_χ, m_α, m_χ. The following purely empirical relations are investigated

$$\sigma_{\mathrm{MD}} = \frac{\sigma_\alpha + \sigma_\chi}{2}, \qquad m_{\mathrm{MD}} = \frac{m_\alpha + m_\chi}{2} \qquad \text{and} \tag{4.11}$$

$$\sigma_{\mathrm{MD}} = \sigma_\chi, \qquad m_{\mathrm{MD}} = m_\chi. \tag{4.12}$$

Choosing one of these relations, we can write the corrected segment fluid viscosity expression as

$$\eta = \tilde{\eta}_0\left(\frac{1}{\tilde{\chi}} + \tilde{\alpha}\tilde{\rho} + \frac{1}{\beta}\tilde{\chi}\tilde{\alpha}^2\tilde{\rho}^2\right) f_{\mathrm{MD}}(\rho m_{\mathrm{MD}}\sigma_{\mathrm{MD}}^3), \tag{4.13}$$

$$f_{MD}(V_0/V) = \begin{cases} 1.0 & \text{if } V_0/V < 0.42, \\ 1.0 + \frac{18}{1.02}(V_0/V - 0.35)^3 & \text{if } 0.42 \leq V_0/V \leq 0.575, \\ 1.0 + \frac{18}{1.02}(V_0/V - 0.35)^3 + \frac{575}{1.02}(V_0/V - 0.575)^3 & \text{if } 0.575 < V_0/V, \end{cases} \tag{4.14}$$

$$V_0/V = \left[N_A/\sqrt{2}\right]\rho m_{\mathrm{MD}}\sigma_{\mathrm{MD}}^3 = \left[6/(\pi\sqrt{2})\right] y_{\mathrm{MD}}. \tag{4.15}$$

Note that the MD correction factor, Eq. (2.42), has been divided by 1.02 to model the zero-density viscosity $\tilde{\eta}_0$ correctly. The corrected segment fluid viscosity expression, Eq. (4.13), the chain length constraint, Eq. (4.1), and Eqs. (4.5) to (4.9) are the defining equations of the Enskog-2σ model for alkanes with hard sphere MD correction factor. The effective diameter σ_α is set to σ_α of methane at the same temperature and will be depicted in Fig. 6.12. The effective chain lengths m_α, m_χ are optimised by minimising the maximum deviation between model and experimental reference correlation for the respective alkane from the dilute gas limit up to the maximum density of the experimental reference correlation.

4.3 Extension to the liquid phase

The Enskog-2σ model for alkanes in the liquid range is based on the same equations as the model for alkanes at supercritical conditions up to high densities described in

section 4.2. The only major difference is that σ_α is set equal to σ_α of methane at the same reduced temperature which will be depicted in Fig. 6.17. We do not derive σ_α from the same temperature as it was done in section 4.2. This would mean that, at most temperatures under investigation, the diameter σ_α in the liquid phase is computed from the σ_α of methane at supercritical conditions. We will avoid this since we will see in section 5.4.2 that the behaviour of σ_α of methane changes qualitatively at the transition from subcritical to supercritical conditions.

4.4 Reference correlations for alkanes

The Enskog-2σ model is applied to alkanes from ethane up to octane. Table 4.1 lists the correlations used. The estimated uncertainties of the reference correlations of ethane, propane, butane and octane are ±5%, ±4%, ±6%, ±5%. For the correlations of pentane, hexane and heptane, there are no estimated uncertainties available. Note also that the correlations of pentane and heptane are only used at liquid conditions since they are valid only for densities larger than the critical density.

Table 4.1: Summary of experimental reference correlations used for alkanes. P_{vap} denotes the vapour pressure.

Fluid	P-range (MPa)	T-range (K)	Viscosity correlation
C_2	0-60	250-500	(Hendl *et al.*, 1994)
C_3	0-100	100-475	(Vogel *et al.*, 1998)
C_4	0-70	150-500	(Vogel *et al.*, 1999)
C_5	P_{vap}-100	195-465	(Assael *et al.*, 1992)
C_6	0-100	245-600	(McLinden *et al.*, 2010)
C_7	P_{vap}-100	245-540	(Assael *et al.*, 1992)
C_8	0-100	295-600	(Huber *et al.*, 2004)

5

Results for simple fluids

In this chapter, the Enskog-2σ model is applied to simple fluids. First, we focus on the results at supercritical conditions up to moderate densities. Then, we extend the density range to high densities and pressures by making use of molecular dynamics corrections. The application of the model to the liquid phase is discussed next. After that, we investigate a variant of the Enskog-2σ model over the full temperature range which extends from low temperatures in the liquid range up to high temperatures at supercritical conditions.

5.1 Supercritical temperature range

This section represents an analysis of the Enskog-2σ model at supercritical conditions up to moderate densities. The results are based on the work by (Umla *et al.*, 2012). First, the correlative power of the Enskog-2σ model and Enskog-1σ model are compared with each other. Then, the temperature dependence of the effective diameters is described and the model sensitivity to those effective diameters is analysed. The magnitude of the model terms is computed exemplarily for some cases. A comparison between the Enskog-2σ model and the VW method follows. After that, the application of the Enskog-2σ model to other transport properties, in particular, to thermal conductivity is discussed. Different definitions of the maximum density of the Enskog-2σ model are investigated next. Finally, we test if the effective diameter exhibit a universal behaviour as a function of reduced temperature which could allow to predict the viscosity of one fluid from the knowledge of the viscosity of a reference fluid.

5.1.1 Correlative power

We first discuss the ability of the Enskog-1σ model and the Enskog-2σ model to correlate the viscosity of the five fluids given in Table 5.1. For each model, the optimal σ's for a given temperature have been computed by the procedure described in section 3.2.

Table 5.1: Summary of the experimental reference correlations used for simple fluids at supercritical temperatures.

Fluid	P-range (MPa)	T-range (K)	Viscosity correlation
Ar	0-400	165-700	(Lemmon & Jacobson, 2004)
CH_4	0-100	200-500	(Vogel *et al.*, 2000)
N_2	0-100	165-600	(Lemmon & Jacobson, 2004)
CO_2	0-300	330-700	(Vesovic *et al.*, 1990; Fenghour *et al.*, 1998)
SF_6	0-50	325-500	(Quiñones-Cisneros *et al.*, 2012)

Fig. 5.1 (a) compares the fitting of the two methods in their ability to reproduce the viscosity of methane at a temperature of 350K. The Enskog-1σ model underestimates the viscosity of methane at medium densities up to 10% and overestimates the viscosity at high densities up to 15%. The Enskog-2σ model, however, reproduces the viscosity within 1% over the whole density interval. The behaviour illustrated in Fig. 5.1 (a) is typical for other temperatures and fluids studied. Further examples are shown in Fig. 5.1 (b) for carbon dioxide at $T = 600K$, Fig. 5.1 (c) for argon at $T = 300K$ and Fig. 5.1 (d) for nitrogen at $T = 250$. For argon at $T = 300K$ for instance, the correlated viscosity deviates less than 2μPa s from the experimental one. Fig. 5.2 (a) summarizes the deviations observed for methane between the experimental reference correlations and the two models as a function of temperature. Although the fitting capability of the Enskog-1σ model improves with increasing temperature, the maximum deviation and absolute average deviation (AAD) observed are always higher than 5.5% and 2.5%, respectively. The Enskog-2σ model, on the other hand, is capable of reproducing the viscosity of methane with deviations of less than 2%. As a further illustration of the fitting capability of the Enskog-2σ model, Fig. 5.2 (b) shows the results for CO_2.

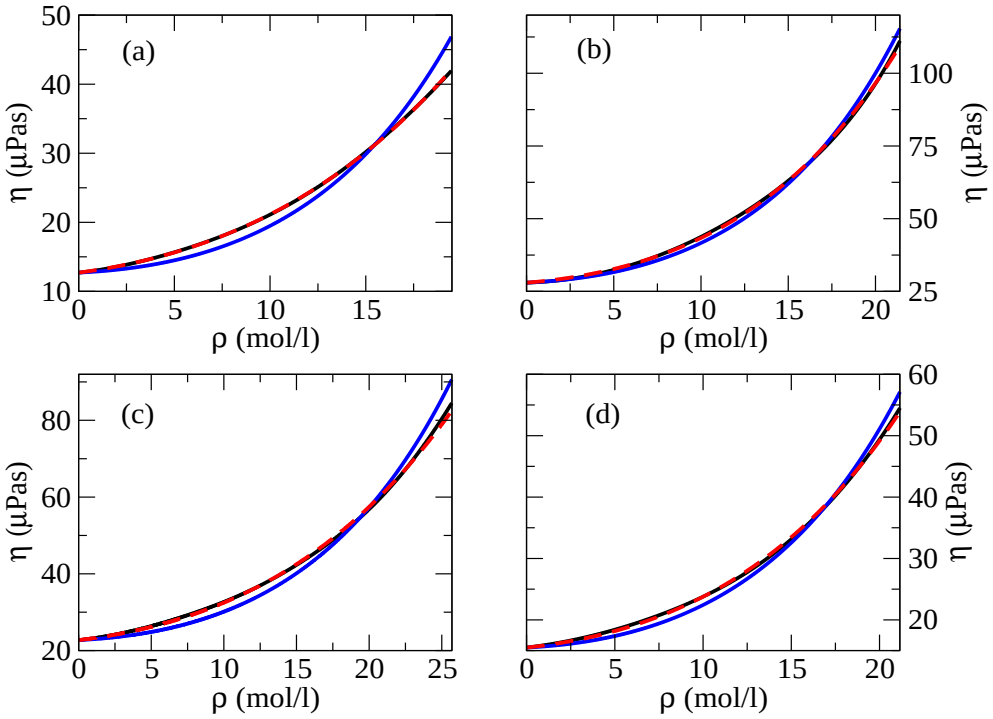

Figure 5.1: Viscosity as a function of density along one isotherm for (a) methane at $T = 350K$, (b) carbon dioxide at $T = 600K$, (c) argon at $T = 300K$, (d) nitrogen $T = 250K$. The black line is the Enskog-2σ model, the blue line is the Enskog-1σ model and the red dashed line is the reference correlation by (a) (Vogel *et al.*, 2000), (b) (Vesovic *et al.*, 1990; Fenghour *et al.*, 1998), (c) and (d) (Lemmon & Jacobson, 2004).

Although the deviations are larger than those observed for methane, it is clear that the Enskog-2σ model is superior to the Enskog-1σ model in correlating the viscosity of a dense fluid. Fig. 5.3 shows the results for argon and nitrogen. At low temperatures, the Enskog-1σ model reaches its largest maximum deviations of 12.6% for argon and 8.6% for nitrogen while the Enskog-2σ model deviates there less than 0.96% for argon and 2.0% for nitrogen. For other temperatures, the difference between the models is less pronounced, however, the Enskog-2σ model outperforms the Enskog-1σ model in correlative power for all temperatures.

All results so far have been obtained by optimizing the effective diameters to minimise the maximum deviation between model and experimental reference correlation for a given temperature T. An alternative procedure to obtain the effective diameters consists in minimising the absolute average deviation (AAD) between model and

experimental reference correlation at each temperature, i.e., minimising

$$\sum_{\rho_i} \frac{|\eta_{\text{model}}(T,\rho_i) - \eta_{\text{corr}}(T,\rho_i)|}{\eta_{\text{corr}}(T,\rho_i)}. \tag{5.1}$$

The densities ρ_i are chosen to lie on an equidistant mesh from 0 to the maximum density at T with a small mesh width of 0.01 mol/l. According to further computations, we have found that both optimisation procedures result in almost identical effective diameters such that both optimisation procedures can be considered as equivalent.

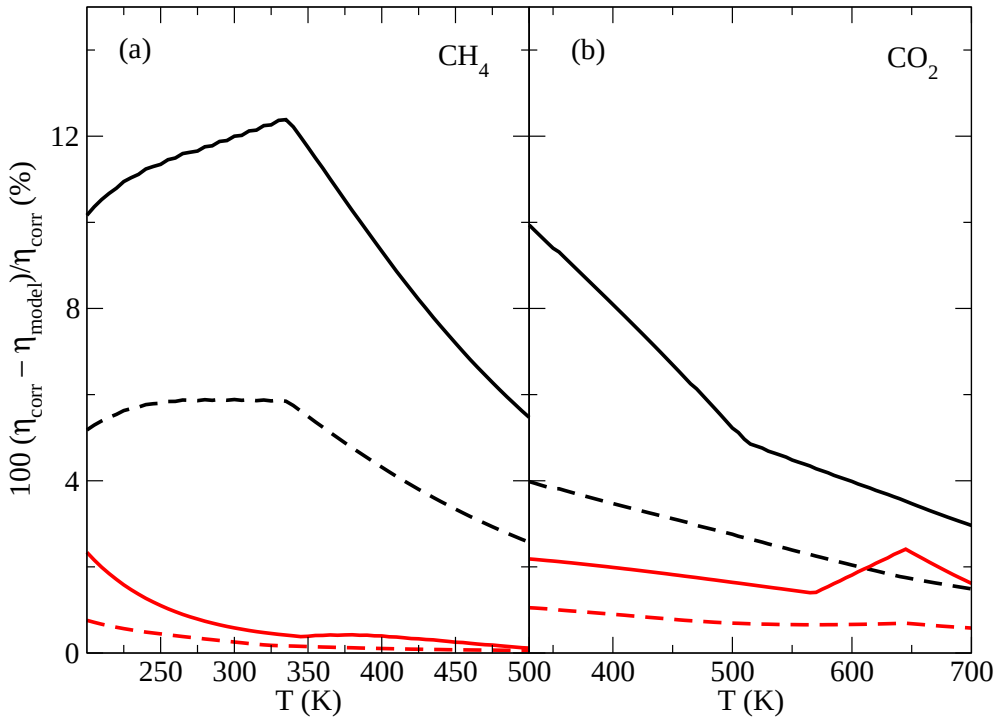

Figure 5.2: Percentage viscosity deviations, $100(\eta_{\text{corr}} - \eta_{\text{model}})/\eta_{\text{corr}}$, obtained with the Enskog-1σ and Enskog-2σ model from the reference correlation for methane (Vogel *et al.*, 2000) and carbon dioxide (Vesovic *et al.*, 1990; Fenghour *et al.*, 1998); the solid lines illustrate maximum deviations, the dashed lines AADs, the black lines the Enskog-1σ model and the red lines depict the Enskog-2σ model. (a) methane, (b) carbon dioxide.

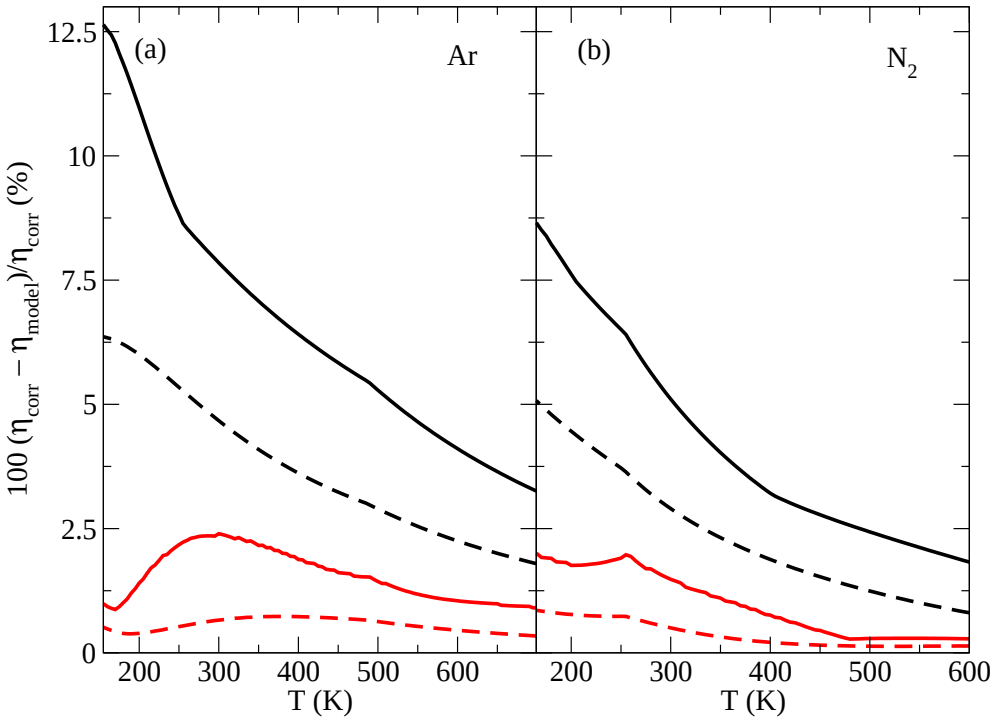

Figure 5.3: Percentage viscosity deviations, $100(\eta_{\mathrm{corr}} - \eta_{\mathrm{model}})/\eta_{\mathrm{corr}}$, obtained with the Enskog-1σ and Enskog-2σ model from the reference correlation for argon and nitrogen by (Lemmon & Jacobson, 2004); the solid lines illustrate maximum deviations, the dashed lines AADs, the black lines the Enskog-1σ model and the red lines depict the Enskog-2σ model. (a) argon, (b) nitrogen.

5.1.2 Comparison with primary experimental data

It is interesting to compare the Enskog-2σ model to the primary experimental data sets on which the experimental reference correlations in table 5.1 are based. The deviations between the Enskog-2σ model and the primary experimental data sets for methane are shown in Fig. 5.4. All experimental data are reproduced with an accuracy better than 3.6%. In Fig. 5.5, we carry out the comparison for argon. The Enskog-2σ model reproduces the experimental data of argon well within 3.8%.

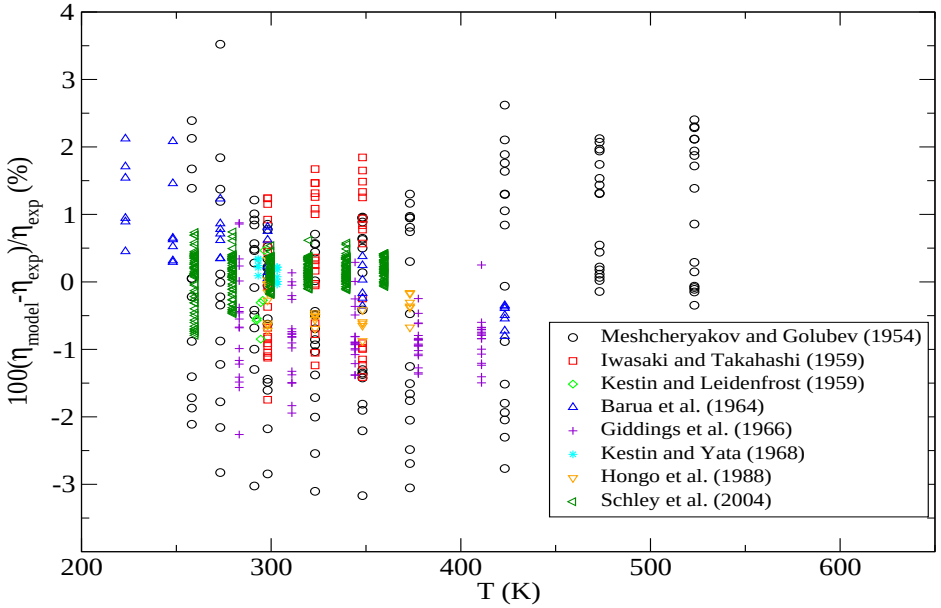

Figure 5.4: Percentage viscosity deviations, $100(\eta_{\text{model}} - \eta_{\text{exp}})/\eta_{\text{exp}}$, between the Enskog-$2\sigma$ model and the primary experimental data sets for methane listed in table 5.2.

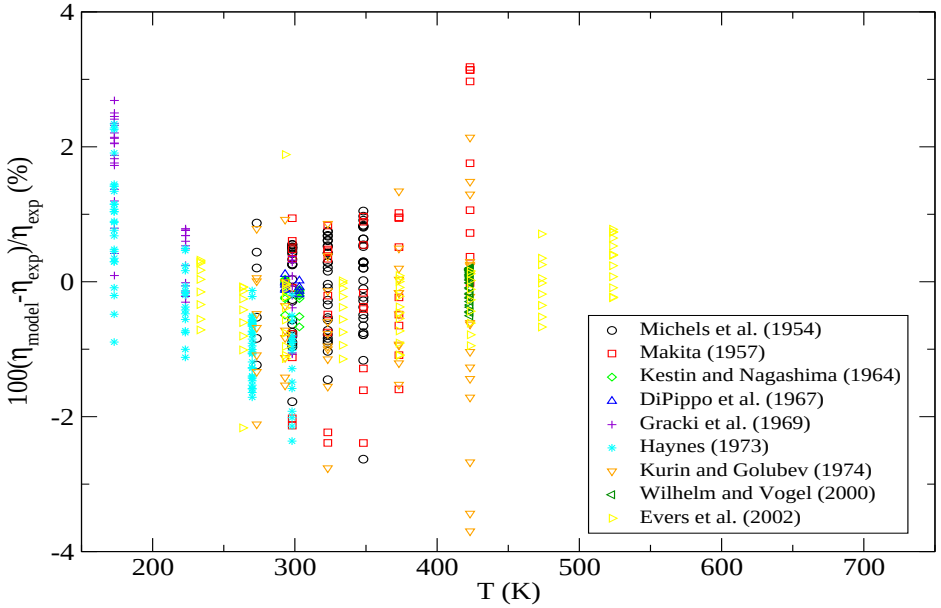

Figure 5.5: Percentage viscosity deviations, $100(\eta_{\text{model}} - \eta_{\text{exp}})/\eta_{\text{exp}}$, between the Enskog-$2\sigma$ model and the primary experimental data sets for argon listed in table 5.3.

Table 5.2: Primary viscosity data sets of methane based on (Vogel *et al.*, 2000).

Data set	P-range (MPa)	T-range (K)
(Meshcheryakov & Golubev, 1954)	1.0-81.1	258-523
(Iwasaki & Takahashi, 1959)	1.7-51.1	298-348
(Kestin & Leidenfrost, 1959)	0.8-7.9	294-296
(Barua *et al.*, 1964)	1.0-17.8	223-423
(Giddings *et al.*, 1966)	0.7-55.2	283-411
(Huang *et al.*, 1966)	4.1-34.5	103-153
(Kestin & Yata, 1968)	0.5-2.6	293-303
(Haynes, 1973b)	vapour pressure	95-185
(Slyusar *et al.*, 1974)	vapour pressure	91-185
(Diller, 1980)	0.6-32.2	100-180
(Hongo *et al.*, 1988)	0.3-5.0	298-373
(Schley *et al.*, 2004)	0.3-29.2	260-360

Table 5.3: Primary viscosity data sets of argon based on (Lemmon & Jacobson, 2004).

Data set	P-range (MPa)	T-range (K)	ρ-range (mol/l)
(Michels *et al.*, 1954)	0.92-202	273-348	0.41-28.9
(Makita, 1957)	0.1-78.5	298-423	0.02-22
(Kestin & Nagashima, 1964)	0.1-5.18	293-303	0.04-2.18
(Van Itterbeek *et al.*, 1966)	0.1-9.79	84.3-89.9	34.5-35.3
(DiPippo *et al.*, 1967)	0.1-5.18	293-303	0.04-0.96
(Gracki *et al.*, 1969)	0.1-2.34	173-298	0.25-21
(Haynes, 1973a)	0.07-34.5	85-298	0.06-35.3
(Kurin & Golubev, 1974)	9.81-380	273-423	2.76-34.9
(van der Gulik & Trappeniers, 1986)	16.1-471	174	20.7-42
(Wilhelm & Vogel, 2000)	0.09-20.1	298-423	0.02-8.49
(Evers *et al.*, 2002)	0.09-28.1	233-523	0.02-6.07

5.1.3 Model sensitivity to the effective diameters

The sensitivity of the Enskog-2σ model to the values of the effective diameters σ_α and σ_χ is illustrated in Fig. 5.6. As can be observed, the Enskog-2σ model is much more sensitive to the choice of σ_α than to the value of σ_χ. In fact, if the optimum σ_α is chosen, one can vary σ_χ by 7% on average from its optimum value and still correlate the viscosity within 4%. However, if the optimum σ_χ is chosen, σ_α can be only varied by 0.6% on average in order to reproduce the viscosity within 4%. This is interesting as it indicates that, for the Enskog-2σ model to predict the viscosity accurately, it is much more important to get the correct geometric effects (excluded volume) than to get the correct collision frequency.

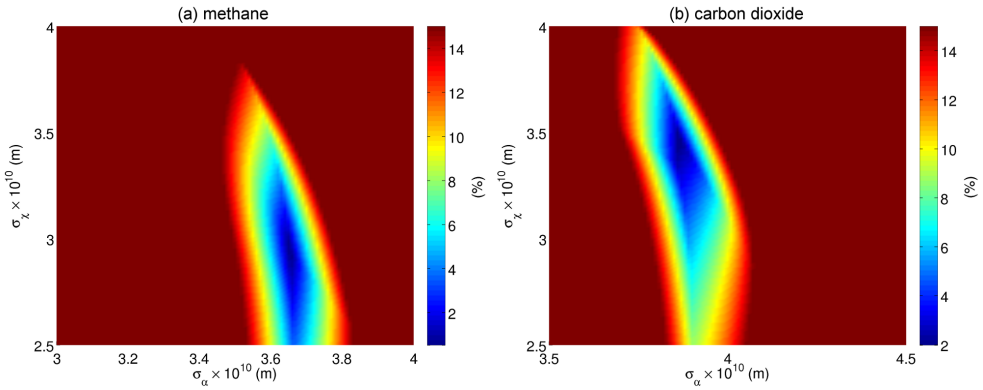

Figure 5.6: Maximum percentage viscosity deviations, at $T = 350K$, of the Enskog-2σ model from the experimental reference correlation for methane (Vogel *et al.*, 2000) and carbon dioxide (Vesovic *et al.*, 1990; Fenghour *et al.*, 1998) for different values of the two effective diameters σ_α and σ_χ. The colour represents the value of the maximum deviation. Maximum deviations larger than 15% are depicted uniformly in dark red. (a) methane, (b) carbon dioxide.

5.1.4 Behaviour of the effective diameters

Next, we examine the behaviour of σ_α, σ_χ as a function of temperature for the five fluids studied. In order to allow for an easier comparison, we show in Fig. 5.7 the behaviour of the effective diameters as a function of the reduced temperature. For the five fluids studied, σ_α exhibits a monotonic decrease with increasing temperature. This decrease with temperature is expected since, at higher temperatures, the fluid particles

have larger thermal energies and hence penetrate the repulsive potential deeper which leads to a smaller collisional diameter σ_α. The slope of each curve is nearly independent of the fluid in question. Furthermore, at each temperature the effective size follows the sequence $\sigma_{SF_6} > \sigma_{CH_4} > \sigma_{CO_2} > \sigma_{N_2} > \sigma_{Ar}$ which is the same as obtained from the Enskog-1σ model and similar to the one obtained from the analysis of the zero-density viscosity (see section 5.1.9), where, however, σ_{CO_2} is slightly larger than σ_{CH_4}. The effective diameter σ_χ, illustrated also in Fig. 5.7, is for a given fluid at a particular temperature always smaller than σ_α. In order to understand this observation, we carried out a number of simulations to ascertain how sensitive the two effective diameters are to the density range used in fitting, by progressively including viscosities at larger densities in the fitting procedure. Fig. 5.8 indicates that for a given density range the effective diameter σ_χ is influenced more by the values of the viscosity at higher density than the effective diameter σ_α. This implies that for a given temperature the effective diameter σ_χ samples further up the repulsive wall of the intermolecular potential. As the repulsive wall for a real fluid is not infinitely steep, but has a negative slope, we observe smaller values of the effective diameter σ_χ compared with those of σ_α.

Although σ_χ also, in general, decreases with temperature, the rate of change is less uniform and σ_χ exhibits a more varied behaviour. The non-uniformity observed can be attributed to the larger uncertainty associated with determining σ_χ. The relative lack of sensitivity of viscosity to σ_χ implies that the uncertainty of the viscosity correlations used will enhance the uncertainty in σ_χ. In order to test this assertion, the viscosity values for all five fluids studied has been computed by assuming a constant, temperature independent value of σ_χ. The overall goodness of fit decreased slightly, but the ability of Enskog-2σ model to correlate the viscosity data remains still very good. For instance, for CH_4 the maximum deviation increased from 2.3% to 3% and the AAD increased from 0.2% to 0.6% while for CO_2 the maximum deviation increased from 2.4% to 2.6% and the AAD increased from 0.8% to 0.9% (for more details, see Fig. 5.9). We conclude that the tests carried out indicate that our knowledge of viscosity is not precise enough to define the exact shape of the effective diameter σ_χ as a function of temperature.

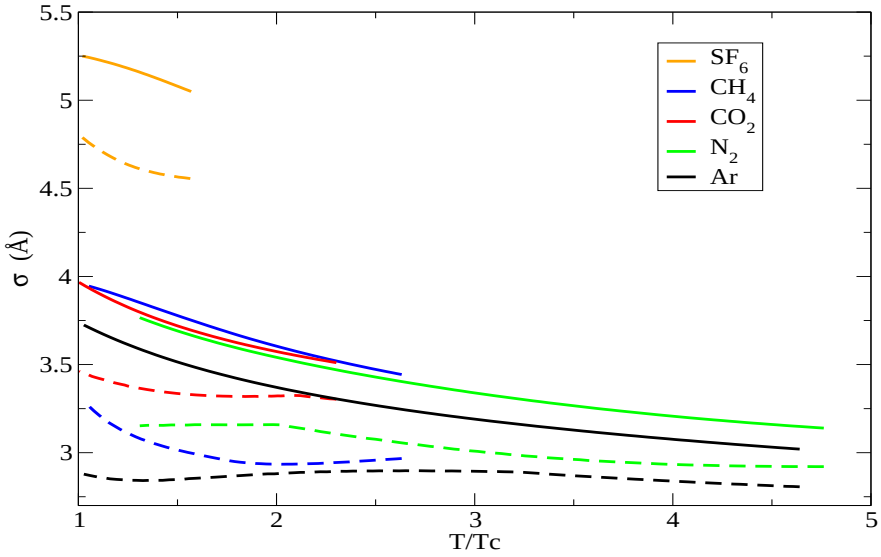

Figure 5.7: Optimised effective diameters as a function of reduced temperature T/T_c. The solid lines depict σ_α and the dashed lines σ_χ.

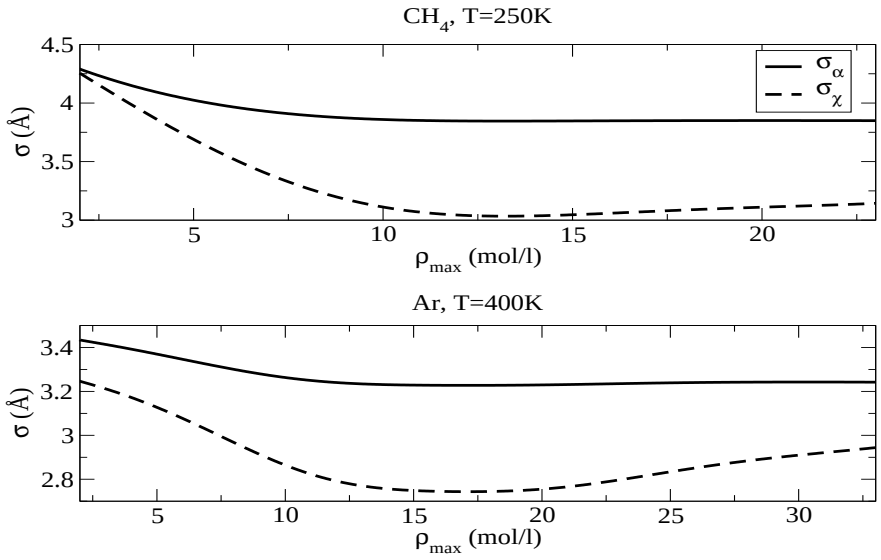

Figure 5.8: Optimised effective diameters as a function of $\rho_{\max}$, where the diameters are obtained by fitting to viscosity data in the interval $0 \leq \rho \leq \rho_{\max}$. The upper plot corresponds to methane at $T = 250K$, the lower plot to argon at $= 400K$. The solid lines depict σ_α, the dashed lines σ_χ.

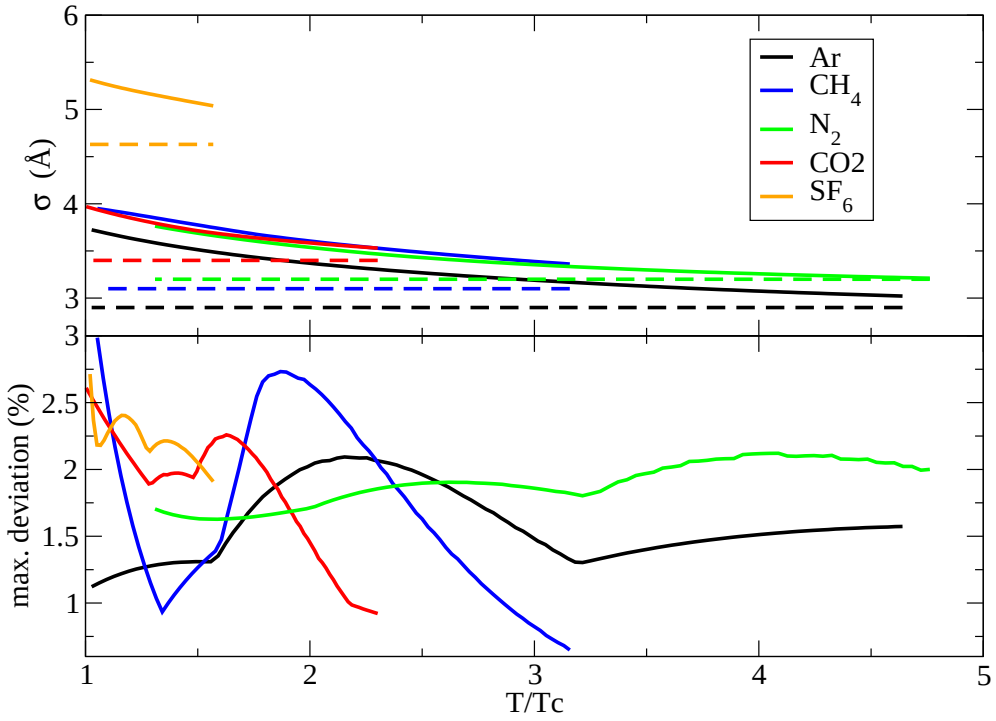

Figure 5.9: Upper plot: Optimised σ_α's (solid lines) for the temperature independent choice of σ_χ's (dashed lines). Lower plot: Corresponding maximum deviations between model and experimental reference correlations.

5.1.5 Magnitude of the model terms

In Fig. 5.10, the magnitude of the viscosity terms in Eq. (3.4) is compared for the Enskog-1σ model (upper plot) and the Enskog-2σ model (lower plot). As an example, the terms are illustrated for carbon dioxide at $T = 600K$. The term $\alpha\rho$ increases linearly with the density ρ, $(\chi/\beta)(\alpha\rho)^2$ grows over-proportionally with ρ and $1/\chi$ decreases almost linearly with ρ. For small densities ρ, the term $1/\chi$ is dominant. Due to the density dependence of the terms, $(\chi/\beta)(\alpha\rho)^2$ and $\alpha\rho$ become larger than $1/\chi$ at $\rho = 11.9$ mol/l and $\rho = 12.7$ mol/l for the Enskog-1σ model and at $\rho = 13.0$ mol/l and $\rho = 13.9$ mol/l for the Enskog-2σ model. At high densities, the term $(\chi/\beta)(\alpha\rho)^2$ is dominant and very sensitive to the density. The optimised effective diameters corresponding to Fig. 5.10 are $\sigma_\alpha = 3.58$Å, $\sigma_\chi = 3.32$Å and $\sigma = 3.6$Å. The sequence $\sigma_\chi < \sigma_\alpha < \sigma$ is typical for high temperatures while the sequence $\sigma_\chi < \sigma < \sigma_\alpha$ is typical at moderate

and low temperatures (see Fig. 5.12 for methane and carbon dioxide). Consequently, the term $1/\chi$ is smaller in the Enskog-1σ model than in the Enskog-2σ model while $\alpha\rho$ is larger in the Enskog-1σ model than in the Enskog-2σ model at high temperatures (as in Fig. 5.10) and smaller at low temperatures. The term $(\chi/\beta)(\alpha\rho)^2$ is larger in the Enskog-1σ model than in the Enskog-2σ model which holds true for all five fluids according to further computations.

Another example for the magnitude of the model terms is given in Fig. 5.11 for argon at $T = 300K$. The corresponding optimised effective diameters are $\sigma_\alpha = 3.37$Å, $\sigma_\chi = 2.88$Å and $\sigma = 3.32$Å. Consequently, the sequence $\sigma_\chi < \sigma < \sigma_\alpha$ holds true and the term $\alpha\rho$ is smaller in the Enskog-1σ model than in the Enskog-2σ model here. The remaining results are qualitatively the same as in Fig. 5.10 for carbon dioxide at $T = 600K$.

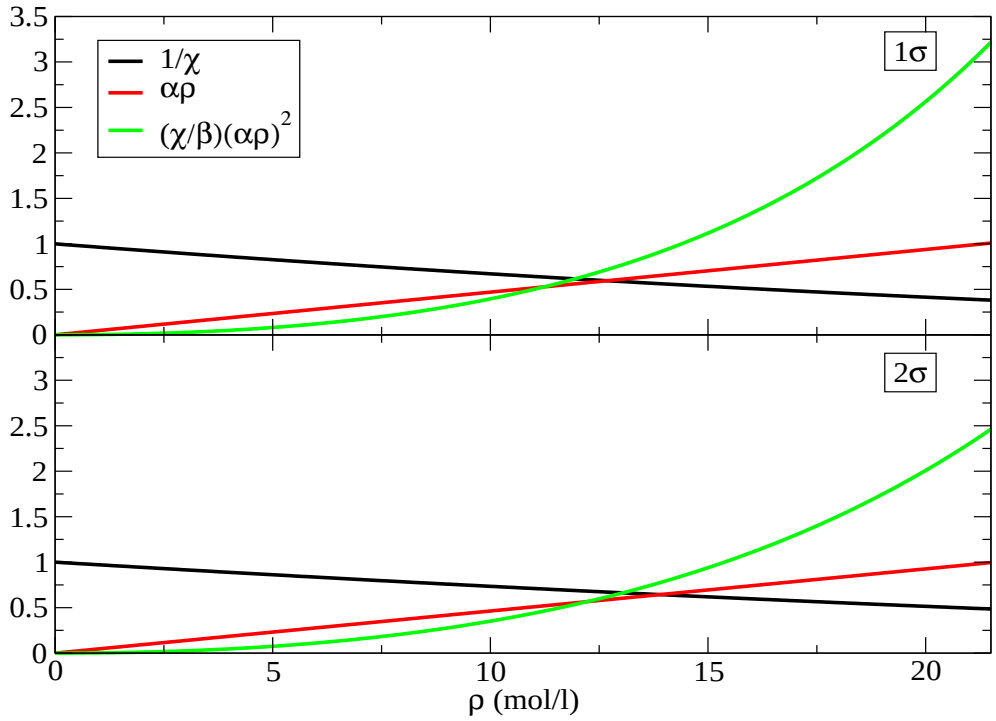

Figure 5.10: Density dependence of the terms in the Enskog-1σ model (upper plot) and Enskog-2σ model (lower plot) for carbon dioxide at $T = 600K$.

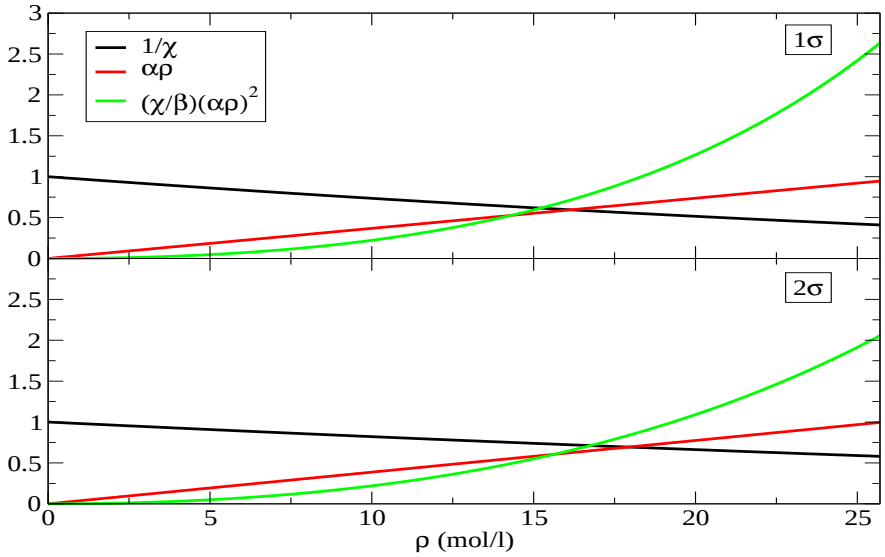

Figure 5.11: Density dependence of the terms in the Enskog-1σ model (upper plot) and Enskog-2σ model (lower plot) for argon at $T = 300K$.

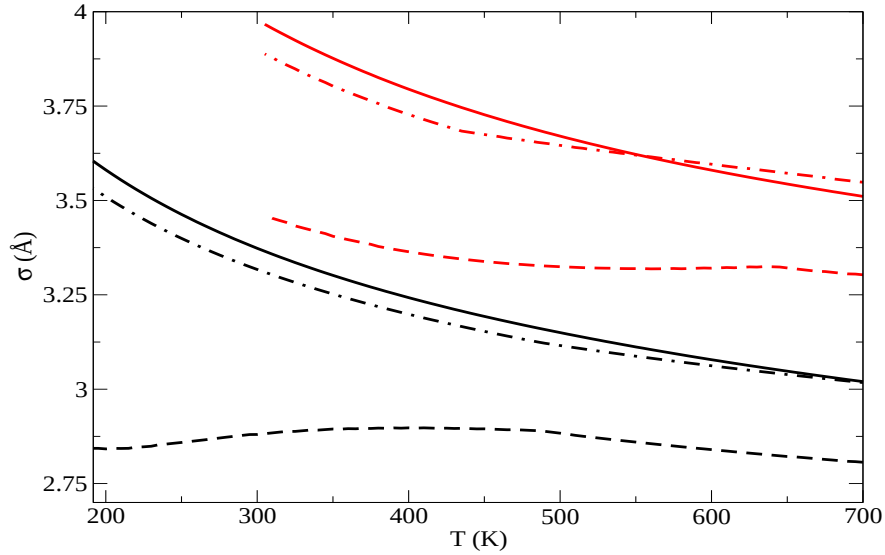

Figure 5.12: Optimised effective diameter σ_α (solid lines), σ_χ (dashed lines) and σ (dash-dotted lines) versus temperature T for argon (black lines) and carbon dioxide (red lines).

5.1.6 Comparison with the VW method

The VW method developed by (Vesovic & Wakeham, 1989b,a) described in section 2.5 has many parallels to the Enskog-2σ model. The VW approach is based as well on Enskog theory and uses a temperature dependent effective diameter σ_α as well as a density and temperature dependent representation of the radial distribution function χ at contact. It is interesting to compare the model parameters of the VW method and the Enskog-2σ model with one another which we will do in this section. According to Fig. 5.13, σ_α obtained from the VW method at the switch-over density is similar to the effective diameter σ_α in the Enskog-2σ model. In particular, both effective diameters σ_α's decrease monotonically with the temperature. The maximum deviation between the σ_α's occurs at $T/T_c = 4.76$ for nitrogen and is about 1.28%. The reason for this deviation can be explained by the fact that the switch-over density, at which the VW σ_α is obtained, is 17.1 mol/l and distinctively exceeds the maximum density of 12.9 mol/l up to which the σ_α of the Enskog-2σ model is computed. The switch-over density decreases with decreasing temperature such that, for nitrogen below $T/T_c = 3.45$, the switch-over density lies within the density interval of the Enskog-2σ model and the deviations between the σ_α's reduces to 0.46%.

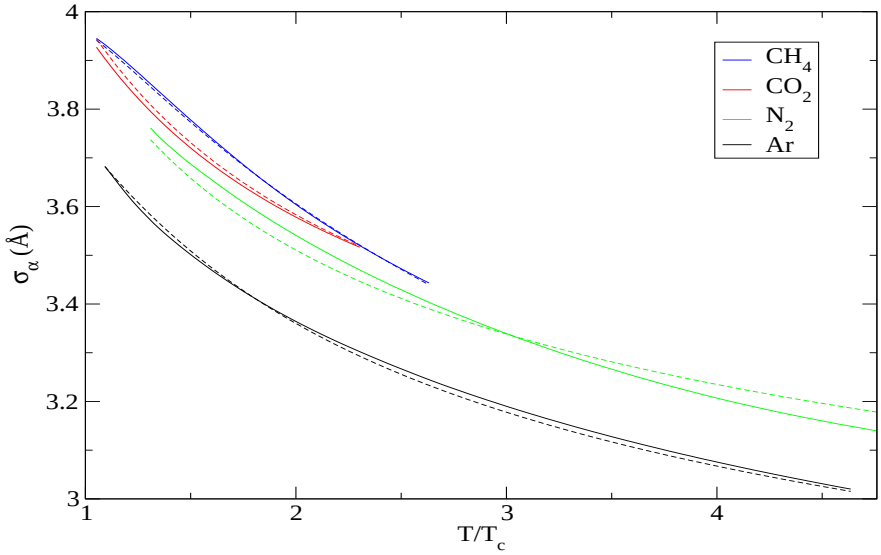

Figure 5.13: σ_α from the Enskog-2σ model (solid lines) and σ_α from the VW method (dashed lines) versus the reduced temperature.

As the σ_α obtained from the VW method at the switch-over density is similar to the σ_α of the Enskog-2σ model, the question arises how well the Enskog-2σ model reproduces the experimental correlations when we set σ_α equal to the VW σ_α. This is done in Fig. 5.14. σ_χ has been obtained by minimising the maximum deviation between model and experimental correlation up to $\rho_{\max}$, defined in section 3.2, and is shown in the upper plot in the figure. According to the lower plot, the model reproduces the experimental reference correlation well within 2.2%, 2.5%, 2.9%, 3.0% for methane, argon, carbon dioxide and nitrogen. We conclude that the VW σ_α gives a good estimate for the σ_α in the Enskog-2σ model.

The χ's obtained from the VW method and the Enskog-2σ model are compared in Fig. 5.15 for a couple of isotherms for methane and argon. By definition, χ increases monotonically with the density. The slope of the Enskog-2σ χ grows by definition with the density while the VW χ is more complex and can have several inflection points as, for example, for the isotherms of methane or argon at $T = 200K$. The largest deviation between the χ's is 4.7% for methane at $T = 500K$, $\rho = 15.3$mol/l, and 11.3% for argon at $T = 200K$, $\rho = 17.5$mol/l. Like the Enskog-2σ model, the VW method uses as input all experimental viscosity data for a given temperature. Thus, although the σ_α's and χ's of both approaches have similar values, one cannot predict the σ's in the Enskog-2σ model from the VW method without knowing the viscosity itself. The prediction of the effective diameters is discussed in section 5.1.9.

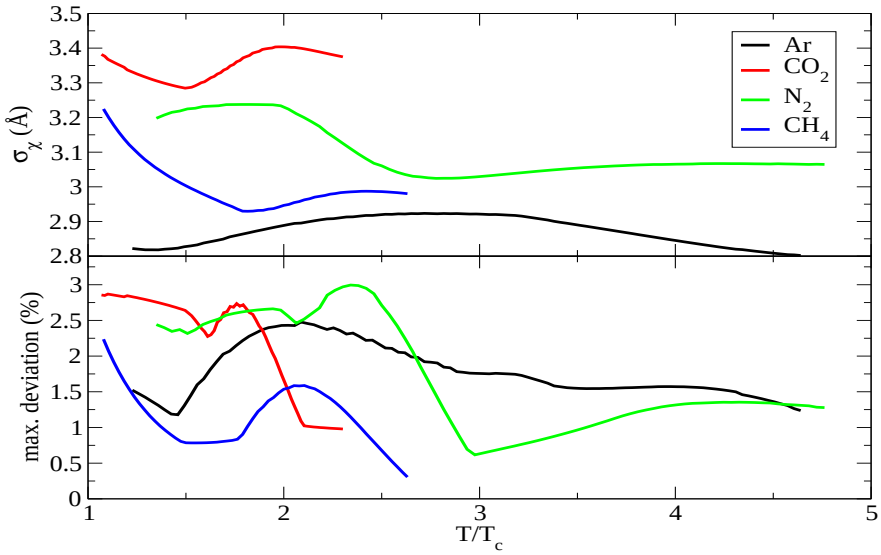

Figure 5.14: Enskog-2σ model with σ_α from the VW method and optimised σ_χ. Upper plot: optimised σ_χ. Lower plot: maximum deviation between model and the experimental reference correlations.

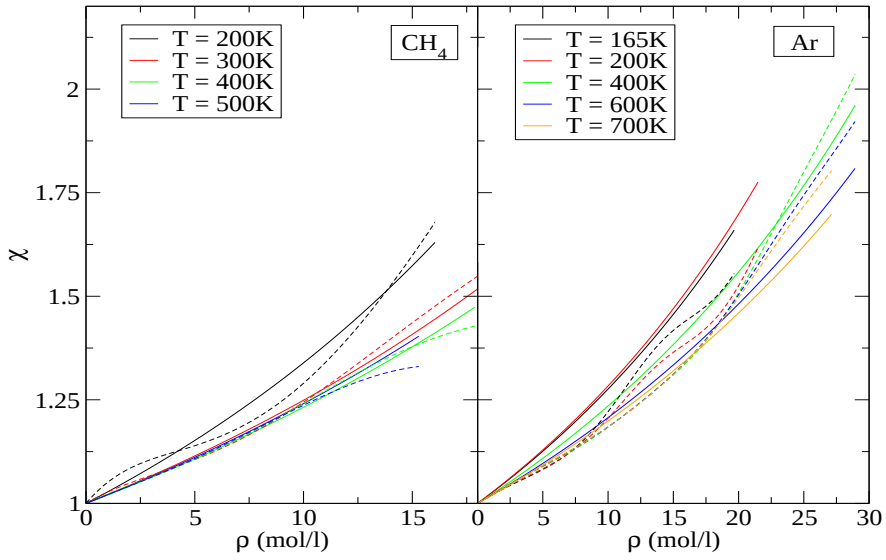

Figure 5.15: χ in the Enskog-2σ model (solid lines) and χ in the VW method (dashed line) versus density for a couple of isotherms of methane and argon.

5.1.7 Application to other transport properties

One cannot envisage that the effective diameters σ_α and σ_χ can be used to evaluate other transport properties of the same fluids. There is evidence, primarily from studies of dilute gases (Hirschfelder *et al.*, 1954; Maitland *et al.*, 1985, 1986), that, in general, the effective parameters which are based on some kinetic theory model are not transferable and that the different transport properties require different effective parameters. The effective diameters do not only account for the difference between the real and hard sphere potential, but also for the deficiencies in Enskog's theory in describing each transport property. As the molecular collisions have a different weighting for different transport properties, Enskog's theory does not describe each transport property with the same accuracy. The assertion of non-transferability of effective diameters has been tested by calculating the background thermal conductivity of methane and carbon dioxide by means of the Enskog-2σ model using the effective diameters obtained from viscosity. To calculate the background thermal conductivity, we make use of of the fact that Enskog's theory is applicable as well to heat transport and gives on the first-order approximation level the heat equation with the following expression for the thermal conductivity

$$\lambda = \lambda_0 \left(\frac{1}{\chi} + \frac{3}{2}\alpha\rho + \frac{1}{\beta^*}\chi\alpha^2\rho^2 \right) \tag{5.2}$$

with the thermal conductivity in the zero density limit λ_0, the numerical constant $\beta^* = 0.845$ and all other quantities as defined in section 2.2.1. The maximum deviations for a given temperature are of the order of 15-40%, see Fig. 5.16. These large deviations might be caused by the fact that the internal degrees of freedom of the fluid molecules contribute to the value of thermal conductivity while they do not play a role for viscosity. Furthermore, this supports the general insight that the effective parameters based on kinetic theory are transport property specific. It was not possible to carry out similar tests for the self-diffusion coefficient due to a lack of accurate experimental data covering large temperature and pressure ranges. However, such large deviations as those observed for thermal conductivity are not expected. Nevertheless, it is worth pointing out that if the effective parameters are used purely as scaling parameters there is plentiful evidence (Assael *et al.*, 1992; Galliéro *et al.*, 2006) that different transport properties can be described by the same effective parameters, albeit with some loss of accuracy.

In Fig. 5.17, the Enskog-2σ model is applied to correlate the thermal conductivity of methane and carbon dioxide. The effective diameters have been optimised to reproduce the thermal conductivity analogously to the optimisation of viscosity. The thermal conductivity can be correlated within 8.3% for methane and within 1.3% for carbon dioxide. The optimised effective diameters are compared to the ones obtained from viscosity in Fig. 5.18 for methane and in Fig. 5.19 for carbon dioxide. The optimised σ_α's for thermal conductivity decrease monotonically with temperature as found for the optimised σ_α's for viscosity. Additionally, we observe that σ_α for thermal conductivity is, except for carbon dioxide at temperatures close to the critical temperature, larger than σ_α for viscosity. The effective diameter σ_χ for thermal conductivity exhibits again a more varied behaviour. The reason is analogous to the one pointed out in section 5.1.4 for viscosity. The effective diameter σ_χ is relatively insensitive to the thermal conductivity λ such that our knowledge of λ is not precise enough to define the exact shape of σ_χ as a function of temperature.

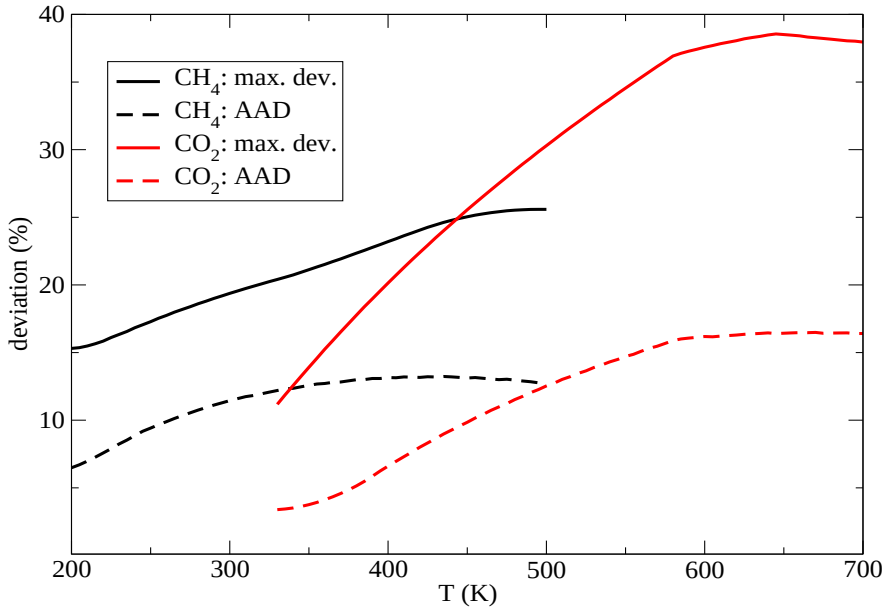

Figure 5.16: Maximum deviation (solid lines) and AAD (dashed lines) of the thermal conductivity between the Enskog-2σ model and the experimental reference correlations (Younglove & Ely, 1987; Vesovic *et al.*, 1990) for methane (black lines) and carbon dioxide (red lines). The effective diameters have been obtained from viscosity and are the same as in Fig. 5.7 for the respective fluid.

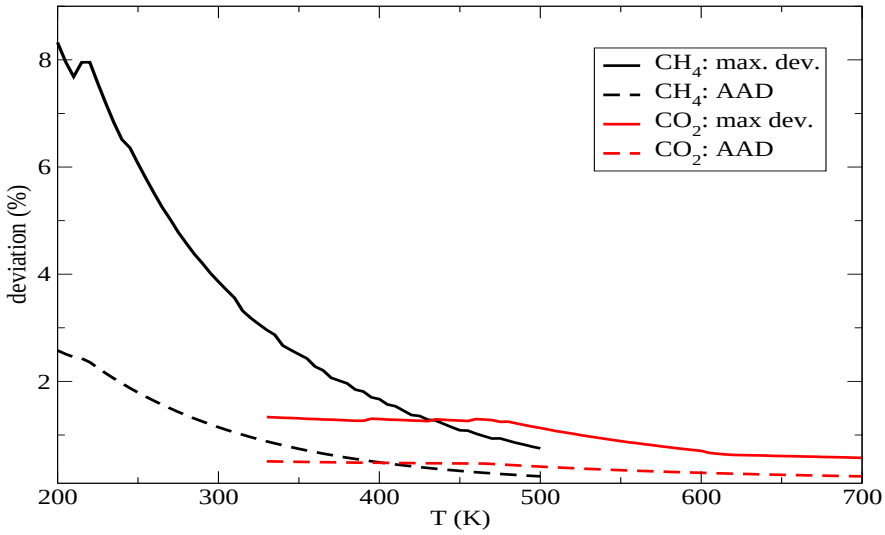

Figure 5.17: Maximum deviation (solid lines) and AAD (dashed lines) of the thermal conductivity between the Enskog-2σ model and the experimental reference correlations (Younglove & Ely, 1987; Vesovic *et al.*, 1990) for methane (black lines) and carbon dioxide (red lines). The effective diameters have been obtained from the correlations for thermal conductivity as described in the text.

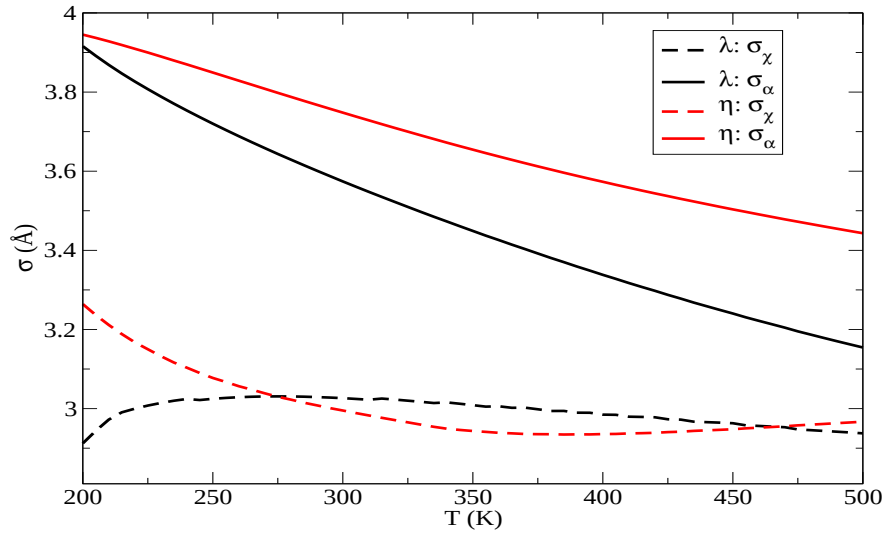

Figure 5.18: Optimised effective diameters for methane. The black lines are obtained from thermal conducivity, the red ones from viscosity. The σ_α's are depicted by the solid lines, the σ_χ's by the dashed ones.

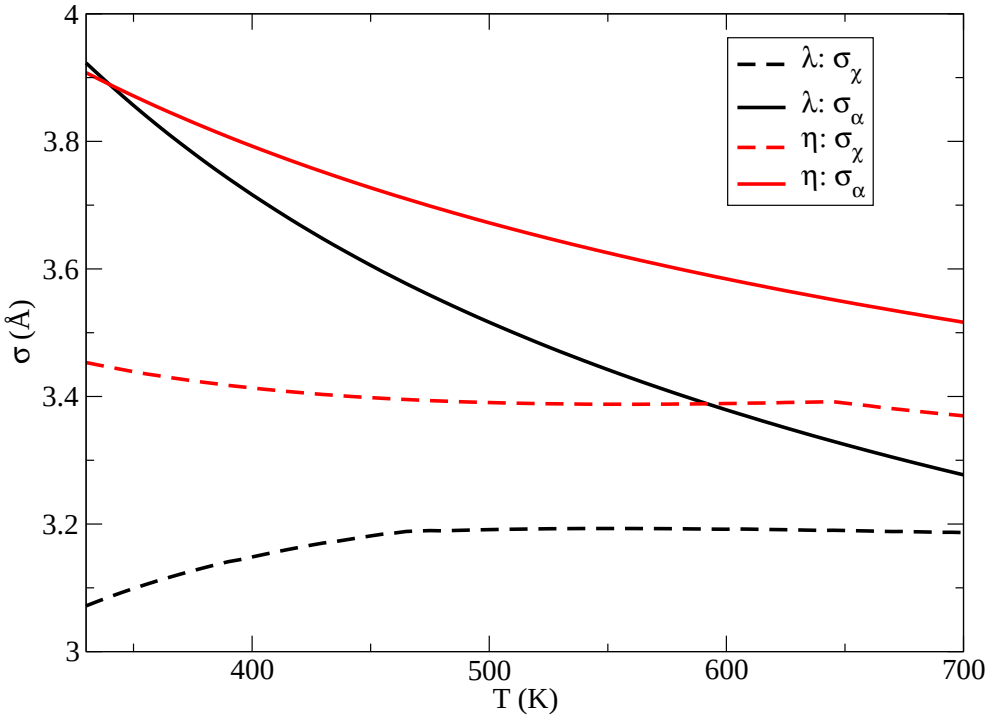

Figure 5.19: Optimised effective diameters for carbon dioxide. The black lines are obtained from thermal conducivity, the red ones from viscosity.The σ_α's are depicted by the solid lines, the σ_χ's by the dashed ones.

5.1.8 Alternative definitions of the maximum density

It is interesting to compare how the choice of the maximum density defined in section 3.2 in the Enskog-2σ model performs compared to alternative choices for the maximum density $\rho_{\max}$. We investigate the following alternative definitions:

- Set $\rho_{\max} = \min(1.5\rho_c, \rho_{\exp})$ where ρ_c is the critical density of the respective fluid and $\rho_{\exp}$ the maximum density of the experimental reference correlation at a given temperature.
- Set $\rho_{\max} = \min(2.0\rho_c, \rho_{\exp})$.
- Set $\rho_{\max} = \min(\rho_{50\text{MPa}}, \rho_{\exp})$ where $\rho_{50\text{MPa}}$ is the density at 50MPa for the respective fluid and temperature.

- Set $\rho_{\max} = \min\left(\rho_{\mathrm{MD,mean}}, \rho_{\exp}\right)$ where

$$\rho_{\mathrm{MD,mean}} = \frac{0.31}{N_A \pi/6(\sigma_\alpha + \sigma_\chi)/2} \tag{5.3}$$

  for the respective fluid and temperature.

The advantage of the first three alternatives is that the maximum densities can be determined directly. In the Enskog-2σ model with the usual choice for $\rho_{\max}$ defined in section 3.2 or the choice under the fourth bullet point, $\rho_{\max}$ depends on the effective diameters and has to be determined iteratively. The results for all approaches are presented in Fig. 5.20 for argon and in Fig. 5.21 for carbon dioxide. Large deviations for the effective diameter σ_α are found at high temperatures between the approach with constant maximum pressure and all other approaches. For argon, the relative deviation reaches a value of 3.7% and, for carbon dioxide, a value of 2.5%. These deviations are caused by the fact that, at high temperatures, the maximum density of the approach with constant maximum pressures is distinctively smaller than for the approaches under bullet point one, two and four (for argon, at least 12.8 mol/l smaller at the highest temperature and, for carbon dioxide, at least 8.1 mol/l smaller at the highest temperature). In Fig. 5.8, we see that such a big difference in the maximum density can lead to the deviations in the effective diameters σ_α of the order of a few percent. The σ_α's of all other approaches deviate less than 0.67% from each other. The behaviour and values of the diameter σ_χ, on the contrary, are again much more varied. This is consistent with Fig. 5.8; σ_χ varies more than σ_α with the maximum density, in particular, at high maximum densities at which σ_α becomes almost independent of the maximum density. The maximum deviation between model and experiment occurs at the smallest temperature for the approaches with a constant maximum density. The Enskog-2σ model with the usual choice for $\rho_{\max}$ or the choice under the fourth bullet point have the beneficial feature to yield a maximum density which decreases with temperature at the lower range of temperatures. This has the effect that the increase in the maximum deviation between model and experiment is diminished with decreasing temperature and even reversed eventually. In particular, for argon, the maximum deviation decreases with decreasing temperature for $T \leq 280K$ as it occurs at the maximum density. For the approach with constant maximum pressure, on the contrary, the maximum density increases with decreasing T thus yielding a relatively

large maximum deviation of 4.7% for argon at $T = 160K$ and 3.4% for carbon dioxide at $T = 305K$. Altogether, the Enskog-2σ model with the usual choice for $\rho_{\max}$ or the choice under the fourth bullet point have an advantageous behaviour of the maximum density (small maximum densities at low temperatures, large maximum densities at high temperatures) but the effective diameters have to be determined iteratively. We have focused section 5.1 on the Enskog-2σ model with the usual choice for $\rho_{\max}$ as the maximum deviations are smaller than for the choice of $\rho_{\max}$ under the fourth bullet point. The latter model, however, will play a role in later sections and its larger maximum density will be found especially beneficial.

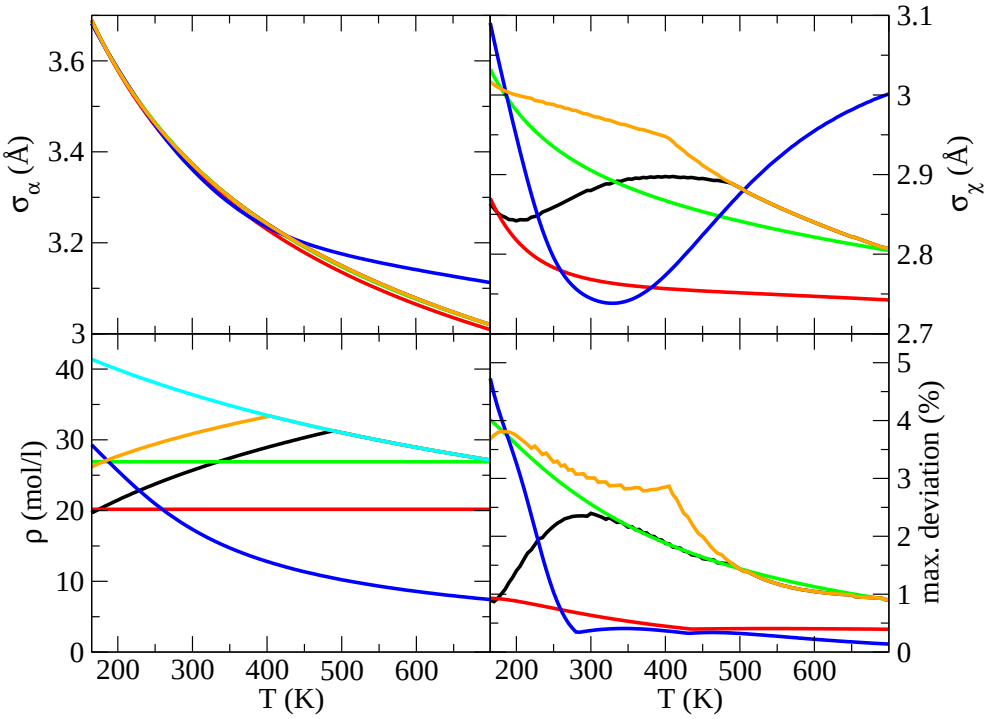

Figure 5.20: Enskog-2σ model with alternative definitions of the maximum density for argon. Plotted versus the temperature, we show σ_α in the upper left plot, σ_χ in the upper right plot, the maximum density in the lower left plot and the maximum deviation between model and experiment in the lower right plot. The Enskog-2σ model corresponds to the black lines, the model with maximum density $1.5\rho_c$ to the red lines, the model with maximum density $2.0\rho_c$ to the green lines, the model with maximum pressure 50MPa to the blue lines and the Enskog-2σ model with $\sigma_{max} = (\sigma_\alpha + \sigma_\chi)/2$ under bullet point four to the orange lines. The cyan line denotes the maximum density of the experimental correlation by (Lemmon & Jacobson, 2004).

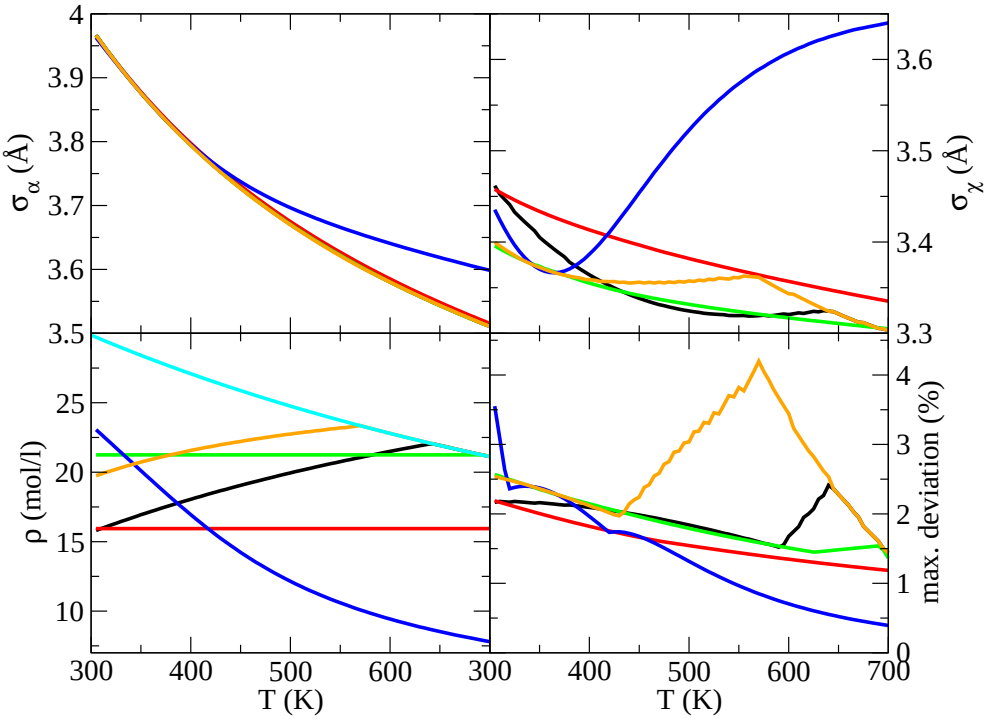

Figure 5.21: Enskog-2σ model with alternative definitions of the maximum density for carbon dioxide. Plotted versus the temperature, we show σ_α in the upper left plot, σ_χ in the upper right plot, the maximum density in the lower left plot and the maximum deviation between model and experimental reference correlation in the lower right plot. The Enskog-2σ model corresponds to the black lines, the model with maximum density $1.5\rho_c$ to the red lines, the model with maximum density $2.0\rho_c$ to the green lines, the model with maximum pressure 50MPa to the blue lines and the Enskog-2σ model with $\sigma_{max} = (\sigma_\alpha + \sigma_\chi)/2$ under bullet point four to the orange lines. The cyan line denotes the maximum density of the experimental reference correlation by (Vesovic *et al.*, 1990; Fenghour *et al.*, 1998).

5.1.9 Universal behaviour

A closer inspection of Fig. 5.7 indicates that the temperature trend of σ_α is very similar for all five fluids studied. It is thus possible, by judicious choice of a scaling parameter, to superimpose all five σ_α curves onto one universal curve by simply shifting each curve in the y-direction. We have chosen argon as a reference fluid and have scaled the effective diameter σ_α for the other four fluids by using a constant scaling parameter, L,

$$\sigma_{\alpha,x}(T/T_{c,x}) = L\sigma_{\alpha,Ar}(T/T_{c,Ar}). \tag{5.4}$$

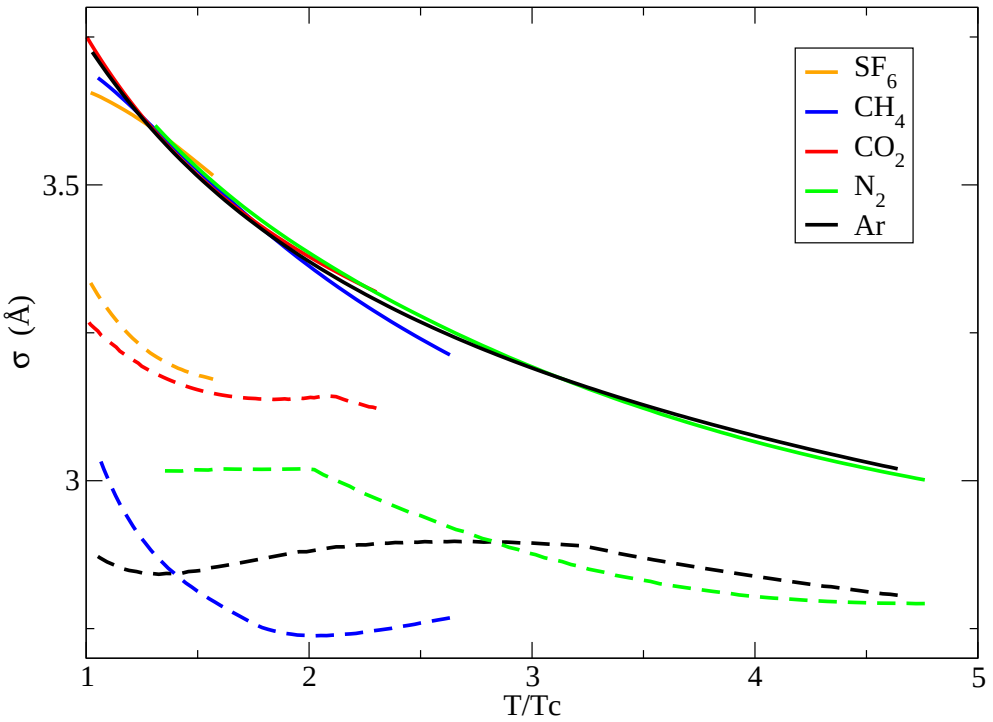

Figure 5.22: Scaled effective diameters as a function of reduced temperature T/T_c. The solid lines depict the scaled σ_α and the dashed lines the scaled σ_χ.

Fig. 5.22 illustrates that using a constant value of the scaling parameter L allows for superimposition of all the σ_α curves on to that of argon. The existence of a universal representation for the effective diameter, σ_α, is not only interesting but also allows for the possibility of predicting the viscosity of one fluid from the knowledge of another, should some relation be found for L. The slightly stronger temperature dependence of the σ_α of methane indicates that methane has a less steep repulsive potential part than the other fluids. Also, as the σ_α of sulphur hexafluoride depends less strongly on the temperature, its repulsive potential seems to be relatively steep. We have used the same parameter L to scale the effective diameter, σ_χ. Fig. 5.22 illustrates that for σ_χ the universal behaviour was not observed and the resulting scaled diameters differ by, at most, 10% from the σ_χ of argon. As the Enskog-2σ model is less sensitive to the choice of σ_χ, it remains to be seen how this choice influences the viscosity prediction. We have made use of the observed universal behaviour of the effective diameter σ_α to

calculate the viscosity of methane, nitrogen, carbon dioxide and sulphur hexafluoride from the knowledge of the viscosity of argon and a single scaling parameter L. For this purpose, we obtain the effective diameters σ_α and σ_χ for a fluid of interest by multiplying the corresponding effective diameters of argon by the scaling parameter L and then making use of the Enskog-2σ model to calculate the viscosity. There are several ways of choosing the scaling parameter L for a given fluid:

(i) by making use of all the available viscosity data and by minimising the maximum deviation between the data and the values predicted by the Enskog-2σ model. This would be equivalent to graphically superimposing σ_α for a chosen fluid to that of argon. As this approach makes use of all the available data, it has no predictive power but rather acts as a base case since it indicates if the universal curve with a single scaling parameter can adequately represent the viscosity data.

(ii) by making use of viscosity data along a single isotherm.

(iii) by making use of a single viscosity value at a given temperature and density.

Table 5.4 presents the values of the scaling parameter L obtained in each case together with how well the viscosity of each fluid is predicted as measured by the AAD and the maximum deviation.

Fig. 5.23 illustrates the deviations observed for all four fluids as a function of the reduced temperature. If all the viscosity data for each fluid are used, the model with a single scaling parameter L is capable of correlating the viscosity of nitrogen and methane almost within their quoted uncertainty. For CO_2 and SF_6 the deviations are larger, reaching a maximum of 6.3% and 7.5%, respectively. For CO_2, these deviations should be seen in the context of the accuracy of the CO_2 correlation, which at supercritical temperatures is of the order of 4%. Fig. 5.24 gives a more detailed illustration of the deviations observed for CO_2 along a number of selected isotherms. For SF_6 the AAD increase rapidly as the temperature approaches the critical temperature, mimicking the weak non-universality displayed by σ_α at these temperatures. In Fig. 5.25, we compare the model directly to experimental primary data of methane. The primary viscosity data is reproduced very well within 4.4%.

Table 5.4: Length scaling parameter L obtained by minimizing the maximum deviation between the Enskog-2σ model and the experimental correlations.

Fluid	Model	L	Max. deviation (%)	AAD (%)
CH_4	all T	1.0686	3.3	0.9
CH_4	$T = 2T_c$	1.0676	3.7	1.0
CH_4	$T = 2T_c$, $\rho = 1.5\rho_c$	1.0687	3.3	0.9
N_2	all T	1.0553	3.1	1.0
N_2	$T = 2T_c$	1.0560	3.2	1.1
N_2	$T = 2T_c$, $\rho = 1.5\rho_c$	1.0533	4.2	0.8
CO_2	all T	1.0750	6.3	3.5
CO_2	$T = 2T_c$	1.0745	6.5	3.4
CO_2	$T = 2T_c$, $\rho = 1.5\rho_c$	1.0682	9.9	2.8
SF_6	all T	1.4476	7.5	2.4
SF_6	$T = 400K \sim 1.3T_c$	1.4450	8.5	2.2
SF_6	$T = 400K$, $\rho = \rho_c$	1.4397	10.5	2.1

Table 5.4 also presents the results when the model with a single scaling parameter L is used in a predictive mode. In the first instance, we focus on the results obtained by evaluating the parameter L from viscosity data along a single isotherm. As an example, we choose for each fluid the isotherm at $T = 2T_c$ in order to evaluate L. For SF_6, this choice would result in a temperature outside the range of validity of the correlation. Instead, we have chosen the 400 K isotherm as it is just below the highest temperature (425 K) where the primary experimental data were available. The deviations quoted in Table 5.4 indicate that calculating L in this fashion gives as good results as in our base case scenario for all four fluids tested. Making use of different isotherms, within the range of validity of the original correlations, would give equally good estimates. For instance, choosing other isotherms to evaluate L, for nitrogen and methane, result in a variation in AAD in the range of $0.8 - 1.1\%$, while for CO_2 and SF_6 the AAD will vary from 2.8% to 3.5% and from 2.2% to 3.5%, respectively. Choosing a single value of viscosity to evaluate L, not surprisingly, leads to a higher overall uncertainty in the predicted viscosity. We have investigated a number of choices. In general, choosing the

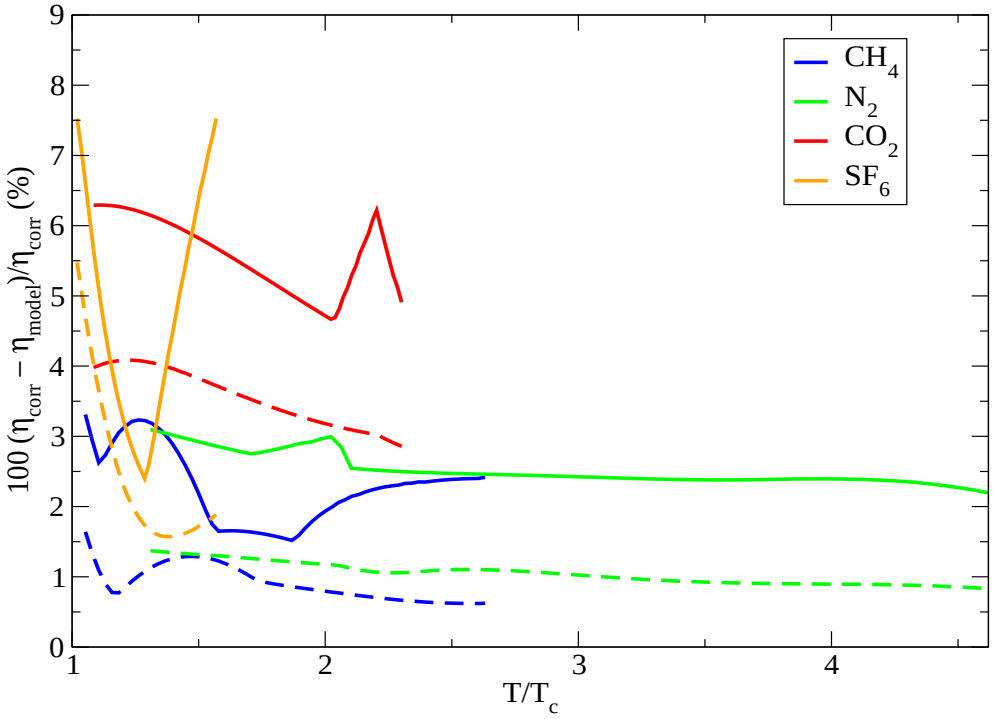

Figure 5.23: Percentage viscosity deviations, $100(\eta_{\text{corr}} - \eta_{\text{model}})/\eta_{\text{corr}}$, obtained with the Enskog-2σ model from the experimental reference correlations in Table 1. The effective diameters for each fluid were obtained by means of Eq. (5.4) using the values of L obtained from the data at all temperatures. The solid lines are the maximum deviations, while the dashed lines are the AAD.

viscosity value at a density higher than the critical leads to more accurate predictions. Table 5.4 presents the maximum deviation and AAD if the choice of L for the four fluids was based on a value of viscosity at $2T_c$ and $1.5\rho_c$. For SF_6, we had to choose a lower density as the choice of $1.5\rho_c$ would lead to densities larger than ρ_{MD}. Although the accuracy with which the viscosity of methane, nitrogen and even sulphur heaxafluoride are predicted has been maintained, there is some decrease in the prediction of the viscosity of CO_2 with the maximum deviation now reaching 9.9%. Choosing other values of viscosity in the range $1.3\rho_c < \rho < \rho_{MD}$ to evaluate L leads to the following variation in AAD: $0.8 - 2.0\%$, $0.6 - 1.3\%$ and $2.8 - 6.6\%$ for methane, nitrogen and carbon dioxide, respectively.

Next, we have explored a number of approaches to obtain an estimate of L from either dilute gas viscosity or thermodynamic data. In particular, the following approaches

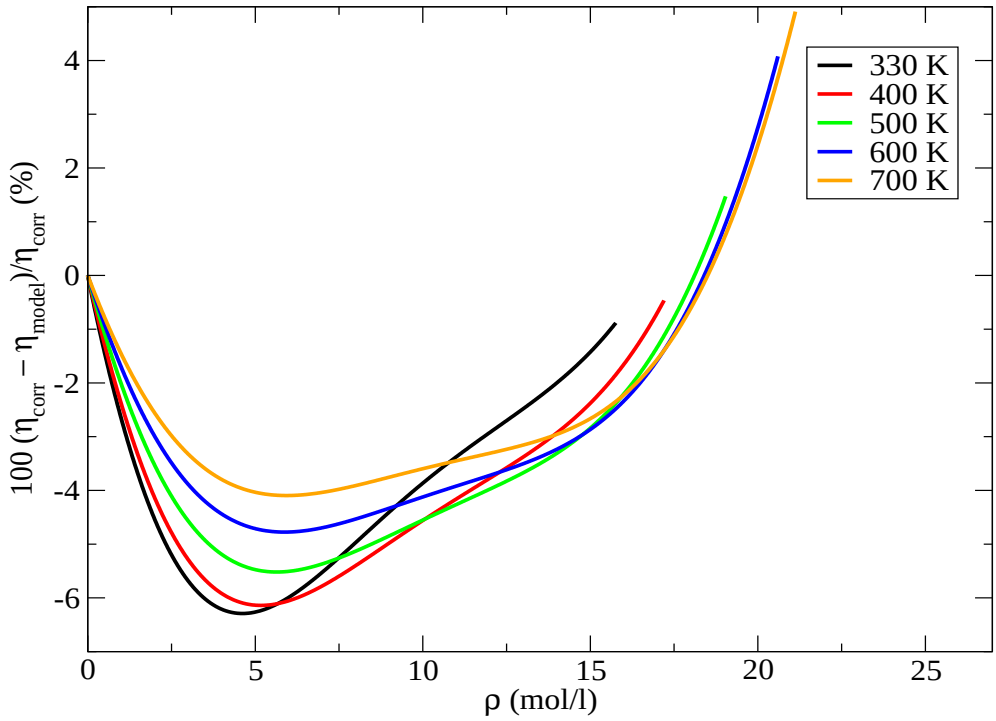

Figure 5.24: Percentage viscosity deviations, $100(\eta_{\text{corr}} - \eta_{\text{model}})/\text{corr}$, obtained with the Enskog-2σ model from the experimental reference correlation for carbon dioxide (Vesovic *et al.*, 1990; Fenghour *et al.*, 1998) as a function of density along a number of isotherms. The effective diameter for carbon dioxide was obtained by means of Eq. (8) using the value of L obtained from the data along the isotherm at $T = 2T_c$.

have been tested:

- Set $L = \sigma_{0,x}/\sigma_{0,Ar}$, where $\sigma_{0,x}$ is length scaling parameter obtained from the dilute gas viscosity by means of a universal correlation (Maitland *et al.*, 1981).
- Set $L = (V_{c,x}/V_{c,Ar})^{1/3}$, where $V_{c,x}$ is the critical volume of the respective fluid and $V_{c,Ar}$ is the critical volume of argon.
- Set $L = \sigma_{\text{CS-vdW},x}/\sigma_{\text{CS-vdW},Ar}$ where $\sigma_{\text{CS-vdW},x}$ is the effective diameter of fluid x obtained from the CS-vdW EOS (Ben-Amotz & Herschbach, 1990). The effective diameter $\sigma_{\text{CS-vdW}}$ is obtained by fitting supercritical pressure-density isotherms. This choice was not possible for SF_6 as no CS-vdW parameters are available for SF_6 (Ben-Amotz & Herschbach, 1990).

- Set $L = \sigma_{\text{SAFT-SW},x}/\sigma_{\text{SAFT-SW},Ar}$ where $\sigma_{\text{SAFT-SW},x}$ is the effective diameter of fluid x obtained with the SAFT-VR SW EOS (Dufal & Haslam, 2012; Gil-Villegas *et al.*, 1997) by fitting vapour-pressures and saturated liquid densities.

- Set $L = \sigma_{\text{SAFT-LJ},x}/\sigma_{\text{SAFT-LJ},Ar}$ where $\sigma_{\text{SAFT-LJ},x}$ is the effective diameter of fluid x obtained with the LJ SAFT-VR Mie EOS (Dufal & Haslam, 2012) by fitting vapour-pressures and saturated liquid densities.

The results summarized in Table 5.5 indicate that, in general, choosing a scaling parameter L in this fashion will lead to large uncertainties in viscosity predictions. We also observe that, whereas for methane the estimated values of parameter L agree to within 4%, for carbon dioxide (the least spherical of the molecules considered here), the agreement is only 7%, while for SF_6, by far the largest molecule studied, the agreement between the largest and the smallest value of L is 14%. It is worth noting that the smallest values of the parameter L correspond to LJ SAFT-VR Mie and the Enskog-2σ model, whereas the largest values were obtained with SAFT-VR SW and from zero-density viscosities for all fluids studied. In future work, it will be interesting to explore other approaches to get good estimates for L.

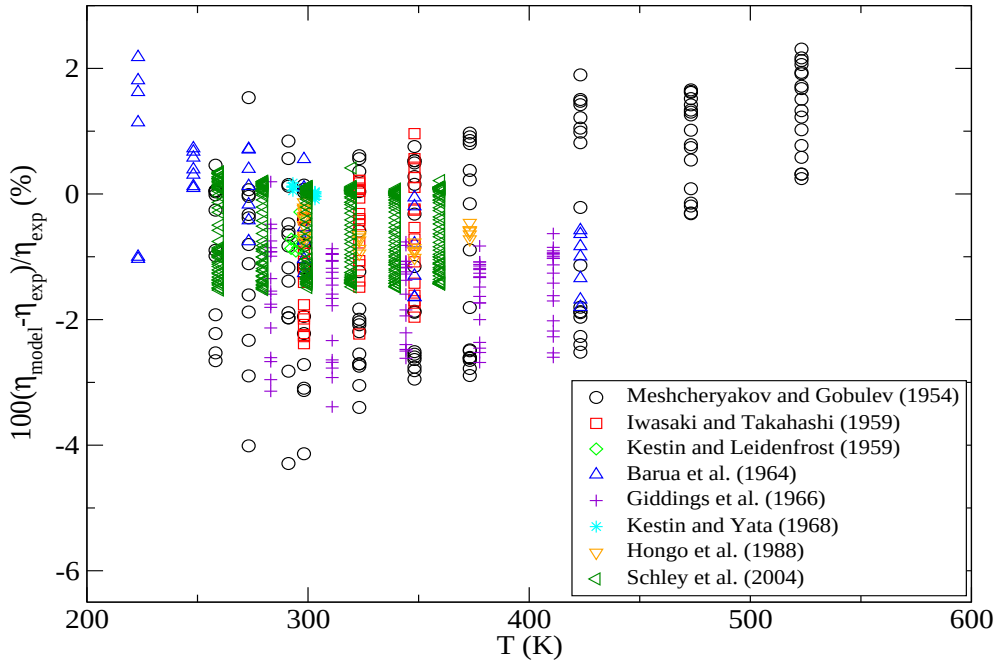

Figure 5.25: Percentage viscosity deviations, $100(\eta_{\mathrm{model}}-\eta_{\mathrm{exp}})/\eta_{\mathrm{exp}}$, between the Enskog-$2\sigma$ model and the primary experimental data sets for methane listed in table 5.2. The effective diameter of methane was obtained by means of Eq. (5.4) using the values of L obtained from the data at all temperatures.

Table 5.5: Length scaling parameter L obtained by the models described in the text. The fourth and fifth column show the maximum deviation and AAD evaluated over the full supercritical range, as described in subsection 5.1.9.

Fluid	Model	L	Max. deviation (%)	AAD (%)
CH_4	$\sigma_{0,x}/\sigma_{0,Ar}$	1.1106	21.7	7.0
CH_4	$(V_{c,x}/V_{c,Ar})^{1/3}$	1.0975	15.1	4.7
CH_4	$\sigma_{\text{CS-vdW},x}/\sigma_{\text{CS-vdW},Ar}$	1.1058	19.3	6.2
CH_4	$\sigma_{\text{SAFT-SW},x}/\sigma_{\text{SAFT-SW},Ar}$	1.1105	21.7	7.0
CH_4	$\sigma_{\text{SAFT-LJ},x}/\sigma_{\text{SAFT-LJ},Ar}$	1.0971	14.9	4.6
N_2	$\sigma_{0,x}/\sigma_{0,Ar}$	1.0842	13.4	5.1
N_2	$(V_{c,x}/V_{c,Ar})^{1/3}$	1.0652	5.9	2.4
N_2	$\sigma_{\text{CS-vdW},x}/\sigma_{\text{CS-vdW},Ar}$	1.0645	5.6	2.3
N_2	$\sigma_{\text{SAFT-SW},x}/\sigma_{\text{SAFT-SW},Ar}$	1.0803	11.6	4.5
N_2	$\sigma_{\text{SAFT-LJ},x}/\sigma_{\text{SAFT-LJ},Ar}$	1.0519	4.9	0.7
CO_2	$\sigma_{0,x}/\sigma_{0,Ar}$	1.1252	24.2	13.7
CO_2	$(V_{c,x}/V_{c,Ar})^{1/3}$	1.0804	6.9	4.5
CO_2	$\sigma_{\text{CS-vdW},x}/\sigma_{\text{CS-vdW},Ar}$	1.1252	24.2	13.8
CO_2	$\sigma_{\text{SAFT-SW},x}/\sigma_{\text{SAFT-SW},Ar}$	1.1504	37.6	18.5
CO_2	$\sigma_{\text{SAFT-LJ},x}/\sigma_{\text{SAFT-LJ},Ar}$	1.0721	18.5	4.0
SF_6	$\sigma_{0,x}/\sigma_{0,Ar}$	1.5679	42.9	18.9
SF_6	$(V_{c,x}/V_{c,Ar})^{1/3}$	1.3740	33.1	10.2
SF_6	$\sigma_{\text{SAFT-SW},x}/\sigma_{\text{SAFT-SW},Ar}$	1.4750	12.3	6.0
SF_6	$\sigma_{\text{SAFT-LJ},x}/\sigma_{\text{SAFT-LJ},Ar}$	1.3819	30.7	9.0

5.2 Molecular dynamics corrections

The aim of this section is to find and compare ways to extend the Enskog-2σ model to higher densities. We will focus on the extension of the Enskog-2σ model to higher densities at supercritical conditions, while, in the section 5.3, the focus will be on the liquid range. Throughout the section, argon will serve as model fluid since the experimental reference correlation for argon by (Lemmon & Jacobson, 2004) extends

to very high densities and pressures.

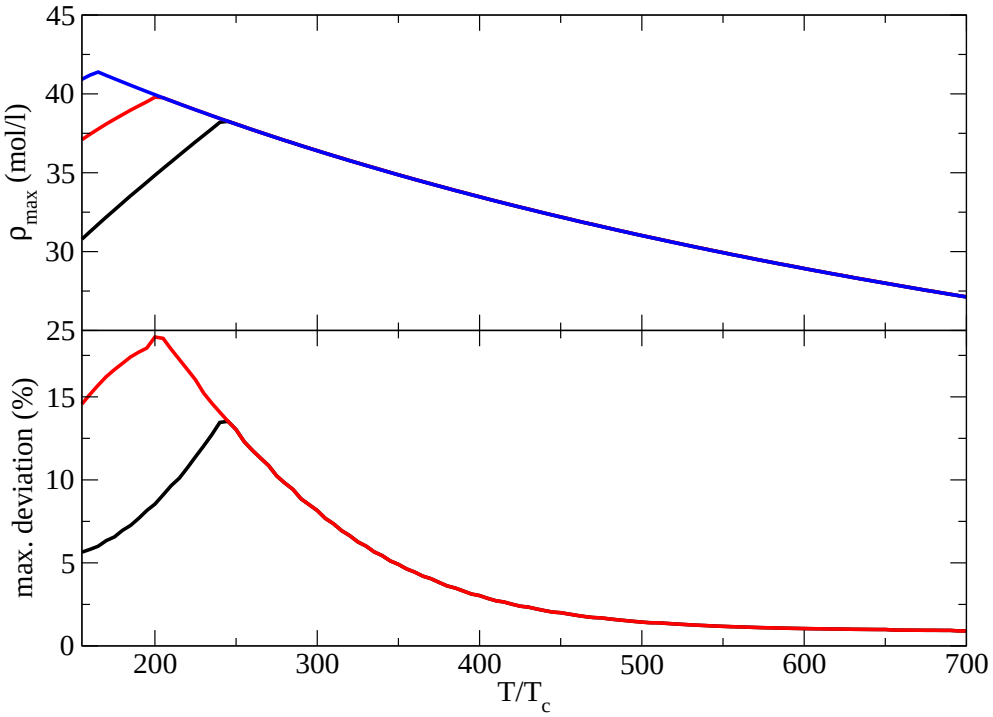

Figure 5.26: Enskog-2σ model without MD corrections up to y_s with $\sigma_{\max} = \sigma_\alpha$ (black lines) and $\sigma_{\max} = \sigma_{\text{mean}}$ (red lines). In the upper plot, the maximum density $\rho_{\max}$ is shown versus the temperature T, in the lower plot, the maximum deviation between model and experimental reference correlation for argon by (Lemmon & Jacobson, 2004). The blue line in the upper plot denotes the experimental maximum density.

5.2.1 Extension to higher densities without MD corrections

We first apply the Enskog-2σ model without MD corrections to illustrate the shortcomings in doing so. We distinguish two cases. In the first case, the maximum density is defined as

$$\rho_{\max,y_{s,\alpha}} = \min\left(\rho_{y_{s,\alpha}}, \rho_{\text{exp}}\right) \quad \text{where} \quad \rho_{y_{s,\alpha}} = \frac{0.494}{N_A \pi/6 \sigma_\alpha^3}, \tag{5.5}$$

in the second case, as

$$\rho_{\max,y_{s,\text{mean}}} = \min\left(\rho_{y_{s,\text{mean}}}, \rho_{\text{exp}}\right) \quad \text{where} \quad \rho_{y_{s,\text{mean}}} = \frac{0.494}{N_A \pi/6 \sigma_{\text{mean}}^3}. \tag{5.6}$$

The diameter σ_{mean} is defined as the mean value $(\sigma_\alpha + \sigma_\chi)/2$ of the effective diameters. The factor 0.494 in Eqs. (5.5) and (5.6) is equal to the packing fraction y_s up to which a hard sphere system represents still a stable fluid, see section 2.3. According to Fig. 5.26, choosing the maximum density $\rho_{\max,y_{s,\text{mean}}}$ yields maximum deviations up to 18.5% with a peak at $T = 200K$. Choosing the maximum density $\rho_{\max,y_{s,\alpha}}$ yields smaller deviations with a peak of the maximum deviation of 13.5% at $T = 245K$, however, the density range covered becomes markedly smaller than for the choice $\rho_{\max,y_{s,\text{mean}}}$. In section 5.2.2, we will see that, by making use of MD corrections, we can describe the experimental viscosity over a larger density range with smaller deviations than it has been possible without MD corrections.

5.2.2 Extension to higher densities with MD corrections

As molecular dynamics simulations show, Enskog's viscosity expression describes a hard sphere fluid up to a packing fraction of $y = 0.31$. Beyond this packing fraction, Enskog's formula deviates from the simulation results and does not describe the hard sphere model fluid correctly. These deviations can be corrected by the use of a multiplicative factor f_{MD} as already discussed in section 2.3. The factor f_{MD} is a function of the packing fraction only and thus depends on the effective diameter σ chosen through y. We denote the corresponding σ as σ_{MD} and investigate the following choices:

- $\sigma_{\text{MD}} = \sigma_\alpha =: \sigma_{\text{MD},\alpha}$,
- $\sigma_{\text{MD}} = \sigma_\chi =: \sigma_{\text{MD},\chi}$,
- $\sigma_{\text{MD}} = (\sigma_\alpha + \sigma_\chi)/2 =: \sigma_{\text{MD,mean}}$,
- $\sigma_{\text{MD}} = \sqrt{\sigma_\alpha \sigma_\chi} =: \sigma_{\text{MD,geo}}$.

For a given choice of σ_{MD}, we define the maximum density $\rho_{\max}$ consistently by

$$\rho_{\max} = \min\left(\rho_{y_s}, \rho_{\text{exp}}\right) \quad \text{where} \quad \rho_{y_s} = \frac{0.494}{N_A \pi / 6 \sigma_{\text{MD}}^3}. \tag{5.7}$$

The maximum densities for the different choices of σ_{MD} are shown in the upper plot in Fig. 5.27. For $\sigma_{\text{MD},\chi}$, the density range extends to the maximum density of the experimental reference correlation by (Lemmon & Jacobson, 2004). For $\sigma_{\text{MD,geo}}$ and $\sigma_{\text{MD,mean}}$, the maximum density is equal to the maximum density ρ_{exp} of the experimental correlation for $T/T_c \geq 1.16$ and up to 0.5 mol/l (0.8 mol/l) smaller than ρ_{exp}

for $T/T_c < 1.16$ and $\sigma_{\mathrm{MD,geo}}$ ($\sigma_{\mathrm{MD,mean}}$). If we choose $\sigma_{\mathrm{MD},\alpha}$, the maximum density becomes, at low temperatures, clearly smaller than the maximum densities for the other choices and reaches only a value of 36.5 mol/l for T close to T_c whereas the maximum density of the experimental correlation is 40.9 mol/l at this temperature.

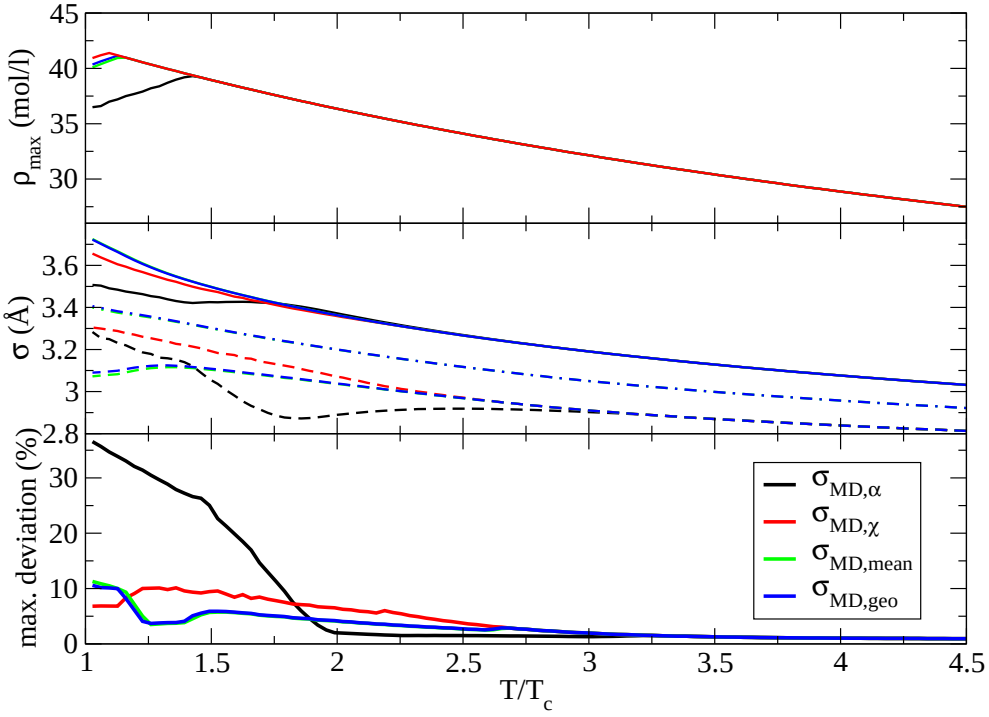

Figure 5.27: Enskog-2σ model with MD corrections applied to argon. In the upper plot, the maximum density is depicted versus the reduced temperature. The black, red, green, blue lines correspond to the Enskog-2σ model with $\sigma_{\mathrm{MD},\alpha}$, $\sigma_{\mathrm{MD},\chi}$, $\sigma_{\mathrm{MD,mean}}$, $\sigma_{\mathrm{MD,geo}}$. The effective diameters are shown in the middle plot; σ_α is denoted by the solid lines, σ_χ by the dashed lines, $\sigma_{\mathrm{MD,mean}}$ by the green dash-dotted line and $\sigma_{\mathrm{MD,geo}}$ by the blue dash-dotted lined. The lower plot depicts the maximum deviation between the models and the experimental reference correlation by (Lemmon & Jacobson, 2004). The maximum density of the experimental reference correlation is equivalent to the red line in the upper plot.

The optimised effective diameter for the approaches with $\sigma_{\mathrm{MD,mean}}$ and $\sigma_{\mathrm{MD,geo}}$ are found to be almost identical and differ less than 0.61% from one another. For $T/T_c \geq 2.89$, the density range does not extend into the region where MD corrections are relevant such that all approaches become equivalent to each other and the effective

diameters take the same value for all approaches. For lower temperatures, on the contrary, the effective diameters depend clearly on the approach chosen. For the lowest temperature, for example, σ_α for $\sigma_{\mathrm{MD},\alpha}$ ($\sigma_{\mathrm{MD},\chi}$) is about 6% (1.9%) smaller than for the model with $\sigma_{\mathrm{MD,mean}}$. Those deviations are relatively large considering how sensitive the viscosity depends on σ_α (compare with section 5.1.3 for example).
According to the lower plot in Fig. 5.27, the approach with $\sigma_{\mathrm{MD},\alpha}$ leads to large deviations up to 36%. The other approaches reproduce the viscosity distinctively better within 11.2%. The models with $\sigma_{\mathrm{MD,mean}}$ and $\sigma_{\mathrm{MD,geo}}$ result in almost identical maximum deviations which reach their peak value at the lowest temperature close to $T = T_c$. The approach with $\sigma_{\mathrm{MD},\chi}$ performs better than the approach with $\sigma_{\mathrm{MD,mean}}$ at low temperatures but results in larger deviations at intermediate temperatures: at $T/T_c = 1.3$ for instance, the maximum deviation between model and experimental correlation is 3.2% for $\sigma_{\mathrm{MD,mean}}$ and 9.8% for $\sigma_{\mathrm{MD},\chi}$. The correlative power of the models with $\sigma_{\mathrm{MD,mean}}$ and $\sigma_{\mathrm{MD},\chi}$ will be compared to each other in greater detail in section 5.2.3 where we test the models directly against primary experimental data.

5.2.3 Comparison with primary experimental data

In the upper plots of Fig. 5.28, we compare the Enskog-2σ model with $\sigma_{\mathrm{MD},\chi}$ from the previous section to primary experimental data for argon. In Fig. 5.29, we do the same for the model with $\sigma_{\mathrm{MD,mean}}$. In the lower plots of the figures, we depict for comparison the deviations between the experimental reference correlation for argon by (Lemmon & Jacobson, 2004) and the primary experimental data.
Both of the models reproduce the bulk of the data within 5% and all data points with densities less than 30mol/l are obtained within 6%. Only for the data sets by (Kurin & Golubev, 1974) and (van der Gulik & Trappeniers, 1986) which extend to densities larger than 30mol/l, deviations larger than 6% are observed. The data points by (Kurin & Golubev, 1974) with deviations larger than 6% appear at pressures larger than 300 MPa and deviate generally in the order of 5% from the viscosity correlation by (Lemmon & Jacobson, 2004) itself. Thus, the data points by (Kurin & Golubev, 1974) might not be as accurate as the other measurements and, consequently, in terms of reliable primary data, the model with $\sigma_{\mathrm{MD},\chi}$ performs as well as the model with $\sigma_{\mathrm{MD,mean}}$ at temperatures above $200K$.

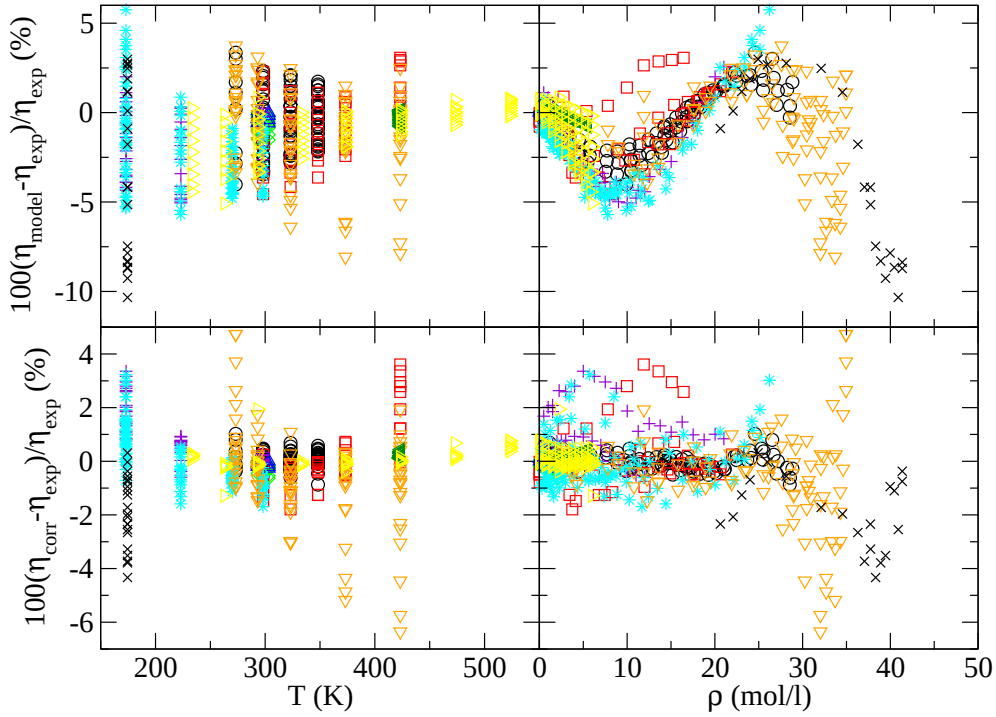

Figure 5.28: Upper plots: Percentage viscosity deviations, $100(\eta_{\mathrm{model}} - \eta_{\mathrm{exp}})/\eta_{\mathrm{exp}}$, between the Enskog-2$\sigma$ model with $\sigma_{\mathrm{MD},\chi}$ and the primary experimental data sets for argon listed in table 5.3. Lower plots: Percentage viscosity deviations, $100(\eta_{\mathrm{corr}} - \eta_{\mathrm{exp}})/\eta_{\mathrm{exp}}$, between the experimental reference correlation for argon by (Lemmon & Jacobson, 2004) and the primary experimental data sets for argon listed in table 5.3. On the left hand side, the deviations are depicted versus the temperature, on the right hand side, versus the density. The black dots refer to the primary experimental data by (Michels *et al.*, 1954), the red squares to the data by (Makita, 1957), the green diamonds to the data by (Kestin & Nagashima, 1964), the blue triangles to the data by (DiPippo *et al.*, 1967), the violet pluses to the data by (Gracki *et al.*, 1969), the cyan stars to the data by (Haynes, 1973a), the orange triangles to the data by (Kurin & Golubev, 1974), the black crosses to the data by (van der Gulik & Trappeniers, 1986), the dark green triangles to the data by (Wilhelm & Vogel, 2000) and the yellow triangles to the data by (Evers *et al.*, 2002).

The measurements by (van der Gulik & Trappeniers, 1986) are performed at $T = 175K$. The model with $\sigma_{\mathrm{MD,mean}}$ reproduces the data points by (van der Gulik & Trappeniers, 1986) within 8.1% and performs slightly better than the model with $\sigma_{\mathrm{MD},\chi}$ which correlates the measurements within 10.4%. Thus, in terms of the primary data, the model with $\sigma_{\mathrm{MD,mean}}$ seems to perform marginally better than the model with

$\sigma_{\mathrm{MD},\chi}$. This result reverses the observation in the last section where it appeared that the model with $\sigma_{\mathrm{MD},\chi}$ reproduces the experimental correlation by (Lemmon & Jacobson, 2004) at lower temperatures better than the model with $\sigma_{\mathrm{MD,mean}}$. Altogether, in terms of the primary data sets available, the models with $\sigma_{\mathrm{MD},\chi}$ and $\sigma_{\mathrm{MD,mean}}$ perform similarly well and one should not attempt to ascribe one of the models better correlative power based on the results in the previous section.

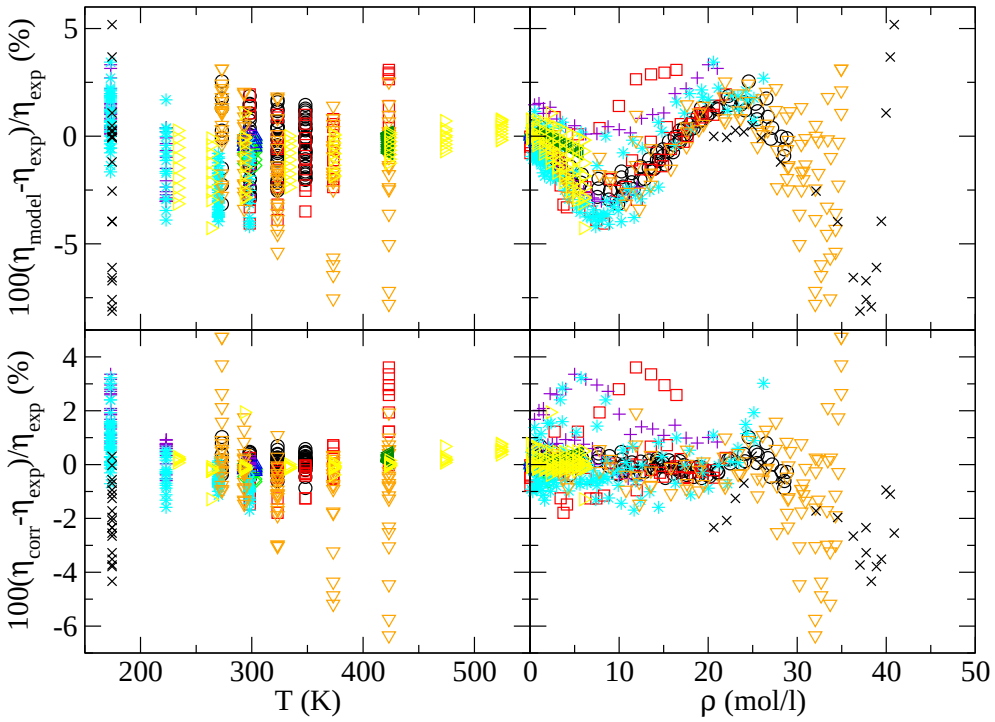

Figure 5.29: Upper plots: Percentage viscosity deviations, $100(\eta_{\mathrm{model}} - \eta_{\mathrm{exp}})/\eta_{\mathrm{exp}}$, between the Enskog-2$\sigma$ model with $\sigma_{\mathrm{MD,mean}}$ and the primary experimental data sets for argon listed in table 5.3. Lower plots: Percentage viscosity deviations, $100(\eta_{\mathrm{corr}} - \eta_{\mathrm{exp}})/\eta_{\mathrm{exp}}$, between the experimental reference correlation for argon by (Lemmon & Jacobson, 2004) and the primary experimental data sets for argon listed in table 5.3. On the left hand side, the deviations are depicted versus the temperature, on the right hand side, versus the density. The black dots refer to the primary experimental data by (Michels *et al.*, 1954), the red squares to the data by (Makita, 1957), the green diamonds to the data by (Kestin & Nagashima, 1964), the blue triangles to the data by (DiPippo *et al.*, 1967), the violet pluses to the data by (Gracki *et al.*, 1969), the cyan stars to the data by (Haynes, 1973a), the orange triangles to the data by (Kurin & Golubev, 1974), the black crosses to the data by (van der Gulik & Trappeniers, 1986), the dark green triangles to the data by (Wilhelm & Vogel, 2000) and the yellow triangles to the data by (Evers *et al.*, 2002).

5.2.4 Magnitude of the MD correction factor

The magnitude of the MD correction factor is investigated in Fig. 5.30. The Enskog-2σ model with $\sigma_{\mathrm{MD,mean}}$ is applied to argon and the MD correction factor is plotted for several isotherms versus the density. The results obtained are very similar for the model with $\sigma_{\mathrm{MD,geo}}$. Up to moderate densities, the Enskog model reproduces correctly a hard sphere fluid, no MD corrections are needed and the MD correction factor has a value of 1. Above 25.1 mol/l for $T = 155K$, 26.4 mol/l for $T = 200K$, 28.2 mol/l for $T = 250K$, 30.0 mol/l for $T = 300K$, the MD correction factors deviates from 1 and starts correcting Enskog's viscosity expression for high density effects. The corresponding pressures for the kick in of the MD corrections are 16MPa, 56MPa, 117MPa and 192MPa at the temperatures $155K$, $200K$, $250K$ and $300K$. With increasing density, the MD correction factor grows monotonically until it reaches a value of 2.06 at $T = 155K$, 1.51 at $T = 200K$, 1.17 at $T = 250K$, 1.07 at $T = 300K$. With increasing temperature, the experimental maximum density ρ_{exp} increases until, for $T > 400K$, ρ_{exp} becomes so small that no MD corrections are needed and the correction factor is equal to 1 over the whole density range. Moreover, since σ_{MD} decreases in general with the temperature, cf. Fig. 5.27, the MD correction factor at a given density decreases as well (unless its value is already 1). Thus, while MD corrections are important at low temperatures, they play a minor role at high temperatures.

5.2.5 Use of MD corrections with optimisation of the effective diameters up to moderate densities

The σ in the MD correction factor Eq. (2.42) corresponds to the diameter of the spheres when the correction factor is used in the Enskog-1σ model. In the Enskog-2σ model, there is no such clear correspondence between σ_{MD} and the effective diameters σ_α and σ_χ. The diameter σ_{MD} is neither directly related to the excluded volume nor to the collision rate. In fact, the relations chosen in section 5.2.2 between σ_{MD} and the effective diameters σ_α and σ_χ is arbitrary and purely empirical. Hence, including the MD correction factor in the optimisation of σ_α and σ_χ, as done in section 5.2.2, weakens the link of the diameters to the excluded volume and the collision rate. In this section, we look at alternatives that do not include the MD correction factor in the optimisation of σ_α and σ_χ and thus keep a full link between the effective diameters

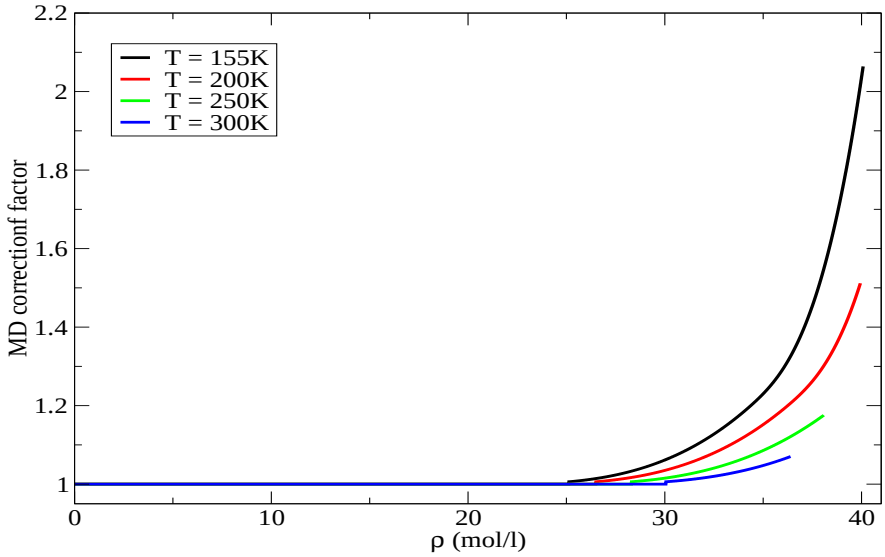

Figure 5.30: Magnitude of the MD correction factor for several isotherms versus the density ρ. The Enskog-2σ model with $\sigma_{\mathrm{MD,mean}}$ is applied to argon.

and the excluded volume as well as the collision rate.

In Fig. 5.31, the effective diameters σ_α and σ_χ have been optimised up to

$$\rho^* = \frac{0.31}{N_A \pi / 6 \sigma_{\mathrm{mean}}^3} \quad \text{with} \quad \sigma_{\mathrm{mean}} = \frac{\sigma_\alpha + \sigma_\chi}{2} \tag{5.8}$$

to minimise the maximum deviation between model and the experimental reference correlation by (Lemmon & Jacobson, 2004) for argon. Up to ρ^*, no MD correction factor is used such that the link between the effective diameters and the excluded volume as well as the collision rate is kept fully. Furthermore, two alternatives are investigated in Fig. 5.31:

(i) σ_{MD} is obtained from

$$\sigma_{\mathrm{MD}} = \sigma_{\mathrm{mean}} =: \sigma_{\mathrm{MD,mean}}, \tag{5.9}$$

(ii) σ_{MD} is optimised at each temperature by minimising the maximum deviation between model and experimental reference correlation

$$\sigma_{\mathrm{MD}} =: \sigma_{\mathrm{MD,opti}}. \tag{5.10}$$

In both cases, we define the maximum density by

$$\rho_{\max} = \min\left(\rho_{y_{s,\mathrm{mean}}}, \rho_{\exp}\right) \quad \text{where} \quad \rho_{y_{s,\mathrm{mean}}} = \frac{0.494}{N_A\pi/6\sigma^3_{\mathrm{mean}}}. \tag{5.11}$$

We find that $\rho_{\exp} \leq \rho_{y_{s,\mathrm{mean}}}$ such that the maximum density is actually given by the maximum density of the experimental reference correlation. As the lower plot in Fig. 5.31 shows, the maximum deviation between model and experimental reference correlation reaches a value of 22.7% for the choice $\sigma_{\mathrm{MD,mean}}$. This deviation is relatively large, so the approach with $\sigma_{\mathrm{MD,mean}}$ is deemed to lack correlative power for the density range chosen. For the choice $\sigma_{\mathrm{MD,opti}}$, the deviations between model and experimental reference correlation remains below 10% for temperatures above $190K$ and reach their peak value of 15.4% at the lowest temperature. The second approach provides more correlative power but, with $\sigma_{\mathrm{MD,opti}}$, an additional effective diameter has to be optimised such that the approach requires the optimisation of three temperature dependent diameters.

5.3 Liquid range

Up to now, we have applied the Enskog-2σ model to supercritical conditions. In this section, we discuss how one can extend the model into the liquid range. Several simple fluids are investigated over the temperature and pressure ranges shown in table 5.6. As no data for sulphur fluoride was available, we included ethane and oxygen in our analysis that are as well simple fluids with non-polar and fairly spherical molecules. First, we investigate the extension of the Enskog-2σ model into the liquid range without MD corrections. Then, we show that it is beneficial to make use of MD corrections and describe ways how this can be done effectively. Finally, we investigate whether the effective diameters exhibit a universal behaviour which could allow to predict the viscosity of one fluid from the knowledge of the viscosity of a reference fluid.

5.3.1 Liquid range without MD corrections

We first apply the Enskog-2σ model without MD corrections to argon in the liquid range. We distinguish three cases with a different choice for the maximum density:

$$\rho_{\max,y_{s,\alpha}} = \min\left(\rho_{y_{s,\alpha}}, \rho_{\exp}\right) \quad \text{where} \quad \rho_{y_{s,\alpha}} = \frac{0.494}{N_A\pi/6\sigma^3_{\alpha}}, \tag{5.12}$$

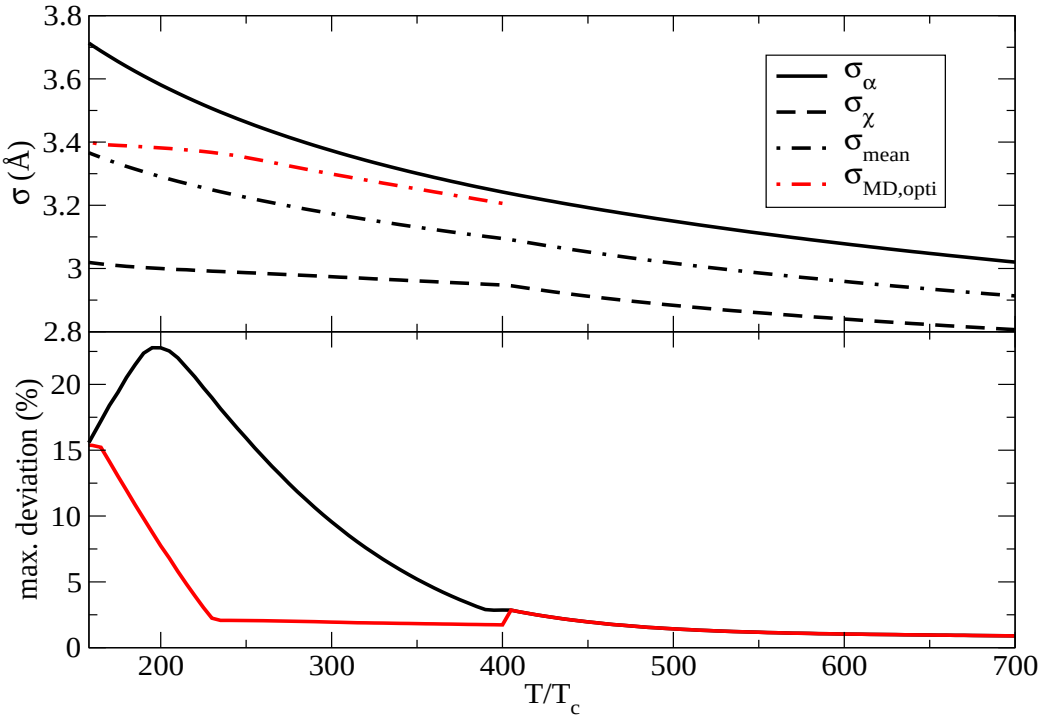

Figure 5.31: Extension of the Enskog-2σ model to high densities with optimisation of σ_α and σ_χ up to moderate densities given by ρ^* in Eq. (5.8). Upper plot: σ_α (solid black line), σ_χ (dashed black line), $\sigma_{\mathrm{MD,mean}}$ (dash-dotted black line) and $\sigma_{\mathrm{MD,opti}}$ (dash-dotted red line). Lower plot: Maximum deviation of the model with $\sigma_{\mathrm{MD,mean}}$ (black line) and the model with $\sigma_{\mathrm{MD,opti}}$ (red line) from the experimental reference correlation by (Lemmon & Jacobson, 2004).

$$\rho_{\mathrm{max},y_{s,\chi}} = \min\left(\rho_{y_{s,\chi}}, \rho_{\mathrm{exp}}\right) \quad \text{where} \quad \rho_{y_{s,\alpha}} = \frac{0.494}{N_A\pi/6\sigma_\chi^3}, \tag{5.13}$$

$$\rho_{\mathrm{max},y_{s,\mathrm{mean}}} = \min\left(\rho_{y_{s,\mathrm{mean}}}, \rho_{\mathrm{exp}}\right) \quad \text{where} \quad \rho_{y_{s,\mathrm{mean}}} = \frac{0.494}{N_A\pi/6\sigma_{\mathrm{mean}}^3}. \tag{5.14}$$

All approaches reproduce the experimental correlation within 10% (see the lower plot in Fig. 5.32). Thus, the accuracy of the models is satisfactory, in particular, for the approach with $\rho_{\mathrm{max},y_{s,\alpha}}$ which reproduces the experimental correlation within 2.6%. The shortcoming of the models without MD corrections can be seen in the upper plot of Fig. 5.32. The maximum densities of the models are clearly smaller than the maximum density of the experimental correlation such that the density ranges covered are relatively small. The reason for the small maximum densities is as follows: neglecting the MD correction factor leads to a viscosity expression which underpredicts

Table 5.6: Summary of the experimental reference correlations for simple fluids used in the liquid range. The pressure range of the correlations extends from the vapour pressure to the maximum pressure stated in the table.

Fluid	Max. pressure (MPa)	T-range (K)	Viscosity correlation
Ar	400	90-150	(Lemmon & Jacobson, 2004)
CH_4	100	115-190	(Vogel *et al.*, 2000)
C_2H_6	60	250-305	(Hendl *et al.*, 1994)
N_2	100	85-125	(Lemmon & Jacobson, 2004)
CO_2	300	270-300	(Vesovic *et al.*, 1990; Fenghour *et al.*, 1998)
O_2	80	85-144	(Lemmon & Jacobson, 2004)

the viscosity of a hard sphere fluid. This results in comparatively large values of the effective diameters (compare middle plot of Fig. 5.32 with the effective diameters calculated in section 5.3.2) and leads according to Eqs. (5.12), (5.13), (5.14) to small maximum densities.

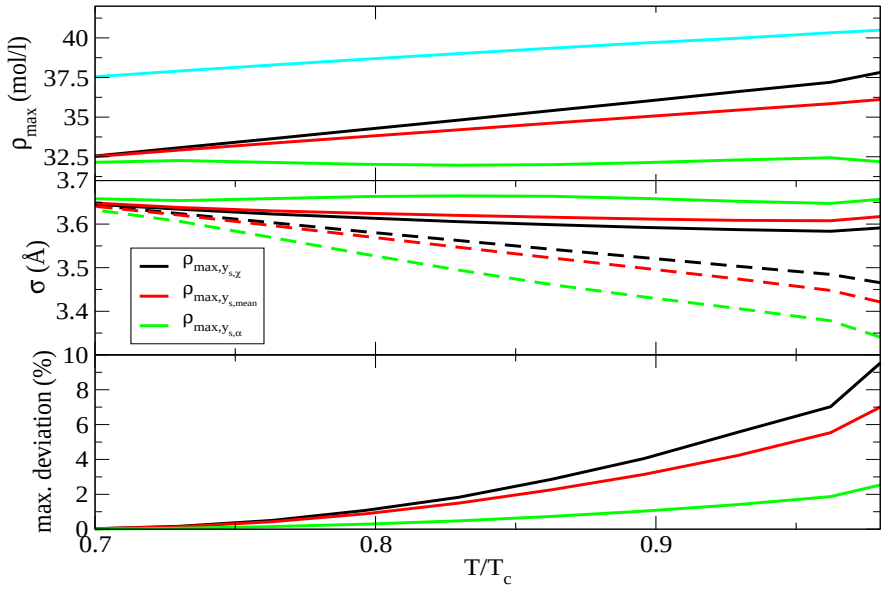

Figure 5.32: Application of the Enskog-2σ model without MD corrections to the liquid range of argon. The model with maximum density $\rho_{\max,y_{s,\chi}}$, $\rho_{\max,y_{s,\mathrm{mean}}}$, $\rho_{\max,y_{s,\alpha}}$ is denoted by the black, red, green lines. The maximum density (upper plot), optimised effective diameters (middle plot) and maximum deviation between model and experimental reference correlation (lower plot) are plotted versus the reduced temperature. The cyan line in the upper plot depicts the maximum density of the experimental reference correlation for argon by (Lemmon & Jacobson, 2004).

5.3.2 Liquid range with MD corrections

The densities of the fluids under investigation are in general large in the liquid range. In section 5.2.2, we have shown that, for the supercritical range, it is beneficial to incorporate MD corrections in the Enskog-2σ model when the model is extended to high densities. We will test now if the incorporation of MD corrections will also improve the results in the liquid range. To do so, we make again use of the factor f_{MD}, Eq. (2.42), which is a function of the packing fraction only and thus depends on the effective diameter σ chosen through y. Analogously to section 5.2.2, we denote the corresponding σ as σ_{MD} and investigate the following choices:

- $\sigma_{\mathrm{MD}} = \sigma_\chi =: \sigma_{\mathrm{MD},\chi}$,
- $\sigma_{\mathrm{MD}} = (\sigma_\alpha + \sigma_\chi)/2 =: \sigma_{\mathrm{MD,mean}}$.

For a given choice of σ_{MD}, we define the maximum density $\rho_{\max}$ consistently by

$$\rho_{\max} = \min\left(\rho_{y_s}, \rho_{\exp}\right), \quad \text{where} \quad \rho_{y_s} = \frac{0.494}{N_A \pi / 6 \sigma_{\mathrm{MD}}^3}. \tag{5.15}$$

The effective diameters σ_α and σ_χ are optimised by minimising the maximum deviation between model and experimental reference correlation from the saturated liquid density obtained from the correlations in table 5.6 to $\rho_{\max}$.

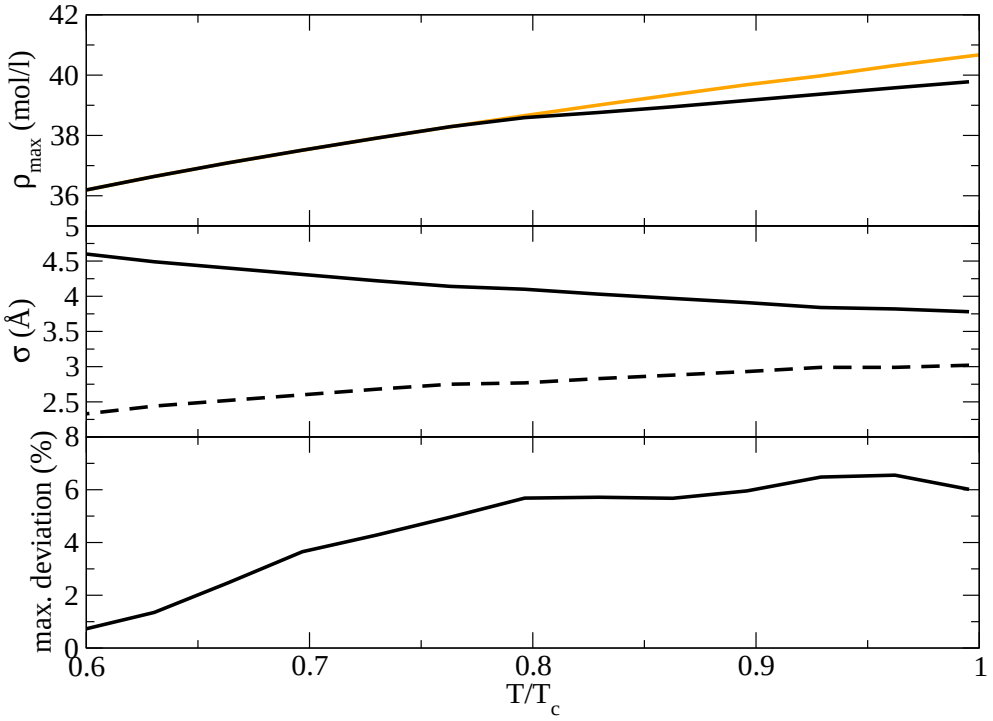

Figure 5.33: Application of the Enskog-2σ model with $\sigma_{\mathrm{MD,mean}}$ to the liquid range of argon. The maximum density (upper plot), optimised effective diameters (middle plot) and maximum deviation between model and experimental reference correlation (lower plot) are depicted versus the reduced temperature. In the middle plot, σ_α is denoted by the solid lines and σ_χ by the dashed lines. The orange the upper plot shows the maximum density of the experimental reference correlation for argon by (Lemmon & Jacobson, 2004).

In Fig. 5.33, we depict the results for argon and the choice $\sigma_{\mathrm{MD,mean}}$. In comparison to the results in the previous section, the maximum density for argon increases from 37.8 mol/l to 39.6 mol/l at $T/T_c = 0.99$ and from 32.4 mol/l to 36.1 mol/l at $T/T_c = 0.7$. The increase in the maximum density leads in particular to an extension of the temperature range from a minimum temperature of $T/T_c = 0.7$ to $T/T_c = 0.6$. According to the

middle plot, σ_α decreases monotonically with the temperature (this behaviour is the same as found before for the supercritical range; see, for example, Fig. 5.7) while σ_χ increases monotonically with T. As the lower plot of the figure shows, the model reproduces the liquid viscosity of argon with a maximum deviation of 6.6%. Fig. 5.34 presents the results of the model with $\sigma_{\mathrm{MD,mean}}$ for carbon dioxide, nitrogen, ethane and oxygen. As the upper plot of the figure shows, the density range of the model extends to the maximum density of the experimental correlation for methane if $T/T_c \geq 0.7$ and, for the other four fluids, at all subcritical temperatures. According to the lower plot in Fig. 5.34, the Enskog-2σ model with $\sigma_{\mathrm{MD,mean}}$ reproduces the liquid viscosity of ethane, methane, oxygen, nitrogen and carbon dioxide with maximum deviations of 1.4%, 2.1%, 5.3%, 5.7% and 6.7%, respectively. The temperature dependence of the corresponding effective diameters is shown in the middle plot of Fig. 5.34. For all five fluids, σ_α decreases again monotonically with the temperature while σ_χ increases monotonically with T except for oxygen for which σ_χ decreases monotonically with T.

The results of the Enskog-2σ model with the choice $\sigma_{\mathrm{MD},\chi}$ are shown in Fig. 5.35. The density range of the model for argon increases in comparison to the choice $\sigma_{\mathrm{MD,mean}}$ and extends now to the maximum density ρ_{exp} of the experimental correlation over the whole temperature range. Furthermore, ρ_{exp} is reached for carbon dioxide, nitrogen, oxygen and ethane over the whole temperature range and, for methane, for $T/T_c \geq 0.63$. According to the lower plot in Fig. 5.35, the Enskog-2σ model with $\sigma_{\mathrm{MD},\chi}$ reproduces the viscosity of carbon dioxide, ethane, nitrogen, oxygen, methane and argon within 2.1%, 2.5%, 2.7%, 3.9%, 4.1% and 4.6%, respectively. As the middle plot of Fig. 5.35 shows, the effective diameters decrease with the temperature in general. The exceptions are σ_α for methane, which increases with T from $T/T_c = 0.78$ to $T/T_c = 0.85$, σ_χ for carbon dioxide, which increases with T from $T/T_c = 0.89$ to $T/T_c = 0.94$, as well as σ_χ for oxygen from $T/T_c = 0.55$ to $T/T_c = 0.62$. All those exceptions are found to be insignificant though. This has been tested as follows: in the temperature interval in which the respective diameter increases with temperature, we set the diameter constant and optimize the other diameter. This approach leads to only marginally larger deviations between model and experimental reference correlation which increase less than 0.5%. Consequently, the liquid viscosity of all fluids can be modelled well within 5% by the Enskog-2σ model with the choice $\sigma_{\mathrm{MD},\chi}$ and effective diameters that decrease monotonically with the temperature.

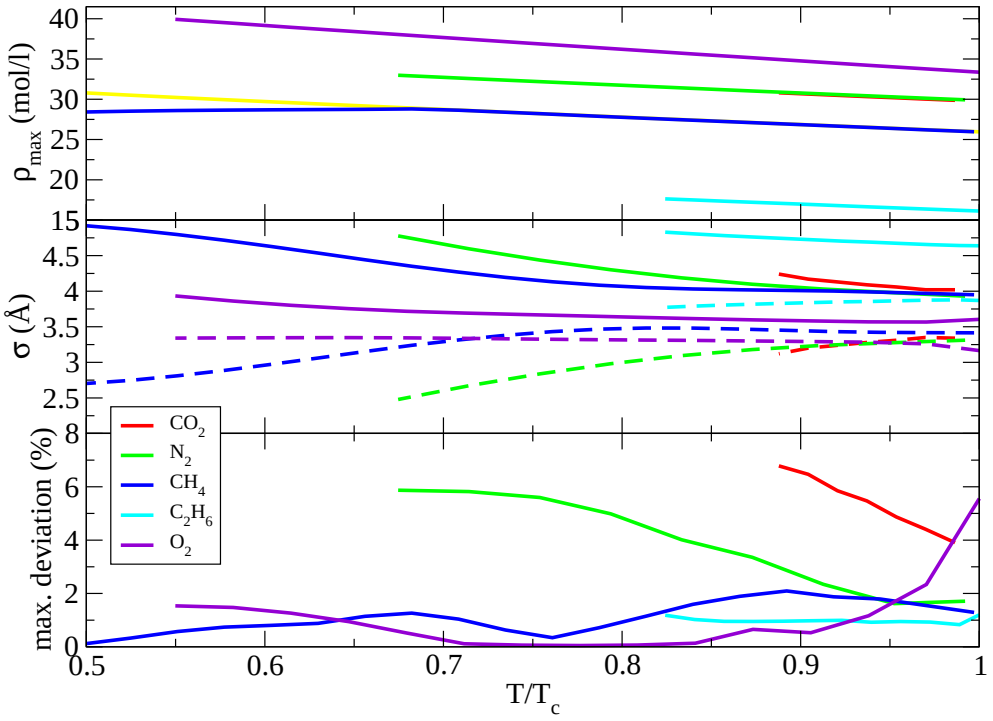

Figure 5.34: Application of the Enskog-2σ model with $\sigma_{\mathrm{MD,mean}}$ to the liquid range of carbon dioxide, nitrogen, methane, ethane and oxygen. The maximum density (upper plot), optimised effective diameters (middle plot) and maximum deviation between model and experimental reference correlation (lower plot) are depicted versus the reduced temperature. In the middle plot, σ_α is denoted by the solid lines and σ_χ by the dashed lines. The yellow line in the upper plot shows the maximum density of the experimental reference correlation for methane by (Vogel *et al.*, 2000).

Altogether, both approaches with MD corrections extend to larger densities than the approaches without MD corrections. Moreover, we find that the Enskog-2σ model with $\sigma_{\mathrm{MD},\chi}$ performs better than the model with $\sigma_{\mathrm{MD,mean}}$ because it (a) extends to higher maximum densities and (b) reproduces the experimental correlation in general more accurately. A further comparison of the accuracy of the models will be given in section 5.3.3 where the models are tested directly against primary experimental data.

The model with the choice $\sigma_{\mathrm{MD}} = \sigma_\alpha$ has also been investigated. The main drawback is that the model extends to relatively small maximum densities. For example, for argon at $T/T_c = 0.86$, the maximum density is only 27.9 mol/l while it is 38.9 mol/l and 39.3 mol/l for the models with $\sigma_{\mathrm{MD,mean}}$ and $\sigma_{\mathrm{MD},\chi}$. Consequently, the model with

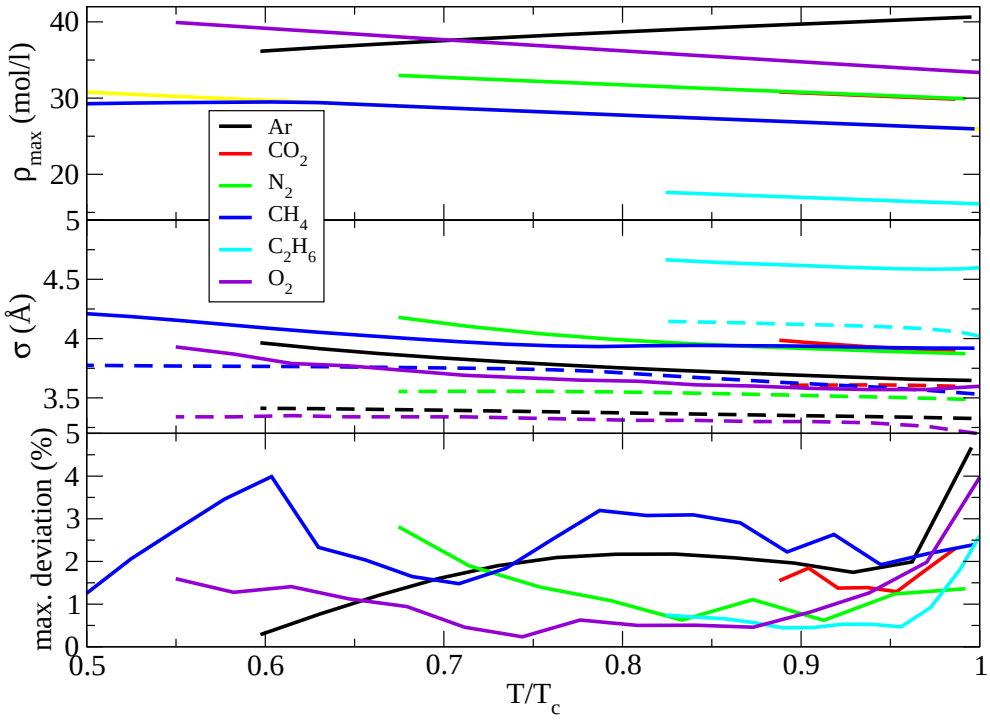

Figure 5.35: Application of the Enskog-2σ model with $\sigma_{\mathrm{MD},\chi}$ to the liquid range of argon, carbon dioxide, nitrogen, methane, ethane and oxygen. The maximum density (upper plot), optimised effective diameters (middle plot) and maximum deviation between model and experimental reference correlation (lower plot) are depicted versus the reduced temperature. In the middle plot, σ_α is denoted by the solid lines and σ_χ by the dashed lines. The yellow line in the upper plot shows the maximum density of the experimental reference correlation for methane by (Vogel *et al.*, 2000).

$\sigma_{\mathrm{MD}} = \sigma_\alpha$ is also restricted to relatively large temperatures, for instance, $T/T_c \geq 0.86$ for argon and $T/T_c \geq 0.79$ for methane.

5.3.3 Comparison with primary experimental data

The Enskog-2σ model with the choice $\sigma_{\mathrm{MD,mean}}$ and the model with the choice $\sigma_{\mathrm{MD},\chi}$ are applied to the primary experimental liquid data of argon in Fig. 5.36. The data is reproduced within 5% except for three data points by (Haynes, 1973a) when the model with $\sigma_{\mathrm{MD},\chi}$ is used. These data points, however, also deviate more than 4% from the experimental reference correlation by (Lemmon & Jacobson, 2004) such that the significance of those points is questionable. If we ignore the three data points, the

model with the choices $\sigma_{\mathrm{MD,mean}}$ and $\sigma_{\mathrm{MD},\chi}$ perform similarly well. In Fig. 5.37, both models are tested against the primary experimental liquid data of methane. Again, both approaches perform similarly well except for two points by (Slyusar *et al.*, 1974) for which the deviations are larger than 5% when the model with $\sigma_{\mathrm{MD},\chi}$ is used. The measured viscosity value at $T = 138K$ by (Slyusar *et al.*, 1974) where the largest deviation of 5.9% occurs deviates also about 3.7% from the experimental reference correlation by (Vogel *et al.*, 2000) and hence its significance is questionable. Finally, Fig. 5.38 shows the deviations between the two models and the primary experimental liquid data of carbon dioxide. At temperatures above 295K, the model show about the same accuracy in reproducing the primary data. This is despite the fact that the model $\sigma_{\mathrm{MD},\chi}$ deviates from two points more than 6% because these measurements deviate also more than 4.4% from the experimental reference correlations by (Vesovic *et al.*, 1990; Fenghour *et al.*, 1998). At $T = 280K$, the model with $\sigma_{\mathrm{MD},\chi}$ correlates the data by (Van der Gulik, 1997) clearly better than the model $\sigma_{\mathrm{MD,mean}}$. This observation agrees with the fact that, at lower temperatures, the model with $\sigma_{\mathrm{MD},\chi}$ reproduces the experimental reference correlation better than the model with $\sigma_{\mathrm{MD,mean}}$ (compare Figs. 5.34 and 5.35).

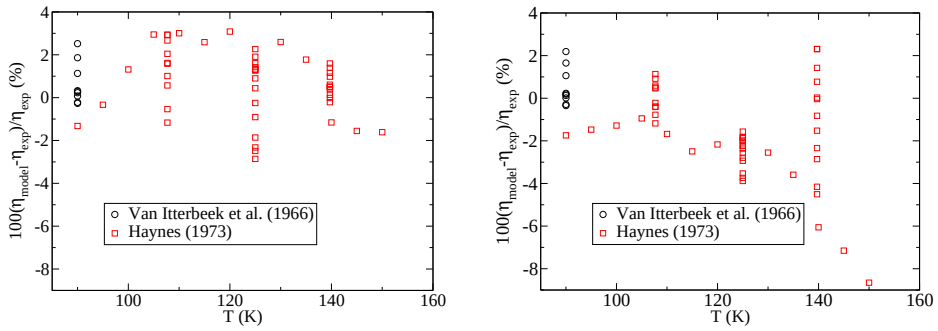

Figure 5.36: Application of the Enskog-2σ model to liquid primary experimental data of argon by (Van Itterbeek *et al.*, 1966) and (Haynes, 1973a). Plot (a) is for the model with the choice $\sigma_{\mathrm{MD,mean}}$, plot (b) for the choice $\sigma_{\mathrm{MD},\chi}$.

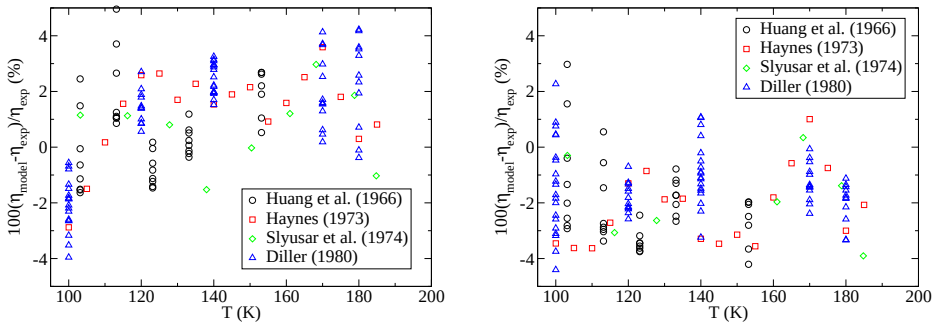

Figure 5.37: Application of the Enskog-2σ model to liquid primary experimental data of methane by (Huang *et al.*, 1966), (Haynes, 1973b), (Slyusar *et al.*, 1974) and (Diller, 1980). Plot (a) is for the model with the choice $\sigma_{\mathrm{MD,mean}}$, plot (b) for the choice $\sigma_{\mathrm{MD},\chi}$.

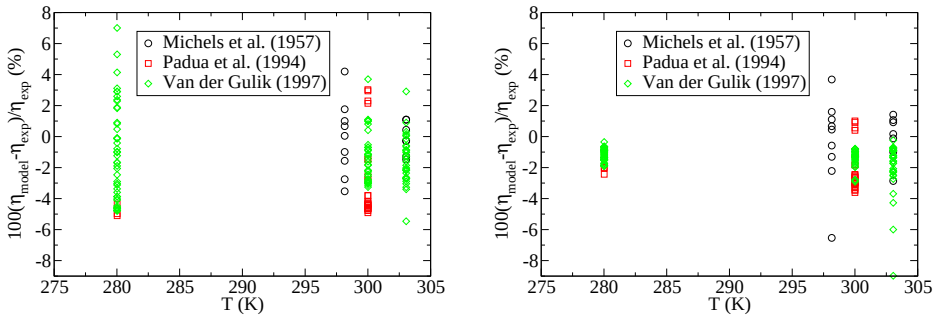

Figure 5.38: Application of the Enskog-2σ model to liquid primary experimental data of carbon dioxide by (Michels *et al.*, 1957), (Padua *et al.*, 1994) and (Van der Gulik, 1997). Plot (a) is for the model with the choice $\sigma_{\mathrm{MD,mean}}$, plot (b) for the choice $\sigma_{\mathrm{MD},\chi}$.

5.3.4 Model sensitivity to the effective diameters

Next, we investigate the sensitivity of the models introduced in section 5.3.2 to the effective diameters σ_α and σ_χ. The Enskog-2σ model with the choice $\sigma_{\mathrm{MD,mean}}$ is analysed in Fig. 5.39. The best choices for the effective diameters lie on an almost straight line. If one of the diameters is chosen with a reasonable value, the other diameter has to be determined quite accurately to reproduce the experimental reference correlation well. For argon, if σ_χ is chosen between 2.6Å and 2.85Å, σ_α can be varied less than 0.9% to obtain deviations smaller than 7.5%, and if σ_α is chosen between 3.6Å and 3.85Å, σ_χ can be varied less than 1.5% to obtain deviations smaller than 7.5%. Analogously for methane, if σ_χ is chosen between 3.25Å and 3.6Å, σ_α can be varied less than 0.8% to obtain deviations smaller than 7.5%, and if σ_α is chosen between 4.0Å and 4.35Å, σ_χ can be varied less than 1.1% to obtain deviations smaller than 7.5%. This situation is different to the one encountered in section 5.1.3 where the Enskog-2σ model was applied without MD corrections to supercritical conditions up to moderate densities and where the model was clearly more sensitive to σ_α than to σ_χ. That the Enskog-2σ model with $\sigma_{\mathrm{MD,mean}}$ is sensitive to both effective diameters can be explained as follows: at the highest density, the MD correction factor equals approximately 1.8 for methane at $T/T_c = 0.75$ and 2.0 for argon at $T/T_c = 0.75$. Thus, a good prediction of the MD correction factor is important to reproduce the viscosity well. Both σ's appear to the power of 9 in the MD correction factor, Eq. (2.42). Consequently, the value of the MD correction factor is equally sensitive to both effective diameters and hence the Enskog-2σ model with $\sigma_{\mathrm{MD,mean}}$ is sensitive to both diameters.

The Enskog-2σ model with the choice $\sigma_{\mathrm{MD},\chi}$ is analysed in Fig. 5.40. Due to the fact that the value of the MD correction factor depends here on σ_χ but not on σ_α, the model is more sensitive to σ_χ than to σ_α. Both effective diameters have to be determined fairly accurate though to correlate the viscosity within 5% as can be seen from the rather small blue to dark-blue region in the figure.

In Fig. 5.41, we depict the sensitivity plots for argon at two further temperatures. In the plot on the left hand side, we set $T/T_c = 0.65$, in the plot on the right hand side, $T/T_c = 0.9$. The maximum deviation is shown between the Enskog-2σ model with $\sigma_{\mathrm{MD,mean}}$ and the experimental reference correlation by (Lemmon & Jacobson, 2004). In both cases, the best choices of the effective diameters lie again on an almost

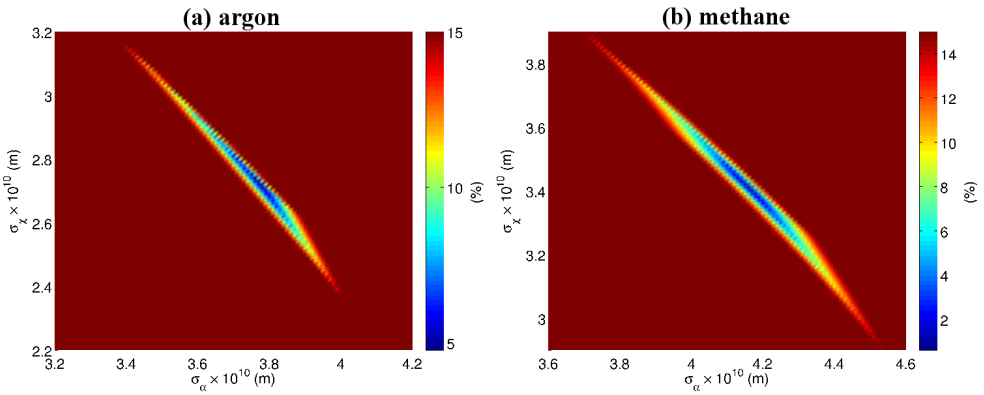

Figure 5.39: Maximum deviation between the Enskog-2σ model with $\sigma_{\mathrm{MD,mean}}$ and the experimental reference correlations at $T/T_c = 0.75$ for different values of the two effective diameters σ_α and σ_χ. The colour represents the value of the maximum deviation. Maximum deviations larger than 15% are depicted uniformly in dark red. (a) argon, (b) methane.

straight line as in Fig. 5.39. Moreover, we find that the model sensitivity to the choice of the effective diameters increases with increasing temperature. The reason being for this observation is that, with increasing temperature, the density interval in which we model the viscosity increases. For $T/T_c = 0.65$, the liquid densities extend from 33.2 mol/l to 36.9 mol/l, while for $T/T_c = 0.9$, the liquid densities range from 25.3 mol/l to 39.1 mol/l. For the same reason, the sensitivity Enskog-2σ model with $\sigma_{\mathrm{MD},\chi}$ to the choice of the effective diameters increases with increasing temperature. The corresponding results are shown in Fig. 5.42.

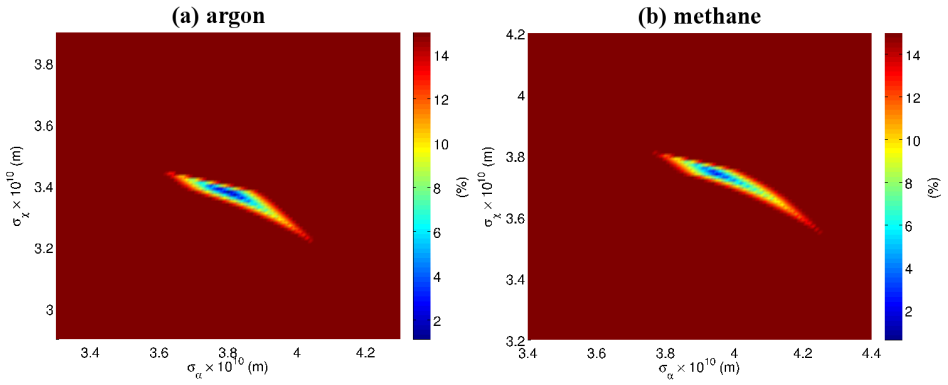

Figure 5.40: Maximum deviation between the Enskog-2σ model with $\sigma_{\mathrm{MD},\chi}$ and the experimental reference correlations at $T/T_c = 0.75$ for different values of the two effective diameters σ_α and σ_χ. The colour represents the value of the maximum deviation. Maximum deviations larger than 15% are depicted uniformly in dark red. (a) argon, (b) methane.

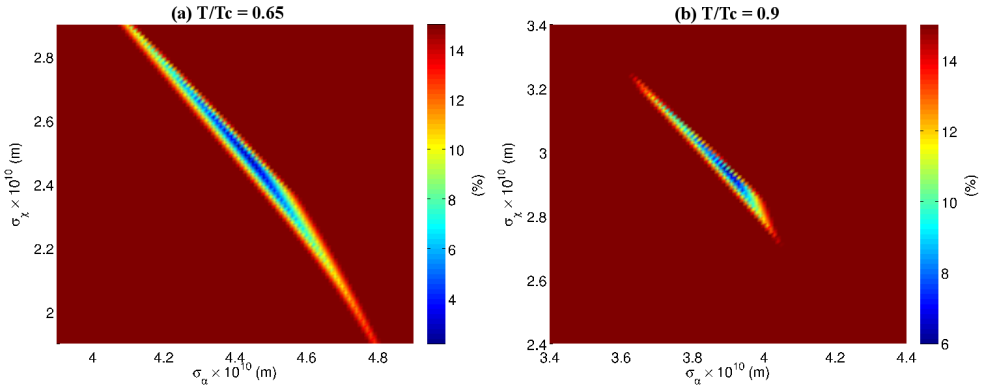

Figure 5.41: Maximum deviation between the Enskog-2σ model with $\sigma_{\mathrm{MD,mean}}$ and the experimental reference correlation for argon and different values of the two effective diameters σ_α and σ_χ. The colour represents the value of the maximum deviation. Maximum deviations larger than 15% are depicted uniformly in dark red. (a) $T/T_c = 0.65$, (b) $T/T_c = 0.9$.

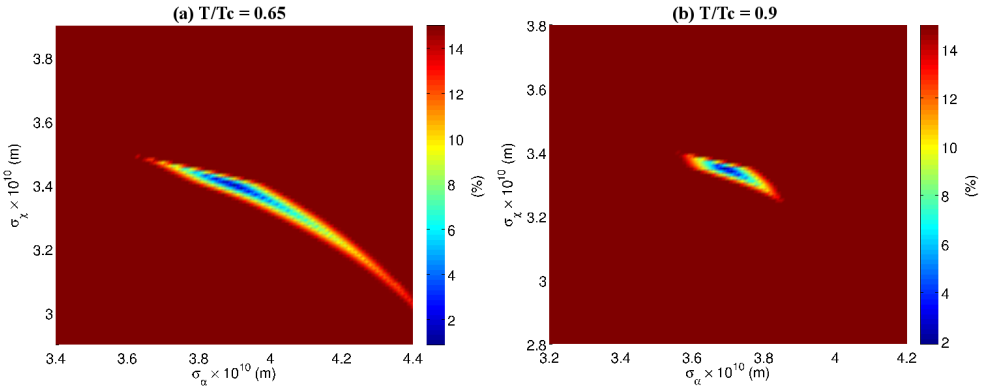

Figure 5.42: Maximum deviation between the Enskog-2σ model with $\sigma_{\mathrm{MD},\chi}$ and experimental reference correlation for argon and different values of the two effective diameters σ_α and σ_χ. The colour represents the value of the maximum deviation. Maximum deviations larger than 15% are depicted uniformly in dark red. (a) $T/T_c = 0.65$, (b) $T/T_c = 0.9$.

5.3.5 Universal behaviour in the liquid range

In section 5.1.9, we have observed a universal behaviour of the effective diameters for the Enskog-2σ model in the supercritical range up to moderate densities. This allowed for the possibility of predicting the viscosity of one fluid from the knowledge of another. In this section, we will investigate whether we can find a universal behaviour for the effective diameters in the liquid range. We focus the analysis on the Enskog-2σ model with $\sigma_{\mathrm{MD},\chi}$ which, according section 5.3.2, has performed best in correlating the viscosity in the liquid range and has reproduced the experimental correlations of all six fluids within 4.6% (see Fig. 5.35). As reference fluid, we choose argon again for which the Enskog-2σ model covers a large temperature and pressure range (from $T/T_c = 0.6$ to $T/T_c = 1.0$ and from the vapour pressure to 400MPa). In the upper plot in Fig. 5.43, we scale the σ_χ's of carbon dioxide, nitrogen, methane, ethane and oxygen such that they superimpose the one of argon and scale the σ_α's with the same constant factor. This approach is motivated by the fact that the model is more sensitive to σ_χ than to σ_α (see section 5.3.4). Choosing the same length scaling factor for both effective diameters leads to deviations up to 5.2% between the optimised σ_α of argon and the scaled σ_α for methane. According to section 5.3.4, the Enskog-2σ model with $\sigma_{\mathrm{MD},\chi}$ is

fairly sensitive to the choice of σ_α. Therefore, the deviations in σ_α are expected to lead to larger deviations between model and experimental reference correlation for methane.

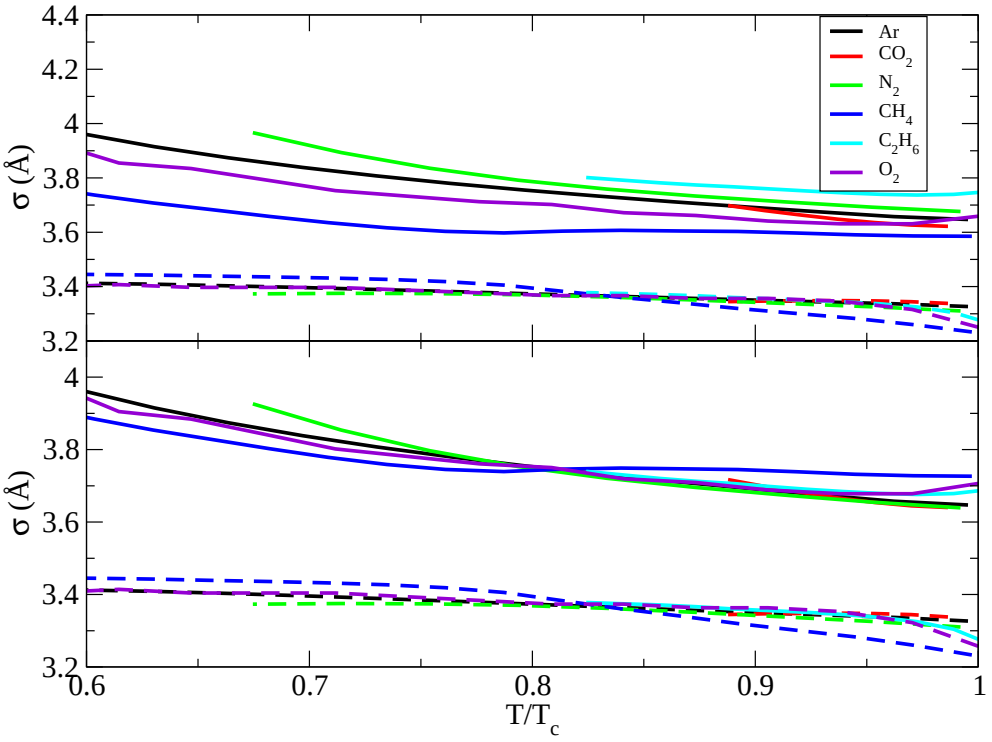

Figure 5.43: Scaled effective diameters in the Enskog-2σ model with $\sigma_{\mathrm{MD},\chi}$ versus reduced temperature T/T_c. The solid lines depict the scaled σ_α and the dashed lines the scaled σ_χ. In the upper plot, both effective diameters are scaled with the same length scaling parameter for a given fluid, in the lower plot, the effective diameters are scaled with two different length scaling parameters for a given fluid.

As further computations show, independent of the choice of the scaling parameter, we encounter indeed deviations up to at least 30% for methane. To obtain better viscosity predictions, we allow for a second constant length scaling parameter with which σ_α is scaled independently of σ_χ. We denote the length scaling parameters as L_α as well as L_χ and scale the effective diameters as follows:

$$\sigma_{\alpha,x}(T/T_{c,x}) = \mathrm{L}_\alpha \sigma_{\alpha,Ar}(T/T_{c,Ar}), \tag{5.16}$$

$$\sigma_{\chi,x}(T/T_{c,x}) = \mathrm{L}_\chi \sigma_{\chi,Ar}(T/T_{c,Ar}). \tag{5.17}$$

By using two different length scaling parameters, the effective diameters of methane,

nitrogen, carbon dioxide, ethane and oxygen can be superimposed with the ones of argon with deviations less than 2% as the lower plot in Fig. 5.43 shows and we can expect to reproduce the experimental viscosity reasonably well.

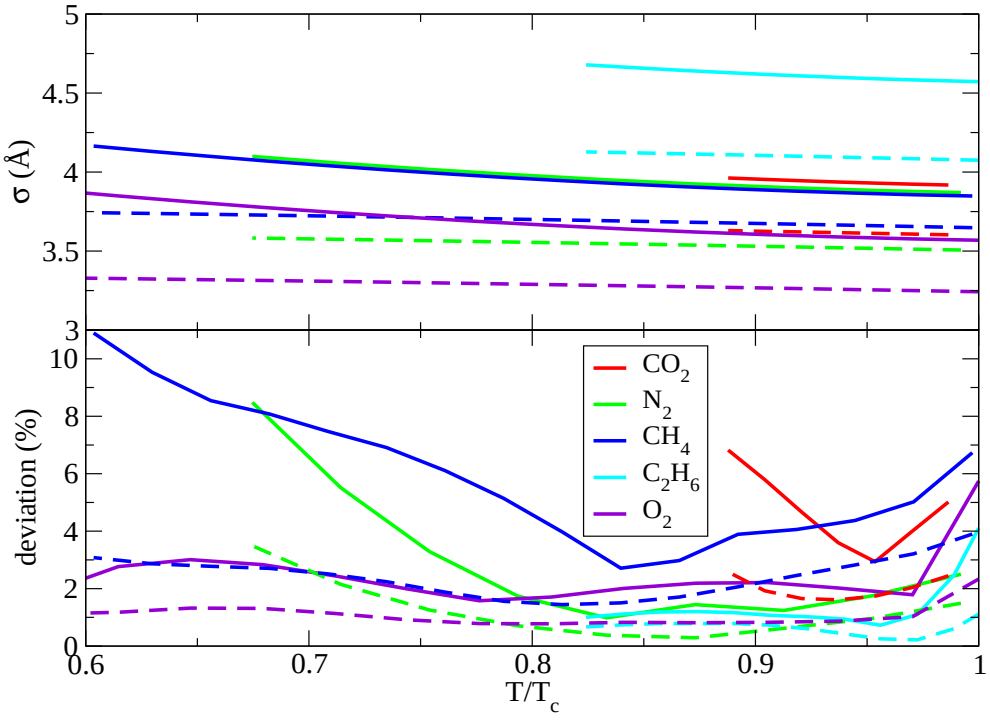

Figure 5.44: Application of the Enskog-2σ model with $\sigma_{\mathrm{MD},\chi}$ to the liquid range of carbon dioxide, nitrogen, methane, ethane and oxygen. The effective diameters in the upper plot have been calculated by scaling the effective diameters of argon with the length scaling parameters obtained by minimising the AAD over all subcritical conditions (see table 5.7 for the scaling parameters). σ_α is denoted by the solid lines and σ_χ by the dashed lines. The lower plot shows the maximum deviation (solid lines) and AAD (dashed lines) between model and experimental reference correlations versus the reduced temperature T/T_c.

We investigate two ways to obtain the length scaling parameters:

(i) choose the length scaling parameters to minimise the AAD between model and the experimental reference correlation for all subcritical conditions, i.e., minimise

$$\mathrm{AAD} = \sum_{\text{all data}} \frac{|\eta_{\mathrm{model}} - \eta_{\mathrm{exp}}|}{\eta_{\mathrm{exp}}}. \tag{5.18}$$

(ii) choose the length scaling parameters to minimise the AAD between model and the experimental reference correlation along the isotherm at $T^* = (T_c - T_{\mathrm{low}})/2$

where T_{low} is the lower bound of the temperature range stated in table 5.6 for a given fluid. Note that, if $T_{\text{low}}/T_c < 0.6$, i.e., if T_{low}/T_c lies outside the range of the reference correlation of argon, we set $T_{\text{lowest}} = 0.6T_c$ (this is the case for methane here).

Table 5.7: Length scaling parameters L_α and L_χ obtained by minimizing the AAD between the Enskog-2σ model and the experimental reference correlations. The maximum deviations and AADs have been computed over the liquid range stated in table 5.6 for $T/T_c \geq 0.6$.

Fluid	Model	L_α	L_χ	Max. deviation (%)	AAD (%)
CH_4	all T	1.0545	1.0967	10.9	2.5
CH_4	$T = T^*$	1.0478	1.1016	6.0	3.0
C_2H_6	all T	1.2531	1.2254	4.9	0.6
C_2H_6	$T = T^*$	1.2515	1.2285	5.3	0.6
N_2	all T	1.0601	1.0537	8.5	1.1
N_2	$T = T^*$	1.0625	1.0521	6.4	1.2
CO_2	all T	1.0727	1.0823	6.8	2.0
CO_2	$T = T^*$	1.0765	1.0794	9.0	2.0
O_2	all T	0.9758	0.9768	5.7	0.8
O_2	$T = T^*$	0.9680	0.9829	8.4	2.0

Table 5.7 presents the values of the scaling parameters obtained in each case together with how well the viscosity of each fluid is predicted as measured by the AAD and the maximum deviation. Fig. 5.44 and Fig. 5.45 illustrate the deviations for case (i) and (ii) observed for carbon dioxide, nitrogen, methane, ethane and oxygen as a function of the reduced temperature. In both cases, the density range covered by the model reaches for all fluids from the saturated liquid density to the maximum density ρ_{exp} of the experimental reference correlations given in table 5.6. As summarised in table 5.7, the experimental viscosity correlations are reproduced fairly well with AADs smaller than 3% (as computed from Eq. (5.18)) and maximum deviations smaller than 10.9%. Case (ii) leads to larger AADs than case (i) as the AAD is minimised just along one isotherm, however, in terms of the maximum deviations, both approaches perform

similarly well. For case (ii), we validate the model against primary viscosity data in the next section.

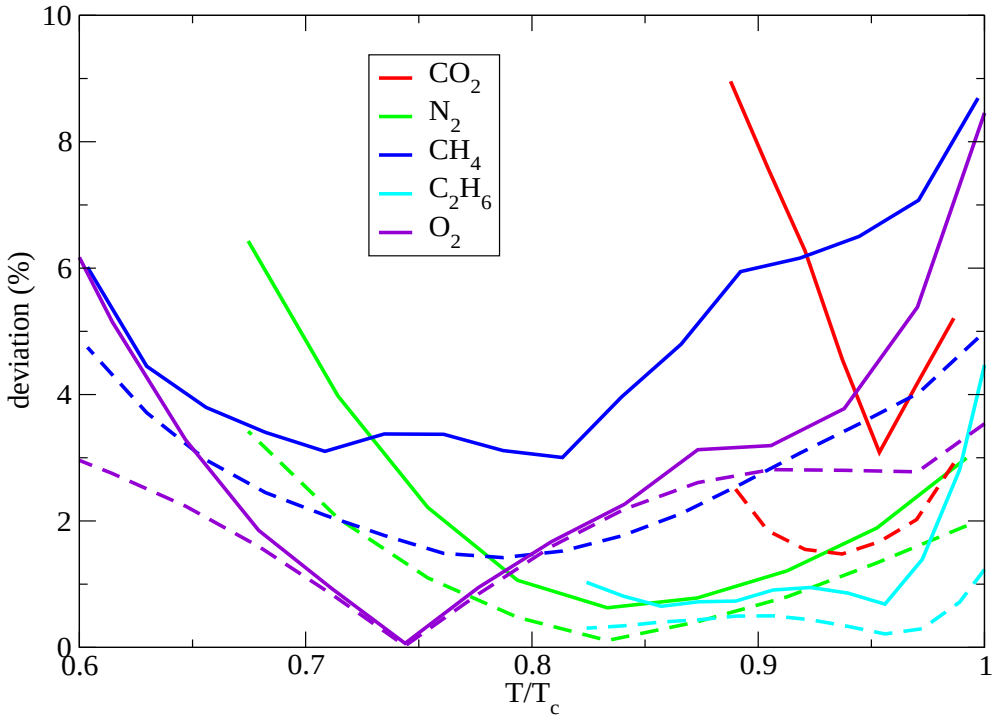

Figure 5.45: Maximum deviation (solid lines) and AAD (dashed lines) between Enskog-2σ model with $\sigma_{\mathrm{MD},\chi}$ and experimental reference correlations versus the reduced temperature T/T_c for carbon dioxide, nitrogen, methane, ethane and oxygen. The effective diameters have been calculated by scaling the effective diameters of argon with the length scaling parameters obtained from the isotherm along T^* (see table 5.7 for the scaling parameters).

5.3.6 Comparison with primary experimental data

The Enskog-2σ model from section 5.3.5 with scaling parameters obtained from one isotherm (case (ii)) is compared to primary experimental data of methane, ethane and carbon dioxide. The results for methane are shown in Fig. 5.46. The model reproduces the primary experimental data of methane within 11%. In general, the model overestimates the viscosity at low temperatures as well as high densities and underestimates the viscosity at high temperatures as well as low densities. The same trends are found for ethane according to Fig. 5.47. The primary data of ethane is

reproduced within 7.8%. As shown in Fig. 5.48, the model correlates the data of carbon dioxide within 6.4%. As for methane and ethane, the model underestimates the experimental viscosity at low densities for the data set by (Van der Gulik, 1997).

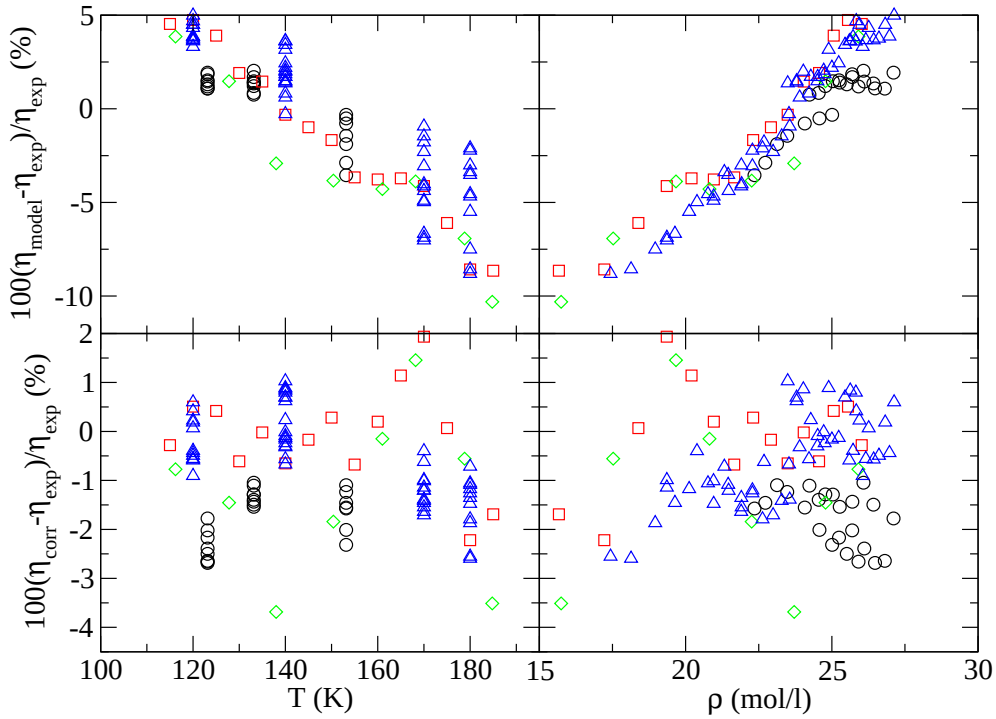

Figure 5.46: Upper plots: Percentage viscosity deviations, $100(\eta_{\mathrm{model}} - \eta_{\mathrm{exp}})/\eta_{\mathrm{exp}}$, between the Enskog-2$\sigma$ model with length scaling parameters from case (ii) in section 5.3.5 summarised in table 5.7 to liquid primary experimental data of methane. Lower plots: Percentage viscosity deviations, $100(\eta_{\mathrm{corr}} - \eta_{\mathrm{exp}})/\eta_{\mathrm{exp}}$, between the experimental reference correlation for methane by (Vogel *et al.*, 2000) and the primary experimental data sets. On the left hand side, the deviations are depicted versus the temperature, on the right hand side, versus the density. The black dots refer to the primary experimental data by (Huang *et al.*, 1966), the red squares to the data by (Haynes, 1973a), the green diamonds to the data by (Slyusar *et al.*, 1974), the blue triangles to the data by (Diller, 1980).

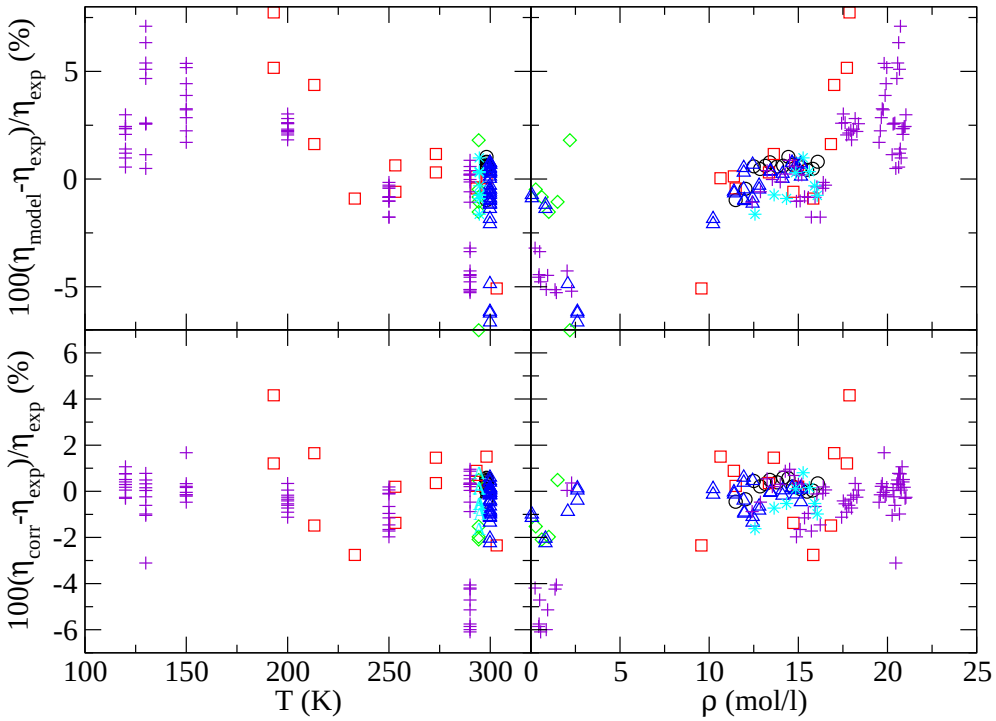

Figure 5.47: Upper plots: Percentage viscosity deviations, $100(\eta_{\mathrm{model}} - \eta_{\mathrm{exp}})/\eta_{\mathrm{exp}}$, between the Enskog-2$\sigma$ model with length scaling parameters from case (ii) in section 5.3.5 summarised in table 5.7 to liquid primary experimental data of ethane. Lower plots: Percentage viscosity deviations, $100(\eta_{\mathrm{corr}} - \eta_{\mathrm{exp}})/\eta_{\mathrm{exp}}$, between the experimental reference correlation for ethane by (Hendl *et al.*, 1994) and the primary experimental data sets. On the left hand side, the deviations are depicted versus the temperature, on the right hand side, versus the density. The black dots refer to the primary experimental data by (Baron *et al.*, 1959), the red squares to the data by (Swift *et al.*, 1960), the green diamonds to the data by (Eakin *et al.*, 1962), the blue triangles to the data by (Carmichael & Sage, 1963a), the violet pluses the data by (Diller & Saber, 1981), the cyan stars the data by (Diller & Ely, 1989).

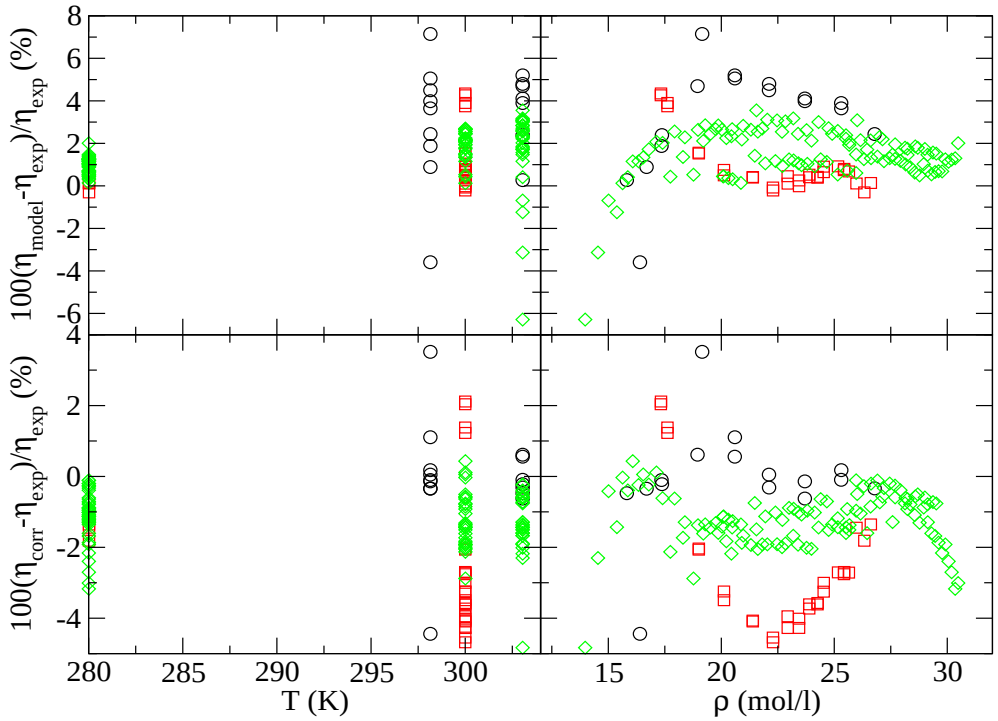

Figure 5.48: Upper plots: Percentage viscosity deviations, $100(\eta_{\text{model}} - \eta_{\text{exp}})/\eta_{\text{exp}}$, between the Enskog-2$\sigma$ model with length scaling parameters from case (ii) in section 5.3.5 summarised in table 5.7 to liquid primary experimental data of carbon dioxide. Lower plots: Percentage viscosity deviations, $100(\eta_{\text{corr}} - \eta_{\text{exp}})/\eta_{\text{exp}}$, between the experimental reference correlation for carbon dioxide by (Fenghour *et al.*, 1998) and the primary experimental data sets. On the left hand side, the deviations are depicted versus the temperature, on the right hand side, versus the density. The black dots refer to the primary experimental data by (Michels *et al.*, 1957), the red squares to the data by (Padua *et al.*, 1994), the green diamonds to the data by (Van der Gulik, 1997).

5.4 Full temperature range

The Enskog-2σ model has been applied to supercritical conditions in section 5.1 and to liquid conditions in section 5.3. In this section, we will discuss the application of the Enskog-2σ model over the full temperature range shown in table 5.8 which extends from low temperatures in the liquid range up to high temperatures in the supercritical range. For example, the temperature range covered for argon extends from $T/T_c = 0.6$ to $T/T_c = 4.6$ and, for nitrogen, from $T/T_c = 0.67$ to $T/T_c = 4.8$. We will also

investigate whether one can observe a conformal behaviour of the effective diameters over the whole temperature range.

Table 5.8: Summary of viscosity correlations used for the full temperature range.

Fluid	P-range (MPa)	T-range (K)	Viscosity correlation
Ar	0-400	90-700	(Lemmon & Jacobson, 2004)
CH_4	0-100	115-600	(Vogel *et al.*, 2000)
C_2H_6	0-60	250-500	(Hendl *et al.*, 1994)
N_2	0-100	85-600	(Lemmon & Jacobson, 2004)
CO_2	0-300	270-700	(Vesovic *et al.*, 1990; Fenghour *et al.*, 1998)
O_2	0-80	85-700	(Lemmon & Jacobson, 2004)

5.4.1 Viscosity correlation over the full temperature range

The Enskog-2σ model with $\sigma_{\mathrm{MD},\chi}$ from section 5.3.2 has successfully correlated the viscosity of argon, methane, ethane, nitrogen, carbon dioxide and oxygen within 5% in the liquid range and will serve as model of choice to be applied over the full temperature range. To achieve this, the model has to be extended in the supercritical range. Hitherto, the effective diameters are optimised at supercritical temperatures by minimising the maximum deviation between model and experimental correlation from the zero density limit up to the maximum density given by

$$\rho_{\max} = \min\left(\rho_{y_s}, \rho_{\exp}\right), \quad \text{where} \quad \rho_{y_s} = \frac{0.494}{N_A \pi / 6 \sigma_\chi^3}. \tag{5.19}$$

As the upper plot of Fig. 5.49 shows, the maximum density is for all fluids and temperatures equal to the maximum density $\rho_{\exp}$ of the experimental correlation. The only exception is $\rho_{\max}$ of methane for $T/T_c \leq 0.63$ (see also Fig. 5.35). The maximum deviations between model and experimental reference correlations are depicted in the lower plot. The Enskog-2σ model with $\sigma_{\mathrm{MD},\chi}$ succeeds in correlating the viscosity fairly well over the whole temperature range with maximum deviations of 4.7%, 6.2%, 6.3%, 6.4%, 6.6%, 9.7% for nitrogen, methane, carbon dioxide, ethane, oxygen and argon. The corresponding effective diameters will be investigated in more detail in section 5.4.2.

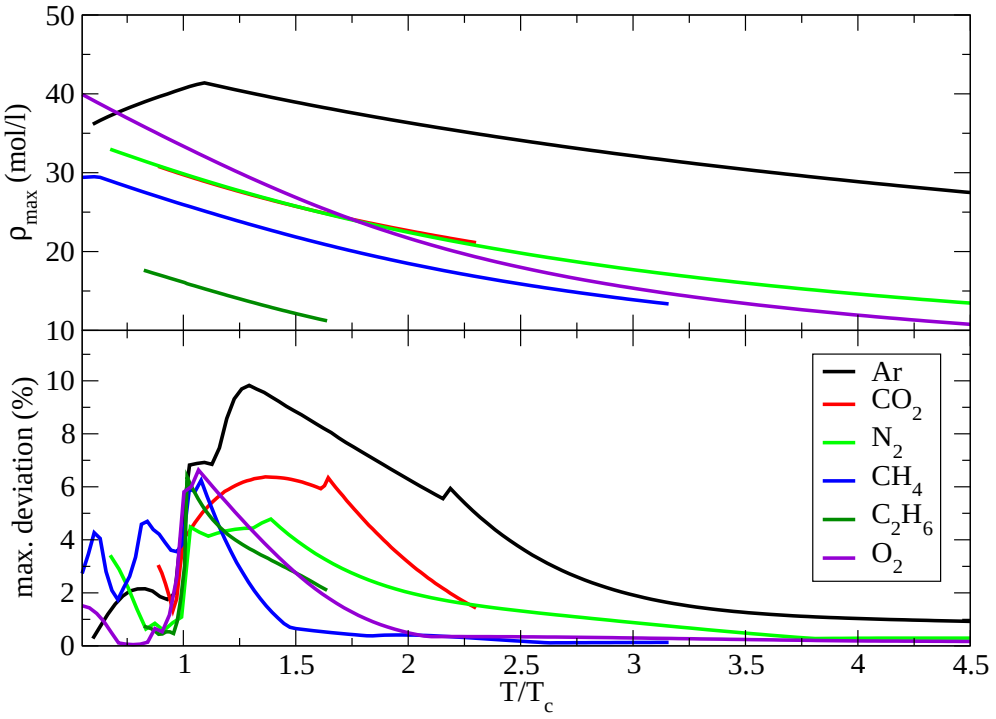

Figure 5.49: Application of the Enskog-2σ model with $\sigma_{\mathrm{MD},\chi}$ to the full temperature range of argon, carbon dioxide, nitrogen methane, ethane and oxygen. The maximum density (upper plot) and maximum deviation between model and experimental reference correlation (lower plot) are plotted versus the reduced temperature T/T_c.

5.4.2 Behaviour of the effective diameters

As we can see in Fig. 5.50, the effective diameters change their behavior around the critical temperature T_c. The diameter σ_α decreases steeply at the transition from the supercritical to the subcritical range, while σ_χ increases rapidly. Also, the curvature of the effective diameters changes markedly from the supercritical to the subcritical regime. Nevertheless, in Fig. 5.51, we attempt to superimpose the effective diameters in Fig. 5.50 with the ones of argon. Although the diameters of a given fluid have been scaled with two different length scaling parameters, larger deviations between the diameters of argon and the scaled diameters of the other fluids are observed: for σ_α, the deviations extend up to 4.2% for methane, for σ_χ, deviations up to 7.3%, 8.0%, 10.2% are encountered for nitrogen, oxygen and methane. Considering the sensitivity of the Enskog-2σ model with $\sigma_{\mathrm{MD},\chi}$ investigated in section 5.3.4 for the liquid range,

these deviations are expected to lead to large deviations in viscosity. Indeed, according to further computations, obtaining the effective diameters over the whole temperature range for a given fluid by scaling the effective diameters of argon with two different length scaling parameters leads to deviations up to 11.2%, 12.5%, 30.1% for ethane, oxygen and methane.

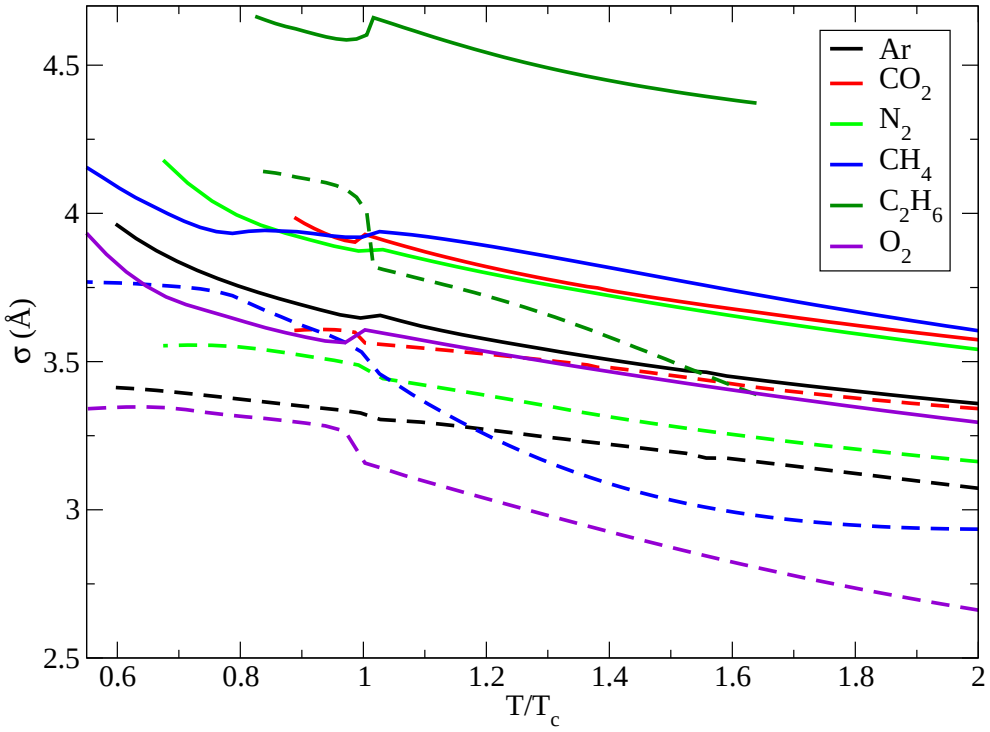

Figure 5.50: Effective diameters of the Enskog-2σ model with $\sigma_{\mathrm{MD},\chi}$ versus the reduced temperature T/T_c. The solid lines depict the optimised σ_α's and the dashed lines the optimised σ_χ's.

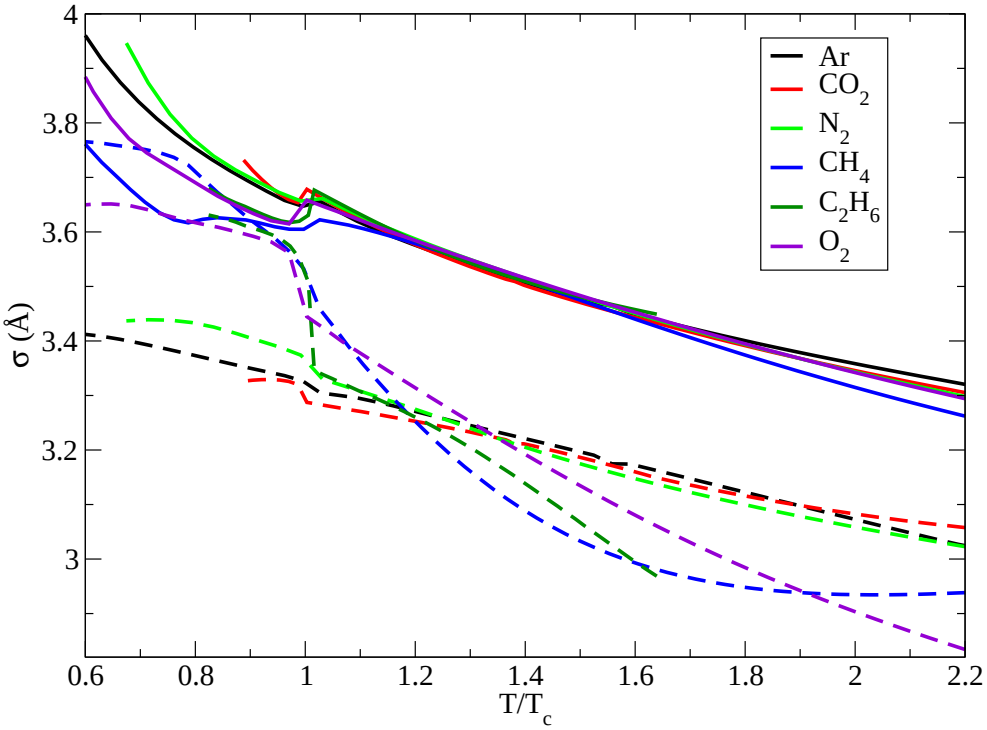

Figure 5.51: Scaled effective diameters of the Enskog-2σ model with $\sigma_{\mathrm{MD},\chi}$ versus the reduced temperature T/T_c. The solid lines depict the scaled σ_α's and the dashed lines the scaled σ_χ's. The effective diameters are scaled with two different length scaling parameters for a given fluid to superimpose the effective diameters of argon.

5.4.3 Choice of the length scaling parameters

Instead of using one set of scaling parameters for the whole temperature range, we recommend to use two different sets of scaling parameters, one for the liquid range and another one at supercritical conditions. The length scaling parameters for the liquid range are given in table 5.7 and the parameters for the supercritical range in table 5.9. The latter have been calculated by minimising the maximum deviation between the Enskog-2σ model with $\sigma_{\mathrm{MD},\chi}$ and the experimental reference correlations in table 5.8 for temperatures $T \geq T_c$. According to table 5.9, the Enskog-2σ model with $\sigma_{\mathrm{MD},\chi}$ and scaled diameters reproduces the viscosity of all fluids within 8.1% in the supercritical range from the dilute gas limit to the maximum density of the experimental reference correlations. In addition, Figures 5.52 and 5.53 show that the model reproduces the

primary experimental data of methane within 6% and the ethane data within 8.6%. The data points of ethane that deviate more than 7% from the model deviate also more than 3.5% from the experimental correlation by (Hendl *et al.*, 1994).

Table 5.9: Length scaling parameters L_α and L_χ obtained by minimising the maximum deviation between the Enskog-2σ model with $\sigma_{MD,\chi}$ and the experimental correlations in table 5.8 for supercritical temperatures $T \geq T_c$.

Fluid	L_α	L_χ	Max. deviation (%)	AAD (%)
CH_4	1.0831	1.0266	8.1	2.0
C_2H_6	1.1614	1.2745	5.9	2.0
CO_2	1.0793	1.0723	6.3	2.7
N_2	1.0577	1.0401	3.7	1.4
O_2	0.9814	0.9680	4.4	2.0

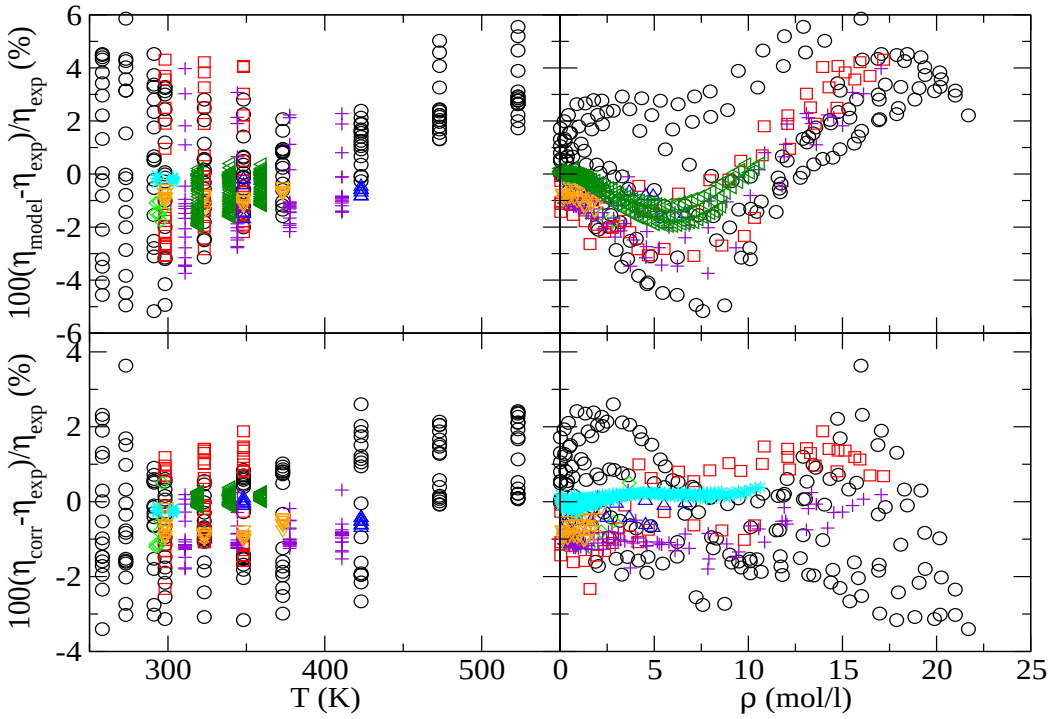

Figure 5.52: Upper plots: Percentage viscosity deviations, $100(\eta_{\mathrm{model}} - \eta_{\mathrm{exp}})/\eta_{\mathrm{exp}}$, between the Enskog-2$\sigma$ model with $\sigma_{\mathrm{MD},\chi}$ and scaled σ's by the scaling parameters from table 5.9 with primary experimental data of methane. Lower plots: Percentage viscosity deviations, $100(\eta_{\mathrm{corr}} - \eta_{\mathrm{exp}})/\eta_{\mathrm{exp}}$, between the experimental reference correlation for methane by (Vogel *et al.*, 2000) and the primary experimental data sets. On the left hand side, the deviations are depicted versus the temperature, on the right hand side, versus the density. The black dots refer to the primary experimental data by (Meshcheryakov & Golubev, 1954), the red squares to the data by (Iwasaki & Takahashi, 1959), the green diamonds to the data by (Kestin & Leidenfrost, 1959), the blue triangles to the data by (Barua *et al.*, 1964), the violet pluses to the data by (Giddings *et al.*, 1966), the cyan stars to the data by (Kestin & Yata, 1968), the orange triangles to the data by (Hongo *et al.*, 1988), the dark green triangles to the data by (Schley *et al.*, 2004).

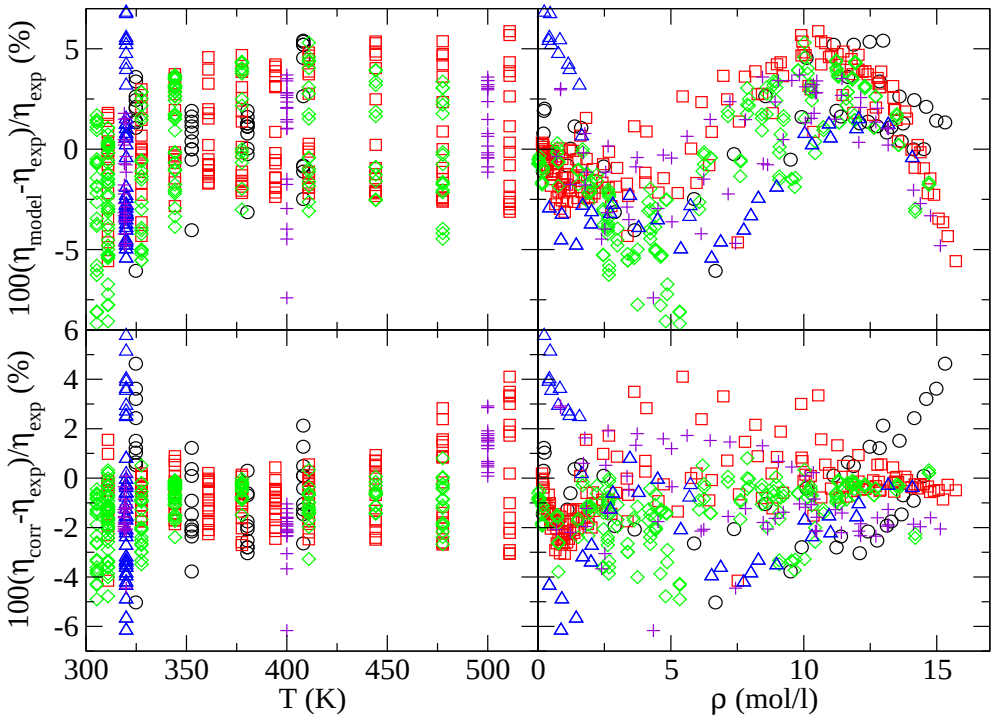

Figure 5.53: Upper plots: Percentage viscosity deviations, $100(\eta_{\mathrm{model}} - \eta_{\mathrm{exp}})/\eta_{\mathrm{exp}}$, between the Enskog-2$\sigma$ model with $\sigma_{\mathrm{MD},\chi}$ and scaled σ's by the scaling parameters from table 5.9 with primary experimental data of ethane. Lower plots: Percentage viscosity deviations, $100(\eta_{\mathrm{corr}} - \eta_{\mathrm{exp}})/\eta_{\mathrm{exp}}$, between the experimental reference correlation for ethane by (Hendl *et al.*, 1994) and the primary experimental data sets. On the left hand side, the deviations are depicted versus the temperature, on the right hand side, versus the density. The black dots refer to the primary experimental data by (Baron *et al.*, 1959), the red squares to the data by (Eakin *et al.*, 1962), the green diamonds to the data by (Carmichael & Sage, 1963a), the blue triangles to the data by (Diller & Saber, 1981), the violet pluses to the data by (Diller & Ely, 1989).

5.5 Conclusions

In this chapter, we have applied the Enskog-2σ model by analysing the viscosity of seven simple fluids (Ar, CH_4, C_2H_6, N_2, CO_2, O_2, SF_6). First, we limited our analysis to the supercritical region from the dilute gas limit up to moderate densities. The Enskog-2σ model correlates the viscosity of Ar, CH_4, N_2, CO_2 and SF_6 within the accuracy of the experimental reference correlations. Thus, in terms of correlative power, the Enskog-2σ model is superior to other approaches based on Enskog theory. This is not simply a result of using two rather than one fitting parameter, but primarily a result of correcting for two independent assumptions made in deriving Enskogs equation. The ability of the Enskog-2σ model to reproduce viscosity within the accuracy of an experimental correlation for each fluid studied is an important confirmation that our choice of effective diameters correctly describes the underlying physics. The success of the VW method (Vesovic & Wakeham, 1989b; Royal *et al.*, 2003; de Wijn *et al.*, 2008) for predicting the viscosity of mixtures, that implicitly uses the same two effective diameters, gives further support to their physical significance. It is found that the σ_α obtained from the VW method at the switch-over density deviates less than 1.3% from the σ_α in the Enskog-2σ model and hence gives a good estimate for σ_α. The effective diameter σ_α exhibits a monotonic decrease with temperature for all fluids studied. If plotted as a function of reduced temperature, σ_α exhibits a universal behaviour, which can be made conformal by use of a single, length-scaling parameter. The effective diameter σ_χ exhibits less regular behaviour, although the real behaviour is masked by the uncertainty in obtaining σ_χ from current viscosity correlations. Based on the universal behaviour of the effective diameter σ_α, we have developed a general model that allows the prediction of the viscosity of one fluid from the knowledge of viscosity of a reference fluid. Using argon as our reference fluid and obtaining the length scaling parameter from the knowledge of the viscosity along a single isotherm, the accuracy of the viscosity prediction is similar to the uncertainty of the original correlation over its entire supercritical range. Estimating the scaling parameter from thermodynamic or zero-density viscosity formulations in most cases leads to poor predictions of viscosity. The Enskog-2σ model was also successfully applied to thermal conductivity. The effective diameter σ_α decreased as for viscosity monotonically with the temperature while σ_χ exhibited a more varied behaviour.

Next, we have demonstrated that the use of the correction factor by (Sigurgeirsson & Heyes, 2003) obtained from molecular dynamics (MD) simulations allows to extend the Enskog-2σ model to higher densities. For this analysis, the experimental reference correlation of argon by (Lemmon & Jacobson, 2004) is used which extends to very high pressures of 400 MPa. The MD correction factor is a function of the packing fraction y only and hence depends on the effective diameter σ_{MD} chosen through y. The choices $(\sigma_\alpha + \sigma_\chi)/2$, $\sqrt{\sigma_\alpha \sigma_\chi}$, σ_χ for σ_{MD} lead all to similar results and allow to correlate the viscosity of argon within 11.2% up to very high pressures and densities. An alternative approach which consists in optimising σ_{MD} independently of σ_α and σ_χ reproduces the viscosity of argon within 15.4%. The advantage of the approach is that σ_α and σ_χ are optimised without the use of an empirical correlation of the two diameters in the MD correction factor such that the link between the effective diameters and the excluded volume as well as the collision rate is kept fully. The disadvantage is that with σ_{MD} a third temperature dependent diameter needs to be optimised.

The Enskog-2σ has been extended to the liquid range and validated against the reference correlations for Ar, CH_4, C_2H_6, N_2, CO_2 and O_2. As the densities in the liquid range are generally high, the use of MD corrections is found to be beneficial. The MD corrections were successfully incorporated with the choices $(\sigma_\alpha + \sigma_\chi)/2$ and σ_χ for σ_{MD} reproducing the experimental reference correlations with maximum deviations less than 6.7% and hence almost within the accuracy of the correlations. The effective diameter σ_α decreases monotonically with the temperature, while the behaviour of σ_χ is again more complex and depends on the choice σ_{MD} and the fluid. We have further demonstrated that, in the liquid range, the effective diameters of CH_4, C_2H_6, N_2, CO_2 and O_2 plotted versus the reduced temperature can be superimposed reasonably well with the diameters of argon when for each effective diameter a different constant length scaling parameter is used. The length scaling parameters can be obtained from a single isotherm such that the experimental correlations of CH_4, C_2H_6, N_2, O_2 and CO_2 are reproduced with maximum deviations less than 9.0%.

Finally, we have applied the Enskog-2σ with the choice $\sigma_{\mathrm{MD}} = \sigma_\chi$ over the full temperature range which extends from low temperatures in the liquid phase to high temperatures in the supercritical phase. The model correlates the viscosity of Ar, CH_4, C_2H_6, N_2, CO_2 and O_2 within 9.7% at all conditions. We have not been able to find a universal behaviour of the effective diameters over the full temperature range though. The

diameters change in general their behaviour at the transition of liquid and supercritical phase. However, in each phase separately, the effective diameters exhibit a universal behaviour. Hence, we recommend two sets of length scaling parameters, one for the liquid phase and one for the supercritical phase. When the effective diameters in the supercritical phase are obtained via two constant length scaling parameters from the diameters of argon, the model correlates the experimental correlations of N_2, O_2, C_2H_6, CO_2 and CH_4 with maximum deviations less than 8.1%.

6

Results for alkanes

Flow processes involving alkanes are ubiquitous in nature and industrial processes, especially, within the petroleum industry. Examples are oil and gas recovery from reservoir rocks and transport of alkane rich fluids through pipelines. In those flow processes, the viscosity of the alkanes is one of key properties and hence modelling this property is of great interest. By extending the Enskog-2σ model to alkanes in this chapter, we introduce a new model for the viscosity of alkanes. Being based on Enskog's theory, the Enskog-2σ model possesses a theoretical foundation. First, the Enskog-2σ model is applied to alkanes at supercritical conditions up to moderate densities. Then, we discuss how the model can be extended to high densities and into the liquid range.

6.1 Supercritical temperature range

The Enskog-2σ model based on the modification of Enskog's viscosity expression for chain fluids by (de Wijn *et al.*, 2008) has been introduced in chapter 4. As for simple fluids, we apply the model at supercritical conditions up to moderate densities first. We investigate how well the Enskog-2σ model correlates the experimental reference correlations stated in table 6.1 and discuss how the number of free parameters can be reduced. Next, we evaluate the model directly against primary experimental viscosity data. Extensions of the model to higher densities are analysed in the last section.

Table 6.1: Summary of experimental reference correlations for alkanes at supercritical conditions.

Fluid	P-range (MPa)	T-range (K)	Viscosity correlation
C_2	0-60	310-500	(Hendl *et al.*, 1994)
C_3	0-100	370-475	(Vogel *et al.*, 1998)
C_4	0-70	425-500	(Vogel *et al.*, 1999)
C_6	0-100	510-600	(McLinden *et al.*, 2010)
C_8	0-100	570-600	(Huber *et al.*, 2004)

6.1.1 Correlative power and behaviour of the model parameters

In this section, we apply the Enskog-2σ model to alkanes at supercritical temperatures up to moderate densities. As outlined in section 4.1, the free parameters in the model are the two effective temperature-dependent chain lengths m_α and m_χ. The effective diameter σ_α is set equal to the σ_α of methane at the same temperature. The corresponding σ_α has been depicted in Fig. 5.7. The effective diameter σ_χ is obtained from the other effective parameters via the chain length constraint equation:

$$\sigma_\chi = \sigma_\alpha \frac{m_\alpha - 1}{m_\chi - 1}. \tag{6.1}$$

The maximum density $\rho_{\max}$ is defined via

$$\rho_{\max} = \min(\rho_{\exp}, \rho^*) \tag{6.2}$$

where ρ^* is given by

$$\rho^* = \rho_{\max,C_1} \frac{\rho_{c,C_n}}{\rho_{c,C_1}} \tag{6.3}$$

with the maximum density $\rho_{\max,C_1}$ of methane shown in Fig. 6.1 evaluated at the same reduced temperature T/T_c as $\rho_{\max}$. ρ_{c,C_1} and ρ_{c,C_n} depict the critical densities of methane and the respective alkane. We compute ρ^* from Eq. (6.3) to limit the model to moderate densities such that MD corrections can be neglected in the first instance. At a given temperature, both effective chain lengths are optimised to minimise the maximum deviation between model and the experimental reference correlation from the dilute gas limit up to $\rho_{\max}$ shown in the upper plot of Fig. 6.2. The optimised m's

are shown in the middle plot of the figure. With increasing carbon number, the chain lengths increase.

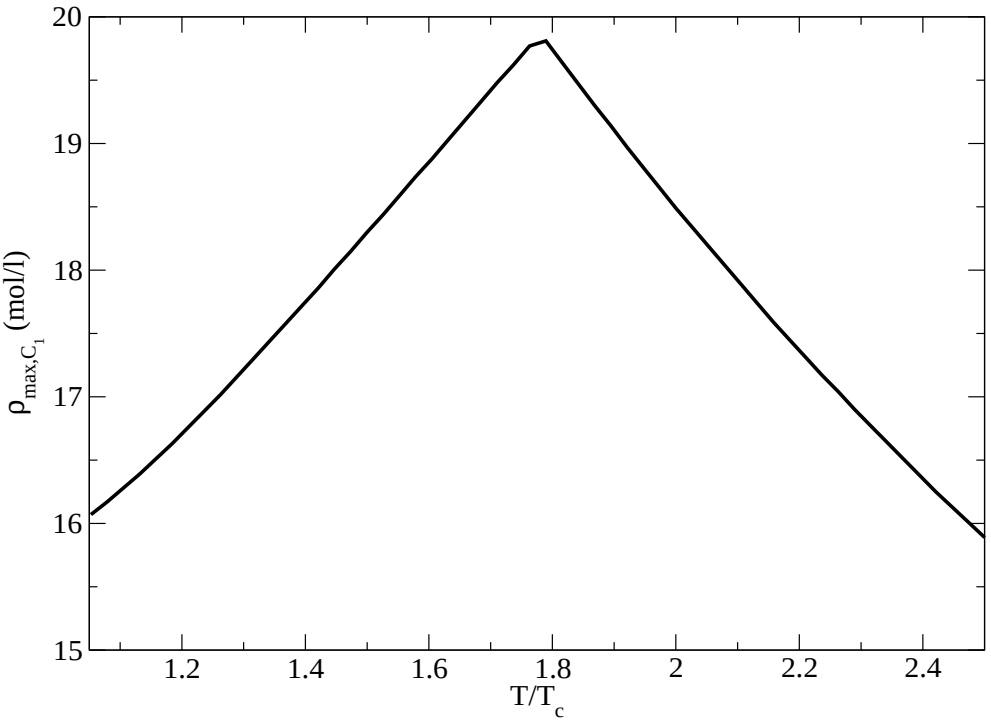

Figure 6.1: Maximum density $\rho_{\max,C_1}$ of methane versus reduced temperature.

The exception is the m_χ of butane which is smaller than m_χ of propane for $T/T_c \geq 1.15$. Moreover, for a given alkane and reduced temperature m_χ is larger than m_α. Again, butane is the exception for $T/T_c \geq 1.09$. We will see in section 6.1.2 that we can choose the chain lengths of butane such that the relation $m_\chi > m_\alpha$ holds true, no crossover with the m's of propane occurs, and the viscosity of butane is reproduced well within 6.5%. Thus, the anomalous behaviour of the chain lengths of butane in Fig. 6.2 is deemed irrelevant in practice. Another important observation is that the m's of ethane, propane, pentane and hexane depend only slightly on the temperature. This result will be used in section 6.1.2 to reduce the number of free model parameters. According to the lower plot of Fig. 6.2 the viscosity of ethane, propane, butane and hexane is correlated within 4% and the viscosity of octane within 6%. The corresponding AAD's averaged over all supercritical temperatures are 0.72%, 0.54%, 0.51%, 0.39%, 2.1% for ethane, propane, butane, hexane and octane. Taking into account that the uncertainty

of the experimental reference correlations is ±5%, these deviations are relatively small. The upper plot in Fig. 6.3 shows the effective diameter σ_χ as obtained from the chain length constraint equation (6.1) from σ_α and the effective chain lengths. The behaviour of σ_χ is varied and does not follow any systematic trend. The same has been observed for simple fluids in section 5.1.4. As for simple fluids, the varied behaviour of σ_χ can be attributed to the fact that the model is fairly insensitive to the value of σ_χ. It is worth noting that the product $\sigma_\chi m_\chi$, as depicted in the lower plot in Fig. 6.3, shows physically reasonable behaviour. It decreases slightly with temperature and increases as expected with increasing carbon number.

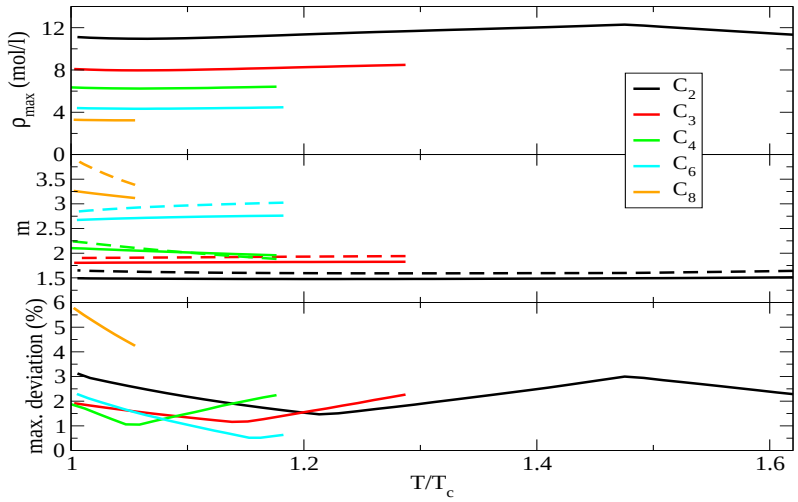

Figure 6.2: Application of the Enskog-2σ model to alkanes up to moderate densities at supercritical temperatures. The upper plot shows $\rho_{\max}$ versus the reduced temperature T/T_c, the middle plot the effective chain lengths (m_α by the solid lines, m_χ by the dashed ones) and the lower plot the maximum deviation between model and the experimental reference correlations given in table 6.1.

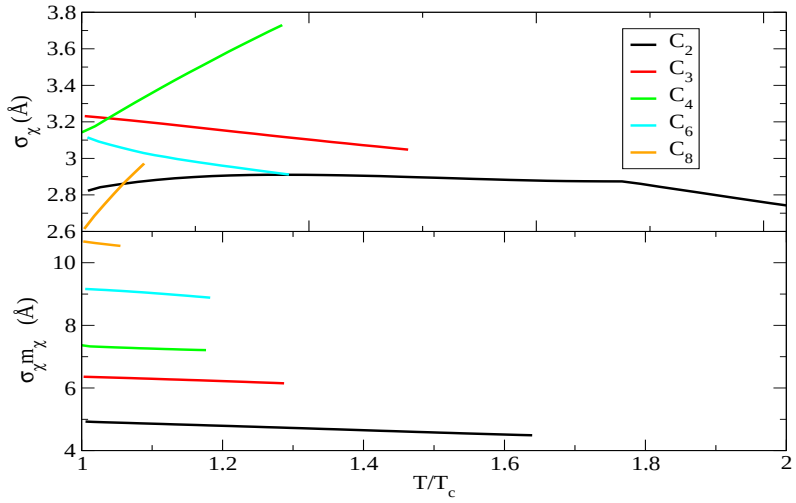

Figure 6.3: Upper plot: Effective diameter σ_χ corresponding to Fig. 6.2 versus the reduced temperature T/T_c. Lower plot: the product $\sigma_\chi m_\chi$ versus T/T_c.

6.1.2 Results for constant chain lengths

As observed in section 6.1.1, the chain lengths of ethane, propane, pentane and hexane vary only slightly with the temperature. In this section, we will assume that the chain lengths are temperature independent and test the correlative power of the resulting approach. This approach has the advantage that the number of free model parameters reduces to only two constant chain lengths. We obtain the constant chain lengths by minimising the maximum deviation between model and experimental reference correlation along the isotherm at the temperature T_{mean}. The temperature T_{mean} is equal to the temperature in the middle of the supercritical T-range of the experimental correlations for a given alkane. The temperature ranges of the correlations can be found in table 6.1. The optimised chain lengths are depicted in the upper plot of Fig. 6.4. The chain length m_χ is found to be larger than m_α for all alkanes. This holds true as well for butane, although both chain lengths have almost the same value here. As expected, the chain lengths increase with increasing carbon number. According to the lower plot of the figure, the model reproduces the experimental correlation of ethane, propane, butane, hexane, octane within 6.4%, 2.8%, 6.3%, 5.8%, 6.4%. The corresponding AAD's averaged over all supercritical temperatures are 1.2%, 0.7%, 1.9%, 1.3%, 2.7%.

Table 6.2: Chain length m_χ for a series of alkanes when m_α is obtained from Eq. (6.4).

Fluid	m_χ
C_2	1.69
C_3	1.85
C_4	2.28
C_6	2.65
C_8	4.09

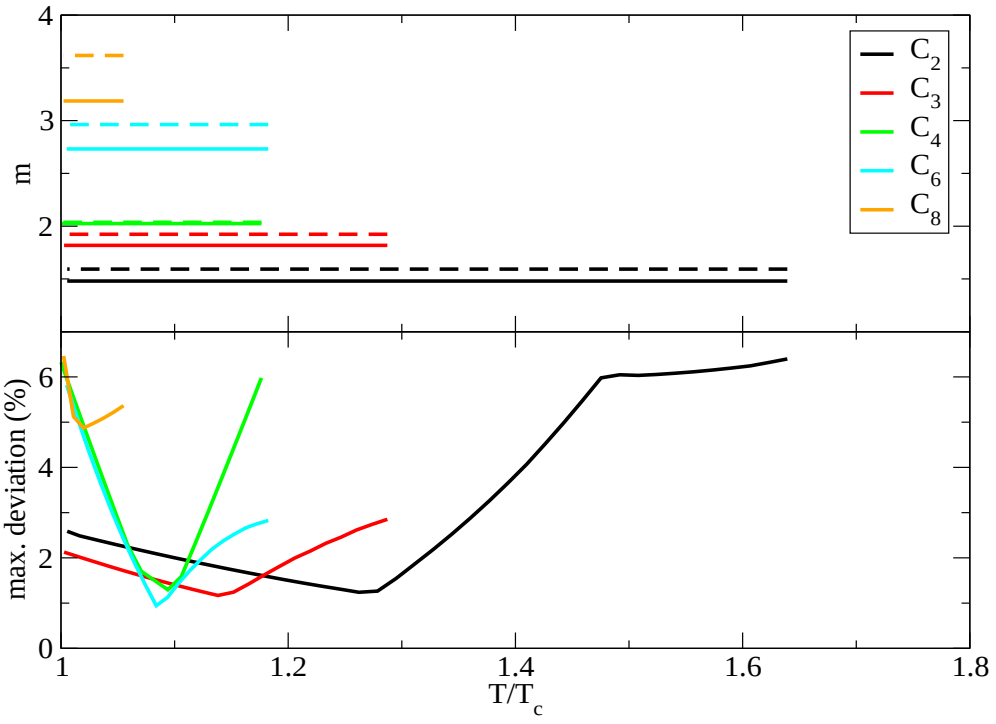

Figure 6.4: Application of the Enskog-2σ model to alkanes up to moderate densities at supercritical temperatures. The temperature-independent chain lengths are shown in the upper plot. m_α is given by the solid lines, m_χ by the dashed ones. The lower plot depicts the maximum deviation between model and the experimental reference correlations given in table 6.1.

In Fig. 6.5, the chain length m_α is plotted against the carbon number N. We find that m_α depends almost linearly on the carbon number. A linear fit results in the straight black line in Fig. 6.5. The linear relationship between N and m_α corresponding is given by

$$m_\alpha = 0.93 + 0.29N. \tag{6.4}$$

If we compute m_α from this relationship and obtain m_χ by minimising the maximum deviation between model and experimental reference correlation along the isotherm at T_{mean}, we get the results in Fig. 6.6. According to the lower plot of the figure, the model reproduces the experimental correlation of ethane, propane, butane, hexane, octane within 7.2%, 2.8%, 9.3%, 6.2%, 6.4%. The corresponding AAD's averaged over all supercritical temperatures are 1.4%, 1.1%, 3.0%, 2.2%, 2.9%. Overall, the accuracy of the model seems to be satisfactory. A more detailed test of the model accuracy will be given in section 6.1.3 where we evaluate the approach directly against the primary experimental data. The chain length m_χ, shown in the upper plot of Fig. 6.6, does not follow a simple relationship with the carbon number. Table 6.2 summarises the values of m_χ.

For methane where $N = 1$, Eq. (6.4) yields $m_\alpha = 1.22$, i.e., methane is not modelled as sphere and hence Eq. (6.4) is not physically meaningful in the limit $N = 1$. This can be explained as follows: n-alkanes are not composed of CH_4 molecules for $n > 1$ but of CH_2 and CH_3 groups. This discrepancy leads to values of m_α that do not extrapolate to 1 in the limit $N = 1$. If we impose the physically meaningful limit $m_\alpha = 1$ for $N = 1$, the best linear fit for m_α is represented by the dashed line in Fig. 6.5 which follows the expression

$$m_\alpha = 0.665 + 0.335N. \tag{6.5}$$

If we compute m_α from this relationship and calculate m_χ as before by minimising the maximum deviation between model and experimental reference correlation along the isotherm at T_{mean}, we obtain the results in Fig. 6.7. The imposition of the physically meaningful limit $m_\alpha = 1$ for $N = 1$, has the disadvantage that the model reproduces the viscosity of the short alkanes ethane and propane rather poorly. The maximum deviations between model and experimental reference correlations extend up to 17.2% and 13.1% for ethane and propane with corresponding AAD's of 9.8% and 7.2%.

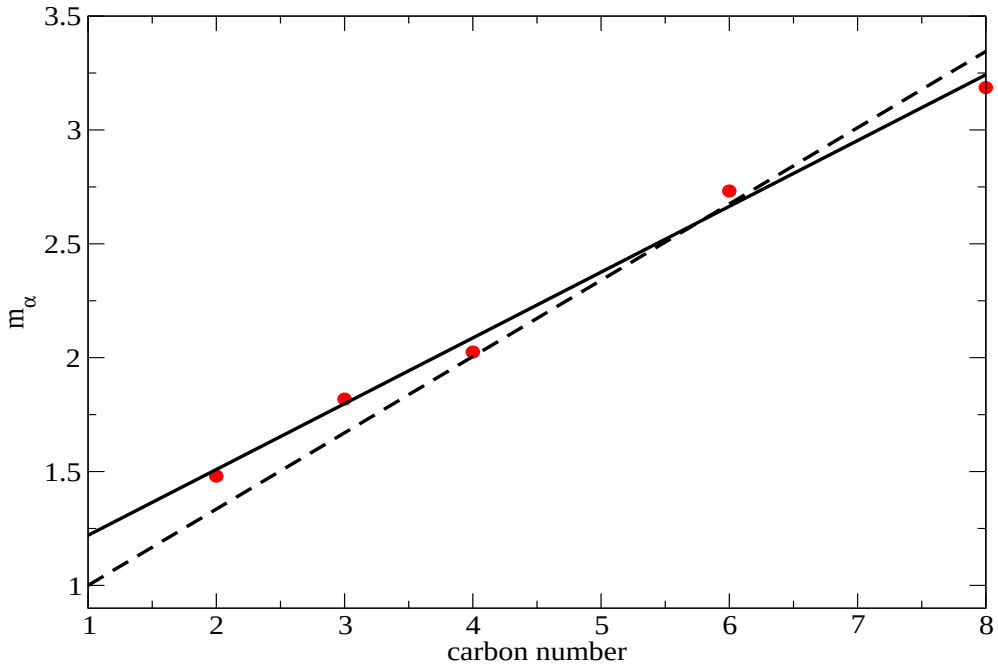

Figure 6.5: Chain length m_α versus the carbon number. The red dots depict m_α from Fig. 6.4, the black solid line the best linear fit for m_α and the black dashed line the best linear fit when $m_\alpha = 1$ for a carbon number of 1.

Butane, hexane and octane, on the contrary, are reproduced satisfactorily well with maximum deviations of 7.7%, 6.1% and 8.1% and corresponding AAD's of 2.0%, 2.1% and 3.4%. Eq. (6.5) resembles closely the chain length expression

$$m = 2/3 + 1/3N \tag{6.6}$$

which is obtained within the SAFT-HS approach, when the critical properties of alkanes are modelled (Jackson & Gubbins, 1989), and from viscosity data in the work by (de Wijn *et al.*, 2008). Moreover, the slope of approximately 1/3 in Eq. (6.5) can be rationalized by the fact that the carbon-carbon bond length in n-alkanes is roughly a third of the diameter of a methane molecule, see again (de Wijn *et al.*, 2008).

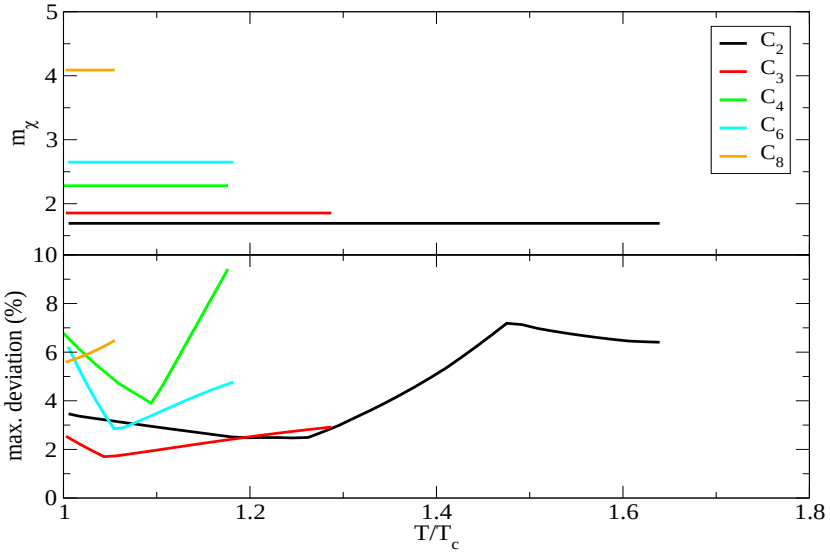

Figure 6.6: Application of the Enskog-2σ model to alkanes up to moderate densities at supercritical temperatures with m_α from Eq. 6.4. The chain length m_χ is shown in the upper plot. The lower plot depicts the maximum deviation between model and the experimental reference correlations given in table 6.1.

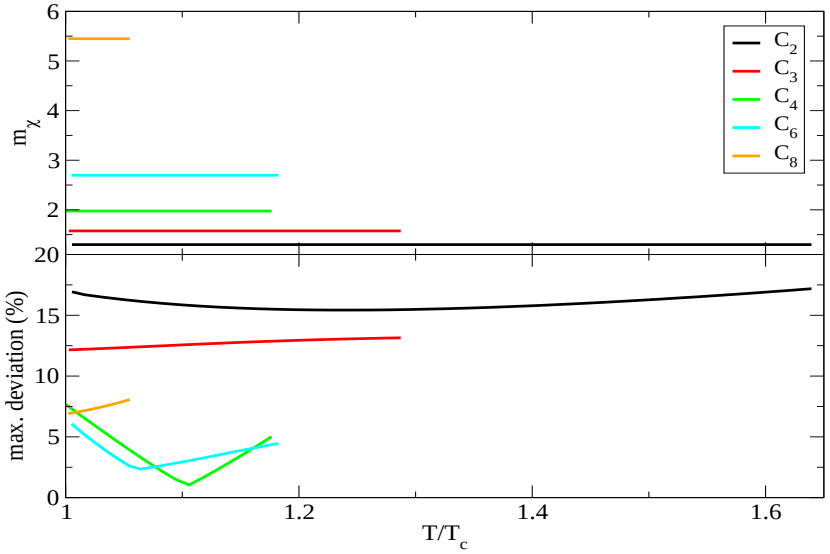

Figure 6.7: Application of the Enskog-2σ model to alkanes up to moderate densities at supercritical temperatures with m_α from Eq. 6.5. The chain length m_χ is shown in the upper plot. The lower plot depicts the maximum deviation between model and the experimental reference correlations given in table 6.1.

6.1.3 Comparison with primary experimental data

In section 6.1.2, we have found that the Enskog-2σ model with m_α from Eq. (6.4) and the optimised m_χ from table 6.2 correlates the experimental viscosity correlations from ethane up to octane reasonable well within 10%. Here, we validate the model directly against the primary viscosity data. Fig. 6.8 shows the results for ethane. The bulk of the data is reproduced with deviations less than 5%. A couple of data points by (Diller & Saber, 1981) deviate more than 5% from the model. These measurements show also larger deviations (from 2.4% to 5.8%) from the experimental reference correlation by (Hendl *et al.*, 1994). It is interesting to compare these data points with the newer viscosity measurements by (Diller & Ely, 1989) which are measured at the same temperature.

Table 6.3: Primary viscosity data sets of ethane, propane and butane based on (Hendl *et al.*, 1994), (Vogel *et al.*, 1998) and (Vogel *et al.*, 1999), respectively.

Fluid	Data set	P-range (MPa)	T-range (K)
C_2	(Baron *et al.*, 1959)	0.7-55.1	325-408
C_2	(Eakin *et al.*, 1962)	0.7-55.1	311-444
C_2	(Carmichael & Sage, 1963a)	0.1-36	311-478
C_2	(Diller & Saber, 1981)	0.6-10	320
C_2	(Diller & Ely, 1989)	1.7-55	319-500
C_3	(Starling *et al.*, 1960)	0.7-55.1	298-411
C_3	(Carmichael *et al.*, 1964)	0.24-34.4	278-478
C_3	(Giddings *et al.*, 1966)	0.7-55.2	278-378
C_4	(Dolan *et al.*, 1963)	0.7-55.2	311-444
C_4	(Carmichael & Sage, 1963b)	0.23-35.3	278-433

The data points lie in the pressure range from 0.6 to 3.2 MPa and the density range from 0.23 to 1.6 mol/l. The data set by (Diller & Ely, 1989) contains a measurement at 0.7 mol/l which is reproduced by the model with a deviation of only -0.2%. Thus, the significance of the data points by (Diller & Saber, 1981) with larger deviations is questionable. The only other point which deviates more than 5% from the model is the measurement by (Eakin *et al.*, 1962) at $477.6K$ and 12.2 mol/l with a deviation of -6.4%. The point occurs near the maximum density of the model at which, according to Fig. 6.6, the deviation between model and the experimental correlation by (Hendl *et al.*, 1994) also extends to about 6%. As the upper right plot of Fig. 6.8 shows, the model underestimates the primary experimental viscosity data at high densities ρ and the errors increase with increasing ρ.

As Fig. 6.9 shows, the primary experimental data for propane is described very well with deviations less 3.5% by the model. Fig. 6.10 depicts the results for butane. Most of the data is reproduced within 5% by the model. The exception are the three data points by (Carmichael & Sage, 1963b) all of which have been measured at $433.15K$ and 4.6 mol/l.

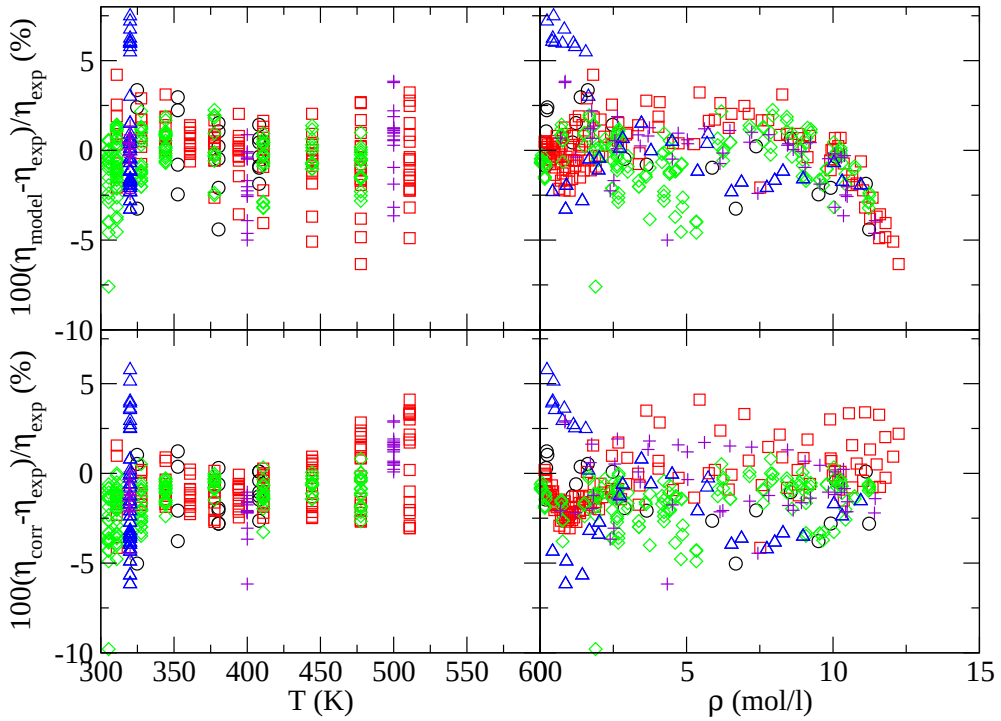

Figure 6.8: Upper plots: Percentage viscosity deviations, $100(\eta_{\mathrm{model}}-\eta_{\mathrm{exp}})/\eta_{\mathrm{exp}}$, between the Enskog-2$\sigma$ model with m_α from Eq. (6.4) and optimised m_χ from table 6.2 and the primary experimental data sets for ethane listed in table 6.3. Lower plots: Percentage viscosity deviations, $100(\eta_{\mathrm{corr}}-\eta_{\mathrm{exp}})/\eta_{\mathrm{exp}}$, between the experimental reference correlation for ethane by (Hendl *et al.*, 1994) and the primary experimental data sets. On the left hand side, the deviations are depicted versus the temperature, on the right hand side, versus the density. The black dots refer to the primary experimental data by (Baron *et al.*, 1959), the red squares to the data by (Eakin *et al.*, 1962), the green diamonds to the data by (Carmichael & Sage, 1963a), the blue triangles to the data by (Diller & Saber, 1981), the violet pluses to the data by (Diller & Ely, 1989).

The measurements differ from each other up to 2% and the point with the largest deviation of −7.3% from the model deviates as well by −5.1% from the experimental correlation by (Vogel *et al.*, 1999). Consequently, the significance of these three data points appears questionable.

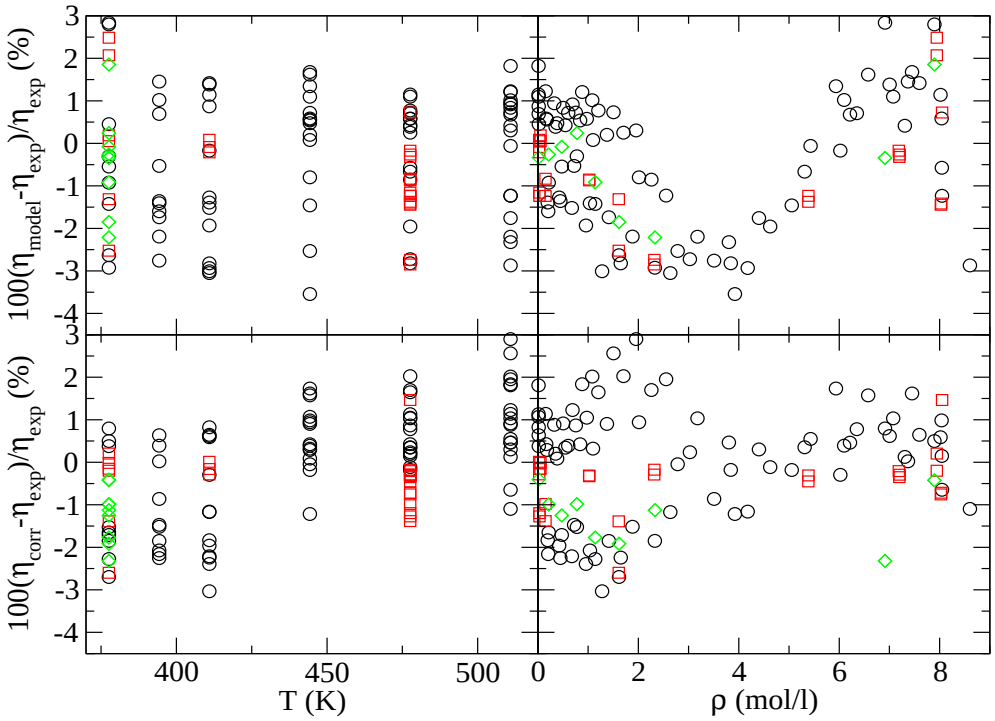

Figure 6.9: Upper plots: Percentage viscosity deviations, $100(\eta_{\mathrm{model}}-\eta_{\mathrm{exp}})/\eta_{\mathrm{exp}}$, between the Enskog-2$\sigma$ model with m_α from Eq. (6.4) and optimised m_χ from table 6.2 and the primary experimental data sets for propane listed in table 6.3. Lower plots: Percentage viscosity deviations, $100(\eta_{\mathrm{corr}}-\eta_{\mathrm{exp}})/\eta_{\mathrm{exp}}$, between the experimental reference correlation for propane by (Vogel *et al.*, 1998) and the primary experimental data sets. On the left hand side, the deviations are depicted versus the temperature, on the right hand side, versus the density. The black dots refer to the primary experimental data by (Starling *et al.*, 1960), the red squares to the data by citepcarmichael64, the green diamonds to the data by (Giddings *et al.*, 1966).

For hexane, we are using the experimental reference correlation by (McLinden *et al.*, 2010). It is unpublished and not clear which primary experimental viscosity data have been used as basis for this correlation. As we could not find any reliable viscosity data sets for hexane at supercritical conditions, we have not included hexane in the discussion here. The experimental reference correlation for octane by (Huber *et al.*, 2004) classifies only a few measurements as primary experimental data in the supercritical range and the correlation at supercritical conditions has been obtained mainly as extrapolation of the fit to primary viscosity data at subcritical conditions. Up to the maximum density ρ_{max} of our model, Eq. (6.2), only two data points by (Badalyan

& Rodchenko, 1986) belong to the primary experimental viscosity data of octane. The measurement at $T = 573K$, $\rho = 3.0$ mol/l is reproduced with a deviation of 5.4% and the measurement at $T = 598K$, $\rho = 2.6$ mol/l is reproduced with a deviation of 2.8%. Altogether, the Enskog-2σ model with m_α from Eq. (6.4) and the optimised m_χ from table 6.2 represents a satisfactorily accurate approach to model the viscosity of alkanes at supercritical temperatures up to moderate densities.

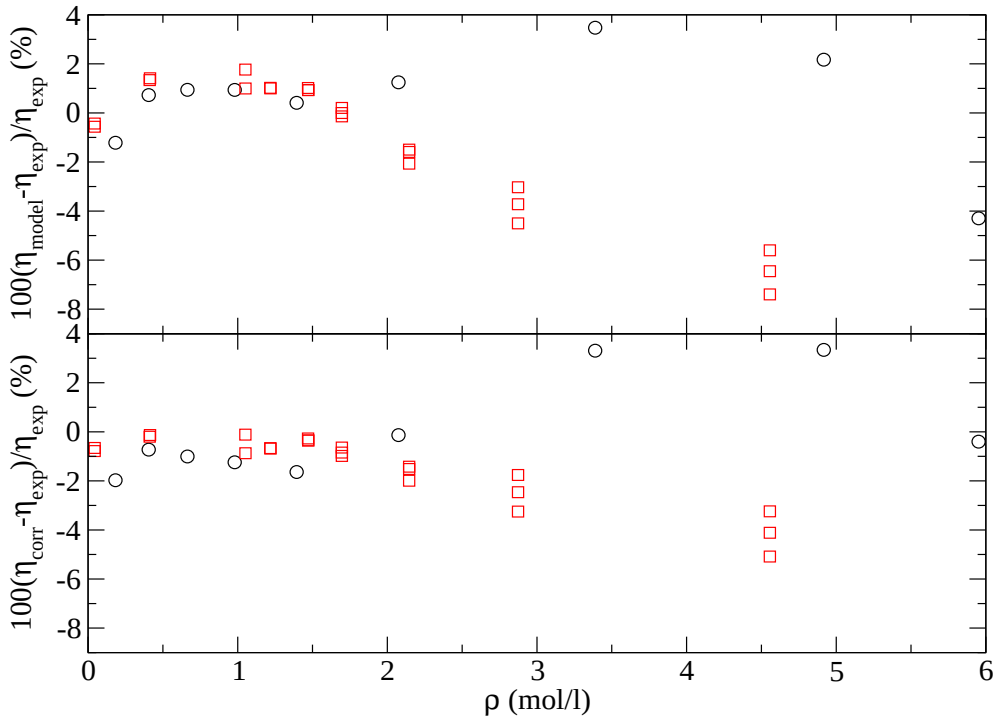

Figure 6.10: Upper plot: Percentage viscosity deviations, $100(\eta_{\text{model}} - \eta_{\text{exp}})/\eta_{\text{exp}}$, between the Enskog-2$\sigma$ model with m_α from Eq. (6.4) and optimised m_χ from table 6.2 and the primary experimental data sets for butane listed in table 6.3. Lower plot: Percentage viscosity deviations, $100(\eta_{\text{corr}} - \eta_{\text{exp}})/\eta_{\text{exp}}$, between the experimental reference correlation for butane by (Vogel *et al.*, 1999) and the primary experimental data sets. The black dots refer to the primary experimental data by (Dolan *et al.*, 1963) at $T = 444.3K$, the red squares to the data by (Carmichael & Sage, 1963b) at $T = 433K$.

6.1.4 Extension up to high densities

So far, the Enskog-2σ model has been applied to alkanes up to moderate densities defined by Eq. (6.2). In this section, we will investigate several variants of the model that extend to the experimental maximum density ρ_{exp} corresponding to the maximum pressures of the reference correlations stated in table 6.1.

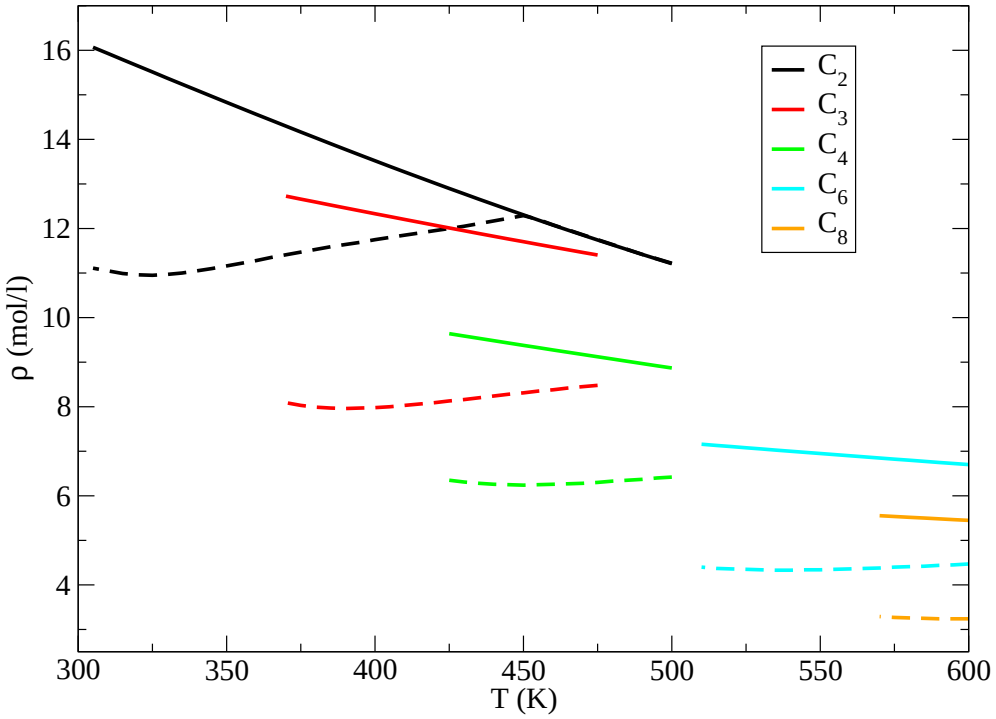

Figure 6.11: Comparison between the experimental maximum density ρ_{exp} (solid lines) and the maximum density ρ_{max} (dashed lines) defined in Eq. (6.2) to limit the model to moderate densities.

The experimental maximum density ρ_{exp} is compared to the maximum density used in the previous sections in Fig. 6.11. Especially, for hexane and octane the increase in the maximum density of the model is substantial and amounts to about 61% and 72%. The increase in the corresponding maximum pressure is even more pronounced. For hexane, the maximum pressure increases from 4.1MPa at $T = 510K$ and 15.4MPa at $T = 600K$ to 100MPa, for octane, from 3.3MPa at $T = 570K$ and 5.7MPa at $T = 600K$ to 100MPa.

The variants discussed are as follows:

(i) The Enskog-2σ model of section 6.1.1 for alkanes without MD corrections up to ρ_{exp}.

(ii) The Enskog-2σ model based on Eq. (4.13) which consists of the modification of Enskog's viscosity expression for chain fluids by (de Wijn *et al.*, 2008) multiplied with the MD correction factor for a hard sphere fluid. The effective diameter σ_{MD} and the effective chain length m_{MD} in the MD correction factor are set equal to $(\sigma_\alpha + \sigma_\chi)/2 =: \sigma_{\text{MD,mean}}$ and $(m_\alpha + m_\chi)/2 =: m_{\text{MD,mean}}$. The effective diameter σ_α is obtained again from methane at the same temperature. Consistently, the σ_α of methane is computed by applying the Enskog-2σ model for simple fluids of section 5.2.2 with $\sigma_{\text{MD,mean}}$ to methane. For all temperatures, the model for methane extends to the maximum density of the experimental reference correlation by (Vogel *et al.*, 2000). The corresponding σ_α is depicted in Fig. 6.12.

(iii) The same model as the model under point (ii) but with $\sigma_{\text{MD}} = \sigma_\chi =: \sigma_{\text{MD},\chi}$, $m_{\text{MD}} = m_\chi =: m_{\text{MD},\chi}$ and σ_α obtained by applying the Enskog-2σ model for simple fluids of section 5.2.2 with $\sigma_{\text{MD},\chi}$ to methane. The model for methane extends again to the maximum density of the experimental reference correlation by (Vogel *et al.*, 2000) and the corresponding diameter σ_α is shown as well in Fig. 6.12.

In all approaches, the effective chain lengths m_α and m_χ are optimised at each temperature to minimise the maximum deviation between model and the experimental reference correlations in table 6.1. Furthermore, the chain length constraint Eq. (6.1) is used to obtain the effective diameter σ_χ. As Fig. 6.12 shows, the σ_α of all approaches are identical to each other above a temperature of $250K$ and, at lower temperatures, deviate only marginally from each other with a maximum deviation of 0.37%. The critical temperature of ethane is approximately $305K$ and longer alkanes have larger critical temperatures. Thus, all models use the same effective diameter σ_α at the supercritical temperatures investigated here.
Fig. 6.13 illustrates the results for the model in case (i). The effective chain lengths increase with the carbon number. The variation of the chain lengths with temperature is rather irregular.

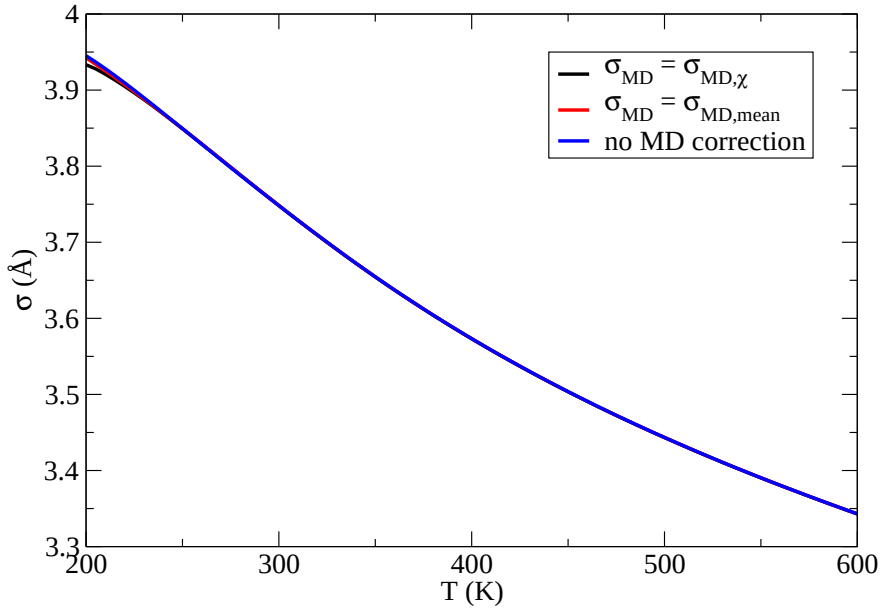

Figure 6.12: Effective diameter σ_α versus temperature T. The black, red, blue line depict σ_α in model case (i), (ii), (iii).

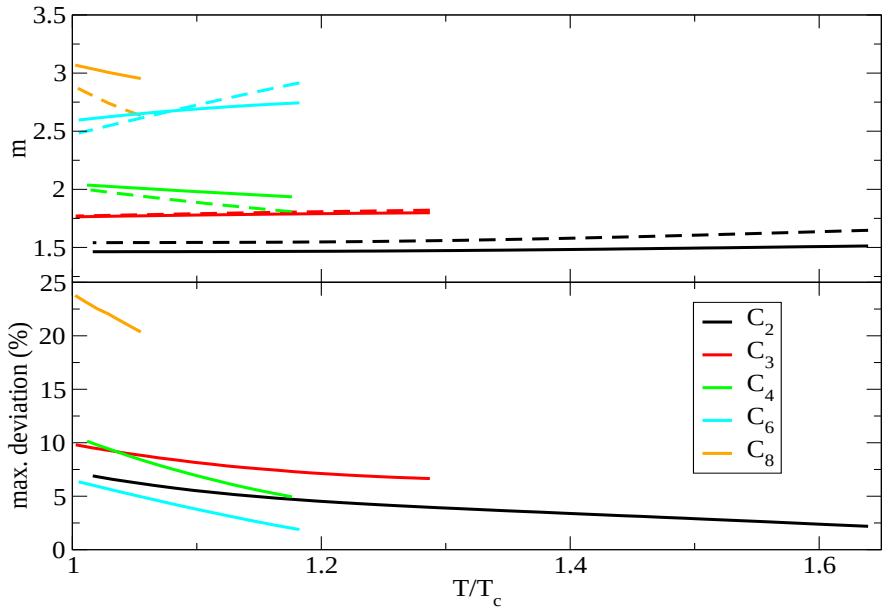

Figure 6.13: Application of the Enskog-2σ model without MD corrections as in case (i). The optimised effective chain lengths are shown in the upper plot. m_α is given by the solid lines, m_χ by the dashed ones. The lower plot depicts the maximum deviation between model and the experimental reference correlations given in table 6.1.

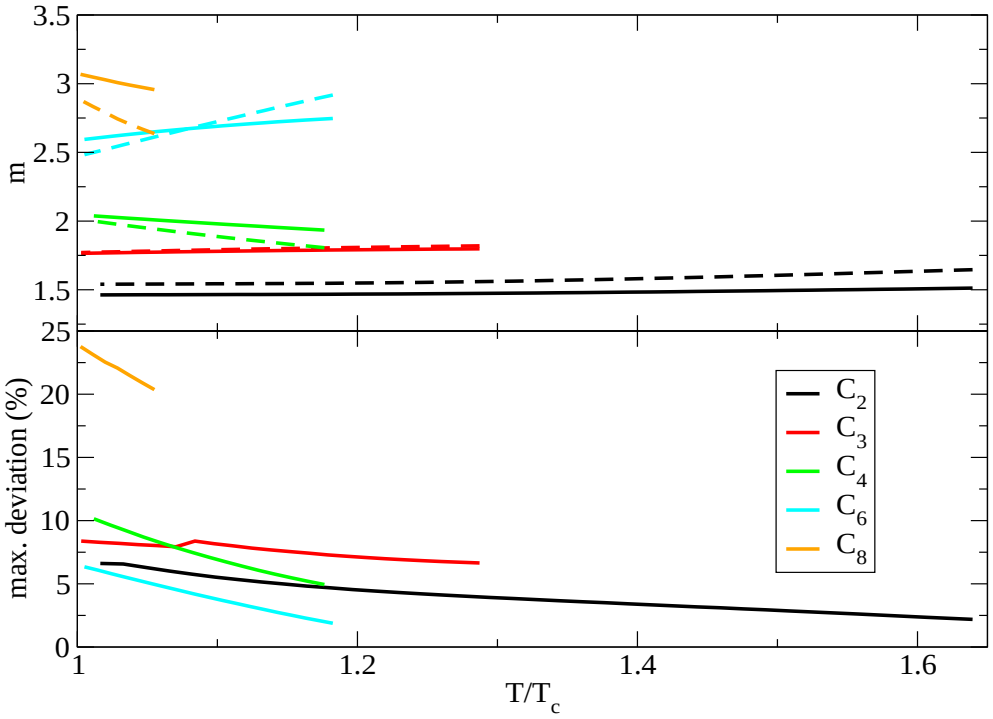

Figure 6.14: Application of the Enskog-2σ model with MD corrections as in case (ii). The optimised effective chain lengths are shown in the upper plot. m_α is given by the solid lines, m_χ by the dashed ones. The lower plot depicts the maximum deviation between model and the experimental reference correlations given in table 6.1.

Dependent on the fluid, the chain lengths are almost independent of the temperature T (as for propane), increase with T (as for hexane) or decrease with T (as for octane). According to the lower plot of Fig. 6.13, the model reproduces the experimental reference correlations of ethane, propane, butane, hexane and octane within 6.9%, 8.4%, 10.1%, 6.3% and 23.8%. As Fig. 6.14 shows, the results of the model in case (ii) are very similar. The chain lengths are barely distinguishable from the ones in Fig. 6.13. The maximum deviations between the model and the experimental reference correlations for ethane, propane, butane, hexane and octane are 6.6%, 9.8%, 10.1%, 6.3% and 23.8%. As an example, Fig. 6.15 shows the deviations between model and experimental reference correlation for butane and octane along several isotherms. The maximum deviation between model and experimental reference correlation occures always at the largest density.

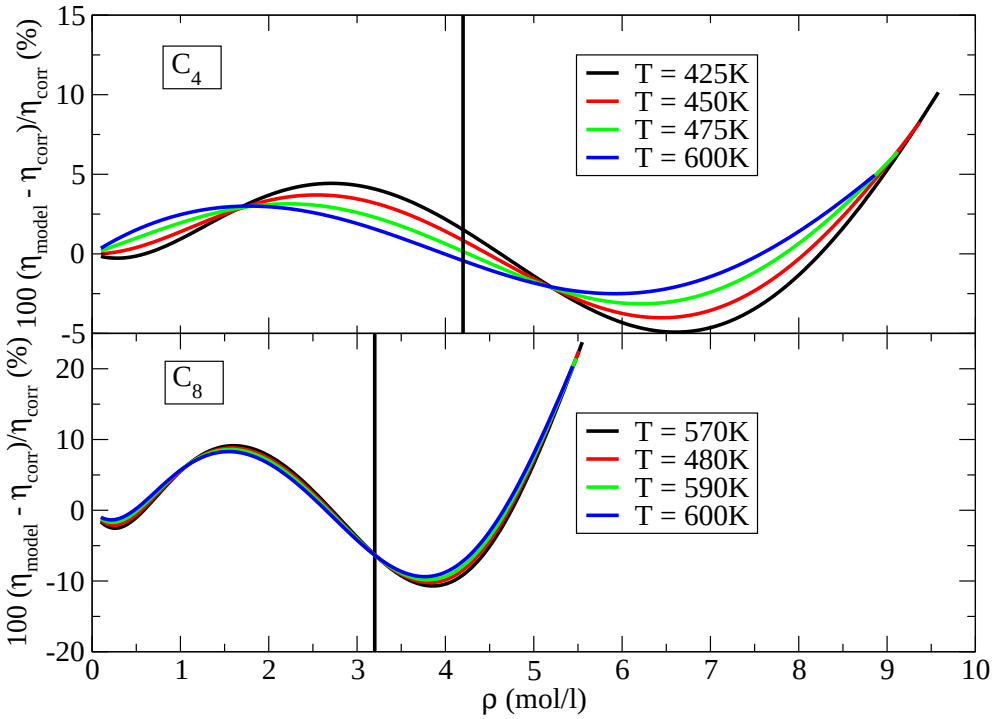

Figure 6.15: Precentage deviations, $100(\eta_{\text{model}} - \eta_{\text{corr}})/\eta_{\text{corr}}$, between the Enskog-2$\sigma$ model with MD corrections as in case (ii) and the experimental reference correlations along several isotherms versus density. Upper plot: butane. Lower plot: octane. The black vertical lines indicate approximately the maximum densities defined by Eq. (6.2).

Furthermore, if we restrict the density to the maximum density, Eq. (6.2), used in the previous sections, the deviations remain less than 4.4% and 9.0% for butane and octane.

According to further computations, the model in case (iii) performs again very similar to the other two cases and reproduces the experimental reference correlations of ethane, propane, butane, hexane and octane within 6.9%, 8.2%, 10.1%, 6.3% and 23.8%. The reason for the fact that all models lead to almost identical results can be understood with the aid of Fig. 6.16. The packing fraction y_{max} at the maximum density ρ_{exp} is plotted versus the reduced temperature T/T_c for model case (ii) and (iii). If y_{max} is smaller than 0.311, no MD correction is used and the model is identical to the model case (i). This holds true for almost all cases. For model case (ii), the exceptions are for ethane at $T/T_c \leq 1.02$ and propane at $T/T_c \leq 1.08$ as well as, for model case (iii), for propane at $T/T_c \leq 1.07$ and butane at $T/T_c \geq 1.08$. For all those exceptions, the

MD correction factor is found to be smaller than 1.02 and hence presents only a slight correction to model case (i).

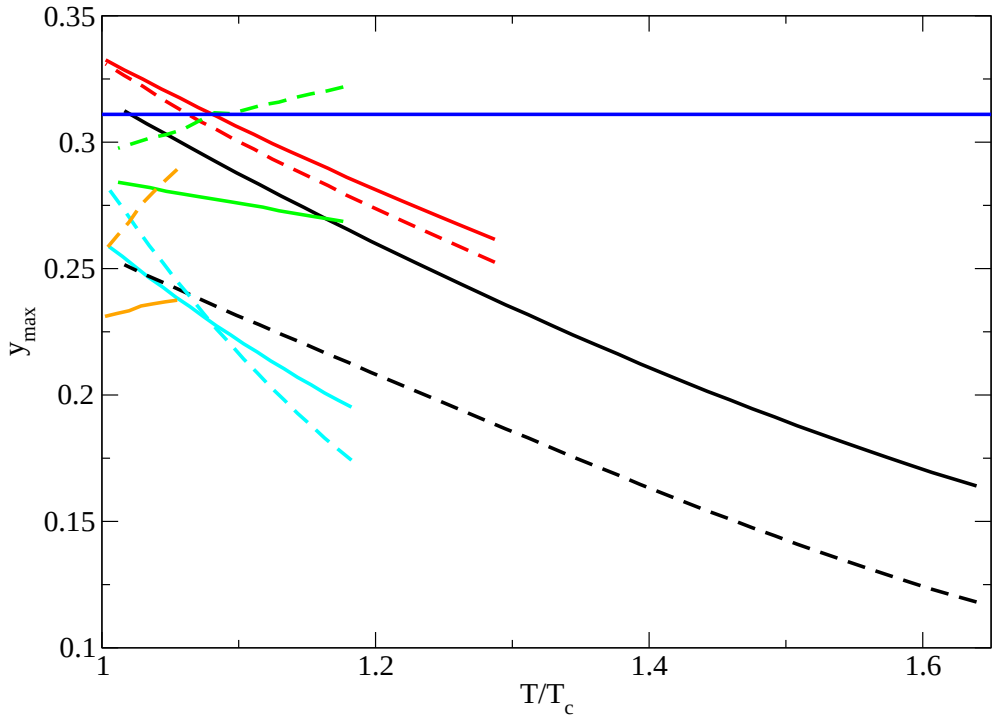

Figure 6.16: Packing fraction $y_{\max}$ at the maximum density $\rho_{\exp}$ versus the reduced temperature T/T_c. The black, red, green, cyan, orange lines refer to ethane, propane, butane, hexane, octane. The solid lines correspond to model case (ii), the dashed ones to case (iii). The horizontal blue line indicates a packing fraction of 0.311 above which MD corrections become relevant.

Overall, for the shorter alkanes ethane and propane, using the MD correction factor for a hard sphere fluid as in model case (ii) leads to slightly smaller deviations than in the model case (i), where no MD correction are used. However, for longer alkanes, the correction factor for a hard sphere fluid does not represent a satisfactory correction at high densities. In particular, for octane, the model cases (ii) and (iii) predict that no MD correction factor is needed but all models deviate up to 23.8% from the experimental reference correlation by (Huber *et al.*, 2004). As the correct MD correction factor for the modification of Enskog's viscosity expression for chain fluids by (de Wijn *et al.*,

2008) was not available, it could not be tested if MD corrections are relevant for octane and if those corrections lead to smaller deviations from the reference correlation.

6.2 Liquid range

In many petroleum reservoir and petroleum engineering processes, the main fraction of alkanes is in the liquid phase. To model the viscosity of liquid alkanes, we apply the Enskog-2σ model based on the modification of Enskog's viscosity expression for chain fluids by (de Wijn *et al.*, 2008) to ethane up to octane as summarised in table 6.4. First, the model is used without MD corrections. Then, we incorporate MD corrections for a hard sphere fluid and discuss how the number of free model parameters can be reduced. As the correct MD correction factor for chain fluids is unknown, the following analysis presents preliminary results. Our preliminary results allow in particular to estimate how well the model with correct MD corrections will work.

Table 6.4: Summary of experimental reference correlations for alkanes at liquid conditions.

Fluid	Max. pressure (MPa)	T-range (K)	Viscosity correlation
C_2	60	250-305	(Hendl *et al.*, 1994)
C_3	100	100-365	(Vogel *et al.*, 1998)
C_4	70	150-425	(Vogel *et al.*, 1999)
C_5	100	195-465	(Assael *et al.*, 1992)
C_6	100	240-505	(McLinden *et al.*, 2010)
C_7	100	245-540	(Assael *et al.*, 1992)
C_8	100	295-565	(Huber *et al.*, 2004)

6.2.1 Liquid range without MD corrections

We test two variants of the Enskog-2σ model without MD corrections. As the liquid range covers mainly high densities at which one can expect MD corrections to be important, the neglect of MD corrections is a rather crude approximation. Both approaches use the viscosity expression for chain fluids by (de Wijn *et al.*, 2008), Eq. (4.13).

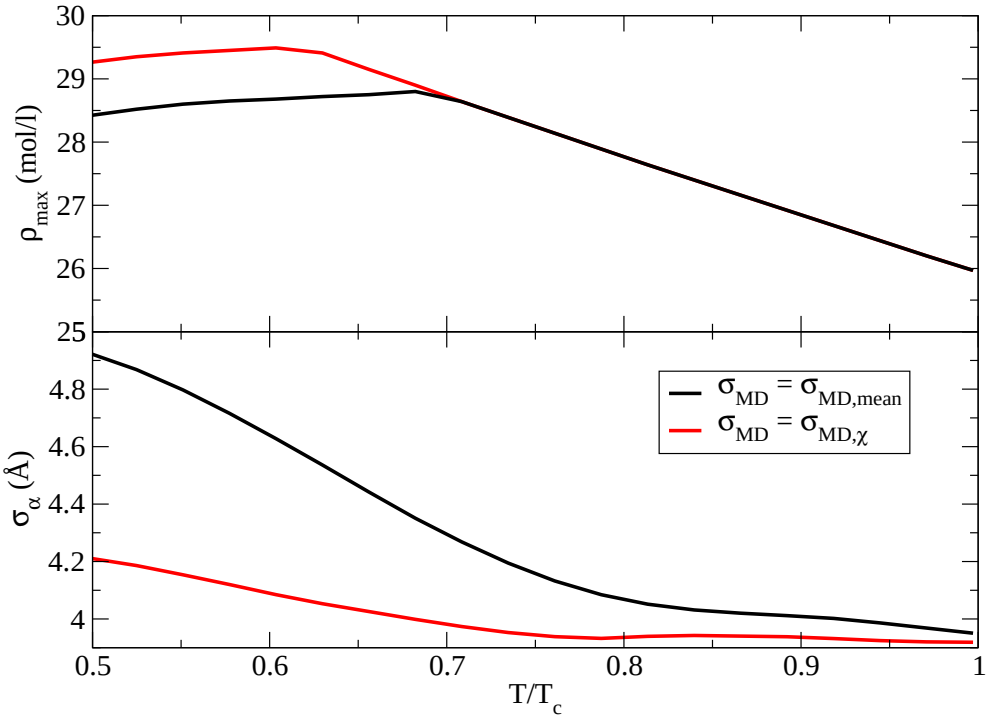

Figure 6.17: Maximum density $\rho_{(\max,\mathrm{mean},C_1)}$ (upper plot) and effective diameter σ_α (lower plot) in the base model for methane versus reduced temperature T/T_c. The black lines refer to the model with $\sigma_{\mathrm{MD,mean}}$, the red ones to $\sigma_{\mathrm{MD},\chi}$. Both models have been investigated in section 5.3.2.

The difference between both alternatives consists in which base model for the reference fluid methane is used.

(i) The first variant uses as base model for methane the model from section 5.3.2 with $\sigma_{\mathrm{MD,mean}}$. From this model, we derive the effective diameter σ_α and the maximum density $\rho_{\max}$. The diameter σ_α for the respective alkane is set equal to σ_α of the base model at the same reduced temperature T/T_c. We do not derive σ_α from the same temperature as it was done in section 6.1. This would mean that, at most temperatures under investigation, the diameter σ_α in the liquid phase is computed from the σ_α of methane at supercritical conditions. We would like to avoid this since we have seen in section 5.4.2 that the behaviour of σ_α changes qualitatively at the transition from subcritical to supercritical conditions. The

maximum density is derived from

$$\rho_{\max} = \min(\rho_{\exp}, \rho^*_{\text{mean}}) \tag{6.7}$$

where $\rho_{\exp}$ is the maximum density of the experimental reference correlation for the respective alkane and ρ^*_{mean} is defined via

$$\rho^*_{\text{mean}} = \rho_{(\max,\text{mean},C_1)} \frac{\rho_{c,C_n}}{\rho_{c,C_1}}. \tag{6.8}$$

The density $\rho_{(\max,\text{mean},C_1)}$ is the maximum density of methane in the model from section 5.3.2 with $\sigma_{\text{MD,mean}}$. The effective diameter σ_α as well as the maximum density $\rho_{(\max,\text{mean},C_1)}$ of methane are plotted in Fig. 6.17 versus the reduced temperature.

(ii) The second variant uses as base model for methane the model from section 5.3.2 with $\sigma_{\text{MD},\chi}$. The effective diameter σ_α as well as the maximum density $\rho_{(\max,\chi,C_1)}$ of methane are shown in Fig. 6.17. From those quantities, the effective diameter σ_α and the maximum density $\rho_{\max}$ are calculated analogously to case (i).

In the following we will refer to these approaches as model (i) and (ii). For both models, we obtain the temperature dependent effective chain lengths m_α and m_χ by minimising the maximum deviation between model and experimental reference correlation from the saturated liquid density up to $\rho_{\max}$ at a given temperature. The effective diameter σ_χ for each alkane is computed from the chain length constraint Eq. (6.1). The experimental reference correlations of the alkanes, their temperature range and maximum pressures are listed in table 6.4. The table contains in particular the correlations by (Assael *et al.*, 1992) for pentane and heptane. These correlations have not been used in the supercritical range as they are valid only at subcritical temperatures and above the critical density. The latter fact does not constitute a problem here as the saturated liquid density of a pure fluid is larger than its critical density.

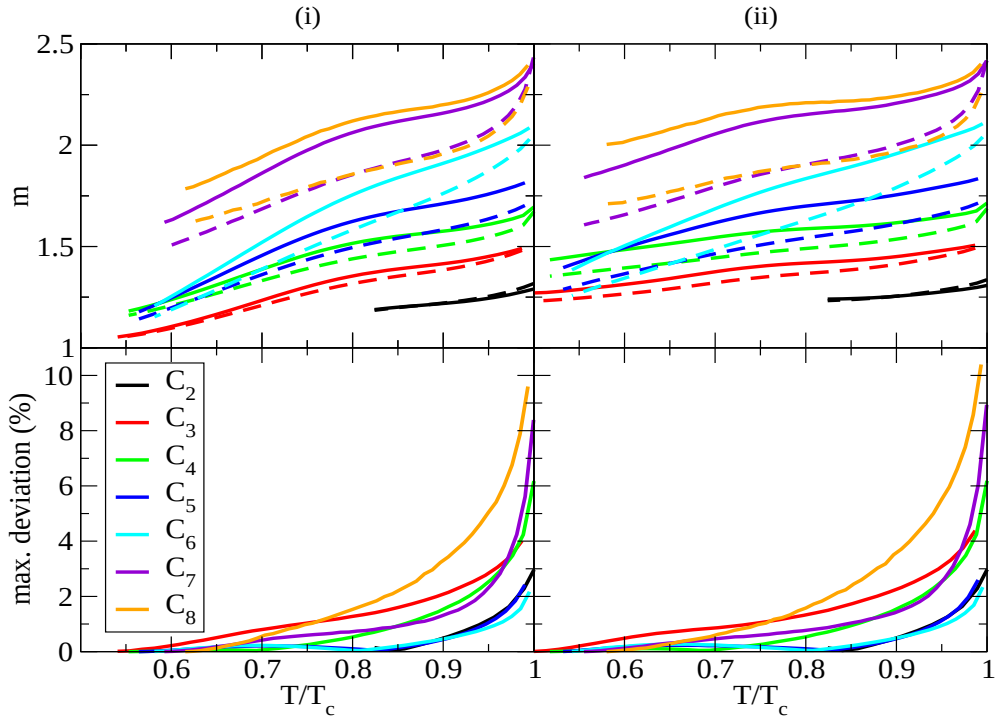

Figure 6.18: Application of Enskog-2σ model without MD corrections to the liquid range of alkanes. Effective optimised chain lengths (upper plots) and maximum deviation between models and experimental reference correlations (lower plots) are plotted versus the reduced temperature T/T_c. The chain length m_α is denoted by the solid lines in the upper plots, m_χ by the dashed lines. The plots on the left hand side refer to model case (i), the ones on the right hand side to (ii).

Fig. 6.18 summarises the results of both models. Both approaches lead to qualitatively similar results. The chain lengths increase in general with increasing temperature. At temperatures above $T/T_c = 0.75$, the chain lengths follow the physically reasonable trend of increasing with the carbon number. The only exception is that the chain length m_{χ,C_7} of heptane is slightly larger than m_{χ,C_8} of octane for $T/T_c \geq 0.8$. At low temperatures, the chain lengths of butane, pentane and hexane crossover and we observe the sequences $m_{\chi,C_6} \leq m_{\chi,C_5} \leq m_{\chi,C_4}$ and $m_{\alpha,C_6} \leq m_{\alpha,C_5} \leq m_{\alpha,C_4}$. As the lower plot of Fig. 6.18 shows, the maximum deviation between the models and the experimental reference correlations is just of the order of 1% for low temperatures. This indicates that the crossover might be avoided by a physically meaningful choice of the chain lengths that still reproduces the experimental reference correlations satis-

factorily. We will address this point in section 6.2.3. According to the lower plots of Fig. 6.18, model (i) and (ii) reproduce the experimental reference correlation of ethane, propane, butane, pentane, hexane, heptane, octane with maximum deviations less than 3.3%, 4.0%, 6.2%, 2.4%, 2.2%, 8.4%, 9.6% and 3.3%, 4.4%, 6.2%, 2.6%, 2.3%, 8.9%, 10.4%. The correlative power of both approaches is better than 5% for $T/T_c \leq 0.93$ and can be deemed overall satisfactory considering the crude approximation inherent in neglecting MD corrections in a density regime where MD corrections can expected to be important.

6.2.2 Liquid range with MD corrections

The liquid range covers mainly high densities at which one can expect MD corrections to be important. As the correct MD correction factor for the modification of Enskog's viscosity expression for chain fluids by (de Wijn *et al.*, 2008) is not available presently, we study the use of the MD correction factor for a hard sphere fluid, Eq. (2.42). We distinguish two model cases with different implementations of the MD correction factor:

(i) The effective diameter σ_{MD} and the effective chain length m_{MD} in the MD correction factor are set equal to $(\sigma_\alpha + \sigma_\chi)/2 =: \sigma_{\mathrm{MD,mean}}$ and $(m_\alpha + m_\chi)/2 =: m_{\mathrm{MD,mean}}$.

(ii) The effective diameter σ_{MD} and the effective chain length m_{MD} in the MD correction factor are set equal to $\sigma_\chi =: \sigma_{\mathrm{MD},\chi}$ and $m_\chi =: m_{\mathrm{MD},\chi}$.

In both cases, the modification of Enskog's viscosity expression for chain fluids by (de Wijn *et al.*, 2008) is multiplied by the respective MD correction factor, see Eq. (4.13). The effective diameter σ_α and maximum density $\rho_{\max}$ in model case (i) are defined as in case (i) in section 6.2.1 for the model without MD corrections. Analogously, σ_α and $\rho_{\max}$ in model case (ii) are defined as in case (ii) in section 6.2.1. In both approaches, the effective diameter σ_χ is computed via the chain length constraint Eq. (6.1) from σ_α and the effective chain lengths. The effective chain lengths m_α and m_χ are calculated by minimising the maximum deviation between model and experimental reference correlation from the saturated liquid density up to $\rho_{\max}$ at a given temperature.

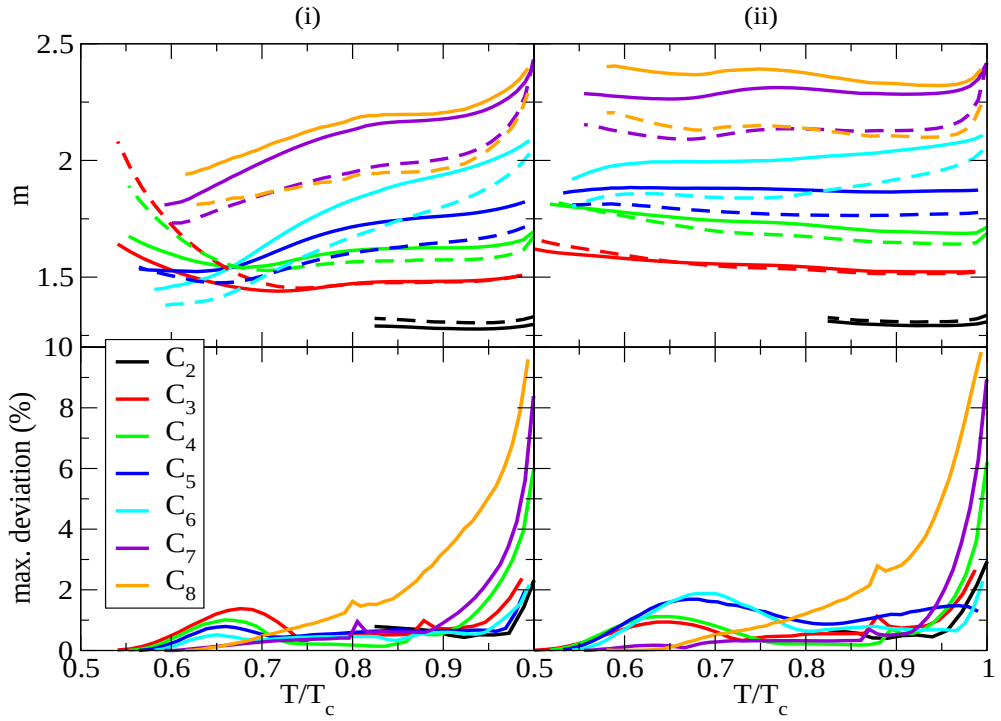

Figure 6.19: Application of Enskog-2σ model with MD corrections for a hard sphere fluid to the liquid range of alkanes. Effective optimised chain lengths (upper plots) and maximum deviation between models and experimental reference correlations (lower plots) are plotted versus the reduced temperature T/T_c. The chain length m_α is denoted by the solid lines in the upper plots, m_χ by the dashed lines. The plots on the left hand side refer to model case (i), the ones on the right hand side to (ii).

According to the lower plots in Fig. 6.19, model (i) and (ii) reproduce the experimental reference correlation of ethane, propane, butane, pentane, hexane, heptane, octane within 3.3%, 2.4%, 6.0%, 2.0%, 2.2%, 8.4%, 9.6% and 3.3%, 2.6%, 6.2%, 1.5%, 2.3%, 8.9%, 9.8%. The chain lengths in both approaches vary irregularly with the temperature. For $T/T_c \geq 0.8$, we find that the effective chain length m_{χ,C_7} of pentane is larger than the chain length m_{χ,C_8} of octane while, from a physical point of view, one would expect $m_{\chi,C_8} > m_{\chi,C_7}$. Moreover, in model case (i), the chain lengths exhibit unphysical behavior at low temperatures: for example, at $T/T_c = 0.6$, we obtain the sequences $m_{\alpha,C_6} \leq m_{\alpha,C_5} \approx m_{\alpha,C_3} \leq m_{\alpha,C_4}$ and $m_{\chi,C_6} \leq m_{\chi,C_5} \leq m_{\chi,C_4} \leq m_{\chi,C_3}$. It remains to be seen whether the chain lengths can be chosen in a physical meaningful way, i.e., increasing chain lengths with increasing carbon number and regular

dependence on temperature. In particular, at lower temperatures where the maximum deviations are less than 2%, there seems to be sufficient flexibility in obtaining a more physical behaviour of the chain lengths. We will test this assertion in section 6.2.3.

6.2.3 Results for constant chain length m_α

The chain lengths obtained for the model cases (i) and (ii) in section 6.2.2 exhibit irregular temperature dependence and partially unphysical dependence on the carbon number. In this section, we will discuss a modification of the approaches that will lead to a sensible behaviour of the chain lengths. The modification consists in setting the chain length m_α to a constant value and only optimising the chain length m_χ at each temperature to minimise the maximum deviation between model and the experimental reference correlations stated in table 6.4. The constant values for m_α are obtained from the following linear relationships in terms of the carbon number N

$$\text{for model case (i):} \quad m_\alpha = 0.997 + 0.15N, \tag{6.9}$$

$$\text{for model case (ii):} \quad m_\alpha = 0.992 + 0.17N. \tag{6.10}$$

The relationships have been calculated from a linear best fit of the optimised chain length m_α at $T/T_c = 0.85$ in section 6.2.2 listed in table 6.5. The m_α values together with the linear best fits are shown in Fig. 6.20. The chain length of heptane has been excluded in obtaining the linear best fits as it does not follow the linear trend of the other chain lengths. Furthermore, we selected the temperature $T/T_c = 0.85$ since, at this temperature, the optimised m_α's lie almost on a straight line and hence show physically sensible behavior. Both linear fits have approximately half the slope as the linear fit of m_α, Eq. (6.6), obtained from the SAFT-HS approach when the critical properties of n-alkanes are modelled.

Fig. 6.21 summarises the results for both model cases with m_α from the linear best fits. As the upper plots of Fig. 6.21 show, the optimised chain length m_χ increase with the carbon number and exhibit a regular temperature dependence; in model case (i), m_χ increases with decreasing temperature, while in model case (ii), m_χ decreases first with decreasing temperature before it increases with decreasing temperature for about $T/T_c \leq 0.72$. We will make use of the universal behaviour of m_χ in section 6.2.5 to reduce the number of free model parameters further on.

Table 6.5: Chain length m_α optimised at $T/T_c = 0.85$ for the models in section 6.2.2 for propane up to octane.

Fluid	m_α, case (i)	m_α, case (ii)
C_2	1.27	1.29
C_3	1.47	1.52
C_4	1.61	1.70
C_5	1.74	1.86
C_6	1.89	2.02
C_7	2.16	2.27
C_8	2.19	2.33

According to the lower plots in Fig. 6.21, model case (i) and (ii) reproduce the experimental reference correlation of ethane, propane, butane, pentane, hexane, heptane, octane up to $T/T_c = 0.97$ within 1.9%, 6.2%, 6.2%, 5.3%, 9.5%, 11.5%, 14.9% and 4.8%, 6.9%, 7.6%, 4.7%, 5.5%, 11.3%, 6.2%. Overall, the results show that, in both model cases, physically reasonable choices for the chain length parameters exist that succeed in reproducing the experimental reference correlations fairly accurately. The accuracy of the approaches in this section is further on evaluated directly against primary experimental viscosity data in section 6.2.4.

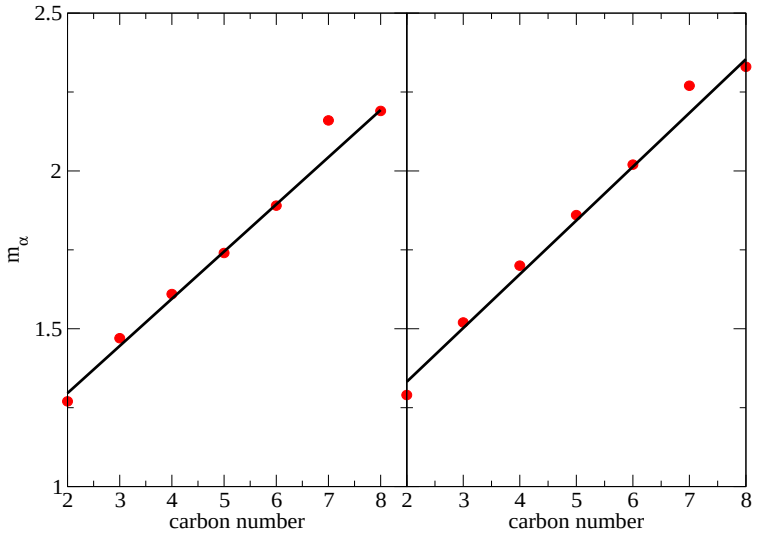

Figure 6.20: Best linear fits (black lines) of the optimised chain length m_α (red dots) at $T/T_c = 0.85$ for the models in section 6.2.2. The plot on the left hand side refer to model case (i), the one on the right hand side to (ii).

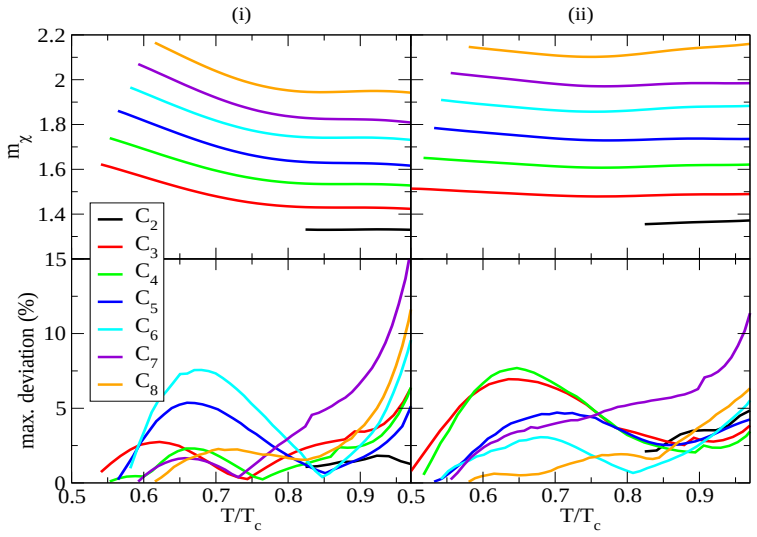

Figure 6.21: Application of Enskog-2σ model with MD corrections for a hard sphere fluid and m_α from the linear relationships Eq. (6.9) and (6.10) to the liquid range of alkanes. Effective optimised chain length m_χ (upper plots) and maximum deviation between models and experimental reference correlations (lower plots) are depicted versus the reduced temperature T/T_c. The plots on the left hand side refer to model case (i), the ones on the right hand side to (ii).

6.2.4 Comparison with primary experimental data

In this section, the accuracy of the models of section 6.2.3 is evaluated against the primary experimental data of ethane, propane and octane listed in table 6.6. Fig. 6.22 shows the results for ethane. Both models reproduce the experimental data sets very well within 4.5%. According to Fig. 6.23, the data sets of propane are correlated within 6.7% in model case (i) and 7.5% in model case (ii). The two data points by (Huang *et al.*, 1966) with deviations larger than 7% in model case (ii) deviate also more than 4.2% from the experimental reference correlation by (Vogel *et al.*, 1998). As Fig. 6.24 illustrates, model case (i) and (ii) reproduce the experimental primary data of octane within 7.7% and 4.0%. The point with the largest deviation occurs at a temperature close to the critical temperature of octane in the lower range of densities. Both models reproduce the primary experimental data satisfactorily. This supports the assertion that, in both model cases, physically reasonable choices for the chain length parameters exist that describe the liquid viscosity of alkanes fairly accurate. Overall, the Enskog-2σ models with MD correction factor for a hard sphere fluid perform fairly well in reproducing the liquid viscosity of alkanes. In future work, when MD corrections for chain fluids are used, we expect to obtain similarly good or even better results.

Table 6.6: Primary viscosity data sets of ethane, propane and octane based on (Hendl *et al.*, 1994), (Vogel *et al.*, 1998) and (Huber *et al.*, 2004).

Fluid	Data set	P-range (MPa)	T-range (K)
C_2	(Swift *et al.*, 1960)	0.2-4.8	193-303
C_2	(Eakin *et al.*, 1962)	0.7-55.1	298
C_2	(Carmichael & Sage, 1963a)	4.4-35.8	300-305
C_2	(Diller & Saber, 1981)	1.3-32.1	95-290
C_2	(Diller & Ely, 1989)	7.6-51.9	295
C_3	(Eakin & Ellington, 1959)	0.7-62.1	298
C_3	(Starling *et al.*, 1960)	0.7-55.1	298-411
C_3	(Carmichael *et al.*, 1964)	0.24-34.4	278-478
C_3	(Giddings *et al.*, 1966)	0.7-55.2	278-378
C_3	(Huang *et al.*, 1966)	6.9-34.5	173-273
C_3	(Strumpf *et al.*, 1974)	3.2-7.2	311
C_3	(Diller, 1982)	1.7-35.1	90-300
C_8	(Dymond & Young, 1980)	vapour pressure	283-393
C_8	(Badalyan & Rodchenko, 1986)	0.159	218-623
C_8	(Knapstad *et al.*, 1989)	vapour pressure	293-370
C_8	(Keramidi & Badalyan, 1982)	vapour pressure	398-569
C_8	(Oliveira & Wakeham, 1992)	0.1253	303-348
C_8	(Harris *et al.*, 1997)	0.1373	283-353
C_8	(Caudwell, 2009)	0.1202	298-473

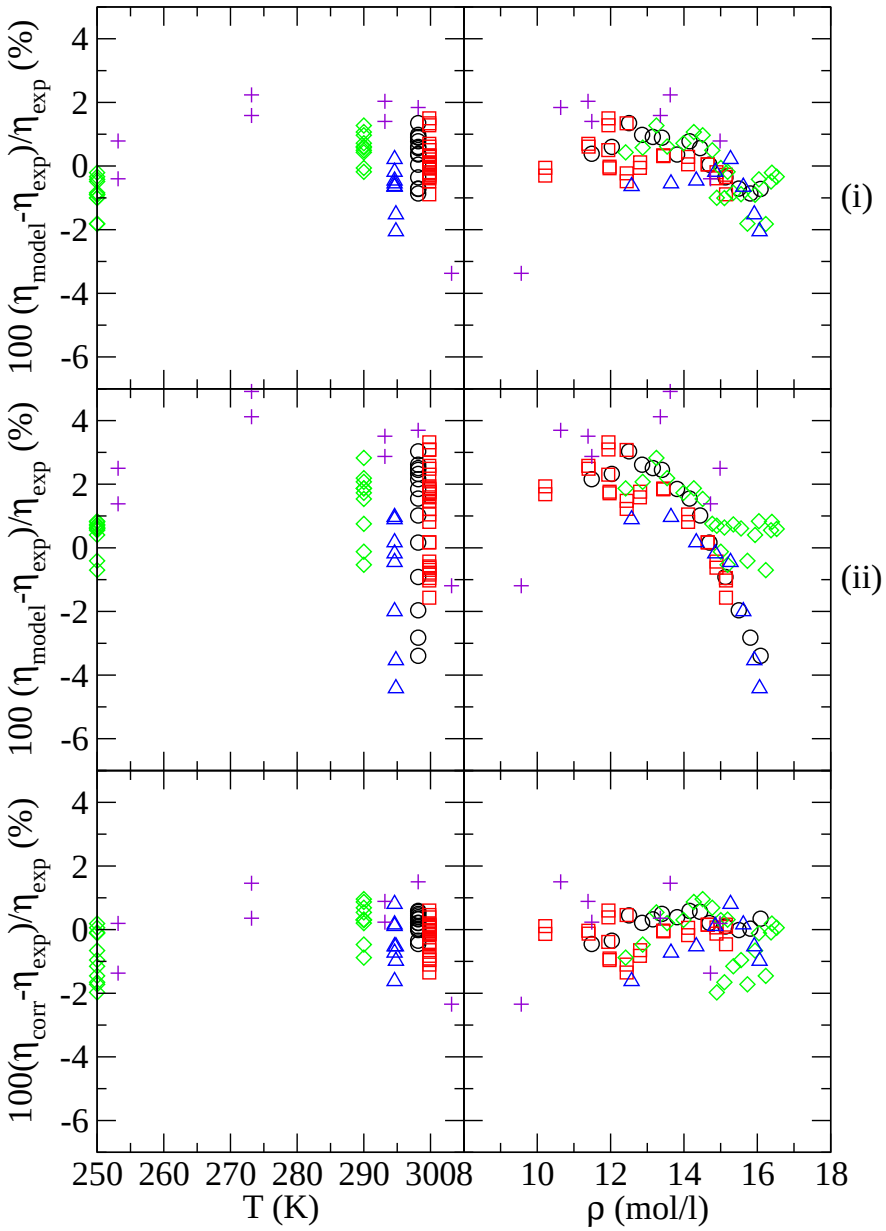

Figure 6.22: Application of the Enskog-2σ model to liquid primary experimental data of ethane. The upper plots are for model case (i), the middle plots for model case (ii) and the lower plots for the comparison between the experimental reference correlation for ethane by (Hendl *et al.*, 1994) and the primary experimental data sets. On the left hand side, the deviations between models and primary experimental data are depicted versus the temperature, on the right hand side, versus the density. The data set by (Baron *et al.*, 1959) is denoted by the black dots, the set by (Carmichael & Sage, 1963a) by red squares, the set by (Diller & Saber, 1981) by green diamonds, the set by (Diller & Ely, 1989) by blue triangles, the set by (Swift *et al.*, 1960) by violet pluses.

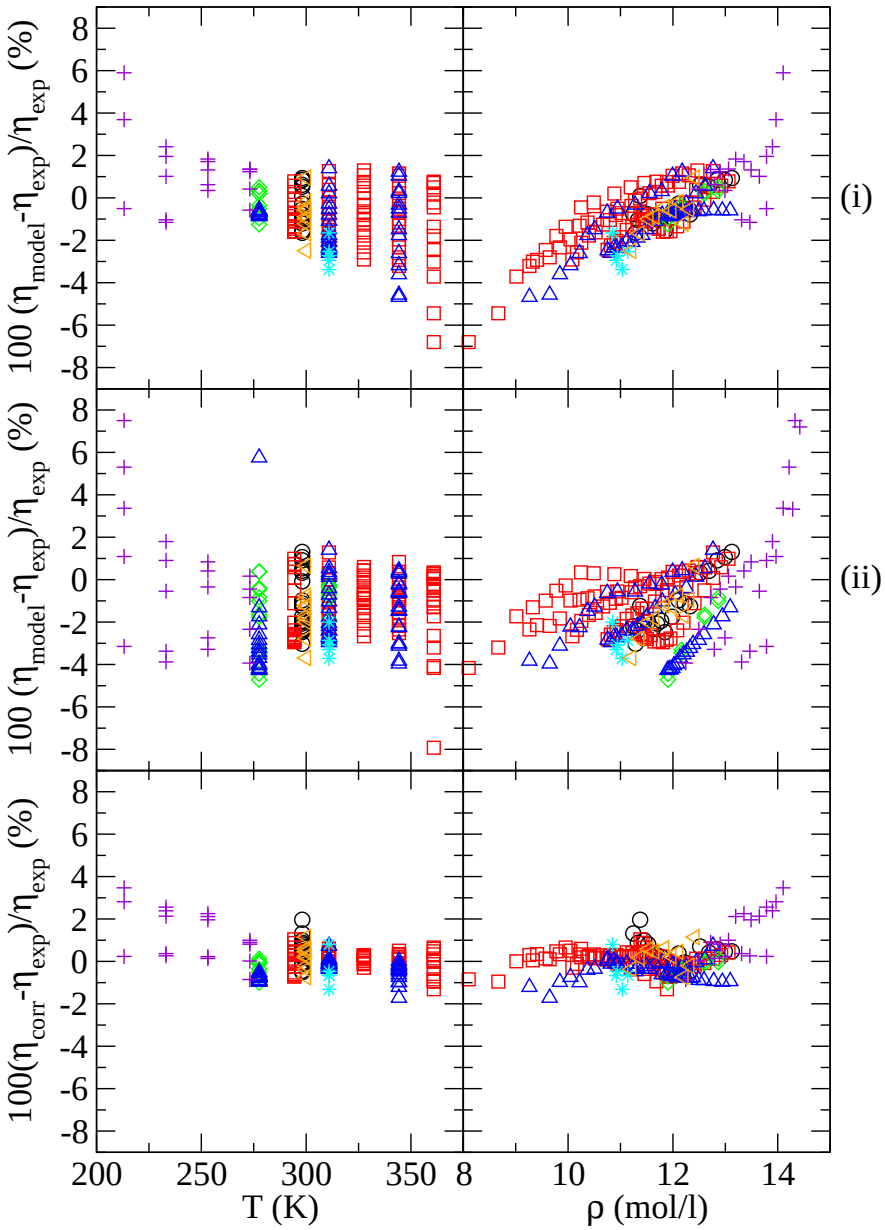

Figure 6.23: Application of the Enskog-2σ model to liquid primary experimental data of propane. The upper plots are for model case (i), the middle plots for model case (ii) and the lower plots for the comparison between the experimental reference correlation for propane by (Vogel *et al.*, 1998) and the primary experimental data sets. On the left hand side, the deviations between models and primary experimental data are depicted versus the temperature, on the right hand side, versus the density. The data set by (Eakin & Ellington, 1959) is denoted by the black dots, the set by (Starling *et al.*, 1960) by red squares, the set by (Carmichael *et al.*, 1964) by green diamonds, the set by (Giddings *et al.*, 1966) by blue triangles, the set by (Huang *et al.*, 1966) by violet pluses, the set by (Strumpf *et al.*, 1974) by cyan stars, the set by (Diller, 1982) by orange triangles.

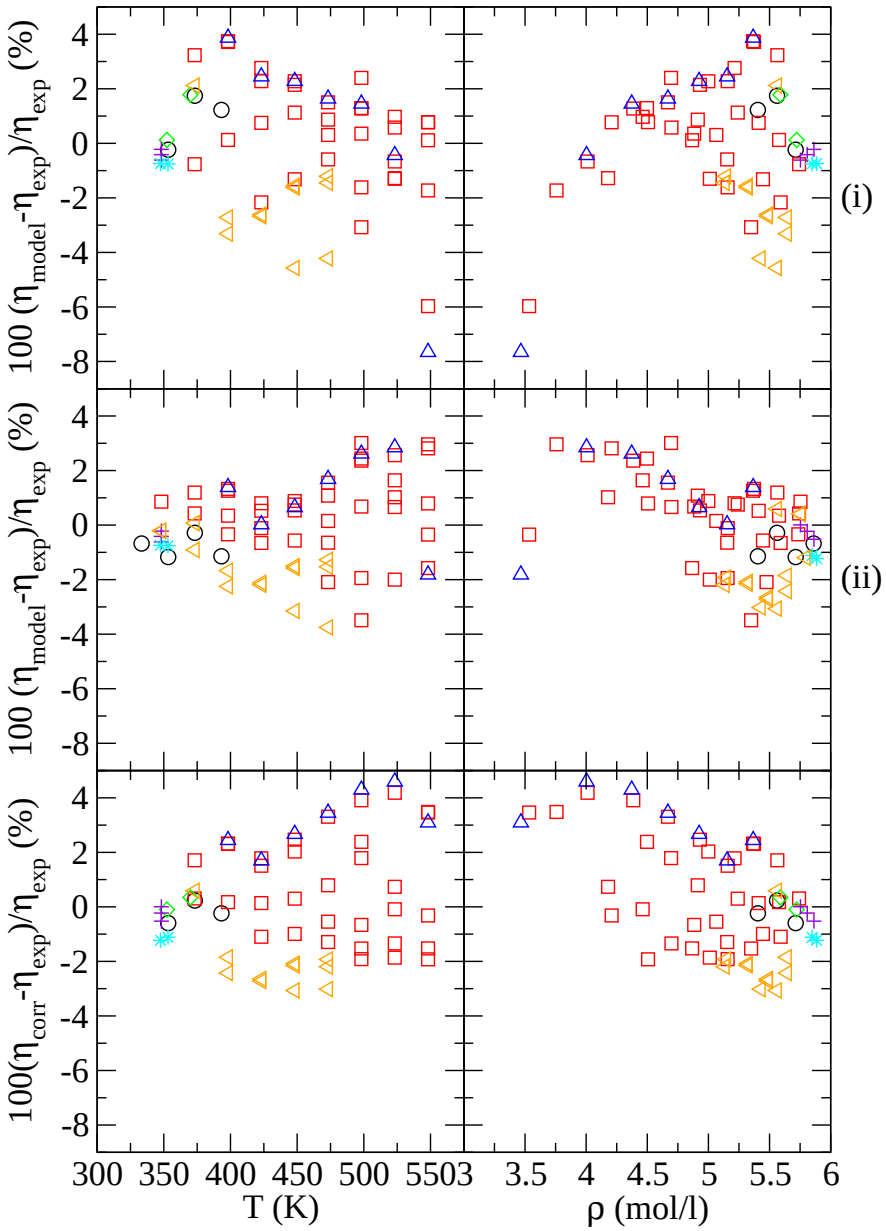

Figure 6.24: Application of the Enskog-2σ model to liquid primary experimental data of octane. The upper plots are for model case (i), the middle plots for model case (ii) and the lower plots for the comparison between the experimental reference correlation for octane by (Quiñones-Cisneros *et al.*, 2012) and the primary experimental data sets. On the left hand side, the deviations between models and primary experimental data are depicted versus the temperature, on the right hand side, versus the density. The data set by (Dymond & Young, 1980) is denoted by the black dots, the set by (Badalyan & Rodchenko, 1986) by red squares, the set by (Knapstad *et al.*, 1989) by green diamonds, the set by (Keramidi & Badalyan, 1982) by blue triangles, the set by (Oliveira & Wakeham, 1992) by violet pluses, the set by (Harris *et al.*, 1997) by cyan stars, the set by (Caudwell, 2009) by orange triangles.

6.2.5 Universal behaviour of m_χ

In section 6.2.3, we have found that the effective chain length m_χ exhibits a regular temperature dependence if m_α is obtained from a linear fit against the carbon number. In the following, we assume that, for model case (i), m_α is obtained from Eq. (6.9), and that, for model case (ii), m_α is obtained from Eq. (6.10). Then, m_χ is computed from scaling the m_χ of butane, m_{χ,C_4}, with a constant length scaling parameter L_{m_χ} at the same reduced temperature, i.e.:

$$m_\chi(T/T_c) = L_{m_\chi} m_{\chi,C_4}(T/T_c). \tag{6.11}$$

The effective chain length m_{χ,C_4} of butane is plotted against the reduced temperature for both model cases in Fig. 6.21. Butane is chosen as reference fluid since it has an intermediate carbon number and since the experimental viscosity correlation of butane extends over a wide range of subcritical temperatures. The scaling parameter L_{m_χ} is calculated by minimising the maximum deviation between model and experimental reference correlation for all subcritical conditions.

Table 6.7: Optimised scaling parameter L_{m_χ} for propane up to octane.

Fluid	L_{m_χ}, case (i)	L_{m_χ}, case (ii)
C_2	0.87	0.84
C_3	0.92	0.92
C_4	1.0	1.0
C_5	1.08	1.08
C_6	1.16	1.16
C_7	1.24	1.23
C_8	1.32	1.32

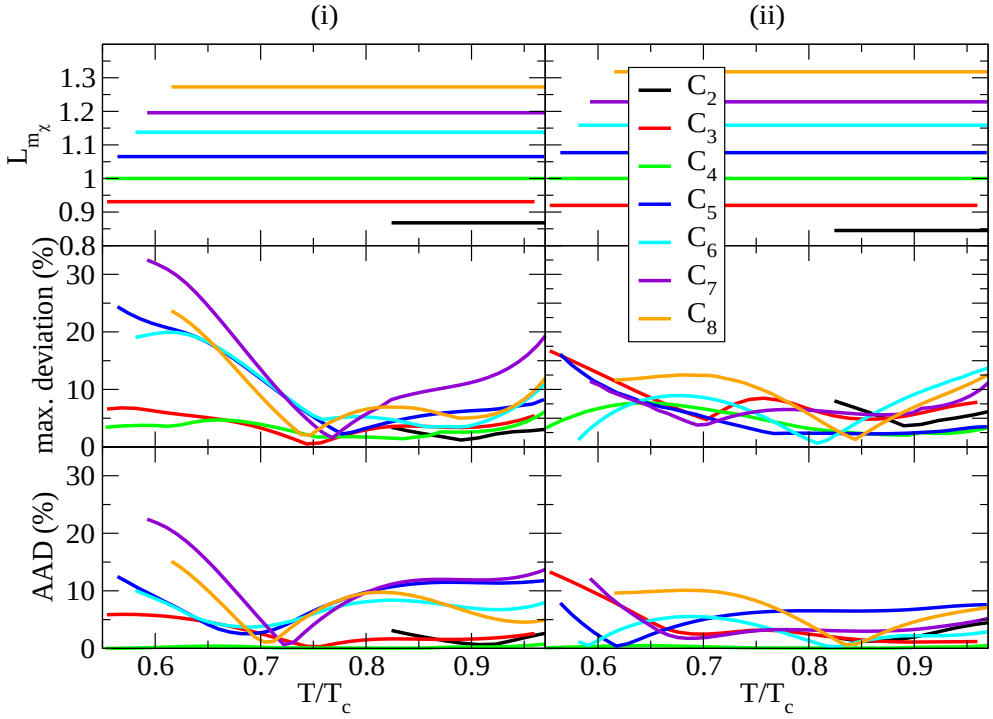

Figure 6.25: Application of the Enskog-2σ model with MD corrections for a hard sphere fluid, m_α from the linear relationships Eq. (6.9) and (6.10) and m_χ from Eq. (6.11) to the liquid range of alkanes. The scaling parameter L_{m_χ} (upper plots), maximum deviation between models and experimental reference correlations (middle plots) and AAD between models and experimental reference correlations (lower plots) are plotted versus the reduced temperature T/T_c. The plots on the left hand side refer to model case (i), the ones on the right hand side to (ii).

The resulting L_{m_χ}'s are summarised in table 6.7 and depicted in the upper plots of Fig. 6.25. According to the middle plots of Fig. 6.25, for model case (i), the experimental reference correlations of ethane, propane, pentane, hexane, heptane and octane are reproduced with maximum deviations less than 3.7%, 6.9%, 13.9%, 12.3%, 22.3% and 14.9%. The largest maximum deviations of alkanes longer than butane occur here for small temperatures. Model case (ii) gives better results for the longer alkanes and results in maximum deviations of 5.6%, 13.4%, 9.2%, 7.7%, 12.4% and 10.8% for ethane, propane, pentane, hexane, heptane and octane. Both model cases possess relatively large AAD's from the experimental reference correlations as can been in the lower plots of Fig. 6.25.

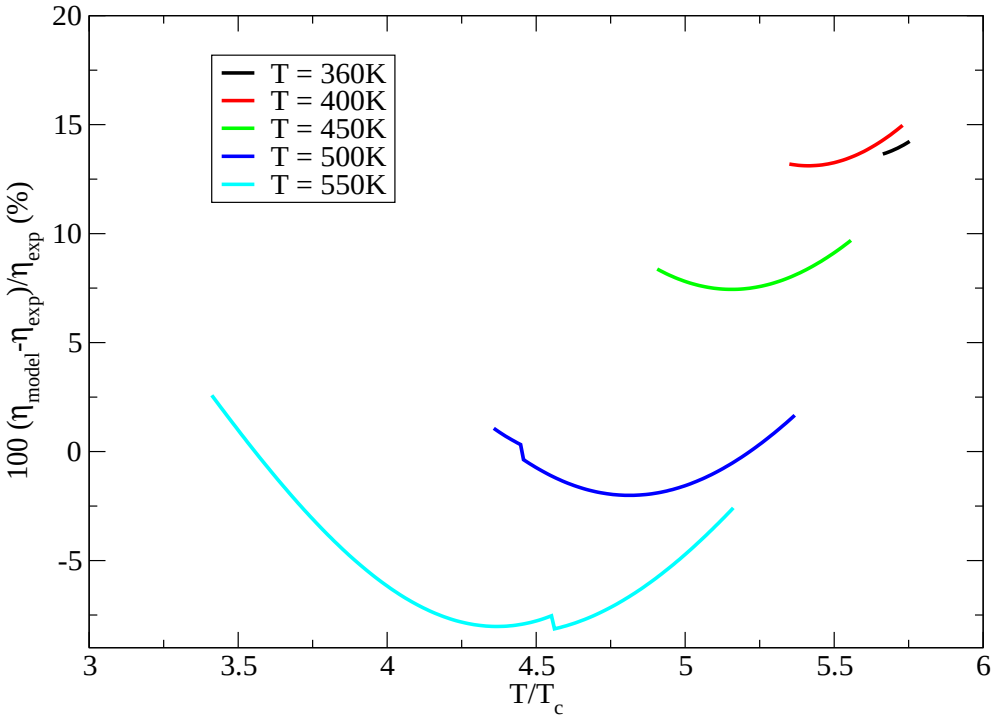

Figure 6.26: Percentage viscosity deviations, $100(\eta_{\text{model}}-\eta_{\text{exp}})/\eta_{\text{exp}}$, between the Enskog-$2\sigma$ model and the experimental reference correlation for octane by (Huber *et al.*, 2004) along several isotherms. The Enskog-2σ model is applied with MD corrections for a hard sphere fluid, m_α from the linear relationships Eq. (6.10) and m_χ from Eq. (6.11) with $L_{m_\chi} = 1.32$ as denoted in table 6.7.

For example, in model case (ii), the AAD from the correlation for octane exceeds 9% for $T/T_c \leq 0.74$. Several isotherms for this case are shown in Fig. 6.26. For $T \leq 450K$, i.e. $T/T_c \leq 0.8$, the model overestimates the viscosity systematically resulting in the large AAD's at low temperatures observed in Fig. 6.25.

As model case (ii), gives overall better results we focus on this case for the following investigations. As Fig. 6.27 shows, the length scaling parameter L_{m_χ} plotted versus the carbon number gives an almost straight line. The best linear fit results in the black line in Fig. 6.27 and reads

$$L_{m_\chi} = 0.68 + 0.079N. \tag{6.12}$$

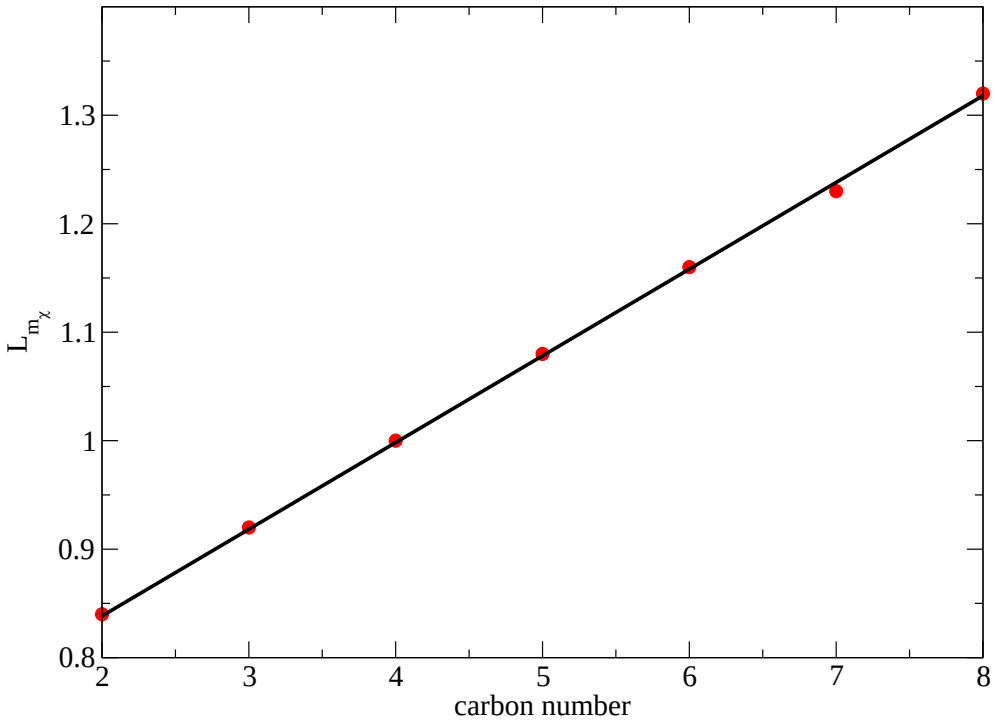

Figure 6.27: Best linear fits (black lines) of the optimised length scaling parameter L_{m_χ} (red dots) in model case (ii).

When L_{m_χ} is obtained from Eq. (6.12), m_χ from Eq. (6.11) and m_α from Eq. (6.10), all free parameters in the Enskog-2σ model are determined. The predictive power of the model is illustrated in Fig. 6.28. The experimental reference correlations are reproduced with maximum deviations less than 6.7%, 16.8%, 9.6%, 8.4%, 14.8% and 11.3% for ethane, propane, pentane, hexane, heptane and octane. The AAD's between model and the experimental reference correlations, denoted by the dashed lines in Fig. 6.28, are again relatively large. It is interesting to test in future work whether the results improve when the correct MD correction factor for the modification of Enskog's viscosity expression for chain fluids by (de Wijn *et al.*, 2008) is used.

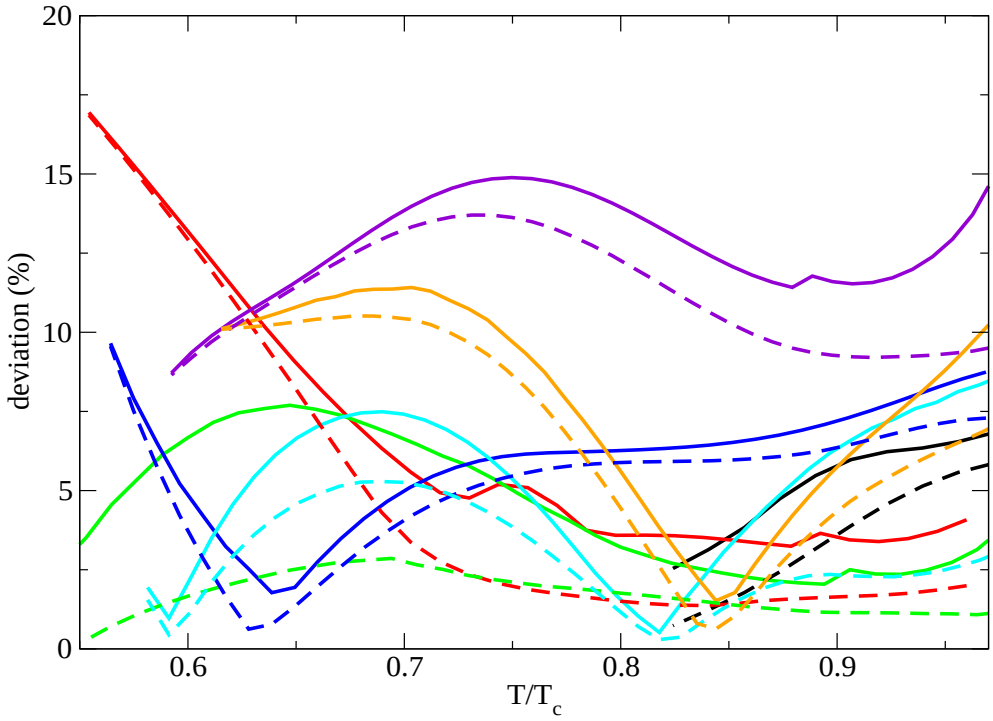

Figure 6.28: Application of Enskog-2σ model with MD corrections for a hard sphere fluid, m_α from Eq. (6.10) and m_χ from Eq. (6.11) with length scaling parameter L_{m_χ} from Eq. (6.12). The solid lines depict the maximum deviations between model and experimental reference correlations, the dashed lines the AADs.

6.3 Conclusions

In this chapter, we have applied the Enskog-2σ model, introduced in chapter 4, to alkanes. The model showed good correlative power up to moderate densities at supercritical conditions: when the two effective chain lengths m_α, m_χ were optimised, the approach reproduced the viscosity of ethane, propane, butane, hexane and octane within 6%. When m_α was obtained from a linear fit versus the carbon number and m_χ was optimised along one isotherm, the model correlated the viscosity of the five alkanes with deviations less than 9.3%. Next, we investigated an extension of the Enskog-2σ model for alkanes to high densities in the supercritical range. Using the MD correction factor for a hard sphere fluid and optimising both effective chain lengths at each temperature, the maximum deviations between the Enskog-2σ model and the experimental reference

correlations for ethane, propane, butane, hexane were found to increase up to 10% and for octane up to 23%. It is interesting to test in future work whether the results can be improved by using the correct MD correction factor for the modification of Enskog's viscosity expression for chain fluids by (de Wijn *et al.*, 2008).

The MD correction factor for a hard sphere fluid was also used to extend the model into the liquid range. When the chain length m_α was obtained from a linear fit versus the carbon number and m_χ is optimised at each temperature, the model reproduced the experimental reference correlations for of all alkanes from ethane to octane satisfactorily within 11%. Furthermore, the optimised m_χ exhibited a universal behaviour versus the reduced temperature T/T_c. When we made use of this observation and obtained m_χ from m_χ of butane by multiplication with a constant length scaling parameter, the model reproduced the experimental reference correlations for of all alkanes from ethane to octane within 13.4%. For some fluids and temperatures, however, this approach systematically overestimated or underestimated the experimental viscosity and resulted in relatively large AAD's from the experimental reference correlations along a given isotherm. Again, it is interesting to see in the future whether the results can be improved by using the correct MD correction factor for chain fluids.

7

Conclusion

The main aim of this work was to develop a new model for viscosity based on Enskog's hard sphere theory that provides us with a realistic and fairly viscosity model for dense fluids. The new viscosity model was derived from Enskog's theory and validated for simple fluids and n-alkanes over a wide range of pressures and temperatures in the supercritical as well as liquid phase.

The new viscosity model was obtained by introducing two effective weakly temperature dependent diameters in Enskog's viscosity expression. Accordingly, the new approach was named Enskog-2σ model. One of the diameters was linked to the collision rate between the fluid molecules, the other diameter to the molecule size.

The Enskog-2σ model was able to reproduce the experimental data of a series of simple fluids (Ar, CH_4, C_2H_6, N_2, CO_2, O_2, SF_6) within the uncertainty of the experimental data at supercritical conditions up to moderate densities. To extend the model to higher densities and pressures, the correction factor by (Sigurgeirsson & Heyes, 2003) obtained from molecular dynamics (MD) simulations was incorporated into the model. For the the effective diameter σ_{MD} appearing through the packing fraction in the MD correction factor, several empirical choices were investigated. The choices $(\sigma_\alpha + \sigma_\chi)/2$, $\sqrt{\sigma_\alpha \sigma_\chi}$, σ_χ for σ_{MD} led all to similar results and allow to correlate the viscosity of Ar, CH_4, C_2H_6, N_2, CO_2 and O_2 fairly well with deviations less than 11% up to very high pressures and densities. In addition, the Enskog-2σ model with MD correction factor reproduced the liquid viscosity data of these simple fluids with deviations less than 10%. Altogether, the correlative power of the Enskog-2σ model for

simple fluids was found to be very good to satisfying over a wide range of temperatures and pressures.

The effective diameters were found to exhibit a universal temperature dependence in several cases. This allowed to derive the σ's of simple fluids following a corresponding states principle from the optimised effective diameters of argon which was chosen as reference fluid. At supercritical conditions up to moderate densities, the diameter related to the molecule size showed conformal behaviour which allowed to reduce the number of free parameters to a single, length-scaling parameter. When this length scaling was obtained from the knowledge of the viscosity along a single isotherm, the accuracy of the viscosity prediction was similar to the uncertainty of the original correlation over its entire supercritical range. At liquid and supercritical conditions up to high densities, the number of free parameters was reduced to two constant length scaling parameters with which the two effective diameters are scaled independently. When the two length scaling parameters are obtained from a single isotherm, the model predicted the viscosity of CH_4, C_2H_6, N_2, CO_2 and O_2 at supercritical and liquid conditions with deviations less than about 9%. As the effective diameters changed their behaviour qualitatively at the transition from the liquid to the supercritical regime, the length scaling parameters at supercritical conditions differed from the ones at the liquid conditions.

Based on the modification of Enskog theory for chain fluids (de Wijn *et al.*, 2008), the Enskog-2σ model was extended to n-alkanes. The model showed good correlative power up to moderate densities at supercritical conditions: when the two effective chain lengths m_α, m_χ were optimised, the approach reproduced the viscosity of ethane, propane, butane, hexane and octane with deviations less than 6%. When m_α was obtained from a linear fit versus the carbon number and m_χ was optimised along one isotherm, the model correlates the viscosity of the five alkanes with deviations less than 9.3%. Using the MD correction factor for a hard sphere fluid and optimising both effective chain lengths at each temperature the model was extended to high densities at supercritical conditions. The maximum deviations between the Enskog-2σ model and the experimental reference correlations for ethane, propane, butane, hexane were found to increase up to 10% and for octane up to 23%.

The MD correction factor for a hard sphere fluid was also used to extend the model into the liquid range. When the chain length m_α was obtained from a linear fit versus the carbon number and m_χ was optimised at each temperature, the model reproduced

the viscosity of all alkanes from ethane to octane satisfactorily with deviations less than 11%. Furthermore, the optimised m_χ exhibited a universal behaviour versus the reduced temperature T/T_c. When m_χ was obtained from the one of butane by multiplication with a constant length scaling parameter, the model reproduced the viscosity of all alkanes from ethane to octane deviations less than 13.4%. For some fluids and temperature, however, this approach systematically overestimated or underestimated the experimental viscosity and resulted in relatively large AAD's from the experimental viscosity along a given isotherm.

7.1 Future work

Attractive proposals for future work are:

- In this work, the Enskog-2σ model has been applied to n-alkanes up to octane. It would be interesting to extend the model to longer alkanes and test if the model parameters can be expressed in terms of the carbon number.
- The Enskog-2σ model for alkanes has been extended to high densities by the use of the MD correction factor for hard spheres. With the aid of MD simulations, the correct MD correction factor for a chain fluids could be derived and subsequently incorporated in the Enskog-2σ model which might improve the results at high densities distinctively.
- The Enskog-2σ model has been restricted to n-alkanes and simple fluids, i.e., fluids with fairly spherical, non-polar molecules. In practice, the viscosity of many non-simple fluids is of great importance and hence it is of interest to extend and validate the Enskog-2σ model for such fluids. Non-simple fluids that play an important role in petroleum industry include water, brines, hydrogen sulfide and methanol.
- The Enskog-2σ model could be used to derive a new model for the viscosity of fluid mixtures. This could be done by developing suitable mixing rules between the model parameters.
- For a given fluid, the Enskog-2σ model relies on viscosity data along at least one isotherm as input to predict the viscosity with good accuracy at other phase

conditions. We tested a series of approaches to predict the viscosity of simple fluids from thermodynamic data or other transport properties but the predictions generally lacked in accuracy. More future work could be devoted to link viscosity of simple fluids to other thermodynamic properties in order to obtain a fully predictive model.

References

Andersen, H., Weeks, J.D. & Chandler, D. (1971). Relationship between the hard-sphere fluid and fluids with realistic repulsive forces. *Phys. Rev. A*, **4**, 15971607.

Andrews, F. (1976). A simple approach to the equilibrium statistical mechanics of Lennard-Jones fluids. *J. Chem. Phys.*, **64**, 1948–1951.

Assael, M., Dymond, J., Papadaki, M. & Patterson, P. (1992). Correlation and prediction of dense fluid transport coefficients. I. n-alkanes. *Int. J. Thermophys.*, **13**, 269 – 281.

Assael, M.J., Dalaouti, N.K. & Wakeham, W.A. (2001). Prediction of the viscosity of liquid mixtures. *Int. J. Thermophys.*, **22**, 1727–1737.

Badalyan, A. & Rodchenko, S. (1986). *Izv. Vyssh. Uchebn. Zaved., Neft i Gaz*, **3**, 61–64.

Barker, J.A. & Henderson, D. (1967). Perturbation Theory and Equation of State for Fluids. II. A Successful Theory of Liquids. *J. Chem. Phys.*, **47**, 4714–4721.

Baron, J.D., Roof, J.G. & Wells, F.W. (1959). Viscosity of Nitrogen, Methane, Ethane, and Propane at Elevated Temperature and Pressure. *J. Chem. Eng. Data*, **4**, 283288.

Barua, A.K., Afzal, M., Flynn, G.P. & Ross, J. (1964). Viscosity of Hydrogen, Deuterium, Methane, and Carbon Monoxide from -50° to 150°C below 200 Atmospheres. *J. Chem. Phys.*, **41**, 374–399.

Ben-Amotz, D. & Herschbach, D.R. (1990). Estimation of effective diameters for molecular fluids. *J. Chem. Phys.*, **94**, 1038–1047.

Bock, S., Bich, E., Vogel, E., Dickinson, A.S. & Vesovic, V. (2002). Calculation of the transport properties of carbon dioxide. I. Shear viscosity, viscomagnetic effects, and self-diffusion. *J. Chem. Phys.*, **117**, 2151–2160.

Bordat, P. & Müller-Plathe, F. (2002). The shear viscosity of molecular fluids: A calculation by reverse nonequilibrium molecular dynamics. *J. Chem. Phys.*, **116**, 3362–3369.

Carmichael, L.T. & Sage, B.H. (1963a). Viscosity of Ethane at High Pressures. *J. Chem. Eng. Data*, **8**, 9498.

Carmichael, L.T. & Sage, B.H. (1963b). Viscosity of Hydrocarbons, n-Butane. *J. Chem. Eng. Data*, **8**, 612616.

Carmichael, L.T., Berry, V.M. & Sage, B.H. (1964). Viscosity of Hydrocarbons. Propane. *J. Chem. Eng. Data*, **9**, 411415.

Carnahan, N.F. & Starling, K.E. (1969). Equation of state for nonattracting rigid spheres. *J. Chem. Phys.*, **51**, 635–636.

Caudwell, D. (2009). *Viscosity Measurements on Dense Fluid Mixtures*. PhD dissertation, Imperial College London.

Chapman, S. & Cowling, T. (1970). *The Mathematical Theory of Non-uniform Gases*. Cambridge University Press, Cambridge.

Ciotta, F. (2010). *Viscosity of asymmetric liquid mixtures under extreme conditions*. PhD dissertation, Imperial College London.

Davis, H.T., Rice, S.A. & Senger, J.V. (1961). On the Kinetic Theory of Dense Fluids. IX. The Fluid of Rigid Spheres with a Square-well Attraction . *J. Chem. Phys.*, **35**, 2210–2233.

de Wijn, A.S., Vesovic, V., Jackson, G. & Trusler, J.P.M. (2008). A kinetic theory description of the viscosity of dense fluids consisting of chain molecules. *J. Chem. Phys.*, **128**, 204901.

de Wijn, A.S., Riesco, N., Jackson, G., Trusler, J.P.M. & Vesovic, V. (2012). Viscosity of liquid mixtures: The Vesovic-Wakeham method for chain molecules . *J. Chem. Phys.*, **136**, 074514.

Diller, D.E. (1980). Measurements of the viscosity of compressed gaseous and liquid methane. *Physica A*, **104**, 417–426.

Diller, D.E. (1982). Measurements of the viscosity of saturated and compressed liquid propane. *J. Chem. Eng. Data*, **27**, 240243.

Diller, D.E. & Ely, J.F. (1989). *High Temperatures - High Pressures*, **21**, 631.

Diller, D.E. & Saber, J.M. (1981). Measurements of the viscosity of compressed gaseous and liquid ethane. *Physica A*, **108**, 143152.

DiPippo, R., Kestin, J. & Oguchi, K. (1967). Viscosity of three binary gaseous mixtures. *J. Chem. Phys.*, **46**, 4758–4765.

Dolan, J.P., Starling, K.E., Lee, A.L., Eakin, B.E. & Ellington, R.T. (1963). Liquid, Gas and Dense Fluid Viscosity of n-Butane. *J. Chem. Eng. Data*, **8**, 396399.

Dufal, S. & Haslam, A. (2012). private communication.

Dymond, J.H. (1974). Corrected Enskog theory and the transport coefficients of liquids. *J. Chem. Phys.*, **60**, 969–973.

Dymond, J.H. (1985). Hard-sphere theories of transport properties. *Chem. Soc. Rev.*, **14**, 317356.

Dymond, J.H. & Alder, B.J. (1966). Van der Waals Theory of Transport in Dense Fluids. *J. Chem. Phys.*, **45**, 2061–2068.

Dymond, J.H. & Young, K.J. (1980). Transport properties of nonelectrolyte liquid mixtures I. Viscosity coefficients for n-alkane mixtures at saturation pressure from 283 to 378 K. *Int. J. Thermophys.*, **1**, 331–344.

Eakin, B.E. & Ellington, R.T. (1959). *Trans. Am. Inst. Min. Metall. Pet. Eng.*, **216**, 85.

REFERENCES

Eakin, B.E., Starling, K.E., Dolan, J.P. & Ellington, R.T. (1962). Liquid, Gas, and Dense Fluid Viscosity of Ethane. *J. Chem. Eng. Data*, **7**, 3336.

Egorov, S.A. (2008). A mode-coupling theory treatment of the transport coefficients of the Lennard-Jones fluid. *J. Chem. Phys.*, **128**, 144508.

Enskog, D. (1922). Kinetic theory of heat conductivity, viscosity, and diffusion in certain condensed gases and liquids. *K. Sven. Vetenskapsakad. Handl*, **63**.

Evers, C., Lösch, H.W. & Wagner, W. (2002). An absolute viscometer-densimeter and measurements of the viscosity of nitrogen, methane, helium, neon, argon, and krypton over a wide range of density and temperature. *Int. J. Thermophys.*, **23**, 1411–1439.

Fenghour, A., Wakeham, W. & Vesovic, V. (1998). The viscosity of carbon dioxide. *J. Phys. Chem. Ref. Data*, **27**, 31–44.

Ferziger, J. & Kaper, H.G. (1972). *Mathematical theory of transport processes in gases*. North-Holland Publishing Company, Amsterdam.

Galliéro, G. & Boned, C. (2009). Shear viscosity of the Lennard-Jones chain fluid in its gaseous, supercritical, and liquid states. *Phys. Rev. E*, **79**, 021201.

Galliéro, G., Boned, C. & Baylaucq, A. (2005). Molecular Dynamics Study of the Lennard-Jones Fluid Viscosity: Application to Real Fluids. *Ind. Eng. Chem. Res.*, **44**, 6963–6972.

Galliéro, G., Boned, C., Baylaucq, A. & Montel, F. (2006). Molecular dynamics comparative study of Lennard-Jones α-6 and exponential α-6 potentials: Application to real simple fluids (viscosity and pressure). *Phys. Rev. E*, **73**, 061201.

Giddings, J.G., Kao, J.T.F. & Kobayashi, R. (1966). Development of a High-Pressure Capillary-Tube Viscometer and Its Application to Methane, Propane, and Their Mixtures in the Gaseous and Liquid Regions. *J. Chem. Phys.*, **45**, 578–586.

Gil-Villegas, A., Galindo, A., Whitehead, P., Mills, S., Jackson, G. & Burgess, A. (1997). Statistical associating fluid theory for chain molecules with attractive potentials of variable range . *J. Chem. Phys.*, **106**, 4168–4186.

Gracki, J., Flynn, G. & Ross, J. (1969). Viscosity of Nitrogen, Helium, Hydrogen, and Argon from - 100 to 25°C up to 150-250 atm. *J. Chem. Phys.*, **51**, 3856–3864.

Guggenheim, E. (1965). Variations on van der Waals' equation of state for high densities. *Mol. Phys.*, **9**, 199–200.

Hanley, H.J.M., McCarty, R.D. & Cohen, E.G.D. (1972). Analysis of the transport coefficients for simple dense fluid: Application of the modified Enskog theory. *Physica*, **60**, 322–356.

Hansen, J. & McDonald, I. (2006). *Theory of simple liquids*. Academic press.

Harris, K.R., Malhotra, R. & Woolf, L.A. (1997). Temperature and Density Dependence of the Viscosity of Octane and Toluene. *J. Chem. Eng. Data*, **42**, 12541260.

Haynes, H. (1973a). Viscosity of gaseous and liquid argon. *Physica*, **67**, 440470.

Haynes, W. (1973b). Viscosity of saturated liquid methane. *Physica*, **70**, 410–412.

Hellmann, R., Bich, E., Vogel, E., Dickinson, A.S. & Vesovic, V. (2008). Calculation of the transport and relaxation properties of methane. I. Shear viscosity, viscomagnetic effects, and self-diffusion. *J. Chem. Phys.*, **129**, 064302.

Hellmann, R., Bich, E., Vogel, E., Dickinson, A.S. & Vesovic, V. (2009). Calculation of the transport and relaxation properties of dilute water vapor. *J. Chem. Phys.*, **131**, 014303.

Hellmann, R., Bich, E., Vogel, E. & Vesovic, V. (2011). Ab initio intermolecular potential energy surface and thermophysical properties of hydrogen sulfide. *Phys. Chem. Chem. Phys*, **13**, 13749–13758.

Hendl, S., Millat, J., Vogel, E., Vesovic, V., Wakeham, W., Luettmer-Strathmann, J., Sengers, J. & Assael, M. (1994). Correlation for the Viscosity of Sulfur Hexafluoride (SF_6) from the Triple Point to 1000 K and Pressures to 50 MPa . *Int. J. Theromphys.*, **15**, 1–31.

Hess, B. (2002). Determining the shear viscosity of model liquids from molecular dynamics simulations. *J. Chem. Phys.*, **116**, 209–217.

REFERENCES

Hirschfelder, J., Curtiss, C. & Bird, R. (1954). *Molecular Theory of Gases and Liquids*. Wiley, New York.

Hongo, M., Yokoyama, C. & Takahashi, S. (1988). Viscosity of Methane - Chlorodifluoromethane (R22) Gaseous Mixtures in the Temperature Range from 298.15 K to 373.15 K and at Pressures up to 5 MPa. *J. Chem. Eng. Jpn.*, **21**, 632–638.

Huang, E.T.S., Swift, G.W. & Kurata, F. (1966). Viscosities of methane and propane at low temperatures and high pressures. *AIChE J.*, **12**, 932936.

Huber, M.L., Laesecke, A. & Xiang, H. (2004). Viscosity correlations for minor constituent fluids in natural gas: n-octane, n-nonane and n-decane. *Fluid Phase Equil.*, **224**, 263270.

Iwasaki, H. & Takahashi, H. (1959). Viscosity of methane under high pressure. *J. Chem. Soc. Jpn.*, **62**, 918–921.

Jackson, G. & Gubbins, K. (1989). Mixtures of associating spherical and chain molecules. *Pure & Appl. Chem.*, **61**, 1021–1026.

Karkheck, J., Stell, G. & Xu, J. (1988). Transport theory for the Lennard-Jones dense fluid. *J. Chem. Phys.*, **89**, 5829–5833.

Keramidi, A. & Badalyan, A. (1982). *Izv. Vyssh. Uchebn. Zaved., Neft i Gaz*, **3**, 58–60.

Kestin, J. & Leidenfrost, W. (1959). An absolute determination of the viscosity of eleven gases over a range of pressures. *Physica*, **25**, 1033–1062.

Kestin, J. & Nagashima, A. (1964). Viscosity of Neon-Helium and Neon-Argon Mixtures at 20°C and 30°C. *J. Chem. Phys.*, **40**, 3648–3655.

Kestin, J. & Yata, J. (1968). Viscosity and Diffusion Coefficient of Six Binary Mixtures . *J. Chem. Phys.*, **49**, 4780–4792.

Kirkwood, J. & Boggs, E. (1942). The radial distribution function in liquids. *J. Chem. Phys.*, **10**, 394–402.

Kirkwood, J.G., Buff, F.P. & Green, M.S. (1949). The Statistical Mechanical Theory of Transport Processes. III. The Coefficients of Shear and Bulk Viscosity of Liquids . *J. Chem. Phys.*, **17**, 988–994.

Knapstad, B., Skjølsvik, P.A. & Øye, H.A. (1989). Viscosity of pure hydrocarbons. *J. Chem. Eng. Data*, **41**, 3743.

Kurin, V. & Golubev, I. (1974). Viscosity of argon, air and carbon dioxide with pressures to 4000 kgs/cm and various temperatures. *Teploenergetika*, **11**, 84–85.

Lado, F. (1984). Choosing the reference system for liquid state perturbation theory. *Mol. Phys.*, **52**, 871–876.

Lemmon, E. & Jacobson, R. (2004). Viscosity and Thermal Conductivity Equations for Nitrogen, Oxygen, Argon, and Air. *Int. J. Thermophys.*, **25**, 21–69.

Leutheuser, E. (1982). Dynamics of a classical hard-sphere gas I. Formal theory. *J. Phys. C*, **15**, 2801–2826.

Lyons, W. & Plisga, G. (2004). *Standard Handbook of Petroleum and Natural Gas Engineering*. Elsevier.

Maitland, G., Rigby, M., Smith, E.B. & Wakeham, W. (1981). *Intermolecular Forces*. Clarendon Press, Oxford.

Maitland, G., Vesovic, V. & Wakeham, W. (1985). The inversion of thermophysical properties II. Non-spherical systems explored. *Mol. Phys.*, **54**, 301 – 319.

Maitland, G., Mustafa, M., Vesovic, V. & Wakeham, W. (1986). The inversion of thermophysical properties. III. Highly anisotropic interactions. *Mol. Phys.*, **57**, 1015 – 1033.

Makita, T. (1957). The viscosity of argon, nitrogen and air at pressures up to 800 kg/cm^2. *Rev. Phys. Chem. Japan*, **27**, 16–21.

McCourt, F., Beenakker, J., Köhler, W. & Kuščer, I. (1991). *Non-Equilibrium Phenomena in Polyatomic Gases, vols. 1 and 2*. Clarendon Press, Oxford.

McLinden, M., Lemmon, E., & Friend, D. (2010). *Thermophysical Properties of Fluid Systems in NIST Chemistry WebBook, NIST Standard Reference Database Number 69*. Eds. P.J. Linstrom and W.G. Mallard, National Institute of Standards and Technology.

Meier, K., Laesecke, A. & Kabelac, S. (2004). Transport coefficients of the Lennard-Jones model fluid. I. Viscosity. *J. Chem. Phys.*, **121**, 3671–3687.

Meshcheryakov, N. & Golubev, I. (1954). Viscosity of gaseous hydrocarbons with high pressures. *Tr. Gos. Inst. Azot. Promsti.*, **4**, 22–35.

Miandehy, M. & Modarress, H. (2003). Equation of state for hard-spheres. *J. Chem. Phys.*, **119**, 2716–2719.

Michels, A., Botzen, A. & Schuurman, W. (1954). The viscosity of argon at pressures up to 2000 atmospheres. *Physica*, **20**, 1141–1148.

Michels, A., Botzen, A. & Schuurman, W. (1957). The viscosity of carbon dioxide between 0°C and 75°C and at pressures up to 2000 atmospheres. *Physica*, **23**, 95102.

Michels, J.P.J. & Trappeniers, N.J. (1980). Molecular dynamical calculations on the transport properties of a square–well fluid : II. The viscosity above the critical density. *Physica A*, **104**, 243–254.

Millat, J., Dymond, J. & de Castro, C. (1996). *Transport properties of fluids: their correlation, prediction and estimation*. Cambridge University Press.

Monnery, W., Mehrotra, A. & Svrcek, W. (1996). Viscosity prediction from a modified square well intermolecular potential model. *Fluid Phase Equil.*, **117**, 378–385.

Monnery, W., Mehrotra, A. & Svrcek, W. (1997). Viscosity prediction from a modified square well intermolecular potential model: polar and associating compounds. *Fluid Phase Equil.*, **137**, 275–287.

Monnery, W., Mehrotra, A. & Svrcek, W. (1998). Viscosity prediction of non-polar, polar, and associating fluids over a wide $p\rho t$ range from a modified square well intermolecular potential model. *Ind. Eng. Chem. Res.*, **37**, 652–659.

Moré, J., Sorenson, D., Garbow, B. & Hillstrom, K. (1984). The MINPACK project. *Sources and Development of Mathematical Software*, 88–111.

Oliveira, C. & Wakeham, W. (1992). The viscosity of five liquid hydrocarbons at pressures up to 250 MPa. *Int. J. Thermophys.*, **13**, 773790.

Padua, A., Wakeham, W.A. & Wilhelm, J. (1994). The viscosity of liquid carbon dioxide . *Physica*, **15**, 767–777.

Polewczak, J. & Stell, G. (2002). Transport Coefficients in Some Stochastic Models of the Revised Enskog Equation. *J. Stat.Phys.*, **109**, 569–590.

Quiñones-Cisneros, S., Huber, M. & Deiters, U. (2012). Correlation for the Viscosity of Sulfur Hexafluoride (SF_6) from the Triple Point to 1000 K and Pressures to 50 MPa . *J. Phys. Chem. Ref. Data*, **41**, 023102.

Rapaport, D.C. (2004). *The art of molecular dynamics simulation*. Cambridge University Press.

Ree, F.H. & Hoover, W. (1964). On the signs of the hard sphere virial coefficients. *J. Chem. Phys.*, **40**, 2048–2059.

Reed, T. & Gubbins, K. (1973). *Applied statistical mechanics*. McGraw-Hill, New York.

Reiss, H., Frisch, H.L. & Lebowitz, J.L. (1959). Statistical Mechanics of Rigid Spheres. *J. Chem. Phys.*, **31**, 369–380.

Royal, D., Vesovic, V., , Trusler, J. & Wakeham, W. (2005). Predicting the viscosity of liquid refrigerant blends: comparison with experimental data. *Int. J. of Refrigeration*, **28**, 311–319.

Royal, D.D., Vesovic, V., Trusler, J.P.M. & Wakeham, W.A. (2003). Prediction of the viscosity of dense fluid mixtures. *Mol. Phys.*, **101**, 339352.

Sandler, S. & Fiszdon, J. (1979). On the viscosity and thermal conductivity of dense gases. *Physica A*, **95**, 602608.

Schley, P., Jäschke, M., Küchenmeister, C. & Vogel, E. (2004). Viscosity of Methane - Chlorodifluoromethane (R22) Gaseous Mixtures in the Temperature Range from 298.15 K to 373.15 K and at Pressures up to 5 MPa. *J. Chem. Eng. Jpn.*, **25**, 1623–1652.

Sengers, J. (1985). Transport properties of fluids near critical points. *Int. J. Thermophys.*, **6**, 203–232.

Sigurgeirsson, H. & Heyes, D.M. (2003). Transport coefficients of hard sphere fluids. *Mol. Phys.*, **101**, 469–482.

Silva, C. & Liu, H. (2008). Modelling of transport properties of hard sphere fluids and related systems, and its applications. *Theory and Simulation of Hard-Sphere Fluids and Related Systems, Lecture Notes in Physics*, **753**, 383–492.

Slyusar, V., Rudenko, N. & Tretyakov, V. (1974). The viscosity of methane at constant density. *Fiz. Zhidk. Sostoyaniya*, 100–104.

Smith, S.W., Hall, C.K. & Freeman, B.D. (1997). Molecular dynamics for polymeric fluids using discontinuous potentials. *J. Comput. Phys.*, **134**, 16–30.

Speedy, R., Prielmeier, F., Vardag, T., Lang, E. & Ludemann, H. (1989). Diffusion in simple fluids. *Mol. Phys.*, **66**, 577.

Starling, K.E., Eakin, B.E. & Ellington, R.T. (1960). Liquid, gas, and dense-fluid viscosity of propane. *AIChE J.*, **6**, 438442.

Strumpf, H.J., Collingsa, A.F., & Pings, C.J. (1974). Viscosity of xenon and ethane in the critical regions. *J. Chem. Phys.*, **60**, 3109–3123.

Swift, G.W., Lohrenz, J. & Kurata, F. (1960). Liquid viscosities above the normal boiling point for methane, ethane, propane, and n-butane. *AIChE J.*, **6**, 415–419.

Thiele, E. (1963). Equation of state for hard spheres. *J. Chem. Phys.*, **39**, 474–479.

Umla, R., Riesco, N. & Vesovic, V. (2012). Viscosity of pure fluids- Enskog-2σ model. *Fluid Phase Equil.*, **334**, 89–96.

van der Gulik, P. & Trappeniers, N. (1986). The viscosity of argon at high densities. *Physica A*, **135**, 1–20.

Van der Gulik, P.S. (1997). Viscosity of carbon dioxide in the liquid phase. *Physica A*, **238**, 81–112.

Van Itterbeek, A., Hellemans, J., Zink, H. & van Cauteren, M. (1966). Viscosity of liquified gases at pressures between 1 and 100 atmosphere. *Physica*, **32**, 2171–2172.

Vesovic, V. & Wakeham, W. (1989a). The prediction of the viscosity of dense gas mixtures. *Int. J. Thermophys.*, **10**, 125–132.

Vesovic, V. & Wakeham, W. (1989b). Prediction of the viscosity of fluid mixtures over wide ranges of temperature and pressure. *Chem. Eng. Sci.*, **44**, 2181–2189.

Vesovic, V., Wakeham, W.A., Olchowy, G.A., Sengers, J.V., Watson, J.T.R. & Millat, J. (1990). The transport properties of carbon dioxide. *J. Phys. Chem. Ref. Data*, **19**, 763–808.

Vesovic, V., Assael, M.J. & Gallis, Z.A. (1998). Prediction of the viscosity of supercritical fluid mixtures. *Int. J. Thermophys.*, **19**, 1297–1313.

Vogel, E., Küchenmeister, C. & Bich, E. (1998). Reference Correlation of the Viscosity of Propane . *J. Phys. Chem. Ref. Data*, **27**, 947–970.

Vogel, E., Küchenmeister, C. & Bich, E. (1999). Viscosity correlation for n-butane in the fluid region. *High Temperatures - High Pressures*, **31**, 173–186.

Vogel, E., Wilhelm, J. & Küchenmeister, C. (2000). High-precision measurements on methane. *High Temperatures - High Pressures*, **32**, 73–81.

Wakeham, W., Nagashima, A. & Sengers, J. (1991). *Measurement of the transport properties of fluids*. Experimental thermodynamics, International Union of Pure and Applied Chemistry. Blackwell Scientific Publications.

Weeks, J.D., Chandler, D. & Andersen, H. (1971). Role of repulsive forces in determining the equilibrium structure of simple liquids. *J. Chem. Phys.*, **54**, 5237–5247.

WERTHEIM, M. (1963). Exact Solution of the Percus–Yevick Integral Equation for Hard Spheres. *Phys. Rev. Lett.*, **10**, 321–323.

WERTHEIM, M. (1964). Analytic Solution of the Percus-Yevick Equation. *J. Math. Phys.*, **5**, 643–651.

WILHELM, J. & VOGEL, E. (2000). Viscosity measurements on gaseous argon, krypton, and propane. *Int. J. Thermophys.*, **21**, 301–318.

YELASH, L.V., KRASKA, T. & DEITERS, U. (1999). Closed-loop critical curves in simple hard-sphere van der Waals-fluid models consistent with the packing fraction limit. *J. Chem. Phys.*, **110**, 3079–3084.

YOUNGLOVE, B.A. & ELY, J.F. (1987). The viscosity of carbon dioxide. *J. Phys. Chem. Ref. Data*, **16**, 577–799.